(4)

CHEMICAL RESEARCH, DEVELOPMENT & ENGINEERING CENTER

CRDEC-CR-88074

OPTICAL CONSTANTS OF MINERALS AND OTHER MATERIALS FROM THE MILLIMETER TO THE ULTRAVIOLET

by R.J. Ball
R.W. Alexander, Jr.
L.A. Newquist
R. Van Diver
M.A. Ordal
L.L. Long
R.E. Paul

UNIVERSITY OF MISSOURI-ROLLA
Rolla, MO 65401

June 1988

U.S. ARMY ARMAMENT MUNITIONS CHEMICAL COMMAND

Aberdeen Proving Ground, Maryland 21010-5423

Disclaimer

The findings in this report are not to be construed as an official Department of the Army position unless so designated by other authorizing documents.

Distribution Statement

Approved for public release; distribution is unlimited.

UNCLASSIFIED

SECURITY CLASSIFICATION OF THIS PAGE

REPORT DOCUMENTATION PAGE

1a. REPORT SECURITY CLASSIFICATION: UNCLASSIFIED

1b. RESTRICTIVE MARKINGS:

2a. SECURITY CLASSIFICATION AUTHORITY:

2b. DECLASSIFICATION / DOWNGRADING SCHEDULE:

3. DISTRIBUTION / AVAILABILITY OF REPORT: Approved for public release; distribution is unlimited.

4. PERFORMING ORGANIZATION REPORT NUMBER(S): CRDEC-CR-88074

5. MONITORING ORGANIZATION REPORT NUMBER(S):

6a. NAME OF PERFORMING ORGANIZATION: University of Missouri-Rolla

6b. OFFICE SYMBOL (If applicable):

7a. NAME OF MONITORING ORGANIZATION:

6c. ADDRESS (City, State, and ZIP Code): Rolla, MO 65401

7b. ADDRESS (City, State, and ZIP Code):

8a. NAME OF FUNDING/SPONSORING ORGANIZATION: CRDEC

8b. OFFICE SYMBOL (If applicable): SMCCR-RSP-B

9. PROCUREMENT INSTRUMENT IDENTIFICATION NUMBER: [illegible]

8c. ADDRESS (City, State, and ZIP Code): Aberdeen Proving Ground, MD 21010-5423

10. SOURCE OF FUNDING NUMBERS:

PROGRAM ELEMENT NO.	PROJECT NO.	TASK NO.	WORK UNIT ACCESSION NO.

11. TITLE (Include Security Classification): Optical Constants of Minerals and Other Materials from the Millimeter to the Ultraviolet

12. PERSONAL AUTHOR(S): Bell, R. J.; Alexander, R. W., Jr.; [illegible] Ordal, M. A.; Long, L. L.; and Paul, R. E.

13a. TYPE OF REPORT: Contractor

13b. TIME COVERED: FROM 85 June TO 87 May

14. DATE OF REPORT (Year, Month, Day): 1988 June

15. PAGE COUNT: [illegible]

16. SUPPLEMENTARY NOTATION: COR: Merrill Milham, SMCCR-RSP-B, (301) 671-3854

17. COSATI CODES

FIELD	GROUP	SUB-GROUP
15	06	03

18. SUBJECT TERMS (Continue on reverse if necessary and identify by block number): Optical Constants; Minerals; Metals; Ultraviolet; Infrared

19. ABSTRACT (Continue on reverse if necessary and identify by block number)

The optical constants of a wide variety of materials were measured for this contract period. Work was performed at two campuses of the University of Missouri—the Rolla Campus and the Kansas City Campus. This report covers the work done at the University of Missouri-Rolla. The work done at the University of Missouri-Kansas City will be submitted separately. The spectral range of the measurements covered from the millimeter to the ultraviolet. The millimeter and submillimeter (far infrared) measurements were made on the Rolla Campus (Bell and Alexander) and the infrared, visible and ultraviolet measurements were made on the Kansas City Campus. This wide spectral range means that Kramers-Kronig analyses can be made with better precision than when reflectance data is available only over a limited spectral range.

(CONTINUED ON REVERSE)

20. DISTRIBUTION/AVAILABILITY OF ABSTRACT: ☒ UNCLASSIFIED/UNLIMITED ☐ SAME AS RPT. ☐ DTIC USERS

21. ABSTRACT SECURITY CLASSIFICATION: UNCLASSIFIED

22a. NAME OF RESPONSIBLE INDIVIDUAL: SANDRA J. JOHNSON

22b. TELEPHONE (Include Area Code): (301) 671-2914

22c. OFFICE SYMBOL: SMCCR-SPS-T

DD FORM 1473, 84 MAR — 83 APR edition may be used until exhausted. All other editions are obsolete.

SECURITY CLASSIFICATION OF THIS PAGE

UNCLASSIFIED

19. ABSTRACT (continued)

Important remote targets.

1. Construction of modulating ellipsometer that is capable of measuring small ellipsometric parameters on samples at ultraviolet wavelengths and samples that are highly absorbing. To our knowledge no other instruments with this capability exist.

2. Measurement of dielectric tensor of gypsum, both as a single crystal and as a powder in the far and near infrared for use as a standard. This goal had originally been proposed in the fiber modeling discussion section of the annual June CRDEC Conference at Aberdeen.

3. Measurement of several types of graphite. We have found that Dixon 200-10 shows a large positive real part of the dielectric constant at low frequencies. This contradicts the usual free electron picture for graphite at low frequencies.

PREFACE

The work described in this report was authorized under Contract DAAA15-85-K-0004. This work was started in June 1985 and completed in May 1987.

The use of trade names or manufacturers' names in this report does not constitute an official endorsement of any commercial products. This report may not be cited for purposes of advertisement.

This report has been approved for release to the public.

Blank

TABLE OF CONTENTS

Blank

Optical Constants of Minerals and Other Materials from the Millimeter to the Ultraviolet

1. SUMMARY

The optical constants of a wide variety of materials were measured for this contract period. Work was performed at two campuses of the University of Missouri--the Rolla Campus and the Kansas City Campus. This report covers the work done at the University of Missouri--Rolla. The work done at the University of Missouri--Kansas City will be submitted separately. The UMKC report will include the financial report for both efforts. The spectral range of the measurements covered from the millimeter to the ultraviolet. The millimeter and submillimeter for infrared measurements were made on the Rolla Campus Bell and Alexander and the infrared, visible and ultraviolet measurements were made on the Kansas City Campus. This wide spectral range means that Kramers-Kronig analyses can be made with better precision than when reflectance data is available only over a limited spectral range.

Important results include
1. Construction of a homodyning interferometer that is capable of measuring small (diameter approximately 1 cm) samples at millimeter wavelengths and samples that are highly absorbing. To our knowledge no other instruments with this capability exist.
2. Measurement of refractive indices of Typerus both as a single crystal and as a powder in the far and near infrared for use as a standard. This goal had originally been proposed in the Friday morning discussion section of the annual June CRDEC Conference at Aberdeen.
3. Measurement of several types of graphite. We have found that Dixon 200-10 shows a large positive real part of the dielectric constant at low frequencies. This contradicts the usual free electron picture for graphite at low frequencies.

2. REPORT OF RESEARCH

2.1 Highlights.

This report will make extensive reference to the quarterly reports submitted during the contract period. The materials studied may be grouped into three classes defined by the tecniques used to measure the refractive indices. These three classes are discussed below, including reference to the work performed at the University of Missouri-Kansas City where necessary. The UMKC work is discussed in more detail in a separate section of this report. Tables of optical constants for the materials measured have been entered into the CRDEC computer data bank. The materials whose optical constants have been measured as part of this contract include: polycrystalline iron, dimethyl methyl phosphonate (DMMP), polycrystalline nickel, stainless

steel, polycrystalline aluminum, diesel fuel, polycrystalline zinc, polycrystalline molybdenum, polycrystalline gold, polycrystalline lead, polycrystalline titanium, polycrystalline tantulum, polycrystalline tungsten, crystalline quartz (two orientations), zinc oxide (powder), fluorapatite (powder), gypsum (powder and three crystal orientations, Dixon 200-10 graphite (powder), and highly oriented pyrolytic graphite (HOPG).

NATURAL MINERALS: Measurements of the refractive indices of natural minerals were made by measuring the reflectance of either single crystals (where available) or of pressed powder pellets. The powders were pressed with no binder. A discussion of this method of sample preparation appears in our recent paper "Preparation dependent properties of pressed pellets of montmorillonite in the far infrared" in Applied Optics.[1] Of particular note is gypsum. At one of the Friday morning "Discussion Sessions" at the annual CRDEC Aberdeen Conference on Obscuration and Aerosol Science, it was decided that gypsum would make an excellent standard for the pressed powder technique for soft materials because it is available in single crystalline form and presses into high quality surface pellets. This project has been completed as a joint effort of the UMR and UMKC groups and a paper is being prepared for publication.[2] Oscillator model fits were made to the reflectance to provide a convenient parameterization of the optical constants. Quartz was discussed as a standard for hard materials. Graphite is discussed under natural minerals because it was measured in pressed pellet and single crystal form even though its optical properties are quite different from the natural minerals. For graphite, a new type of interferometer was developed to allow measurements on (relatively) small samples at millimeter wavelengths. This unique instrument has allowed measurements of optical properties at millimeter wave lengths of very lossy materials not available in large sample sizes for the first time.

METALS: The measurement of the optical constants of metals at long wavelenths -- greater than 100 micrometers -- is very difficult because metals are so highly reflecting. Two technigues are available, stacked plane parallel waveguides[3] and non-resonant cavities.[4,5] Both techniques were tried in our laboratory and the non-resonant cavity method proved superior and required smaller amounts of sample. As part of our feasibility study of plane parallel waveguides, we measured the absorption coefficient of Teflon in the submillimeter.[6] The results were published in Applied Optics. For the nonresonant cavity, we improved the analysis used to obtain the optical constants from the measurements and measured a large number of metals. Almost no data existed in the literature for submillimeter wavelengths for metals prior to our measurements. In order to obtain optical constants over a wide frequency range, our UMR data was combined with infrared, visible and UV measurements made at UMKC or with data from the literature. The resulting data sets covered a very wide frequency range allowing a good Kramers-Kronig analysis of the measure reflectance to give optical constants. The Drude model for metals was found to fit the data for many metals in the

submillimeter frequency region.

LIQUIDS: The UMKC laboratory is well-known for its measurements of the optical properties of liquids in the infrared and visible. These were made by measuring the reflectance of a horizontal pool of the sample liquid and the performing a Karmers-Kronig analysis to obtain refractive indices. This technique is difficult to extend to the far infrared and instead, we measure transmittances of liquids in cells with either TPX or silicon windows. Very few measuements of liquids have been made in the far infrared. DMMP proved to be very strongly absorbing in the submillimeter and a special cell was constructed to allow very thin samples to be measured.

2.2 Natural Minerals.

GYPSUM: Gypsum was studied, at least in part, because it was decided at one of the Friday morning informal discussions at the annual CRDEC Aberdeen Conference on Obscuration and Aerosol Research that it would make a good standard for studies of natural minerals using the pressed powder technique. The pressed powder technique had originally been shown to be useful for natural minerals by the UMKC laboratory. The conferees chose gypsum because it was anisotropic, available as a single crystal and pressed to form pellets with very smooth surfaces. We have just published a paper discussing the pressed pellet technique in the far infrared. An important observation we made was that the pressed pellet has a surface skin that is denser than the average pellet density. This means that the optical constants measured from the pressed pellet are nearer the bulk values than the average density of the pellet would indicate. For gypsum, we also measured the optical constants for all three crystalline axes. A comparison of the pressed pellet optical constants with those of the single crystal allowed us to conclude that the pellet had an effective density 0.91 that of the single crystal and that all three crystalline orientations were represented equally on the sample surface. That is, the pressing operation resulted in little preferential orientation of the crystallites on the pellet surface. This is further discussed in this contract's first quarterly report dated 26 August 1985 and in a paper now in preparation.[2]

Figures 1 through 8 show the measured reflectance and the derived optical constants for the three orientations of the gypsum single crystal and the pressed powder gypsum sample. The reflectance was measured from 10 to 400 cm^{-1} at UMR and from 400 to 4,000 cm^{-1} at UMKC. The dispersion analysis was done on the combined data set. Table 1 gives the oscillator fit parameters for the three crystalline axes. The form of the dielectric constant used to fit the reflectance data was

$$\epsilon(\omega) = \epsilon_\infty + \sum_j \frac{A_j\,\omega_{oj}^2}{\omega_{oj}^2 - \omega^2 - i\gamma_j\omega}$$

In general, our experience was that the oscillator fit gave better results than a Kramers-Kronig analysis, especially in regions were k was small. However, a good oscillator fit required the reflectance to be measured over a wide frequency range, necessitating measurements at both the UMR and UMKC laboratories. An oscillator fit is often called a dispersive analysis. The details of the oscillator fit model were discussed in our fifth quarterly report dated 11 September 1986.

TABLE 1: OSCILLATOR FIT PARAMETERS FOR GYPSUM

j	A_j	γ_j (cm^{-1})	ω_{oj} (cm^{-1})
X-axis			
1	0.2421	10.170	1123.1
2	0.0956	8.844	666.5
3	0.4265	91.816	447.6
4	1.0642	120.976	222.1
5	2.6027	97.899	220.4
6	1.1337	17.840	207.9
7	2.9672	8.364	117.6

$\epsilon_\infty = 2.625$

j	A_j	γ_j (cm^{-1})	ω_{oj} (cm^{-1})
Y-axis			
1	0.0432	53.718	3520.1
2	0.0105	23.195	1684.7
3	0.0943	16.953	1131.2
4	0.1422	8.832	1121.0
5	0.1740	37.910	594.8
6	1.9611	103.472	545.6
7	0.1033	81.043	412.2
8	0.3038	30.126	302.0
9	0.5991	25.179	217.3
10	0.5799	7.367	191.3
11	1.2839	27.557	165.3

$\epsilon_\infty = 2.147$

Z-axis

1	0.0379	55.059	3403.0
2	0.0166	10.335	1622.6
3	2.5834	13.904	1108.0
4	0.1623	23.915	592.8
5	0.1434	85.412	542.2
6	0.6468	42.698	295.8
7	1.1131	40.671	220.2
8	1.0278	19.926	175.1

ε_∞ = 2.162

FLUORAPATITE: Fluorapatite, $Ca_5(PO_4)_3F$, or calcium phosphate with fluorine is one of the most common phosphates. It crystalliizes in the hexagonal system, C_{6h}^2. The length of the a and c axes are 9.39 and 6.89 A, respectively. This mineral is uniaxial negative with the index of refraction for the ordinary ray, n_o = 1.633, and extraordinary ray, n_e = 1.630 at the sodium D line, 5983 A. It thus has a very small birefringence. On the Mohs hardness scale fluorapatite is rated at 5 and thus can be scratched with a knife blade. It has a specific gravity ranging from 3.1 to 3.4.

Pressed powder samples were made by applying 16,000 lbs of force to a 13mm diameter die. This produced a whitish green pellet. The reflectance spectrum of this pellet is shown in Fig. 9. An oscillator fit was made to Eq. (1) and n and k derived from this fit are shown in Fig. 10. The oscillator fit parameters are given in Table 2.

TABLE 2: OSCILLATOR FIT PARAMETERS FOR FLUORAPATITE

j	A_j	γ_j (cm^{-1})	ω_{oj} (cm^{-1})
1	0.6677	59.843	331.34
2	0.2248	18.922	282.89
3	0.6636	31.992	237.97
4	0.3165	18.751	196.56
5	0.6934	21.943	99.23
6	3.3869	87.180	73.08

ε_∞ = 3.6556

ZINC OXIDE: Zinc oxide, or zincite is a very soft material (Moh hardness 4) that pressed into pellets under moderate pressure. These pellets had a smooth, mirror-like surface. Zinc oxide also crystallizes in the hexagonal system. The lengths of the a and c axes are 3.25 and 5.21 A, respectively. It is positive uniaxial with n_o = 2.013 and n_e = 2.029 at the sodium D line. Its specific gravity ranges from 5.64 to 6.68.

The measured reflectance in the 10 to 350 cm^{-1} range is shown in Fig. 11. Bear in mind that this material was not measured at shorter wavelengths. Such measurements will be needed if a Kramers-Kronig analysis to obtain optical constants is wanted.

QUARTZ: Reflectance data for quartz was available in the literature. Kramers-Kronig analysis was used to find n and k. For the spectral range from 20 to 370 cm^{-1}, the data of Russell and Bell was used.[7] Spitzer and Kleinman's [8] measurements were used from 370 to 1,600 cm^{-1}. Table 3 contains n and k for both the ordinary ray and the extraordinary ray. Figure 12 shows n and k for the ordinary ray, while Fig. 13 shows the same for the extraordinary ray. The oscillator fit parameters are shown in Table 4 for the two crystalline axes. The reflectances calculated from the oscillator fit parameters for the ordinary and extraordinary ray are shown in Figs. 12 and 13, respectively.

TABLE 4: OSCILLATOR FIT PARAMETERS FOR QUARTZ

j	A_j	γ_j (cm^{-1})	ω_{oj} (cm^{-1})
Ordinary Ray			
1	0.009	134.	1227
2	0.010	6.98	1163
3	0.67	7.61	1072
4	0.11	7.17	797
5	0.018	8.36	697
6	0.852	4.05	450
7	0.36	2.76	394
8	0.050	7.36	263
9	0.0006	4.49	128.4

ϵ_∞ = 2.356

Extraordinary Ray

1	0.011	183.	1220
2	0.67	7.45	1000
3	0.10	7.78	778
4	0.006	21.56	539
5	0.05	7.13	509
6	0.699	4.56	495
7	0.72	5.10	364

$\varepsilon_\infty = 2.383$

Sources of Quartz data were refs. 7 and 8.

==========

GRAPHITE: Pellets pressed from Dixon 200-10 graphite were measured at both UMR and UMKC. Reflectance of these pellets was measured at UMR from 20 to 400 cm^{-1} using our Fourier Transform Spectrometer. This data was combined with the UMKC data at shorter wavelengths and Kramers-Kronig analyzed. In Figure 14 the real and imaginary parts of the dielectric function (ε_1 and ε_2, respectively) are plotted versus wavenumber. For frequencies below 20 cm^{-1} the Kramers-Kronig analysis was extrapolated to zero frequency as shown.

To extend our measurements to millimeter wavelengths, we invented a new type of interferometer, a homodyning interferometer. This instrument uses a monochromatic microwave source and the detector looks at the interference between the beam transmitted directly from the source and the beam reflected from the sample. Currently our source operates at 1.10 cm^{-1} (corresponding to a wavelength of 9 mm). The sample is moved by a micrometer and the signal is measured as a function of distance. This signal versus displacement is fit using "Asystant" (McMillan and Co.). Figure 15 shows a plot of the measured signal versus displacement (dots) and the fit obtained using "Asystant." Using the fit parameters and our theory, we have obtained both the amplitude and phase of the reflection coefficient of graphite relative to Ag. Using the Drude model values for silver, allows the determination of the graphite values. The measured reflectivity is 0.939 +/- 0.003 and the measured phase angle of the reflection coefficient is J(0) = 0.2^o-0.3^o. From the amplitude and phase of the reflection coefficient, we can obtain ε_1 and ε_2 at 1.10 cm^{-1}. These points are shown in Fig. 14, along with the Kramers-Kronig results. Our best estimates for error bars are shown also.

The diagram of our homodyne interferometer is shown in Fig. 16. Note that the chopper modulates only the beam from the sample, which eliminates the strong signal from the direct source

horn to detector horn path. Stray radiation was reduced by using an antireflection cone behind the sample. This cone reduces back reflected radiation from behind the sample. The system can be used without the chopper in a dc mode. This reduces the stray radiation from the chopper, but we have obtained better signal to noise ratios from the ac method (using the chopper.) With better dc amplifiers we may go back to the dc method. The homodyning interferometer is described more fully in the paper appearing in the CRDEC Scientific Conference on Obscuration and Aerosol Research for 1987. [9] Note that to our knowledge, this homodyning interferometer is the only instrument capable of measuring optical constants at millimeter wavelengths for such small samples, or for samples which are so highly absorbing.

Our current picture of these graphite pressed pellets is that they are made up of thin platelets of crystalline graphite. Our scanning electron microscope pictures of these pellets show a high degree of parallel orientation of the platelets. These platelets are sufficiently thin that we have adapted a model where the carriers are in a quantum well in the z-direction (thin dimension of platelet) and large in the other two (x and y) directions. Such a theory yields $\epsilon_1(\omega)$ and ϵ_2 that have the form of Sellmeier's equation (harmonic oscillator resonance). Note from Fig. 14 that ϵ_1 is positive at low frequencies and hence cannot be fit with a simple free carrier (Drude) model. Our preliminary fit to the thin platelet model suggests the graphite is a p-type semimetal with a resistivity of about 2.4 x 10^{-3} Ω-cm. More details of this model can be found in our second quarterly report dated 1 December 1988.

In Fig. 17 we report the reflectance of polycrystaline HOPG graphite from the UV to the millimeter wavelength ranges. The reflectance is rather complicated compared to the Dixon 200-10 reflectance. We have KK analyzed the data for the ϵ_1 and ϵ_2 and have qualitative agreement with the Dixon 200-10 pressed pellets; however, the magnitude swings for the HOPG sample are rather large. Also, the values of ϵ_1 at very low frequencies are positive and not negative in contraction to Phillip's data. We've also seen the positive range of ϵ_1 values at very low frequencies for Dixon 200-10. The physics of graphite at low frequencies is far from certain despite the fact that many scientists have only observed semimetal behavior at high frequencies. It is advisable to take more data, which we're actively doing. Soon we plan to use the new homodyning interferometer to measure ϵ_1 and ϵ_2 at 1.1 cm^{-1} for HOPG graphite.

In Fig. 18 we present the reflectance of POCO graphite in the FIR and submillimeter wavelength range as taken at UMR. We don't have the higher frequency data but it will be measured at high frequencies at UMKC. In addition, we'll use the homodyning interferometer to measure ϵ_1 and ϵ_2 at 1.1 cm^{-1}.

2.3 Metals.

The optical constants of metals are particularly difficult to measure in the far infrared and millimeter spectral regions because they are so highly reflecting. Two techniques have been employed which in effect make use of a large number of reflections. These are the plane parallel waveguide method (described in ref. 3) and the non-resonant cavity method (described in our recent paper, ref. 5). After considerable experimentation, we decided that the non-resonant cavity method is better in the 10 to 350 cm^{-1} spectral range. We developed an improved theory to analyze the non-resonant cavity measurements. This is described in our third quarterly report (dated 14 March 1986) and our paper entitled "Optical properties of Au, Ni, and Pb at submillimeter wavelengths", published in Applied Optics.[5]

IRON: A polycrystalline sample of iron was measured using the nonresonant cavity from 80 to 320 cm^{-1}. The reflectance of the iron sample was measured from 400 to 4,000 cm^{-1} at the UMKC laboratory. Literature values for iron were used from 4,000 to 242,000 cm^{-1}. This large data sent was then Kramers-Kronig analyzed to obtain $\epsilon_1(\omega)$ and $\epsilon_2(\omega)$. Figure 19 shows $r(\omega)$, the normalized surface impedance as a function of wavenumber for iron. The points with error bars show our non-resonant cavity results, the dashed dot line is from the data set including the UMKC reflection measurements and literature values.[10] Figure 20 shows ϵ_1 and ϵ_2 as functions of wavenumber. Our improved method of analyzing the nonresonant cavity and details of Kramers-Kronig analysis appear in our third quarterly report (dated 14 March 1986), in our papers (refs. 4 and 5) and a submitted paper (see Appendix B). The third quarterly report includes tables of n, k, ϵ_1, ϵ_2, and R (reflectance) as a function of wavenumber.

ALUMINUM: A polished polycrystalline aluminum sample was measured using the nonresonant cavity. The measured normalized surface impedance is shown in Fig. 21 as points with error bars. Literature values (from ref. 10) are shown at shorter wavelengths. The values of ϵ_1 and ϵ_2 obtained from combining our long wavelength measurements with data from ref. 10 and performing a Kramers-Kronig analysis are shown in Fig. 22. Our seventh quarterly report, dated 6 March 1987, contains a table of ϵ_1, ϵ_2, n, k, and R versus wavenumber for aluminum. This data is being prepared for publication (see Appendix B).

TITANIUM: A polished polycrystalline titanium sheet was measured using the nonresonant cavity. Our measured real part of the normalized surface impedance is shown in Fig. 23. Data at shorter wavelengths from ref. 10 are shown as the dot dash line. Figure 24 shows ϵ_1 and ϵ_2 derived from the Kramers-Kronig analysis of our data combined with the short wavelength data from ref. 10. Table 3 of Appendix B gives n, k, ϵ_1, ϵ_2, and R as a function of wavenumber for titanium. This data is being prepared for publication (see Appendix B).

TUNGSTEN: Polished polycrystalline tungsten sheet was measured with the nonresonant cavity. Figure 25 plots the measured normalized surface resistance with error bars and data from ref. 10 for shorter wavelengths (dash dot and dotted line). Once again the dielectric constant was obtained from a Kramers-Kronig analysis of our data and the ref. 10 data. The results are shown as the solid lines in Fig. 26. The dash dot and dotted lines show the ref. 10 only results. Table 5 of Appendix B gives n, k, ϵ_1, ϵ_2 and R as a function of wavenumber. This data is being prepared for publication (See Appendix B).

TANTULUM: A polished polycrystalline tantulum sheet was studied in the nonresonant cavity. Figure 27 shows the normalized surface impedance. Our nonresonant cavity data are plotted as the points with error bars and the data from ref. 10 is plotted as the dash dot line. Once again, our data was combined with the literature data and Kramers-Kronig analyzed to obtain ϵ_1 and ϵ_2. The results are plotted in Fig. 28 as the solid lines. The dash dot line (almost on top of the solid line) is the literature values alone. Table 4 of Appendix B gives n, k, ϵ_1, ϵ_2 and R as a function of wavelength. This data is being prepared for publication (see Appendix B).

MOLYBDENUM: A polished polycrystalline molybdenum sheet was studied in the nonresonant cavity. In Fig. 29 is plotted our measured points for the normalized surface resistance. The dash dot line shows the datum from ref. 10. Again, Kramers-Kronig analysis yielded ε_1 and ε_2. They are plotted in Fig. 30. Table 6 of Appendix B contains n, k, ε_1, ε_2 and R.

ZINC: A polished polycrystalline zinc sheet was measured with the nonresonant cavity at UMR and in a standard reflection geometry at UMKC. Because of problems in obtaining a good surface finish, our measurements were not extended into visible and uv. This means that the data set does not extend to sufficiently short wavelengths for a good Kramers-Kronig analysis. Figure 31 is a plot of the measured real part of the surface resistance, r, versus wavenumber for zinc. The reflectance at shorter wavelengths is shown in the UMKC portion of this report.

STAINLESS STEEL: A sheet of polished stainless steel was measured in the nonresonant cavity. The measured real part of the surface resistance is plotted versus wavenumber in Fig. 32. We have not attempted a Kramers-Kronig analysis because of the lack of reflectance measurements at shorter wavelengths.

2.4 Liquids.

The UMR group has measured the transmission spectra of two liquids, diesel fuel and dimethyl methyl phosphonate (DMMP). Measuring just the transmission spectrum allows a determination of only the absorption coefficient (or equivalently, the imaginary part of the refractive index, k). Difficulties with absorption in the vapor phase in our instrument have prevented reflection measurements such as have been made at shorter wavelengths by the UMKC laboratory.

DIESEL FUEL: The transmission spectrum of diesel fuel was measured with our Fourier Transform Spectrometer in a specially constructed cell with TPX windows. The details of the data analysis were discussed in our second quarterly report (dated 1 December 1985) and in our CRDEC annual conference paper[11]. Briefly, the transmission spectra were measured for a empty cell and diesel fuel filled cells of varying thickness. The log of the ratio of the transmission of the filled cell to the empty cell is plotted as a function of the cell thickness. The slope of this line is the absorption coefficient, $\alpha(\omega)$. The imaginary part of the refractive index, k can be obtained from α by the relation $k = 2\pi\alpha/\lambda$. Figure 33 shows our measured absorption coefficient for diesel fuel. The imaginary part of the refractive index is plotted in Fig. 34.

DMMP: DMMP is a much more strongly absorbing material than is diesel fuel. As a result a cell that allowed much shorter path lengths was required. This was purchased. Experimentation showed that path lengths in the 25 to 100 micrometers range were required. This caused some difficulties in assuring proper cell loading. Silicon windows were used because DMMP was found to interact slowly with the TPX windows. The same measurement techniques as described for diesel fuel were used for the DMMP (with, of course, the exception

of different cell lengths). The measured absorption coefficient versus wavenumber is shown in Fig. 35. Figure 36 presents our measured values of k versus wavenumber. These results were reported at the June 1987 CRDEC Conference on Obscuration and Aerosol Science and will appear in the procedings of this conference.

2.5 FIGURES

1. Reflectance for the X-axis of Gypsum. The solid line is the dispersive analysis fit. The squares are the measurements.
2. Optical Constants for the X-axis of Gypsum. The solid line is the real part of the refractive index, n, and the dashed line the imaginary part, k.
3. Reflectance for the Y-axis of Gypsum. The solid line is the dispersive analysis fit. The squares are the measurements.
4. Optical Constants for the Y-axis of Gypsum. The solid line is the real part of the refractive index, n, and the dashed line the imaginary part, k.
5. Reflectance for the Z-axis of Gypsum. The solid line is the dispersive analysis fit. The squares are the measurements.
6. Optical Constants for the Z-axis of Gypsum. The solid line is the real part of the refractive index, n, and the dashed line the imaginary part, k.
7. Reflectance of a Pressed Powder Gypsum Sample. The solid line is a fit with an average over the three crystalline orientations.
8. Optical Constants of Gypsum from a Pressed Pellet Sample.
9. Reflectance of a Pressed Pellet of Fluorapatite. The squares are the measured values and the straight line is the dispersive analysis fit.
10. Optical Constants for a Pressed Pellet of Fluorapatite. The solid line is n and the dashed k.
11. Reflectance of a Pressed Pellet of Zinc Oxide.
12. Optical Constants for the Ordinary Ray of Quartz. The solid line is n and the dashed line is k.
13. Optical Constants for the Extraordinary ray of Quartz. The solid line is n and the dashed line is k.
14. ϵ_1 and ϵ_2 for Dixon 200-10 graphite pressed pellet from KK analysis. Data points from Homodyning Interferometer.
15. Measured signal versus displacement (dots) for the homodyne intereferometer and fit (solid line).
16. Schematic Diagram of Homodyne Interferometer.
17. Reflectance of HOPG Graphite. This data from our data and that of Phillips (ref.).
18. Reflectance of POCO Graphite versus Wavenumber.
19. Real Part of the Normalized Surface Impedance for Iron. Points with error bars are from our nonresonant cavity measurements. Dashed dot line is from data of ref. 10.
20. ϵ_1 and ϵ_2 for Iron. Solid lines are the Kramers-Kronig results from combining our long wavelength measurements with literature values of Weaver, et al. (tabulated in ref. 10). The dashed dot curve are the measurements of Bolotin, et al. (also tabulated in ref. 10).
21. Real part of the Normalized Surface Resistance for Aluminum. Points with error bars are our nonresonant cavity measurements, while the dashed and dash dot curves for shorter wavelengths are from ref. 10.
22. ϵ_1 and ϵ_2 for Aluminum.

23. Real Part of the Normalized Surface Resistance of Titanium. Our nonresonant cavity measurements are show as data points with error bars. Data from ref. 10 are shown as the dash dot line.
24. ε_1 and ε_2 for Titanium. The solid curves show the Kramers-Kronig results for a data set consisting of our long wavelength nonresonant cavity data and literature data (ref. 10). The dash dot curve is the ref. 10 data alone.
25. Real Part of the Normalized Surface Resistance for Tungsten. Our nonresonant cavity measurements are shown by the points with error bars. The shorter wavelength data shown by the dash dot and dotted lines are from ref. 10.
26. ε_1 and ε_2 for Tungsten. The solid curves are for our data plus the short wavelength data. The dotted and dash dot curves are the ref. 10 data alone.
27. Real Part of the Normalized Surface Resistance for Tantulum. Our nonresonant cavity measurements are shown by the points with error bars. The shorter wavelength data shown by the dash dot line are from ref. 10.
28. ε_1 and ε_2 for Tantulum. The solid curves are for our data plus the short wavelength data. The dash dot curves are the ref. 10 data alone.
29. Real Part of the Normalized Surface Resistance for Molybdenum. Our nonresonant cavity measurements are shown by the points with error bars. The shorter wavelength data shown by the dash dot line are from ref. 10.
30. ε_1 and ε_2 for Molybdenum. The solid curves are for our data plus the short wavelength data. The dash dot curves are the ref. 10 data alone.
31. Real Part of the Normalized Surface Resistance for polycrystalline zinc.
32. Real Part of the Normalized Surface Resistance, r, versus wavenumber for Stainless Steel.
33. Absorption Coefficient, α, versus wavenumber for diesel fuel.
34. Imaginary Part of the Refractive Index versus wavenumber for diesel fuel.
35. Absorption Coefficient, α, versus wavenumber for DMMP.
36. Imaginary Part of the Refractive Index versus wavenumber for DMMP.

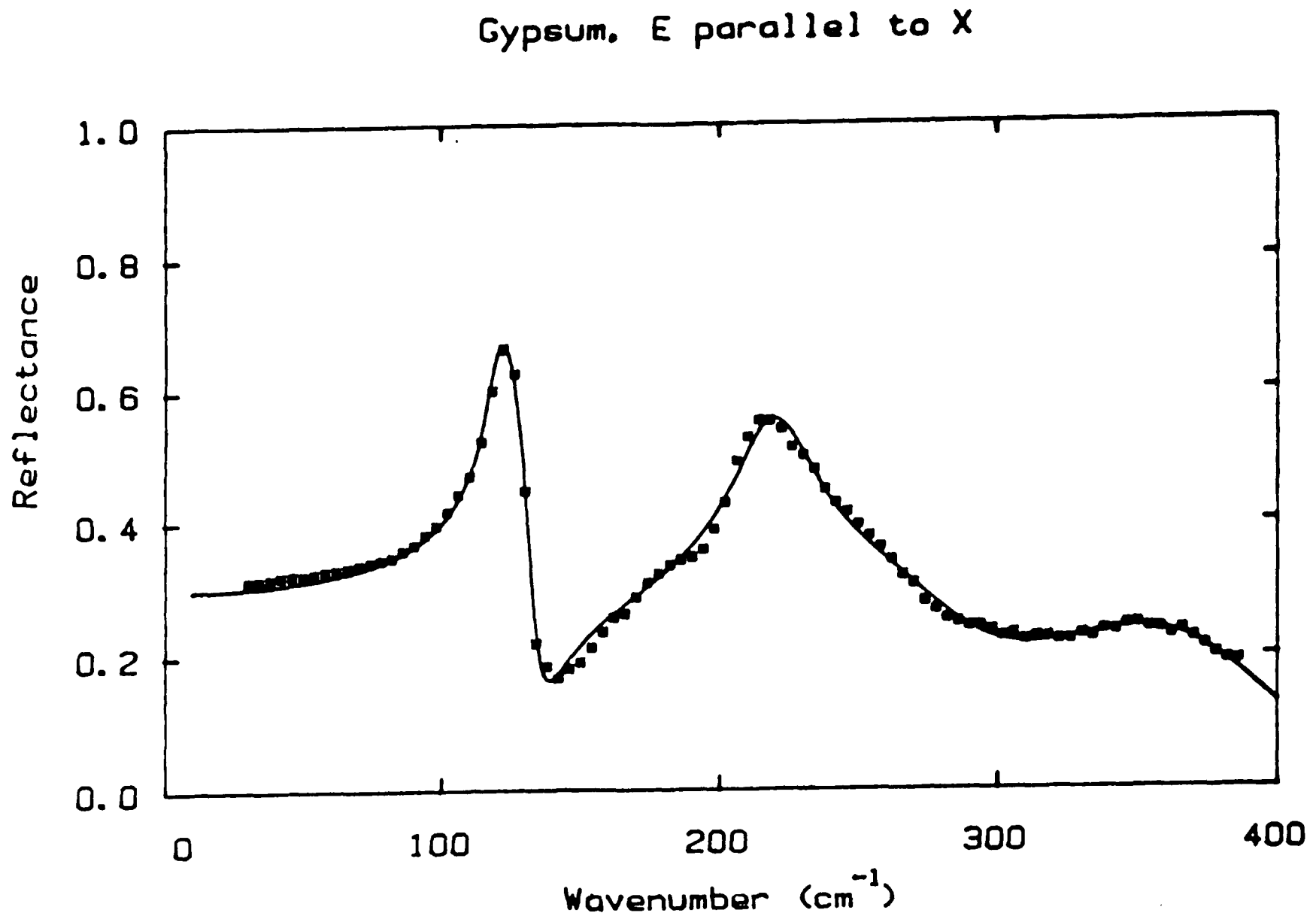

Fig. 1 Reflectance for the X optical axis of gypsum. The solid line is the dispersive analysis fit. The squares represent the data.

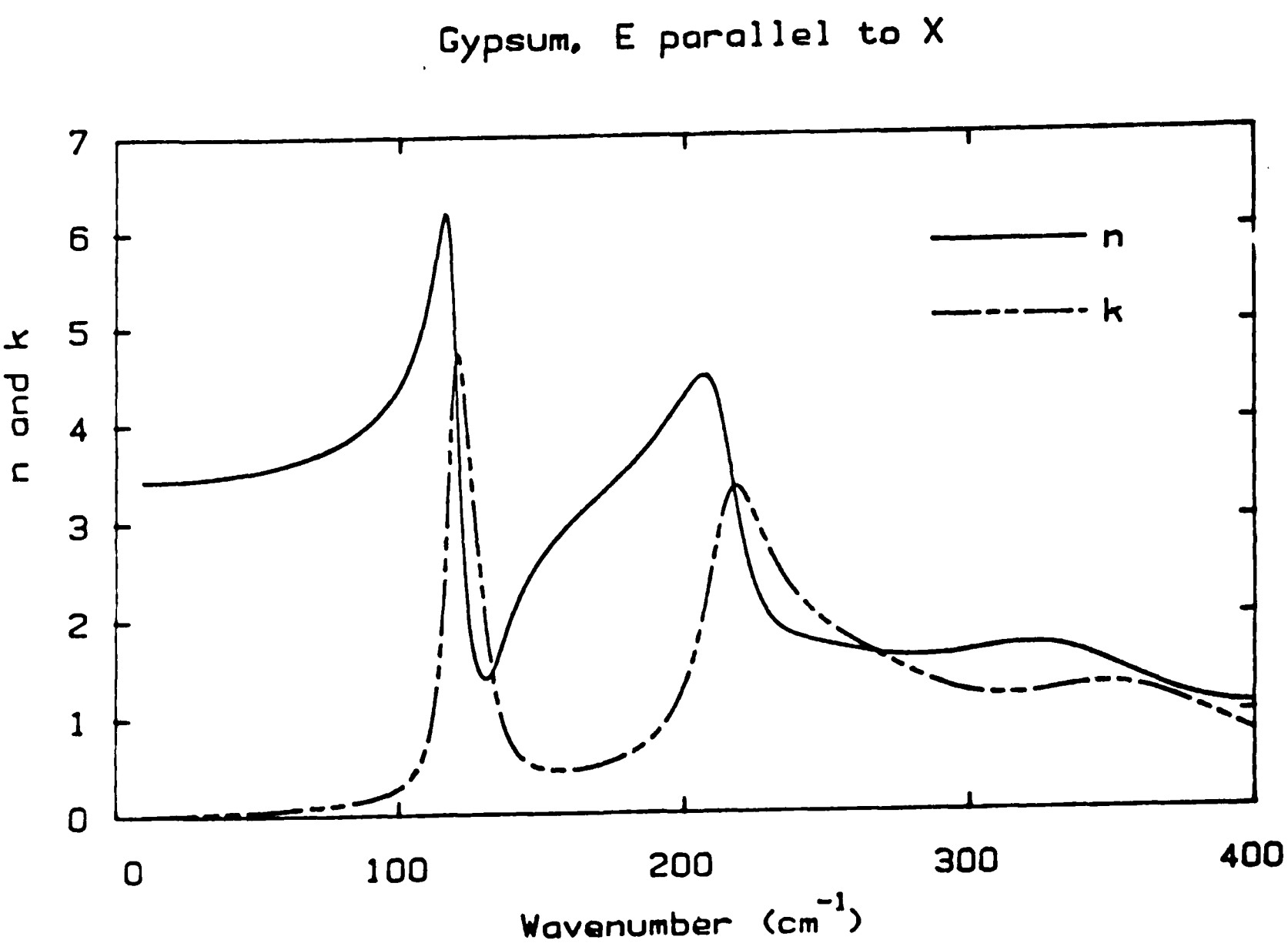

Fig. 2 Optical properties for the X optical axis of gypsum. The solid line is the real part of the index of refraction. The dashed line represents the imaginary part.

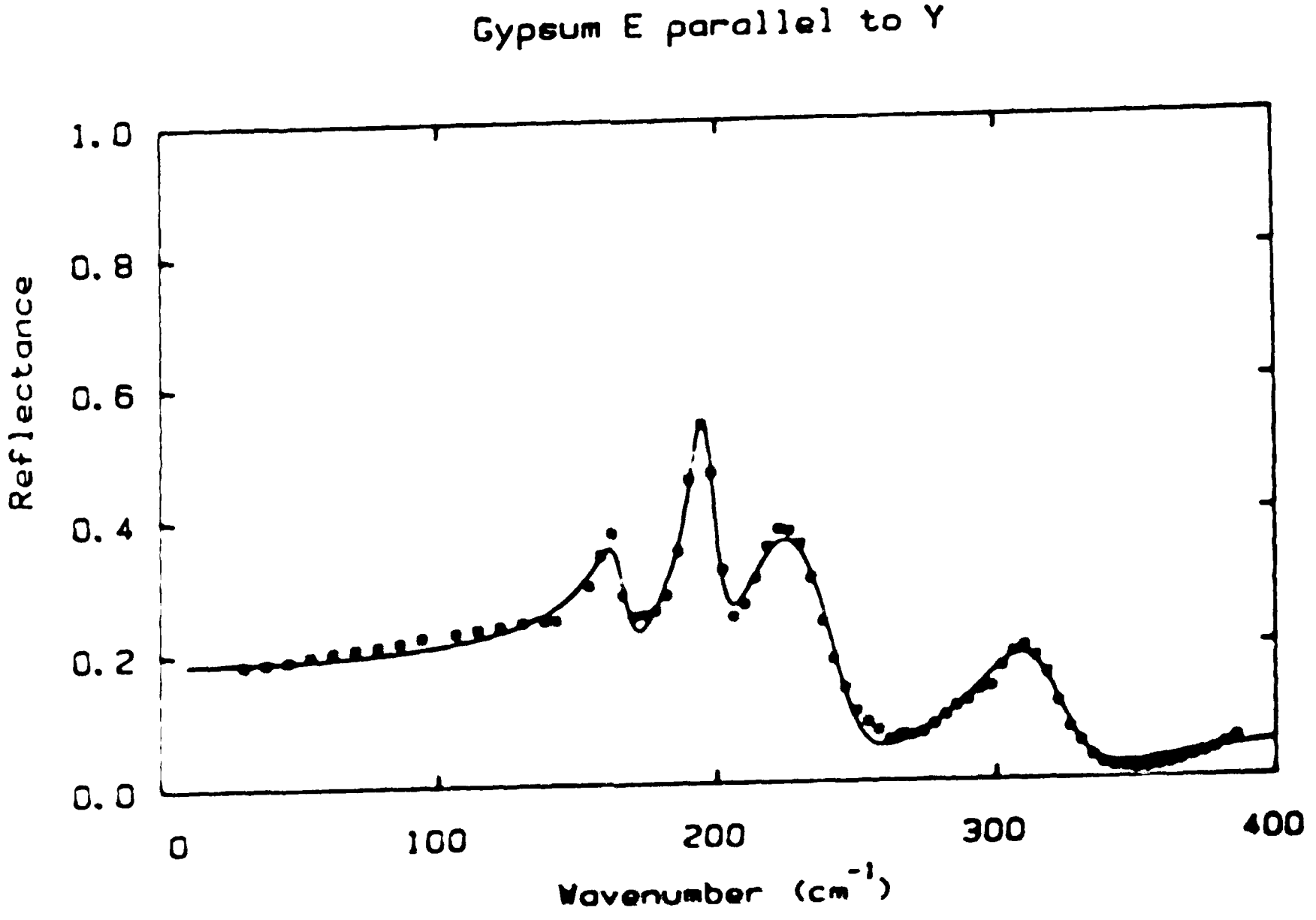

Fig. 1. Reflectance for the Y optical axis of gypsum. The solid line is the dispersive analysis fit. The squares represent the data.

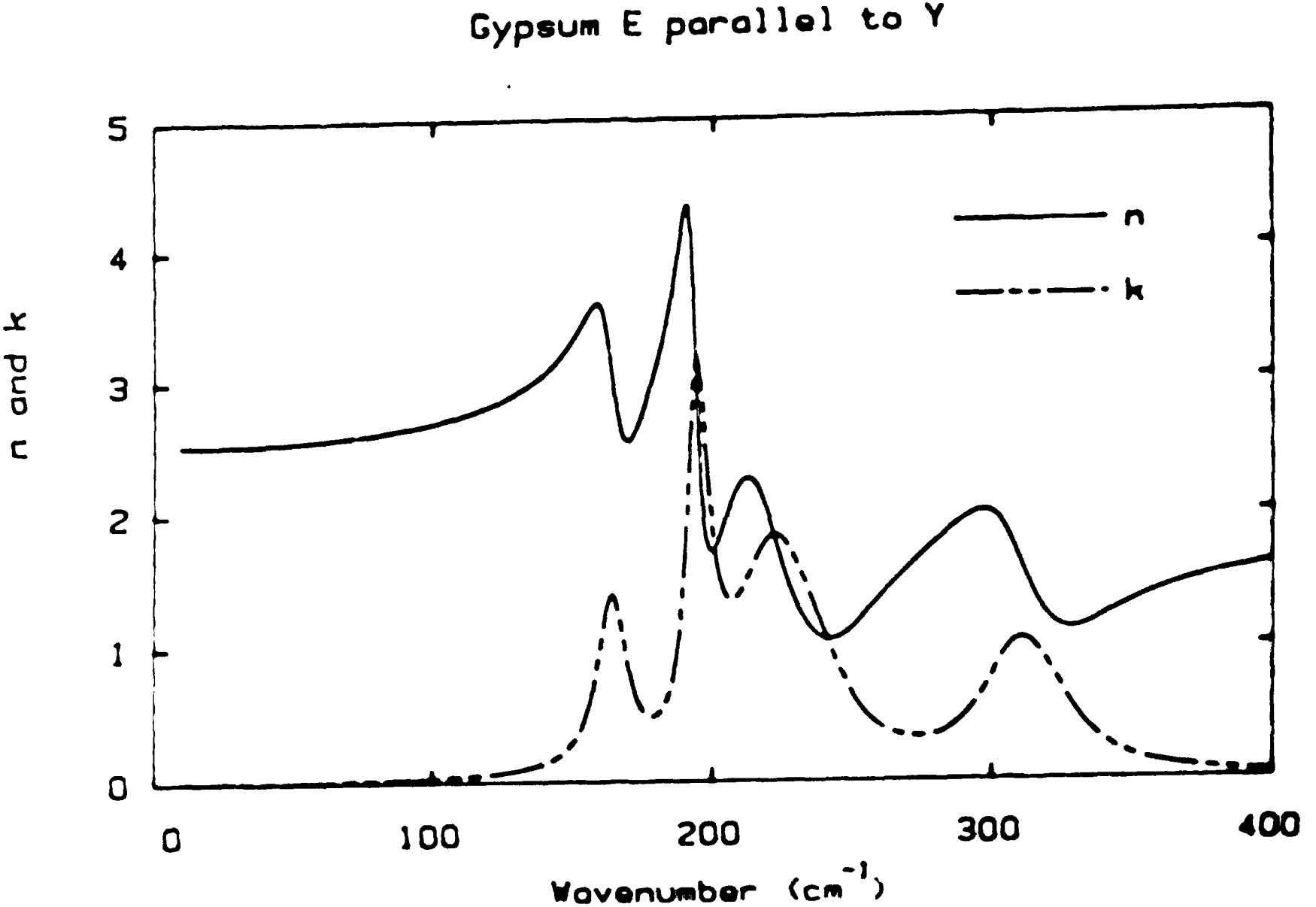

Fig. 4. Optical properties for the Y optical axis of gypsum. The solid line is the real part of the index of refraction. The dashed line represents the imaginary part.

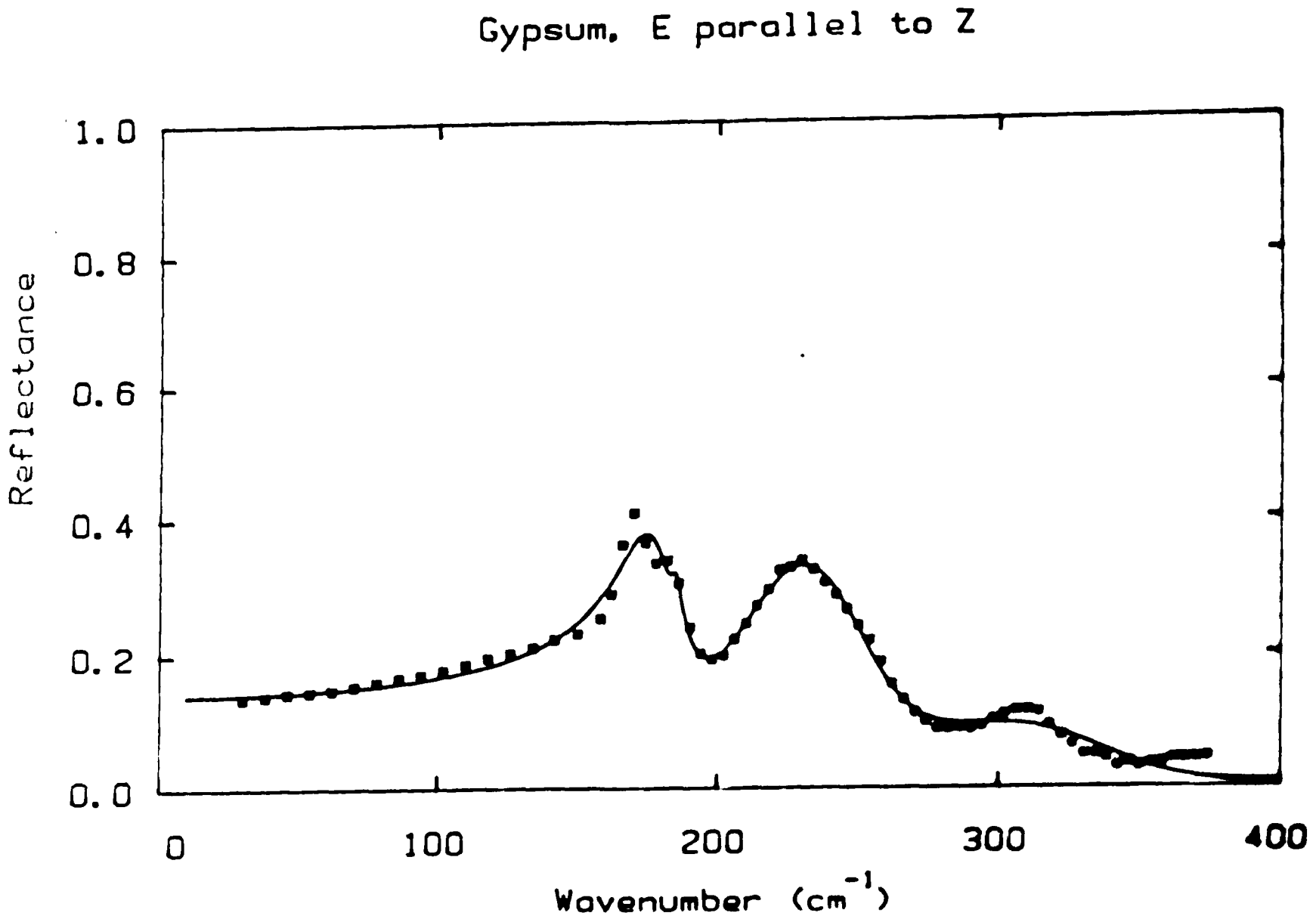

Fig. 5 Reflectance for the Z optical axis of gypsum. The solid line is the dispersive analysis fit. The squares represent the data.

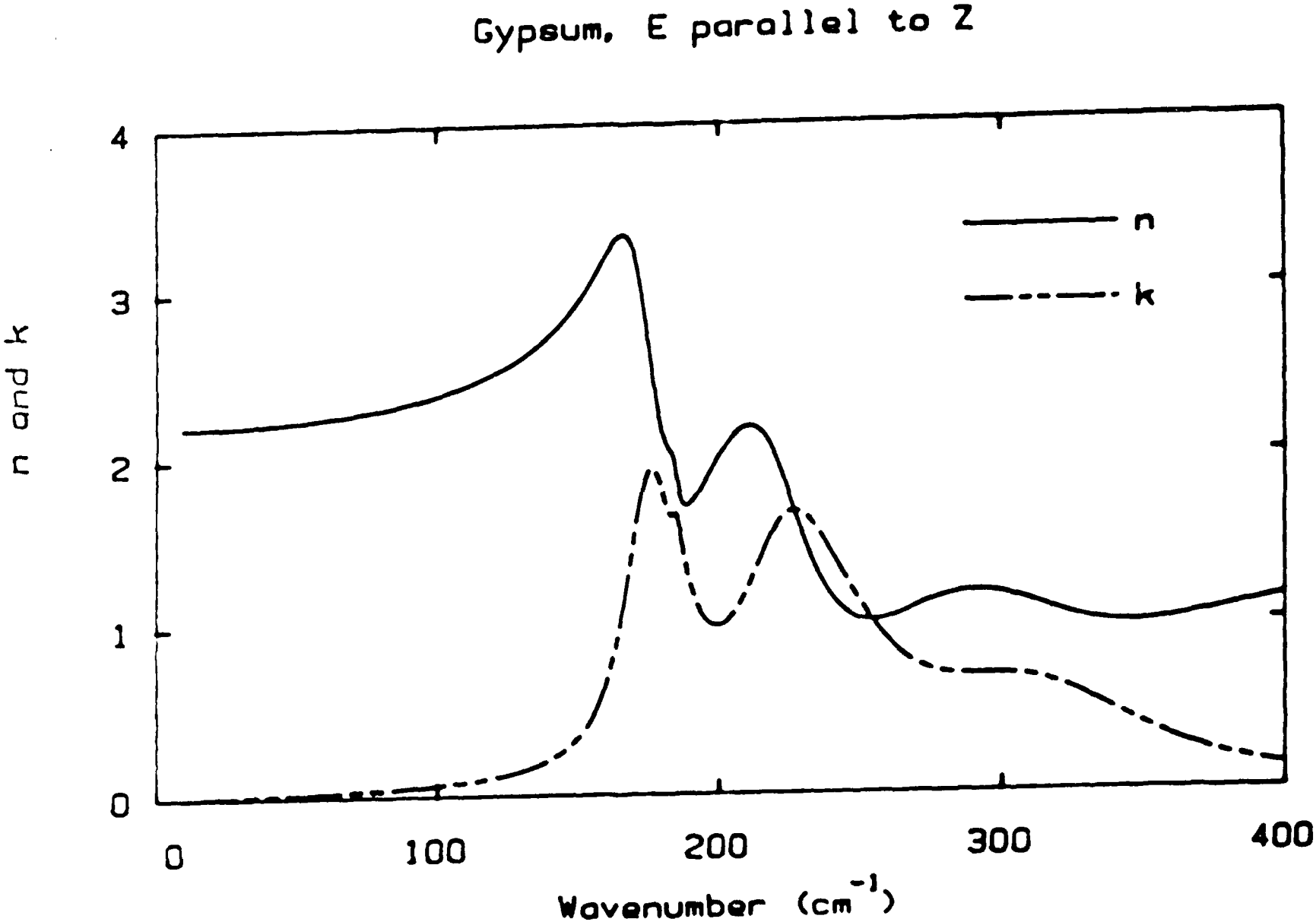

Fig. 6 Optical properties for the Z optical axis of gypsum. The solid line is the real part of the index of refraction. The dashed line represents the imaginary part.

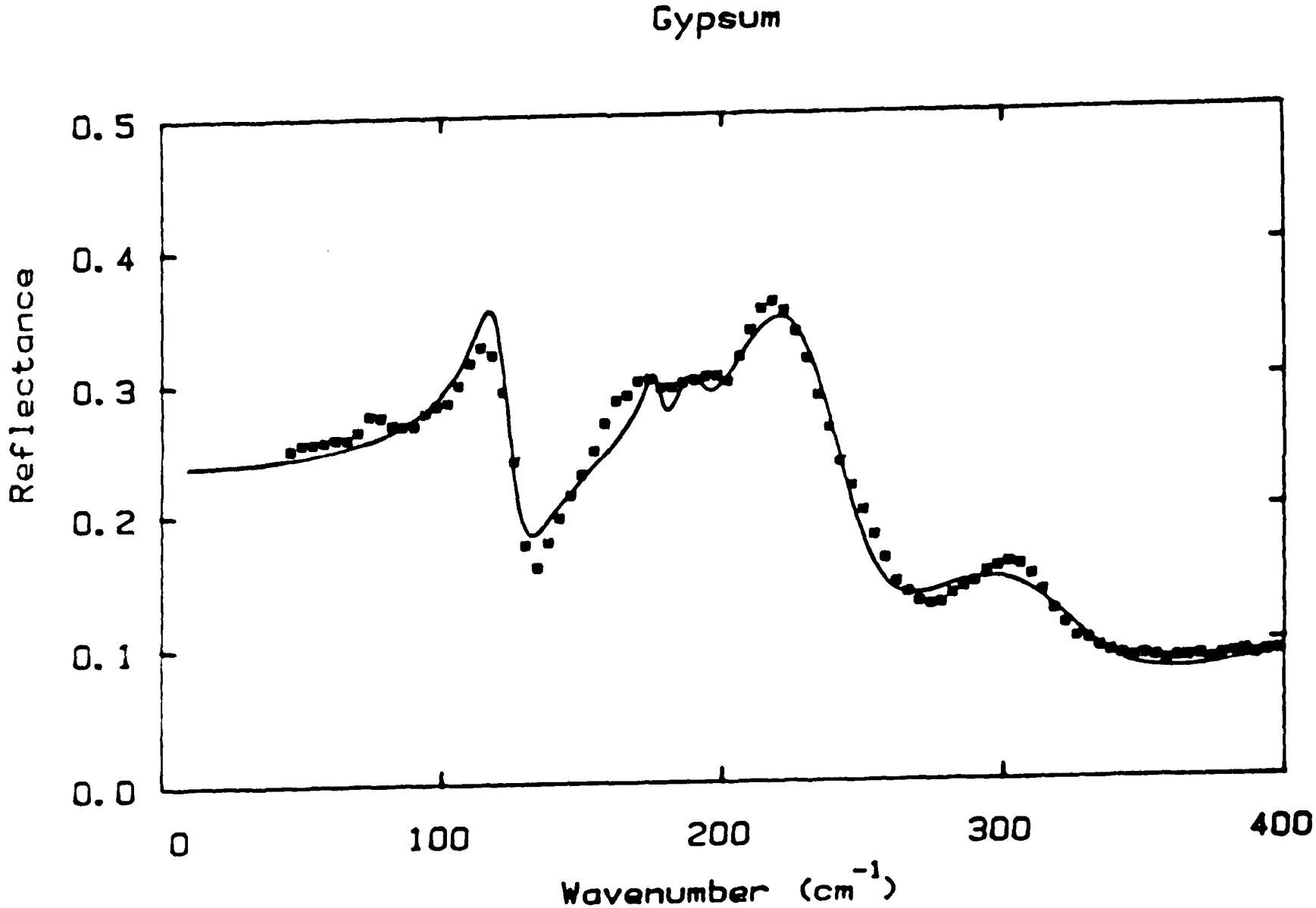

Fig. 7 The solid line represents the powdered gypsum data and the dashed line is the simulated powdered data.

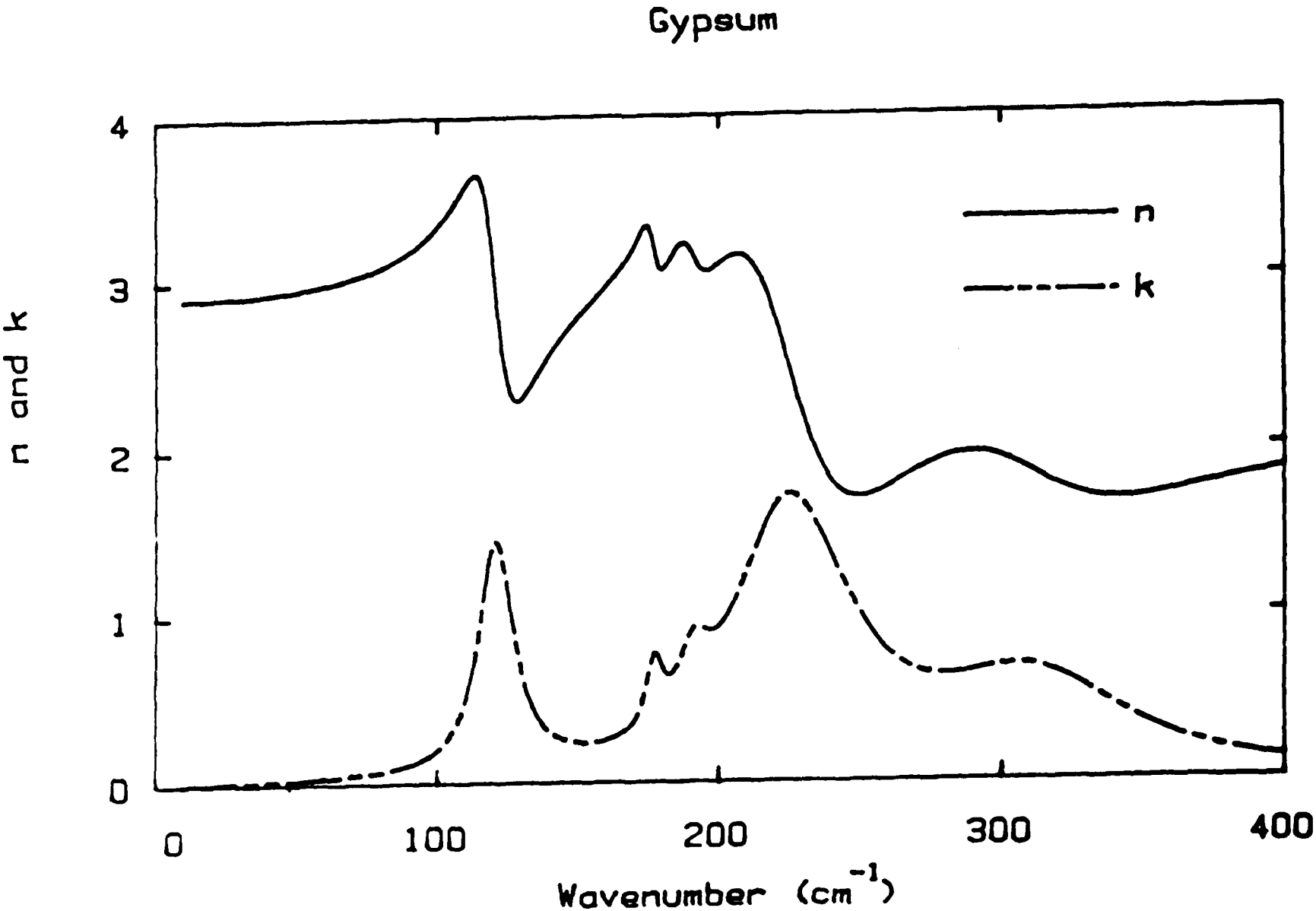

Fig. 8 Refractive index of gypsum from a pressed pellet.

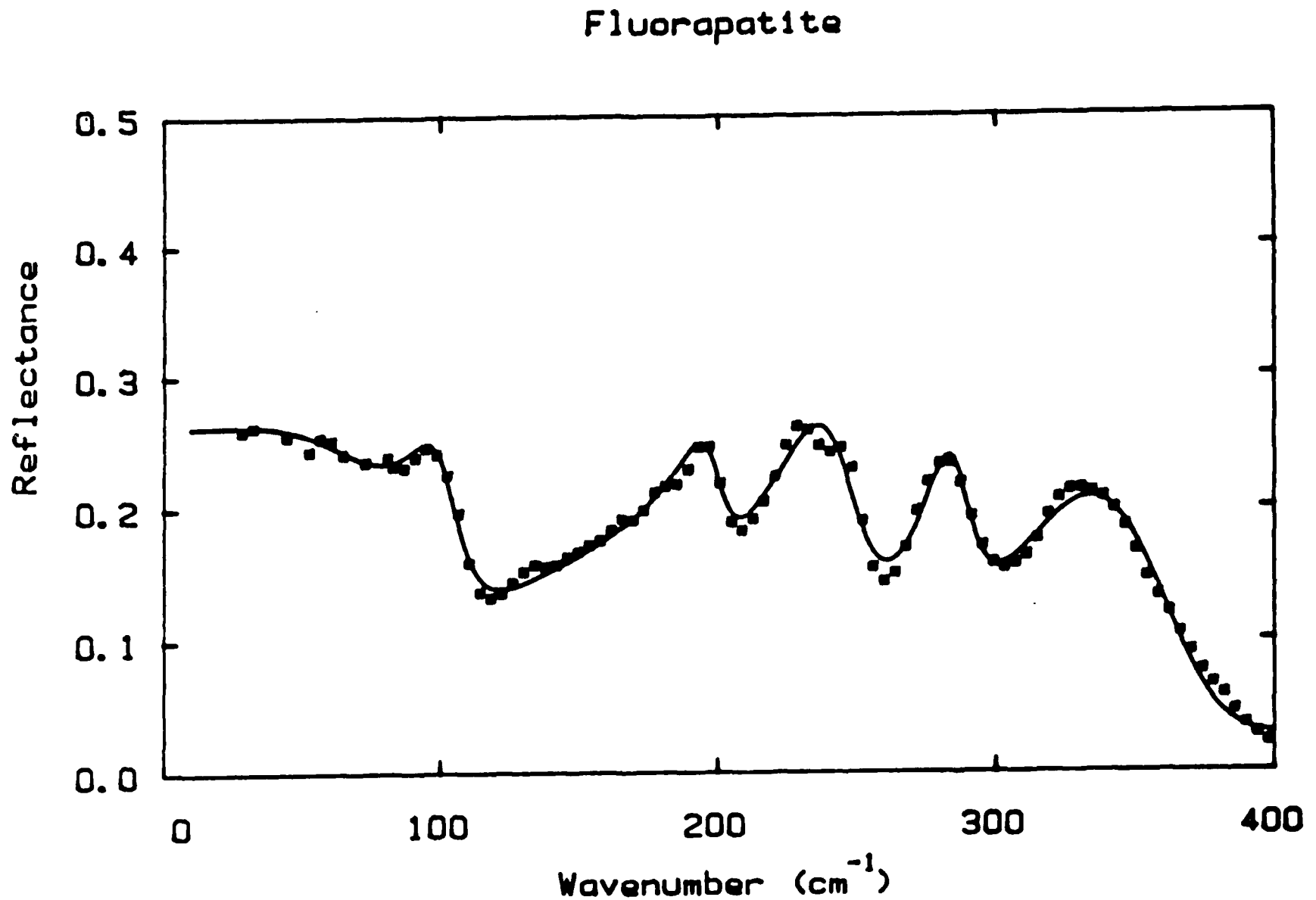

Fig. 9 Reflectance of a Pressed Pellet of Fluorapatite. The squares are the measured values and the straight line is the dispersive analysis fit.

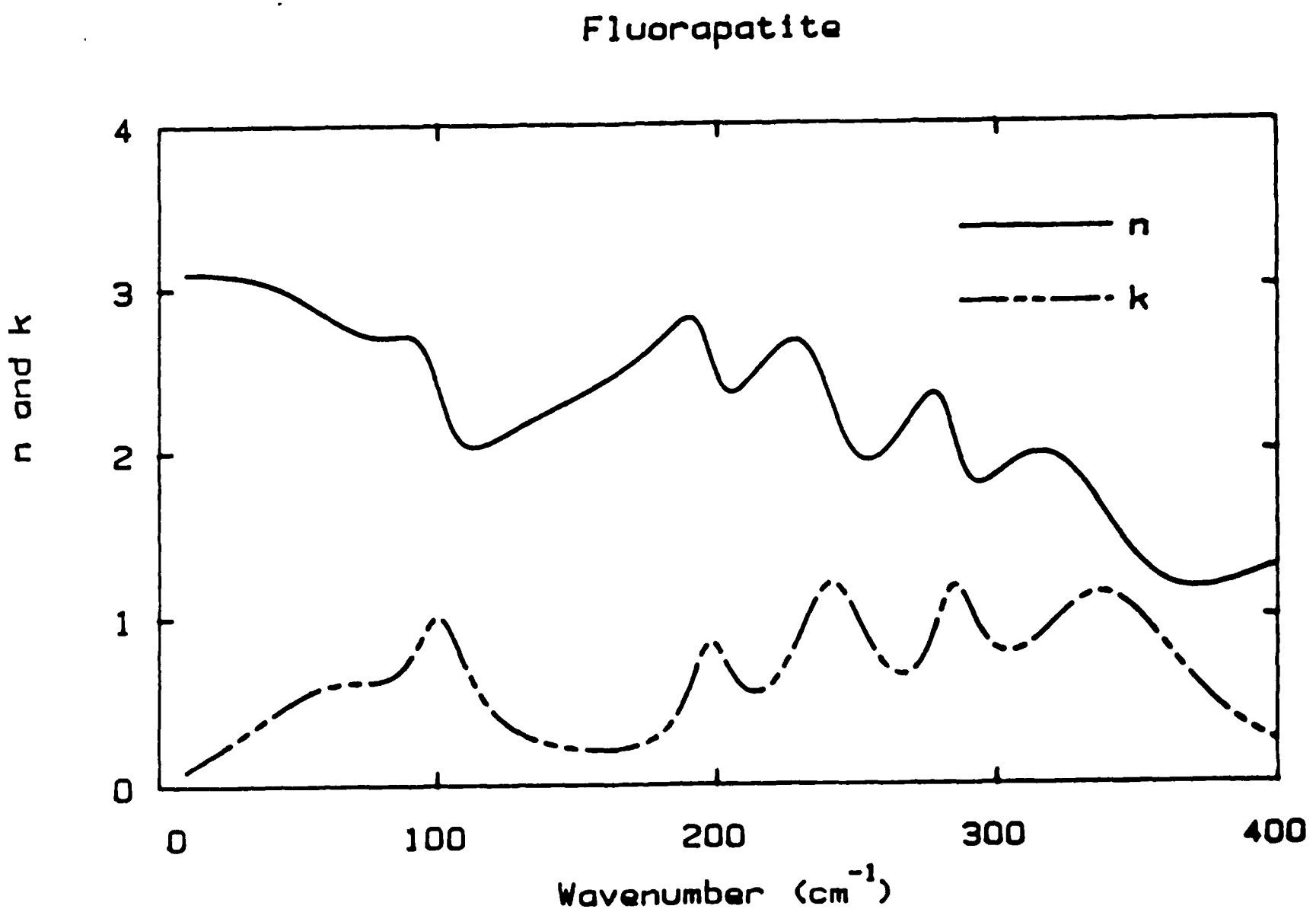

Fig. 10 Optical Constants for a Pressed Pellet of Fluorapatite. The solid line is n and the dashed k.

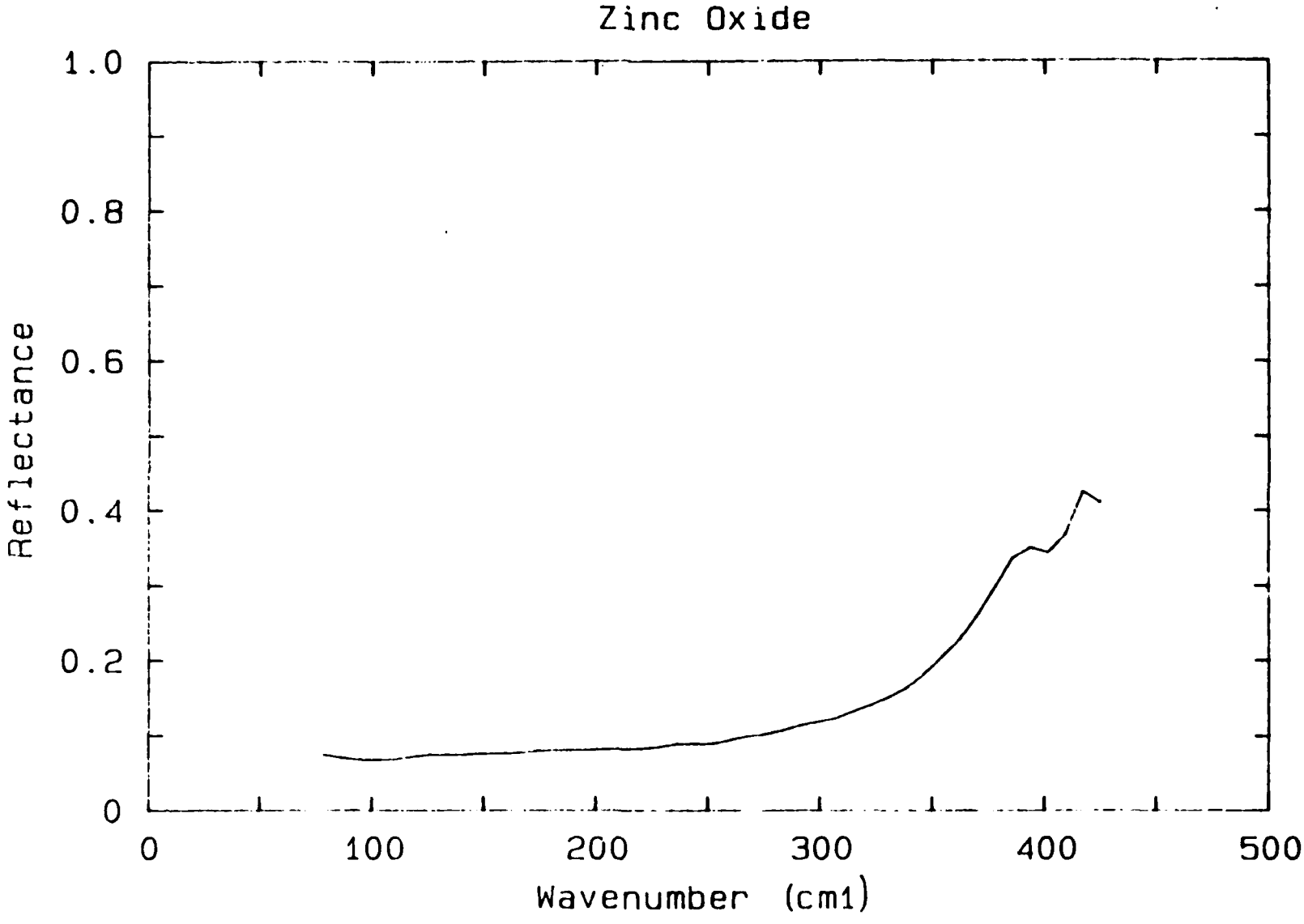

Fig. 11 Reflectance of a Pressed Pellet of Zinc Oxide.

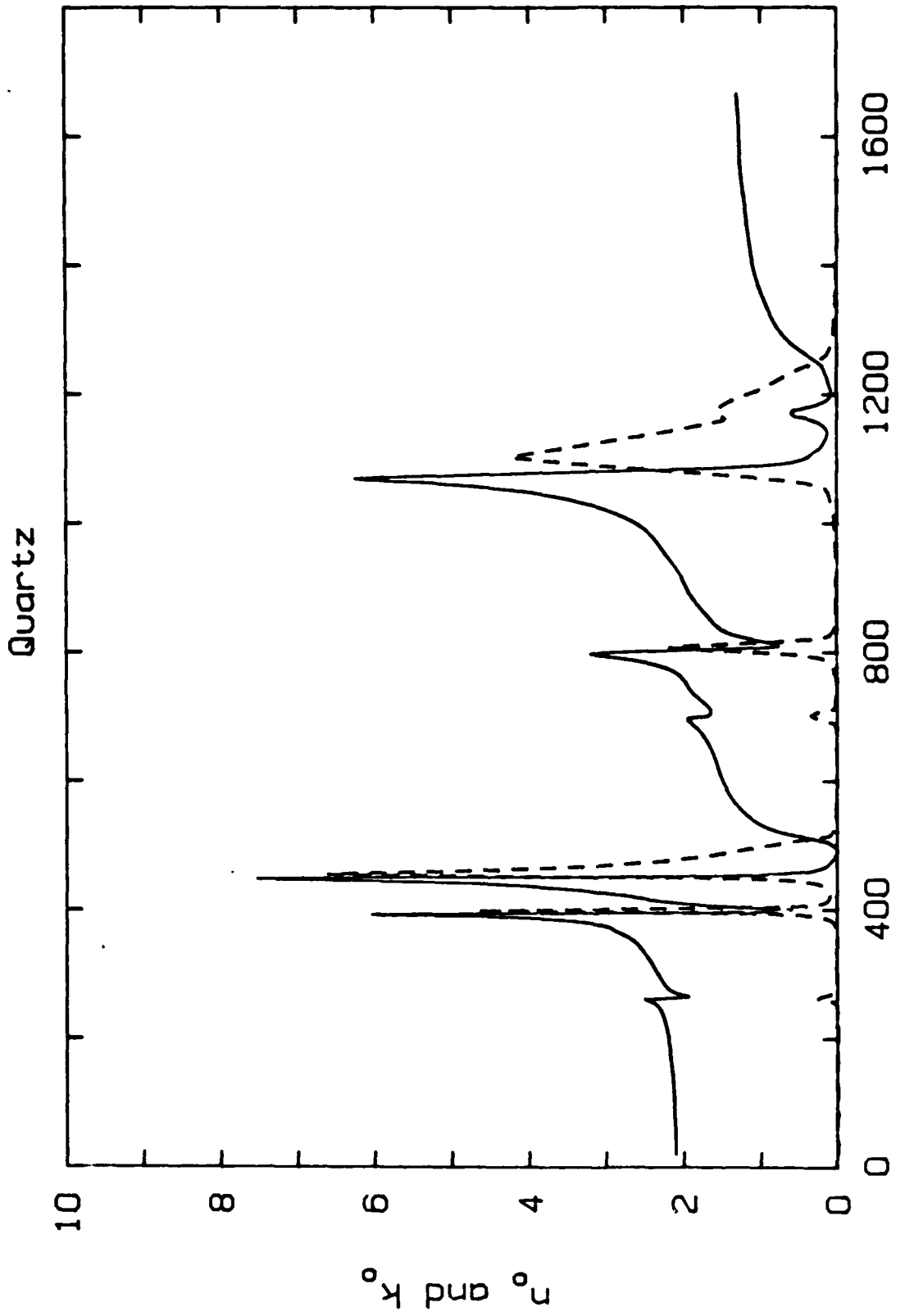

Fig. 12 Optical Constants for the Ordinary Ray of Quartz. The solid line is n and the dashed line is k.

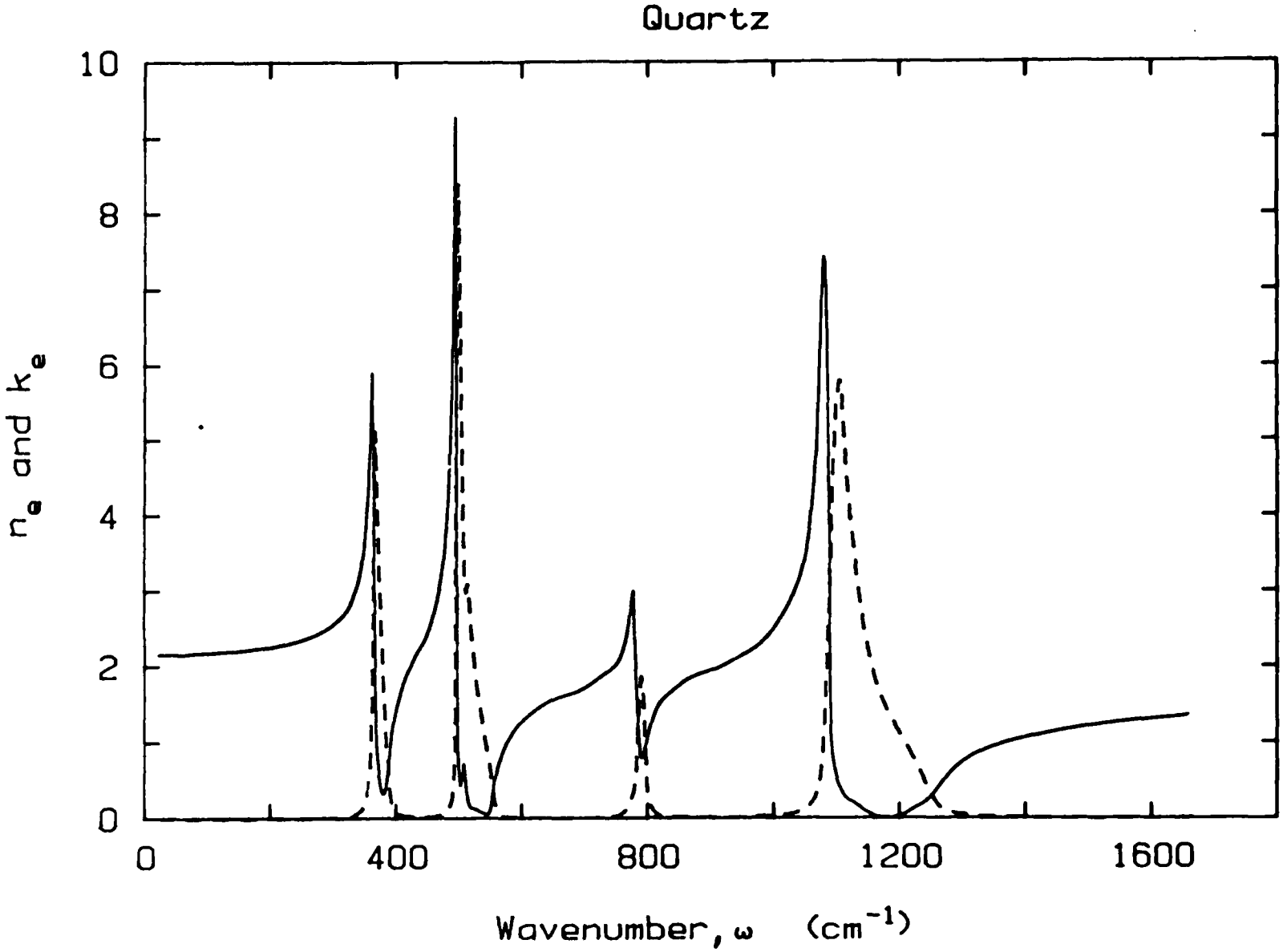

Fig. 13 Optical Constants for the Extraordinary ray of Quartz. The solid line is n and the dashed line is k.

HOMODYNING GIVES R = 0.939 AND J(0) = 0.216° AT ω = 1.10 cm^{-1}

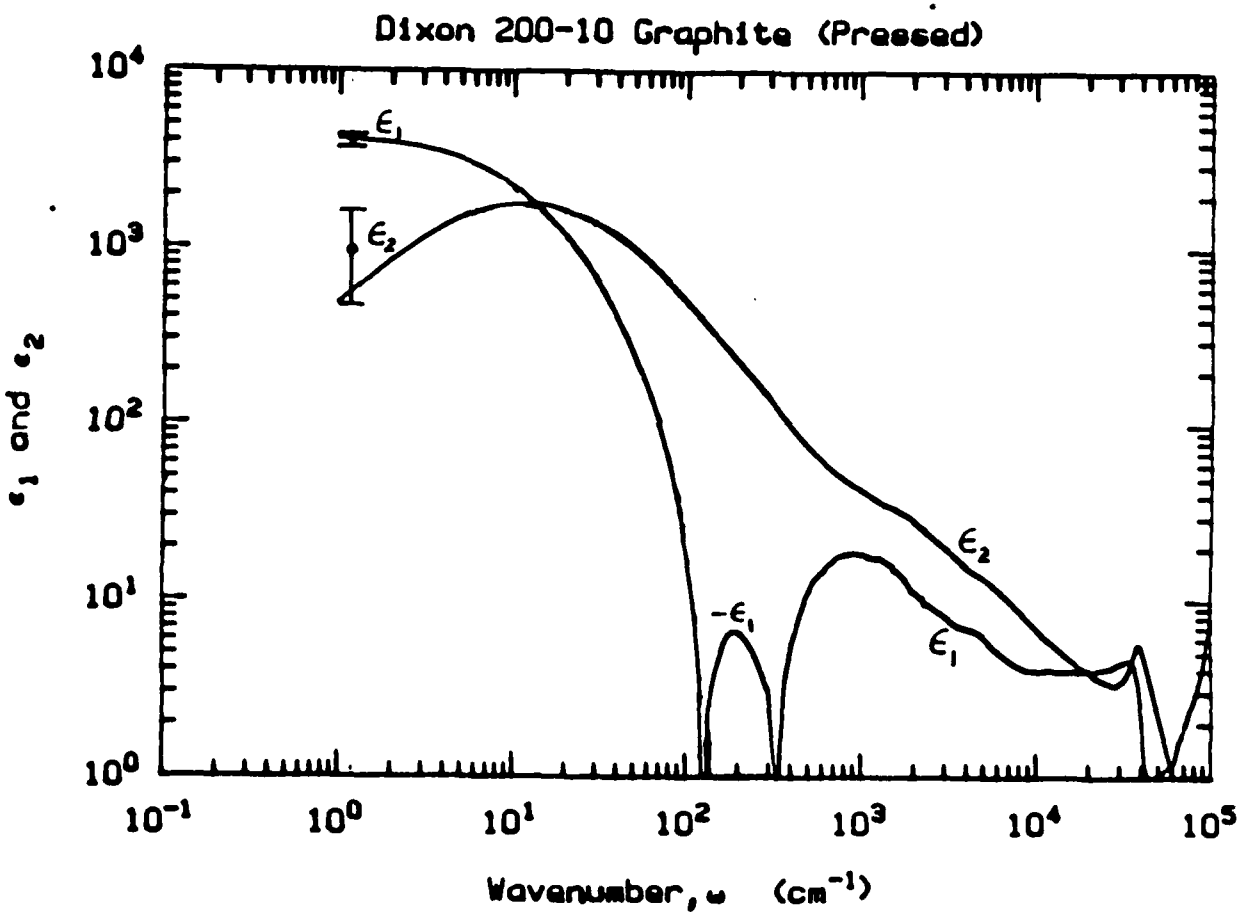

Fig. 14 ϵ_1 and ϵ_2 for Dixon 200-10 graphite pressed pellet from KK analysis. Data points from Homodyning Interferometer.

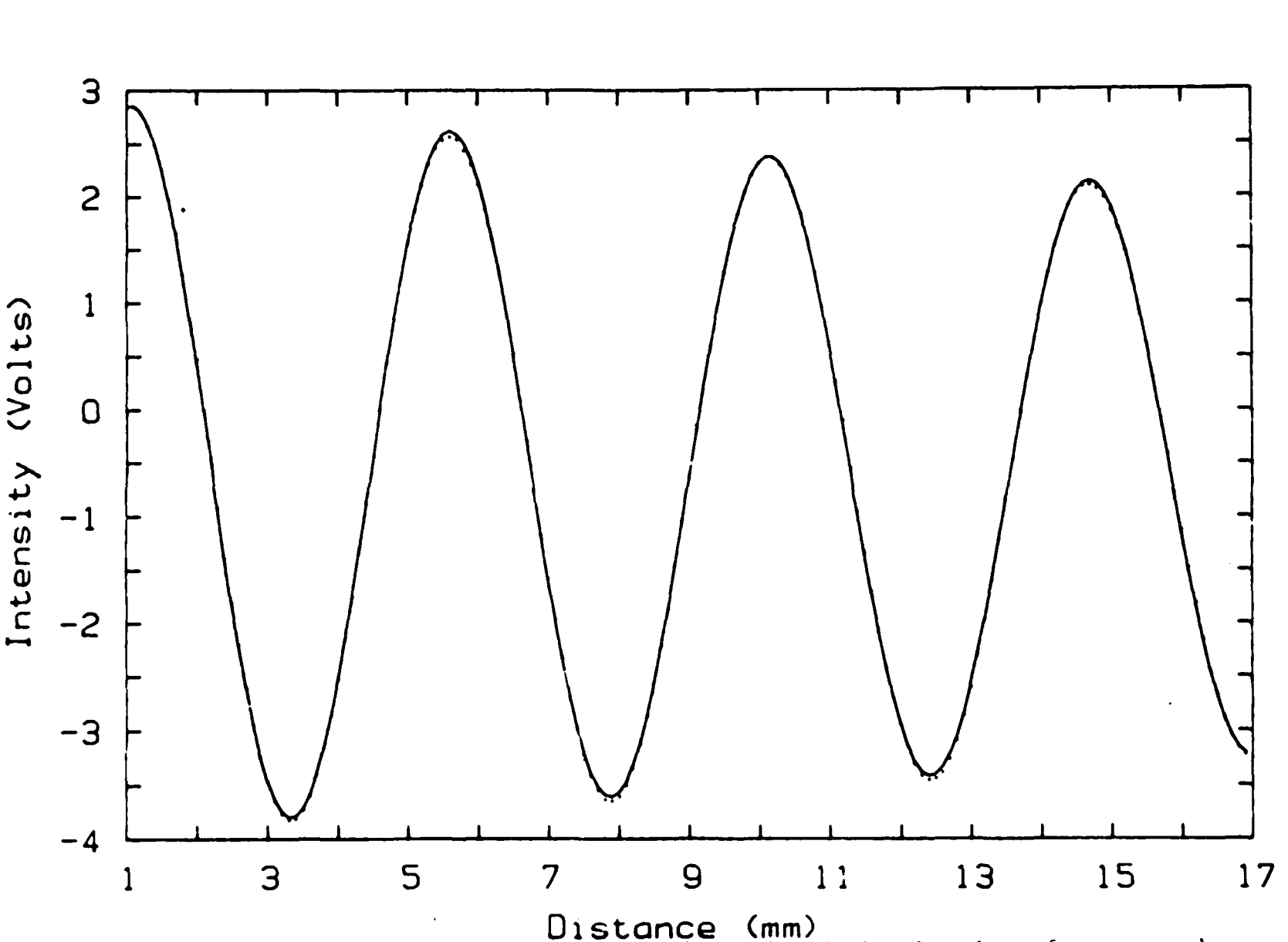

Fig. 15 Measured signal versus displacement (dots) for the homodyne intereferometer and fit (solid line).

HOMODYNEING SPECTROMETER

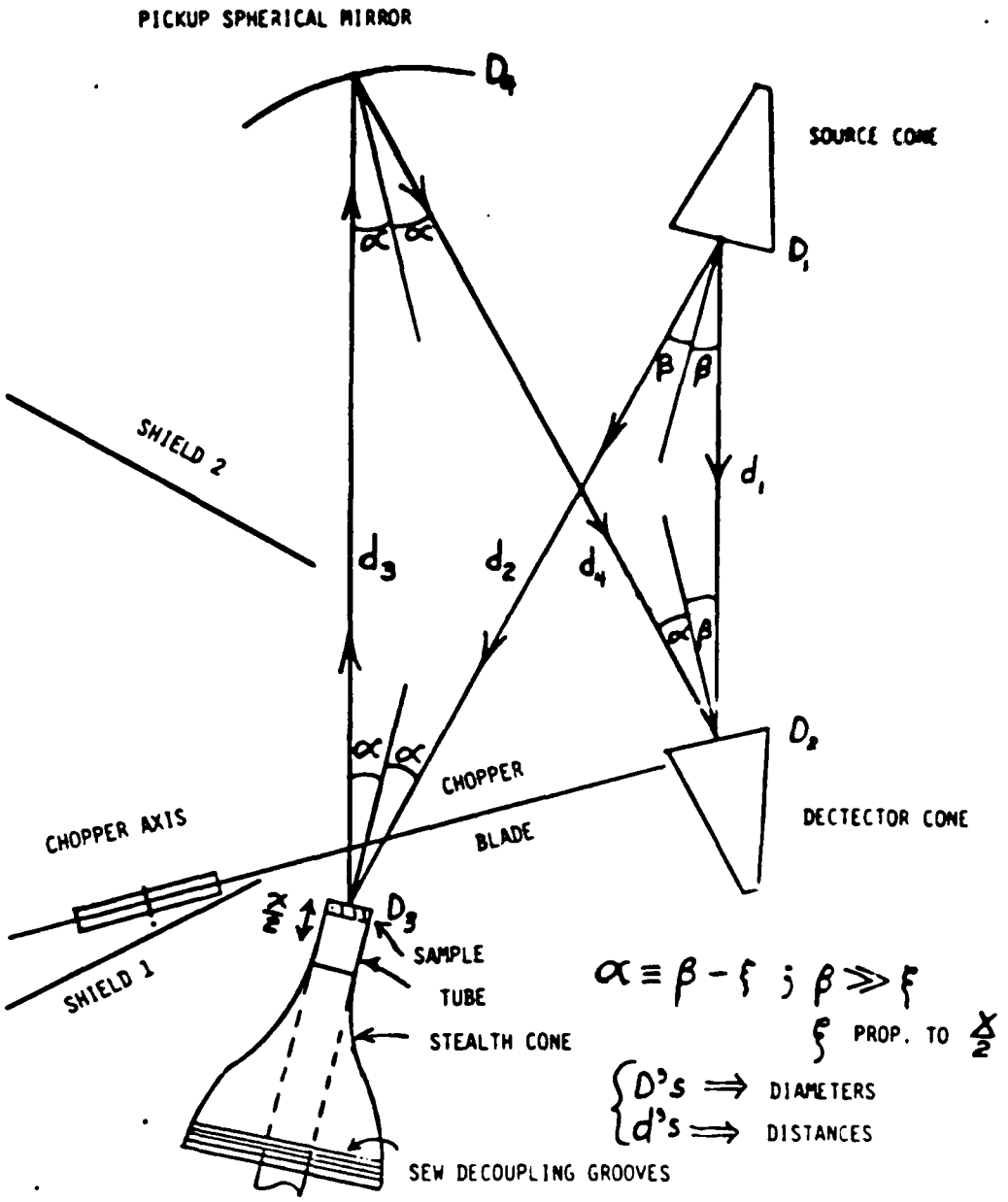

Fig. 16 Schematic Diagram of Homodyne Interferometer.

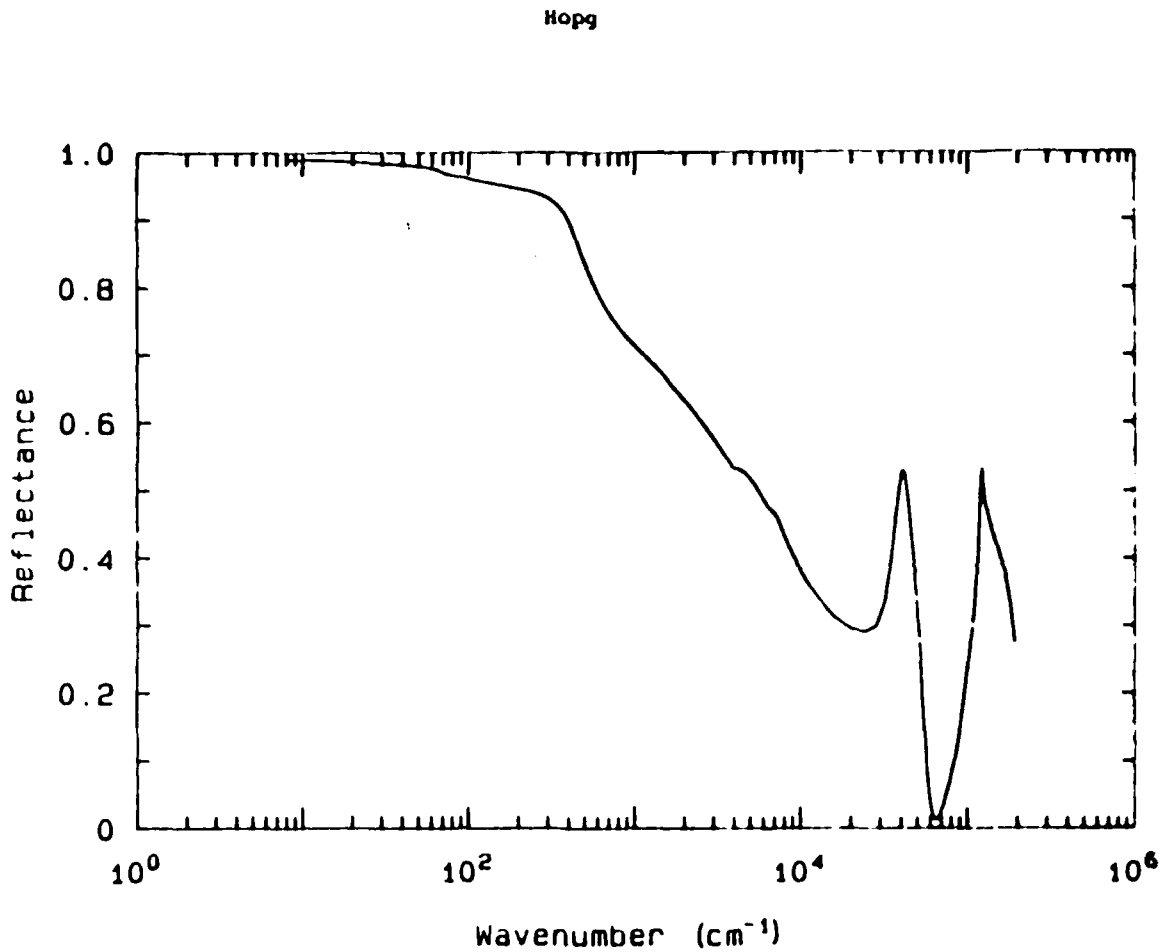

Fig. 17 Reflectance of HOPG Graphite. This data from our data and that of Phillips.

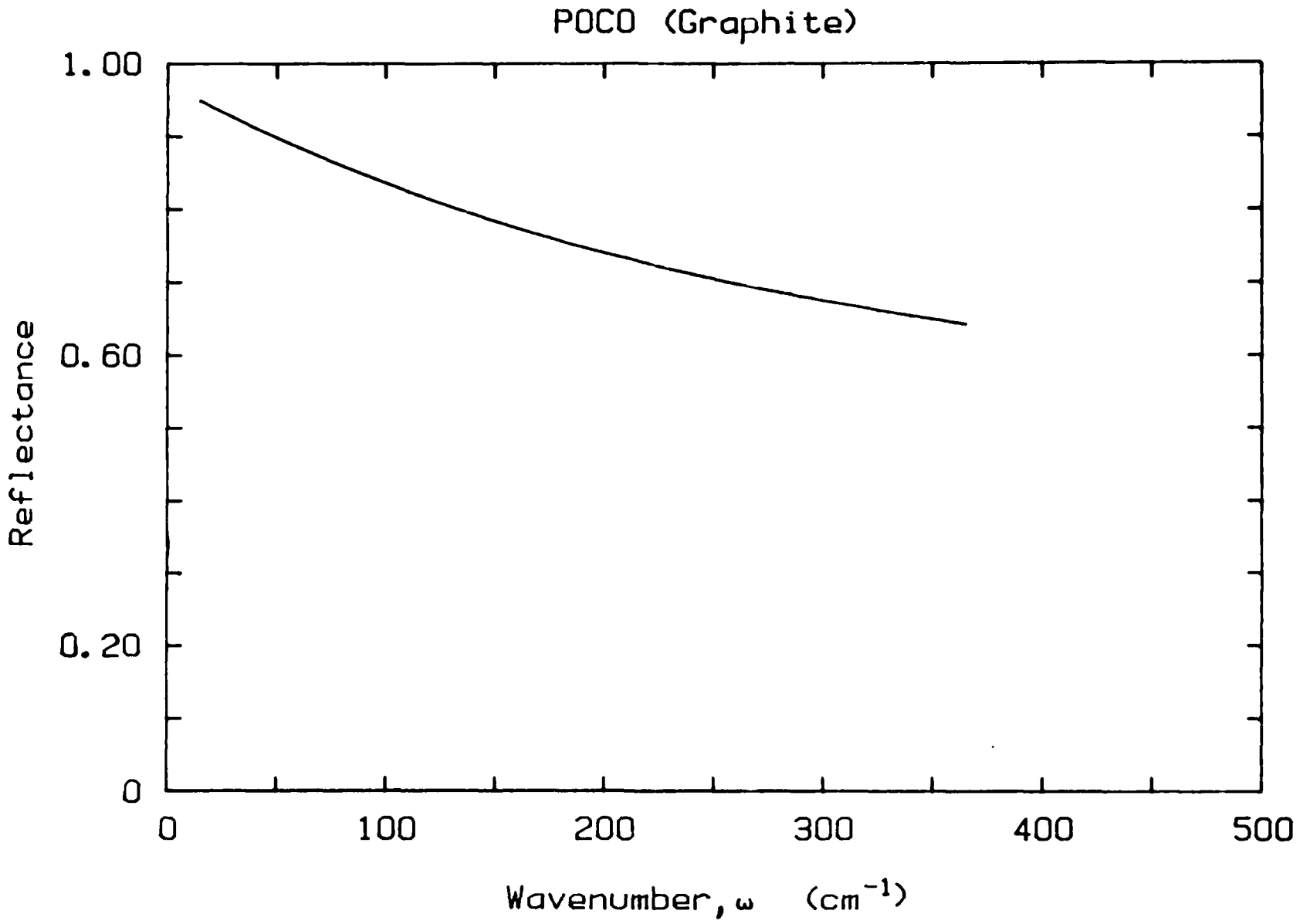

Fig. 18 Reflectance of POCO Graphite versus Wavenumber.

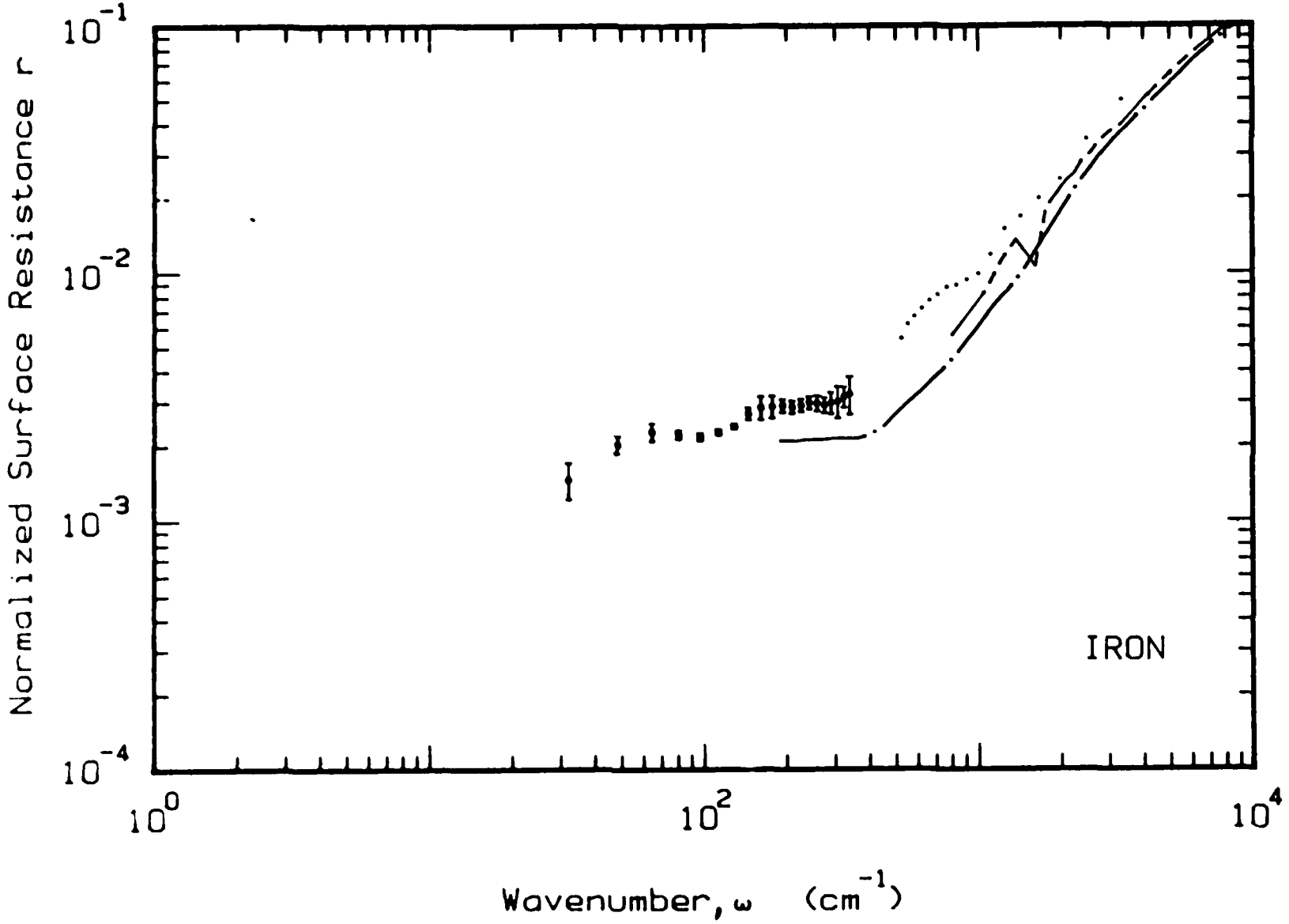

Fig. 19 Real Part of the Normalized Surface Impedance for Iron. Points with error bars are from our nonresonant cavity measurements. Dashed dot line is from data of ref. 10.

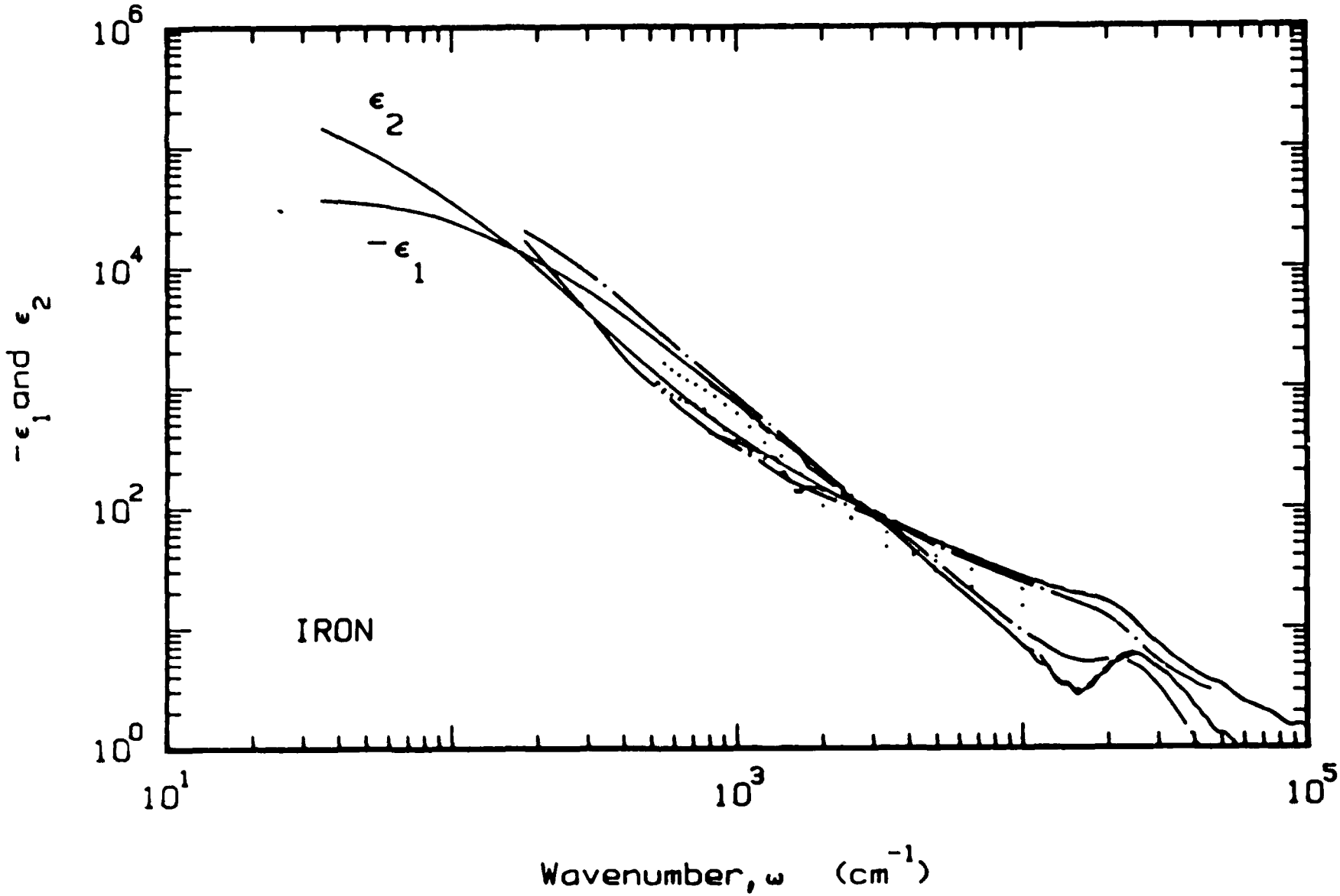

Fig. 20 ϵ_1 and ϵ_2 for iron. Solid lines are the Kramers-Kronig results from combining our long wavelength measurements with literature values of Weaver, et al. (tabulated in ref. 10). The dashed dot curve are the measurements of Bolotin, et al. (also tabulated in ref. 10).

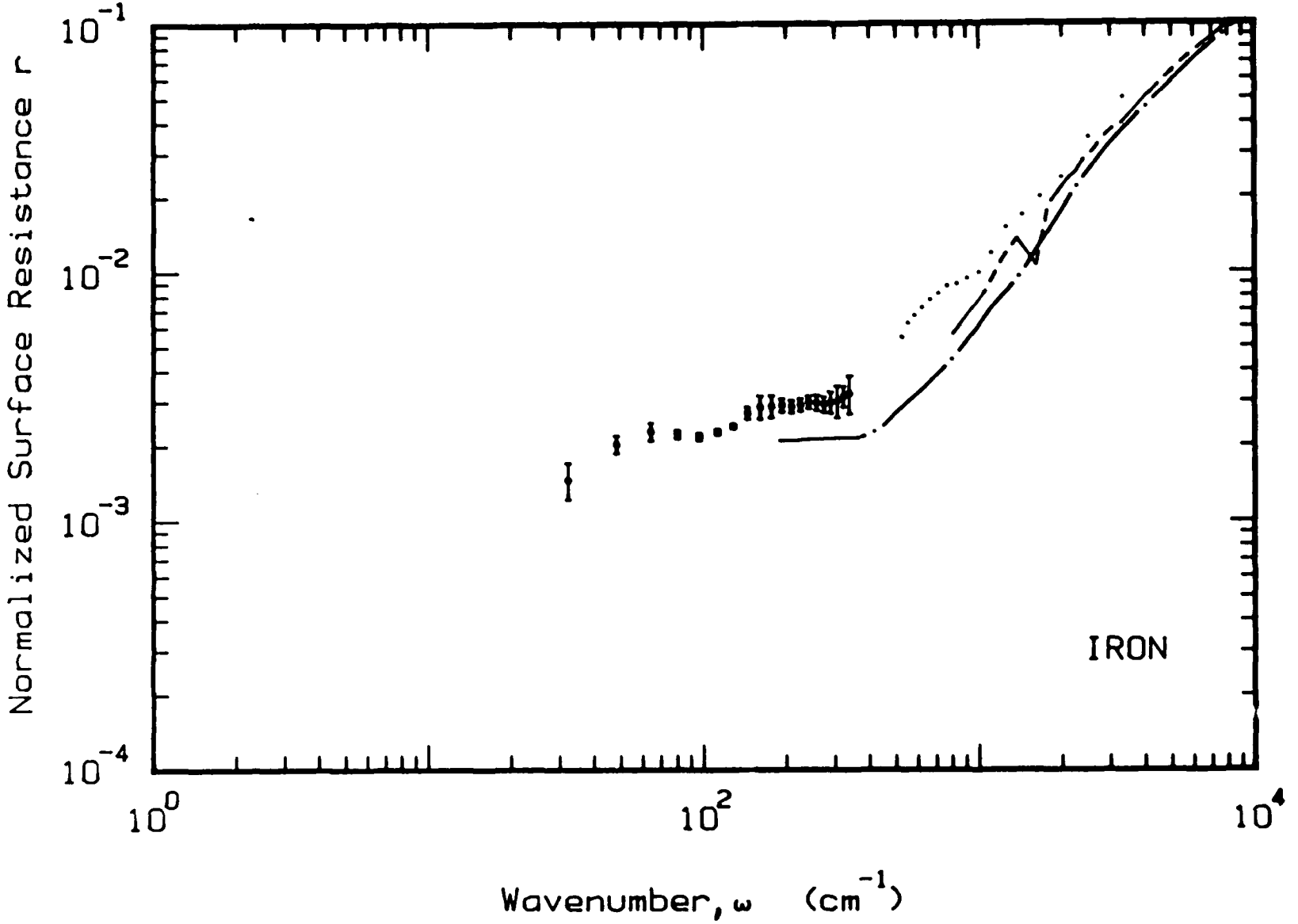

Fig. 19 Real Part of the Normalized Surface Impedance for Iron. Points with error bars are from our nonresonant cavity measurements. Dashed dot line is from data of ref. 10.

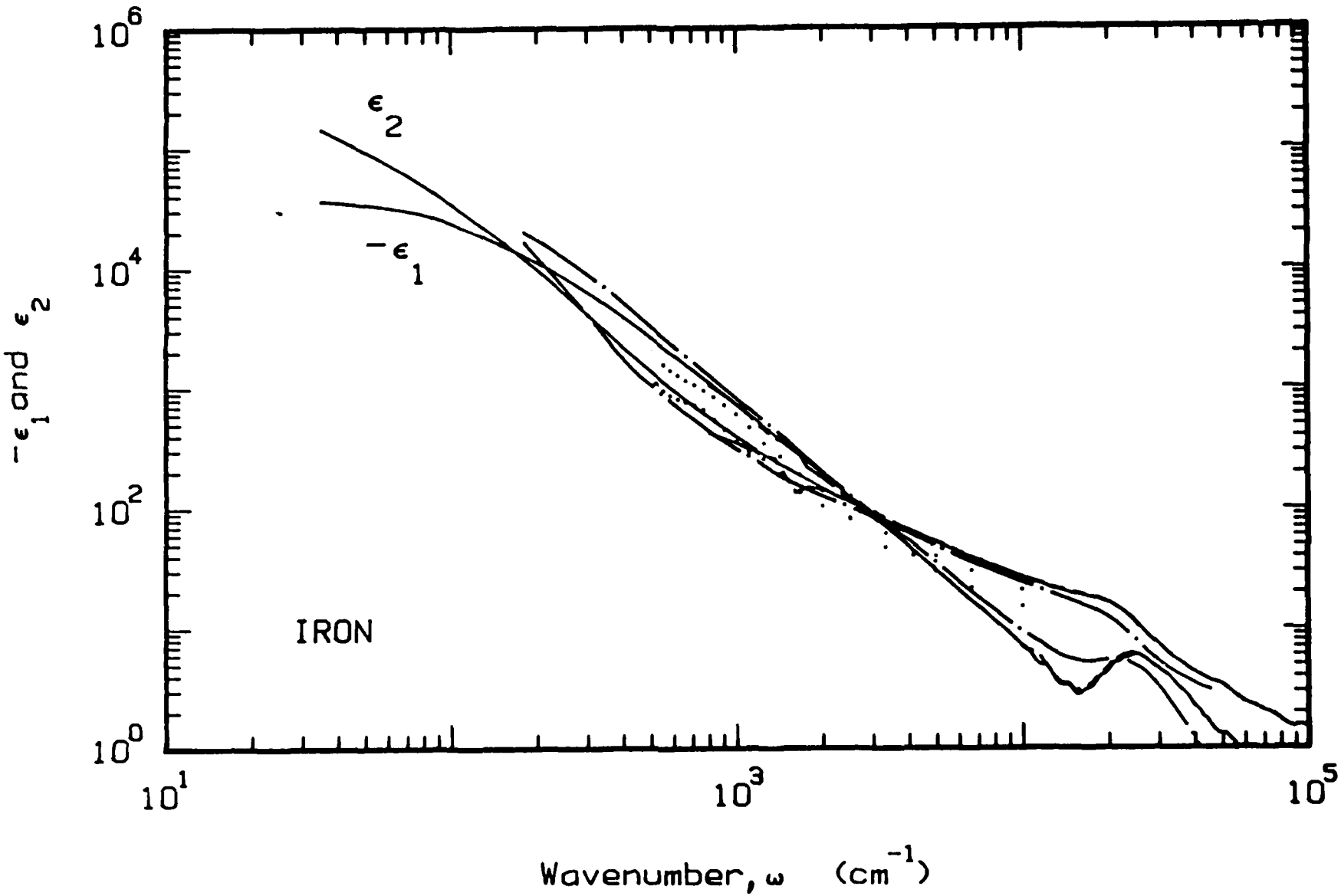

Fig. 20 ϵ_1 and ϵ_2 for iron. Solid lines are the Kramers-Kronig results from combining our long wavelength measurements with literature values of Weaver, et al. (tabulated in ref. 10). The dashed dot curve are the measurements of Bolotin, et al. (also tabulated in ref. 10).

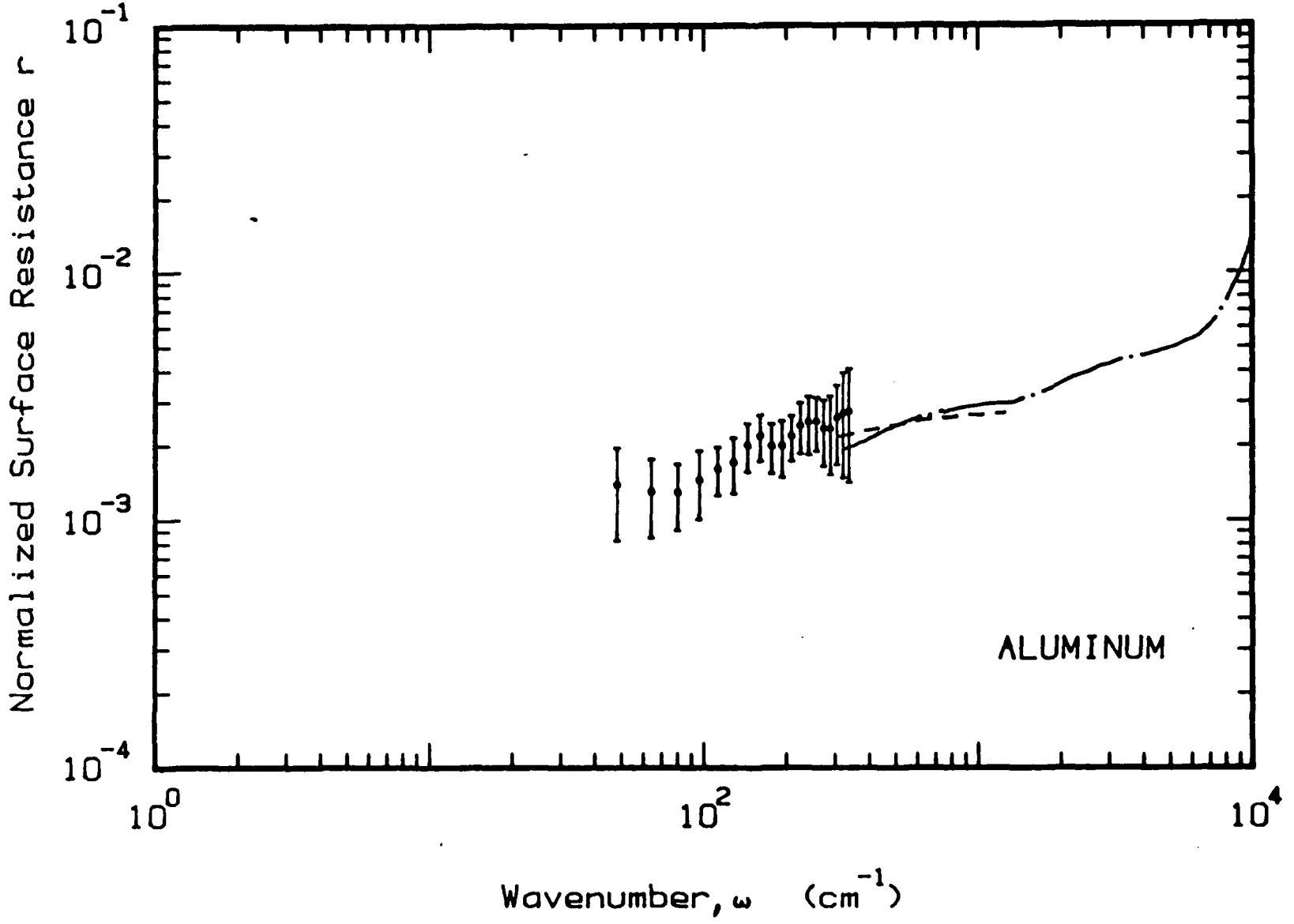

Fig. 21 Real part of the Normalized Surface Resistance for Aluminum. Points with error bars are our nonresonant cavity measurements, while the dashed and dash dot curves for shorter wavelengths are from ref. 10.

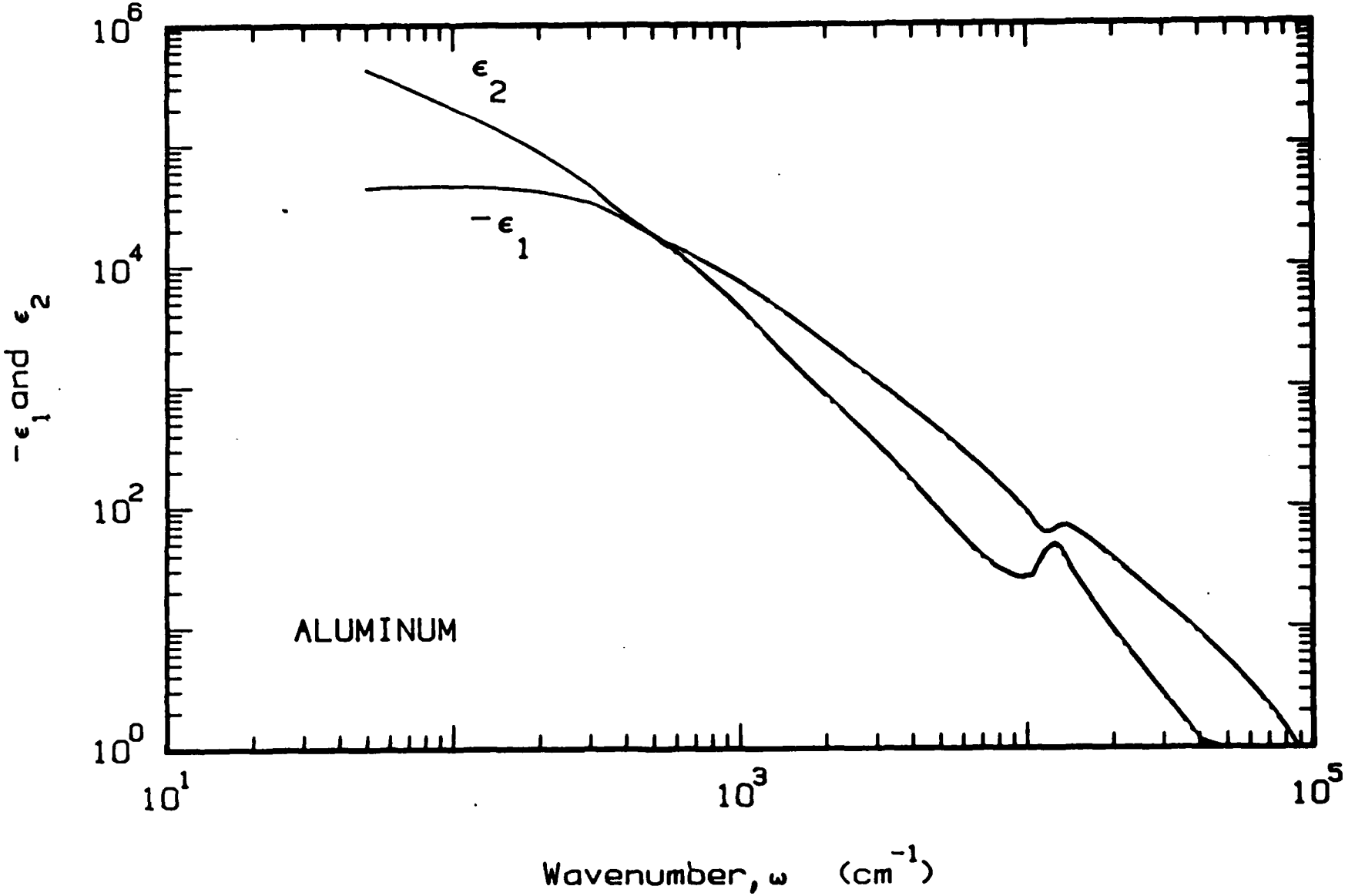

Fig. 22 ϵ_1 and ϵ_2 for Aluminum.

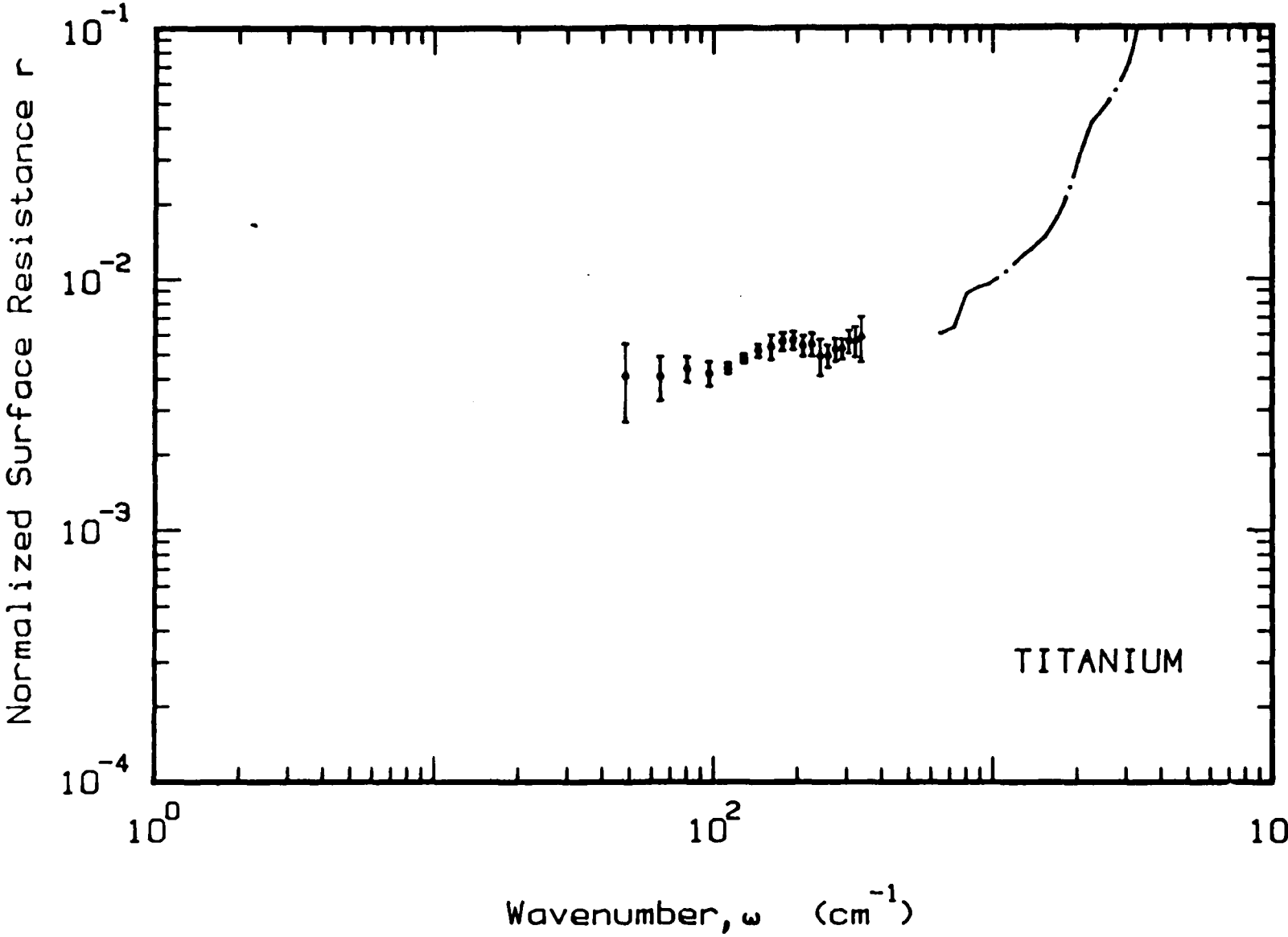

Fig. 23 Real Part of the Normalized Surface Resistance of Titanium. Our nonresonant cavity measurements are shown as data points with error bars. Data from ref. 10 are shown as the dash dot line.

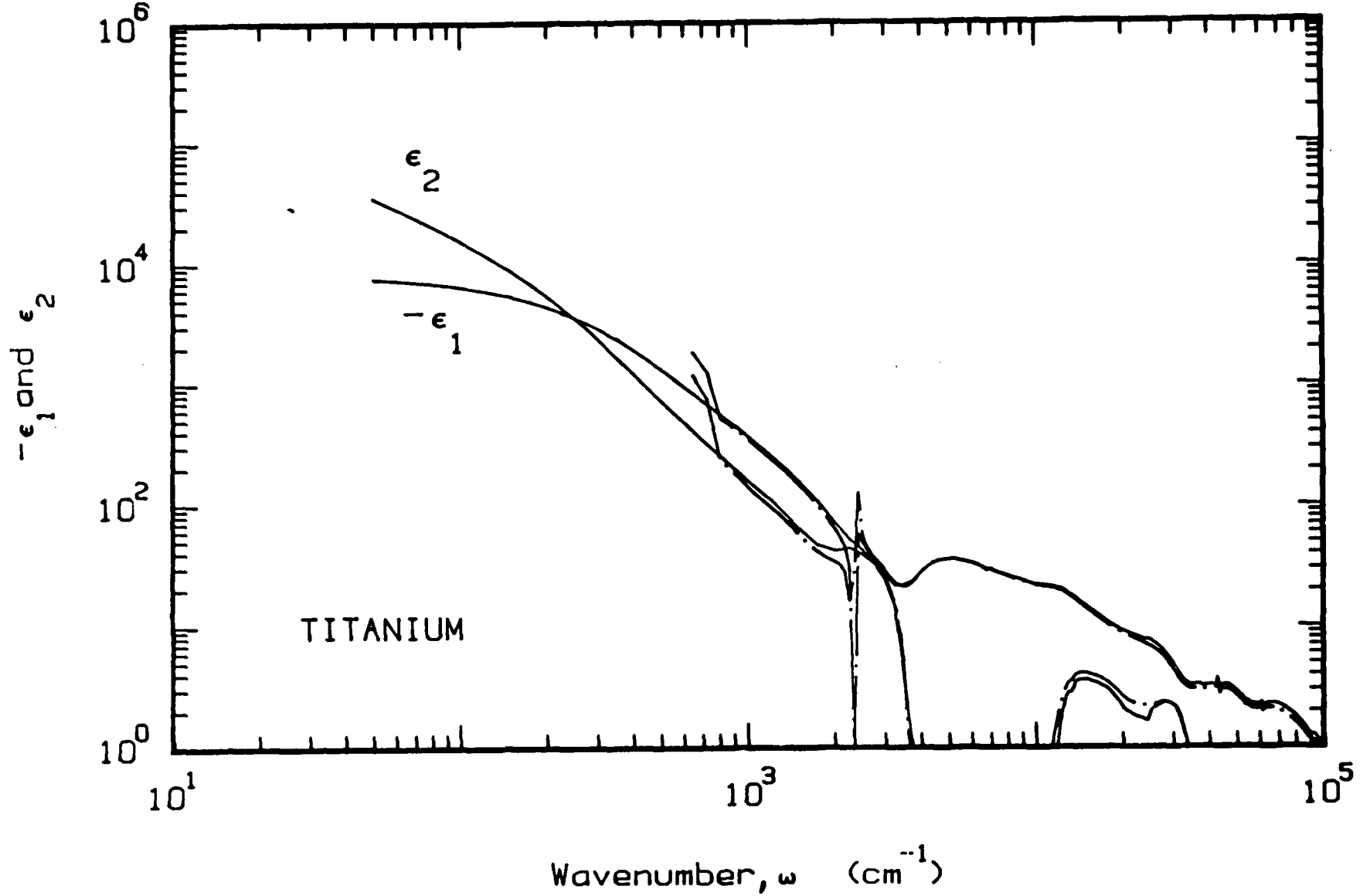

Fig. 24 ϵ_1 and ϵ_2 for Titanium. The solid curves show the Kramers-Kronig results for a data set consisting of our long wavelength nonresonant cavity data and literature data (ref. 10). The dash dot curve is the ref. 10 data alone.

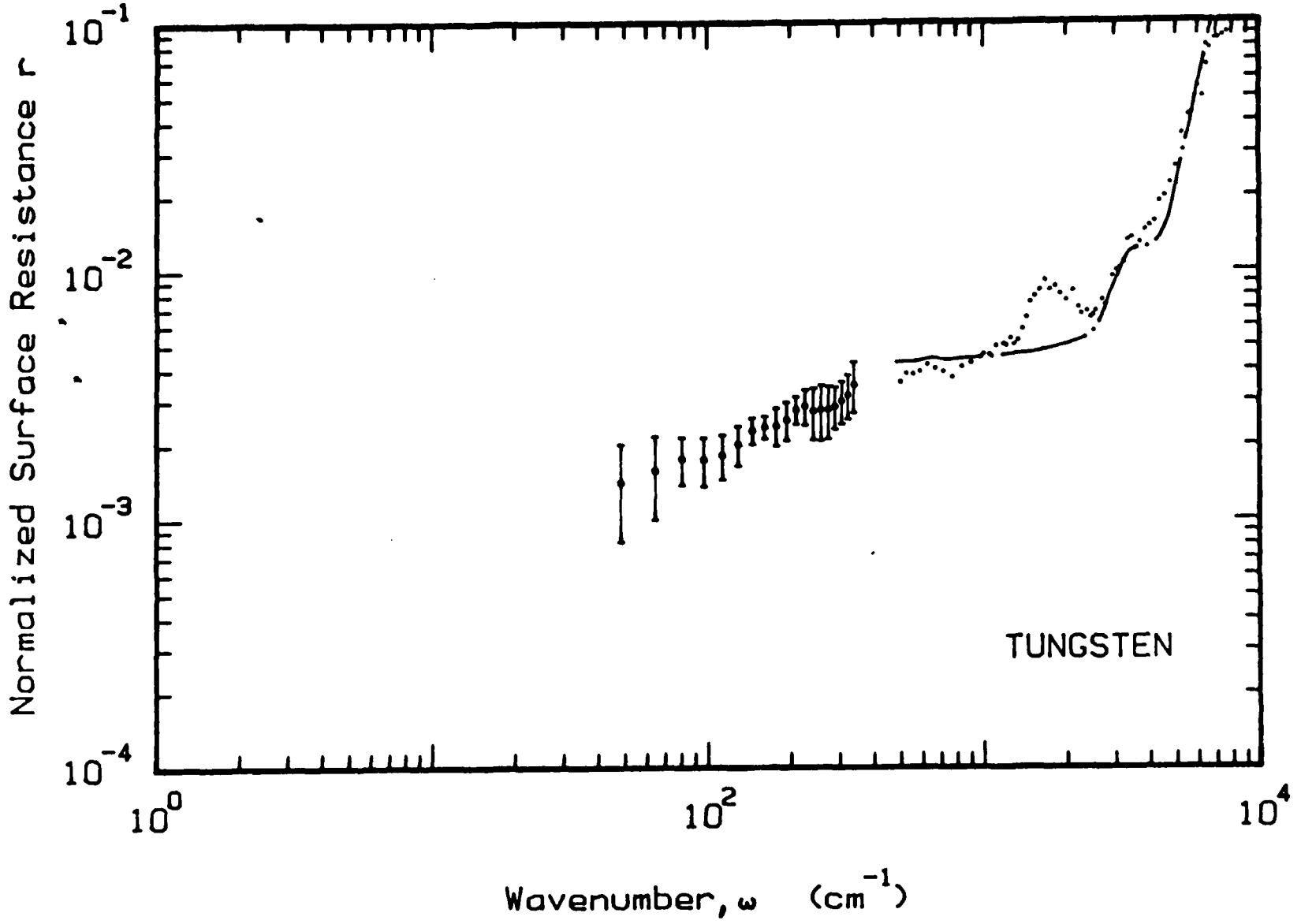

Fig. 25 Real Part of the Normalized Surface Resistance for Tungsten. Our nonresonant cavity measurements are shown by the points with error bars. The shorter wavelength data shown by the dash dot and dotted lines are from ref. 10.

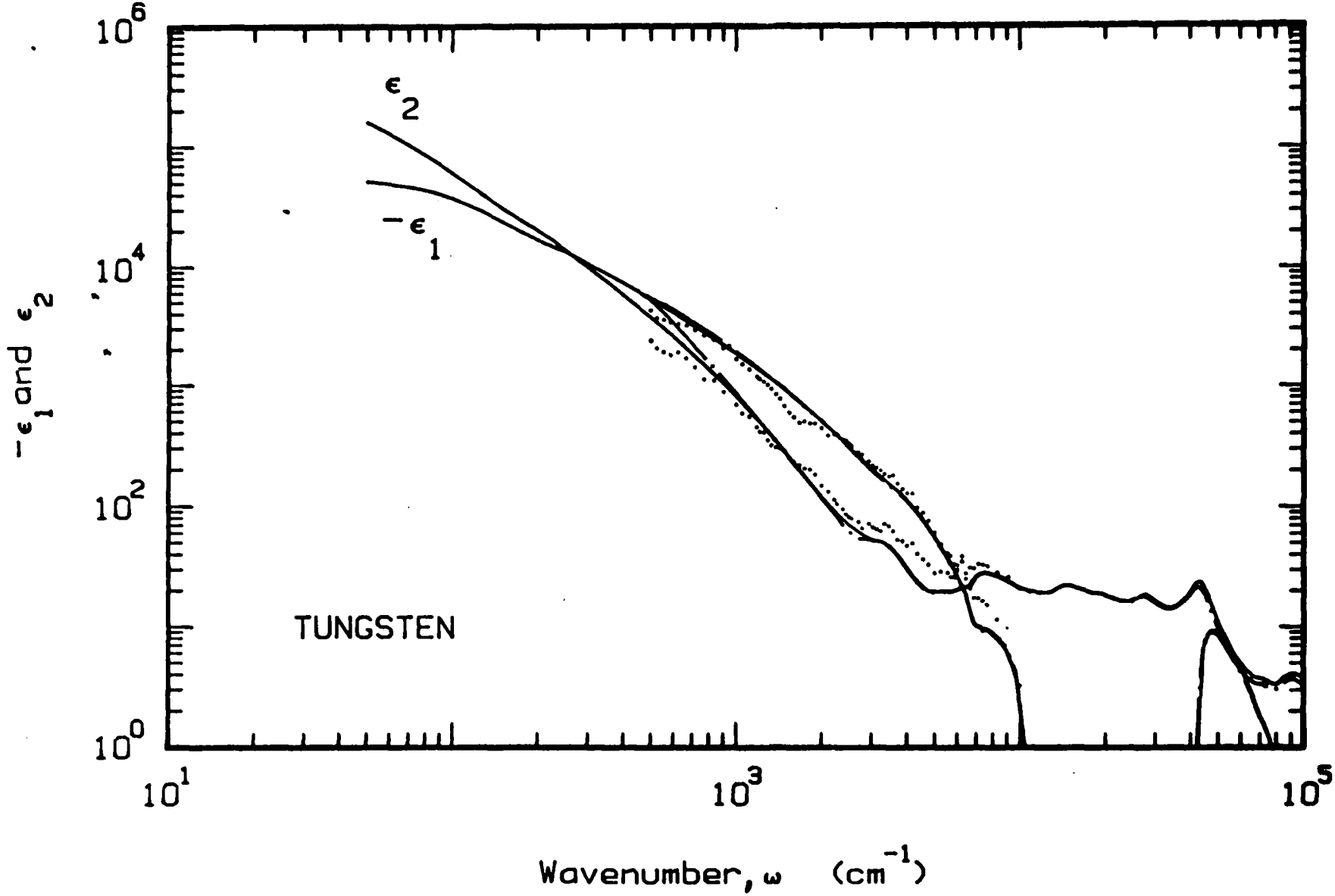

Fig. 26 ϵ_1 and ϵ_2 for Tungsten. The solid curves are for our data plus the short wavelength data. The dotted and dash dot curves are the ref. 10 data alone.

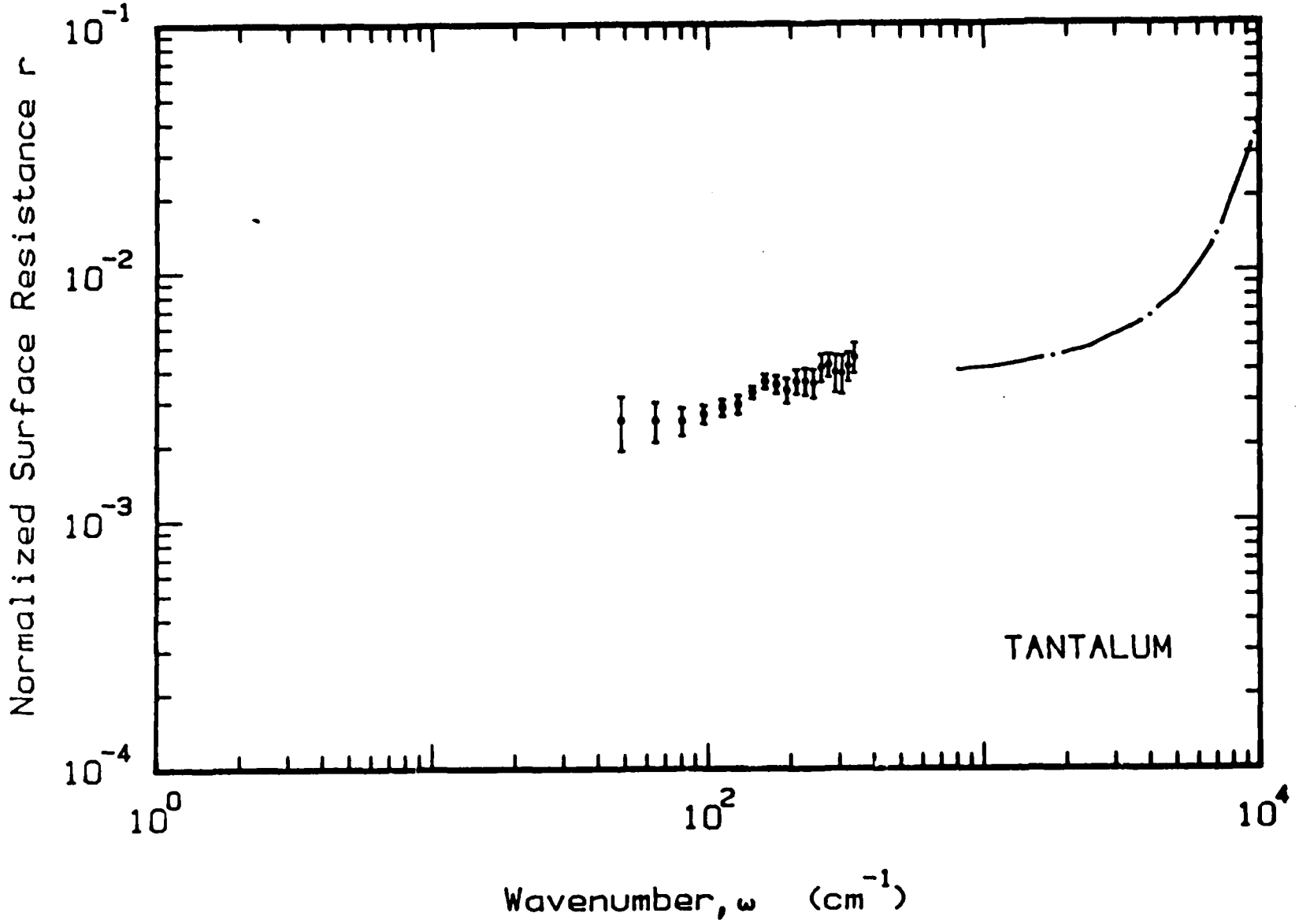

Fig. 27 Real Part of the Normalized Surface Resistance for Tantulum. Our nonresonant cavity measurements are shown by the points with error bars. The shorter wavelength data shown by the dash dot line are from ref. 10.

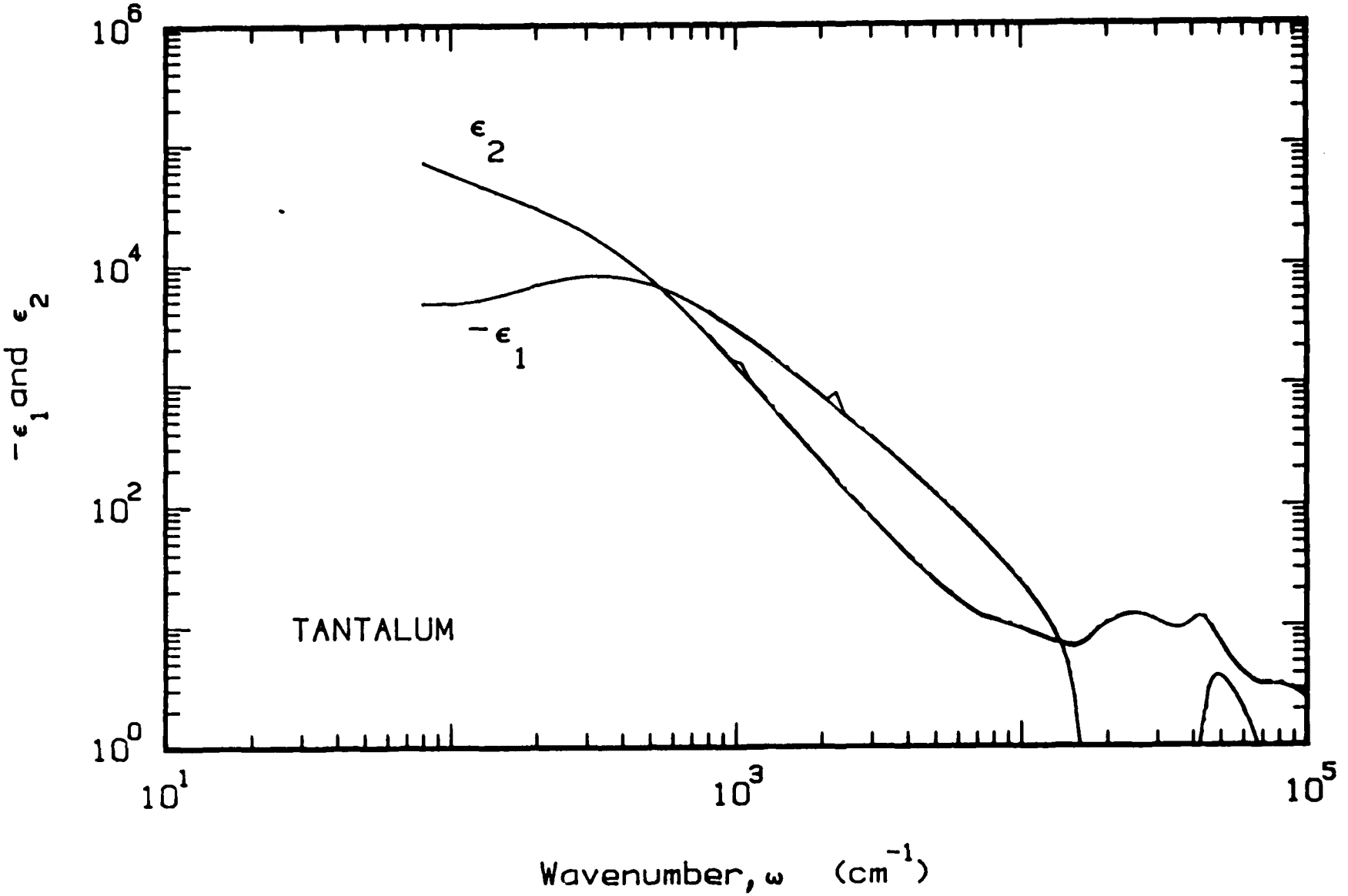

Fig. 28 ϵ_1 and ϵ_2 for Tantulum. The solid curves are for our data plus the short wavelength data. The dash dot curves are the ref. 10 data alone.

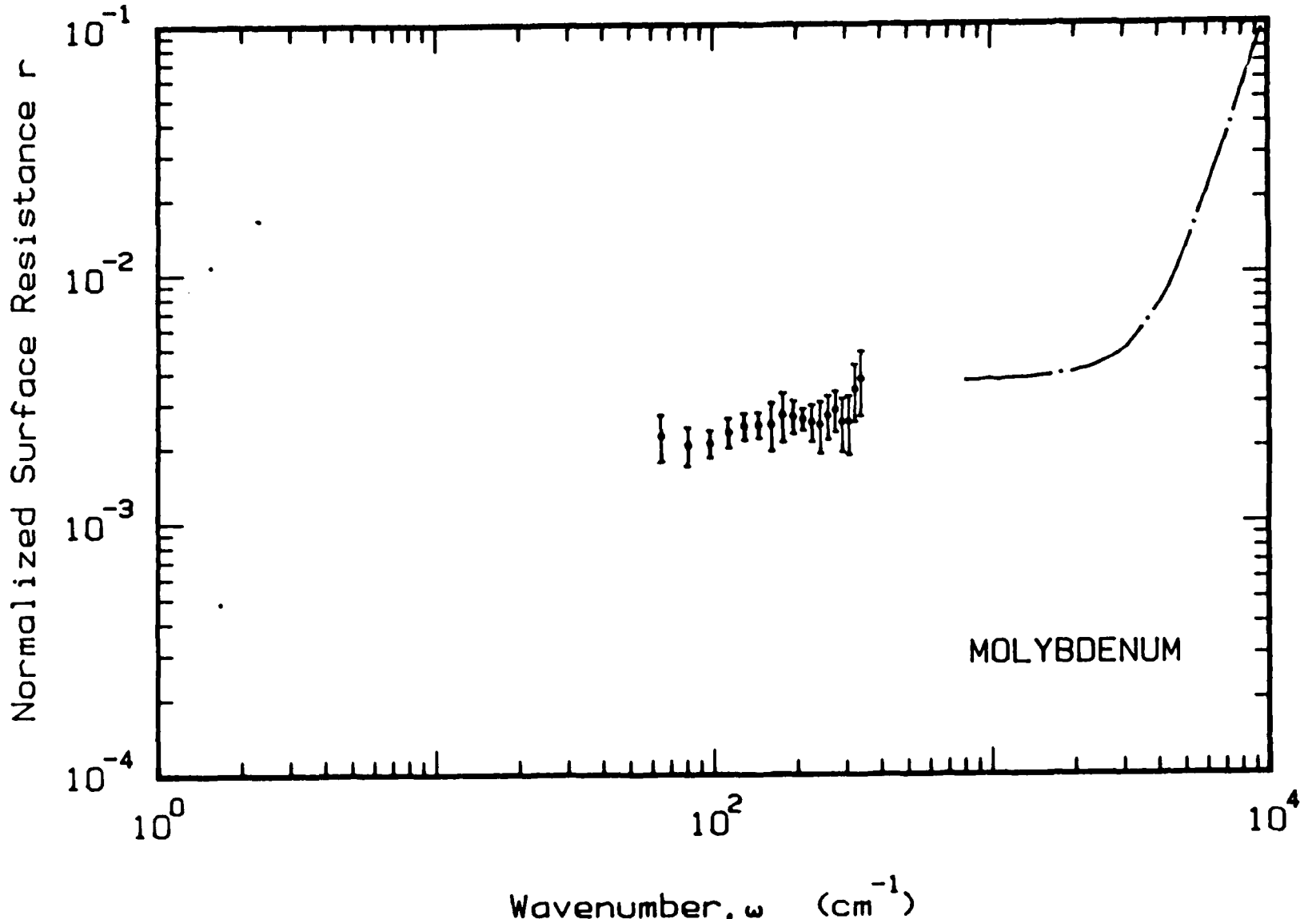

Fig. 29 Real Part of the Normalized Surface Resistance for Molybdenum. Our nonresonant cavity measurements are shown by the points with error bars. The shorter wavelength data shown by the dash dot line are from ref. 10.

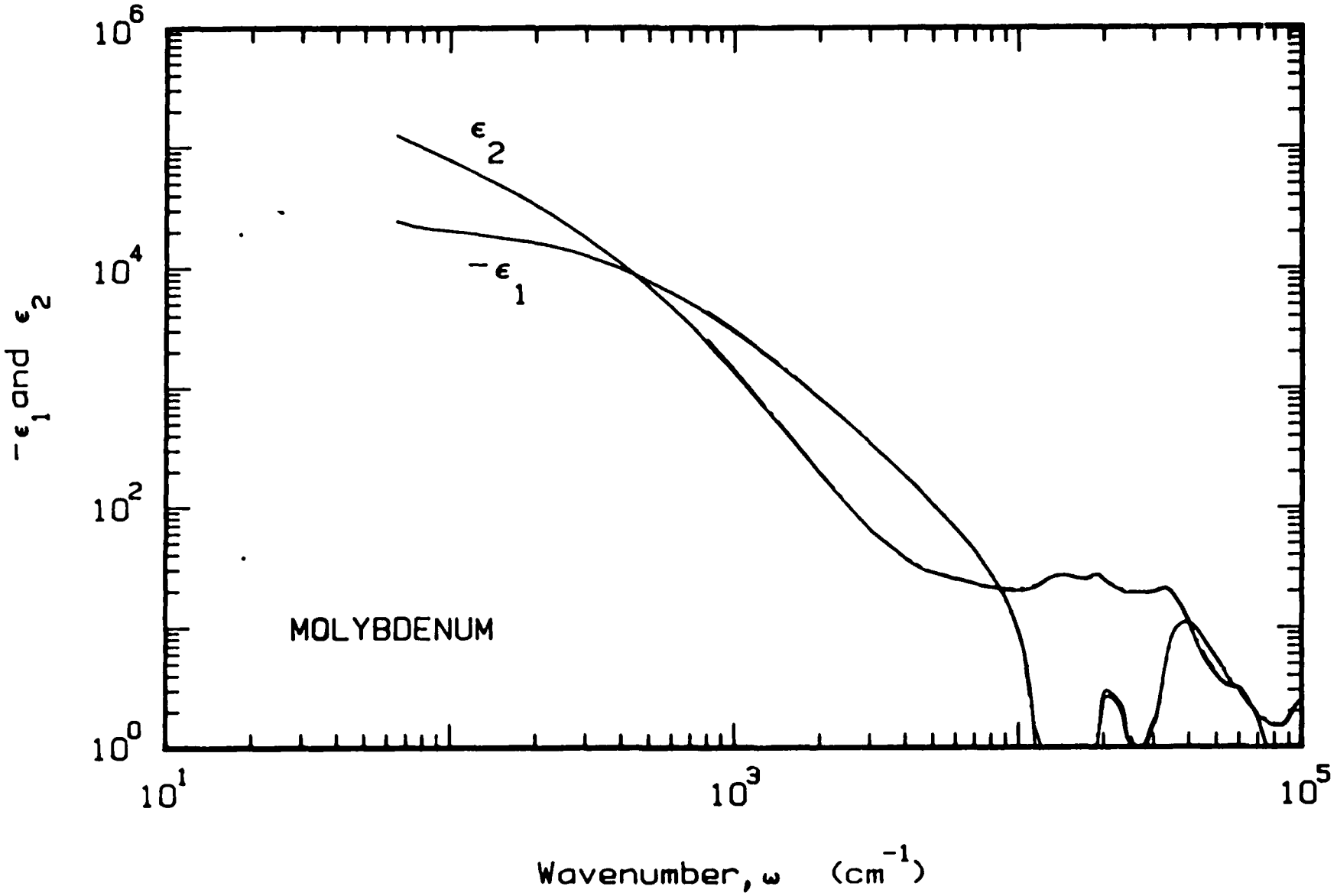

Fig. 30 ϵ_1 and ϵ_2 for Molybdenum. The solid curves are for our data plus the short wavelength data. The dash dot curves are the ref. 10 data alone.

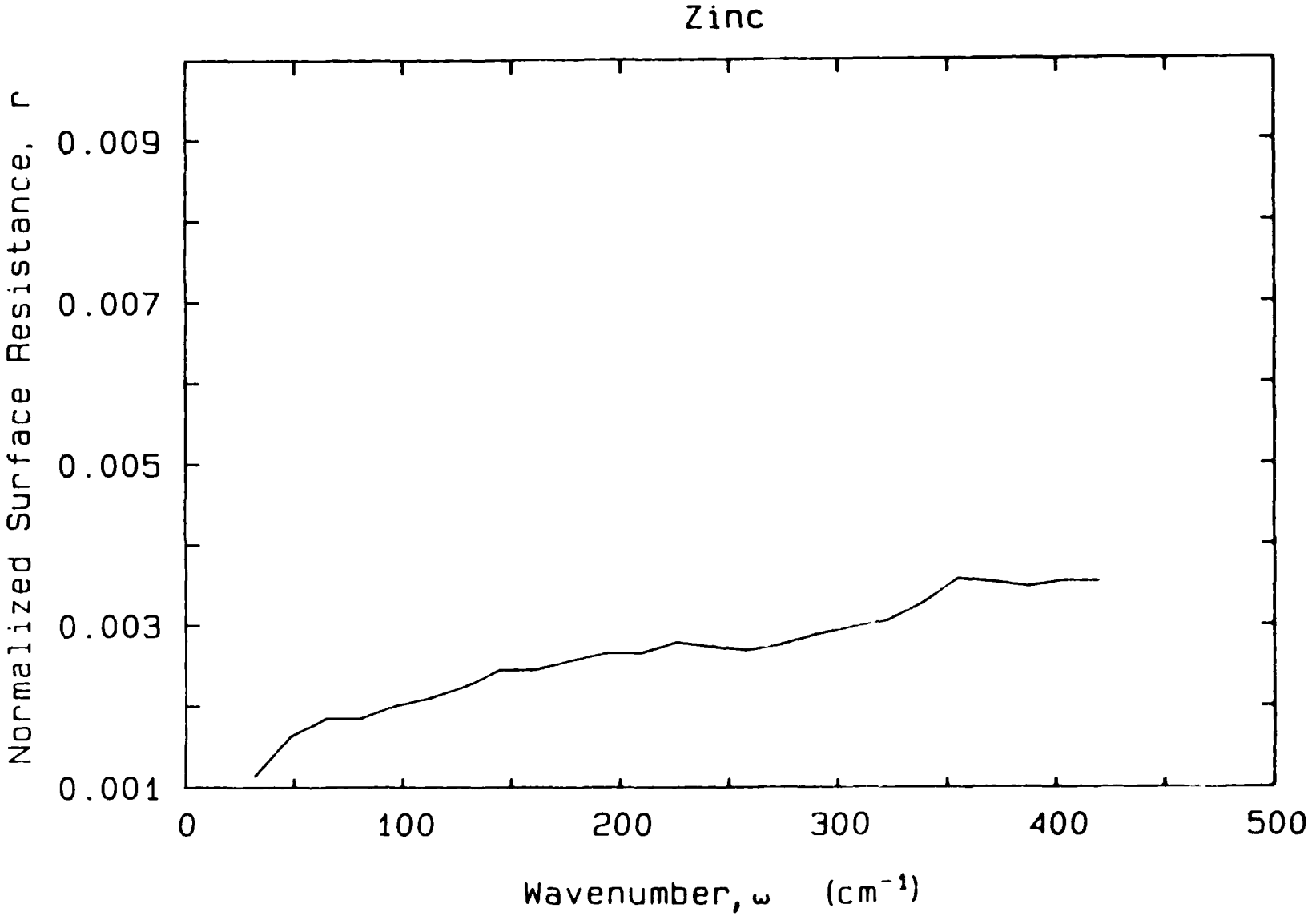

Fig. 31 Real Part of the Normalized Surface Resistance for polycrystalline zinc.

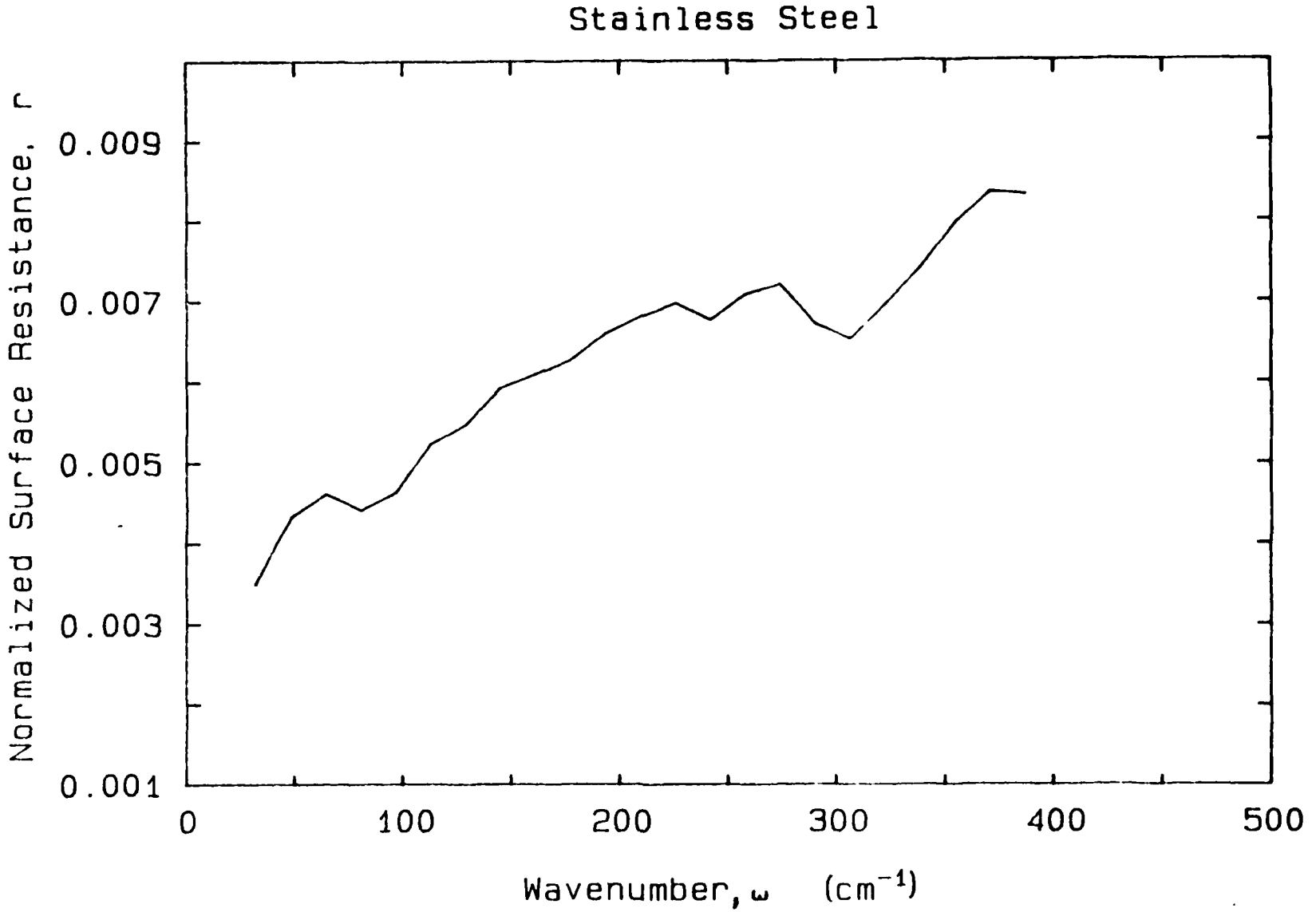

Fig. 32 Real Part of the Normalized Surface Resistance, r, versus wavenumber for Stainless Steel.

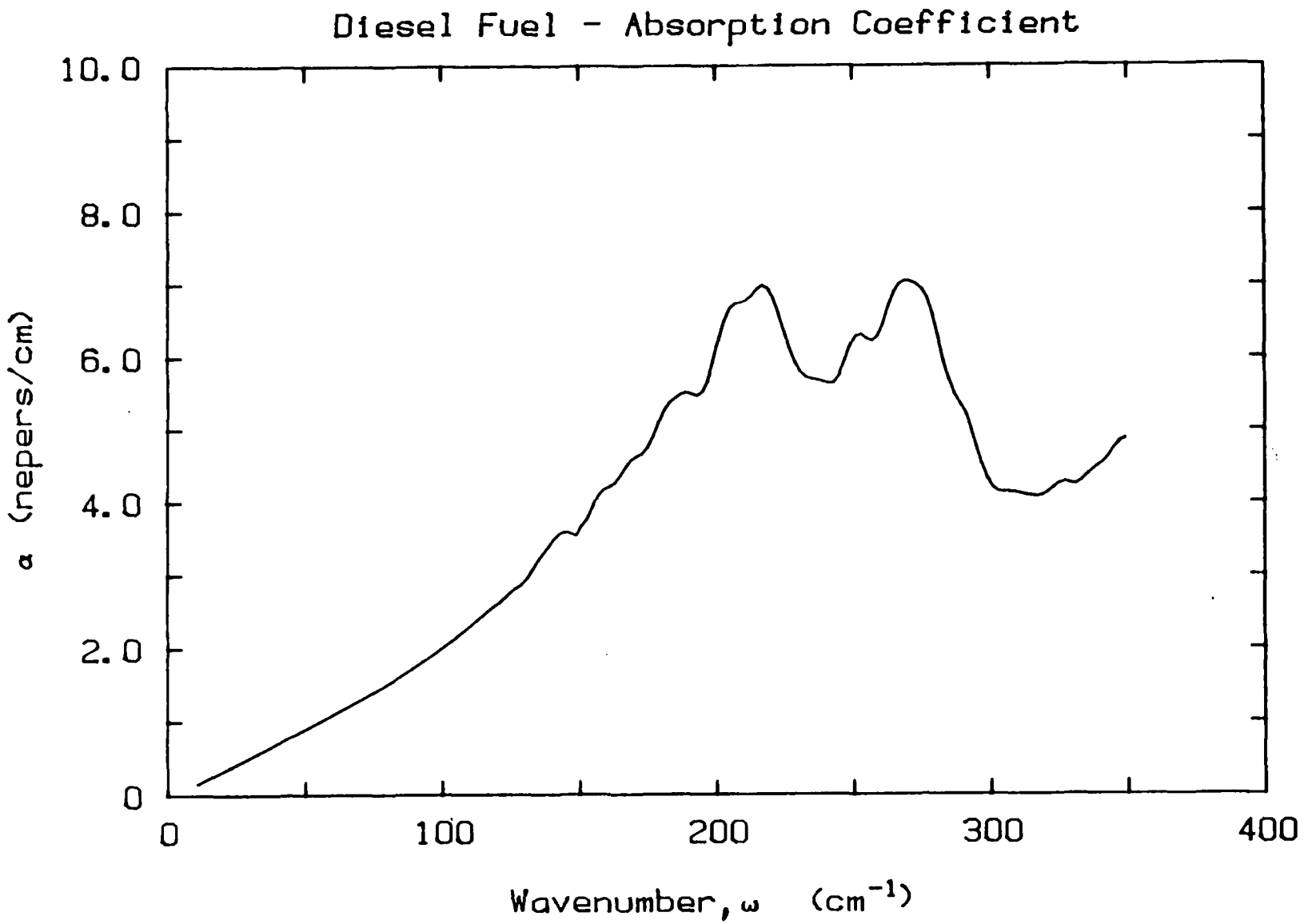

Fig. 33 Absorption Coefficient, α, versus wavenumber for diesel fuel.

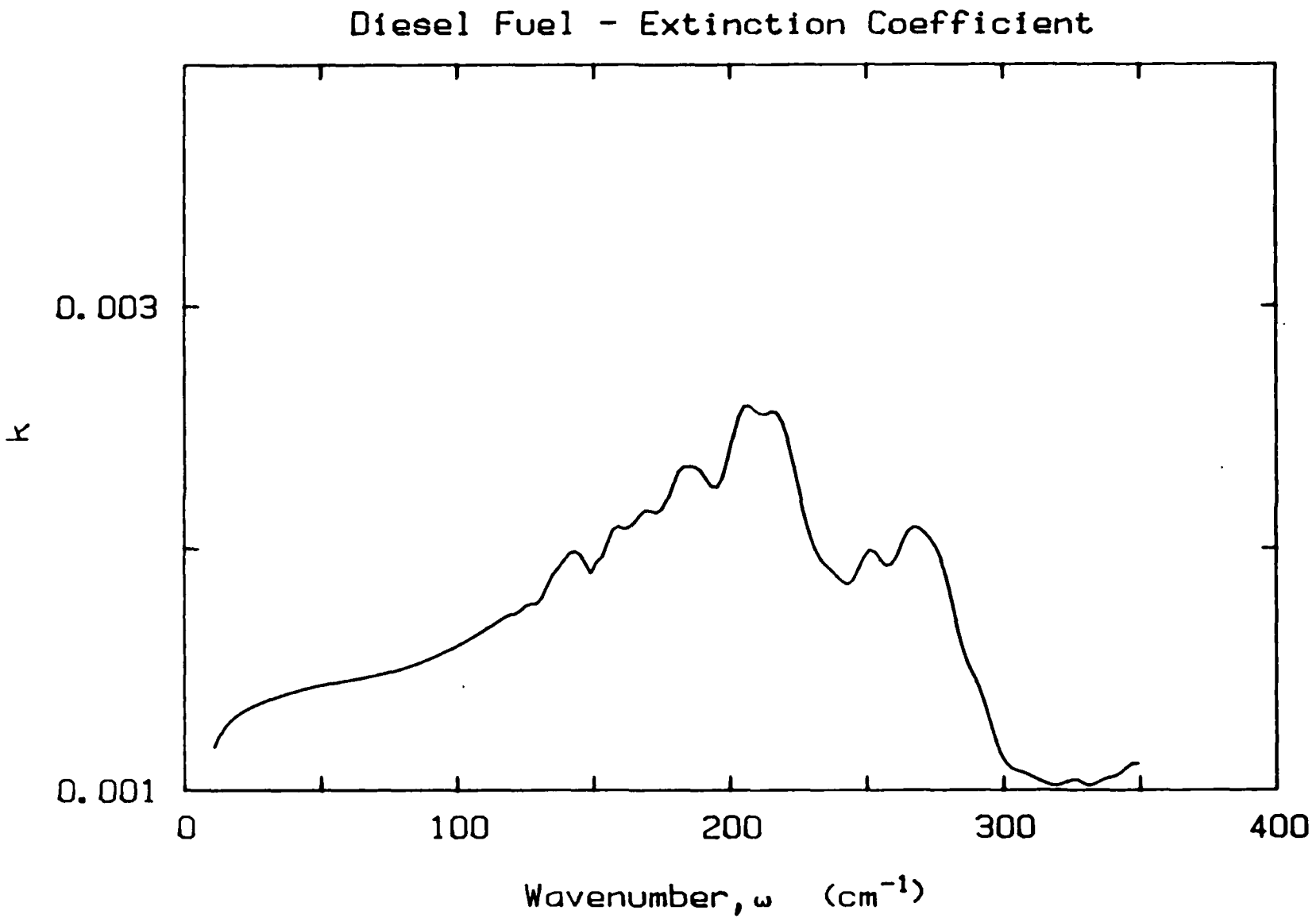

Fig. 34 Imaginary Part of the Refractive Index versus wavenumber for diesel fuel.

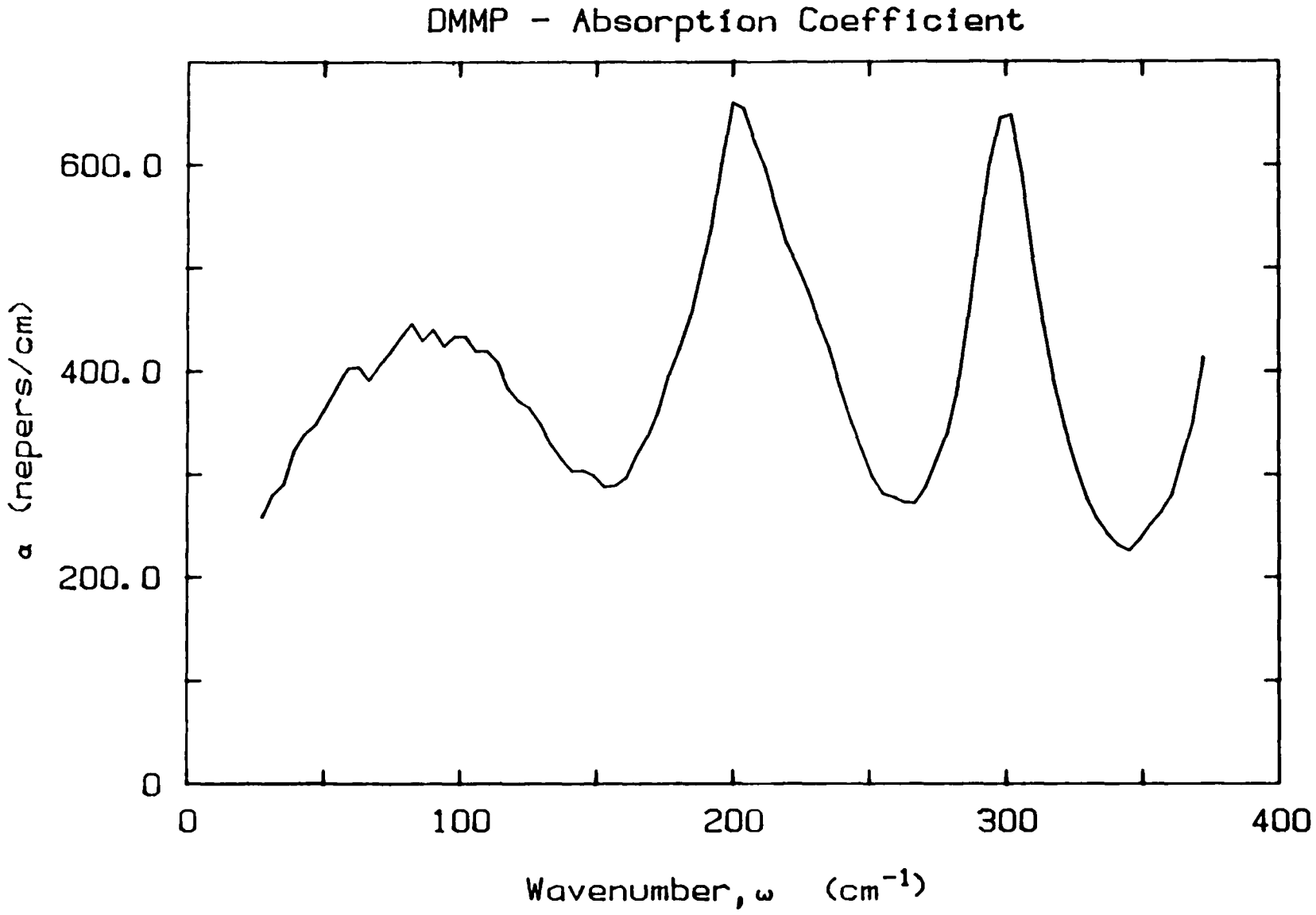

Fig. 35 Absorption Coefficient, α, versus wavenumber for DMMP.

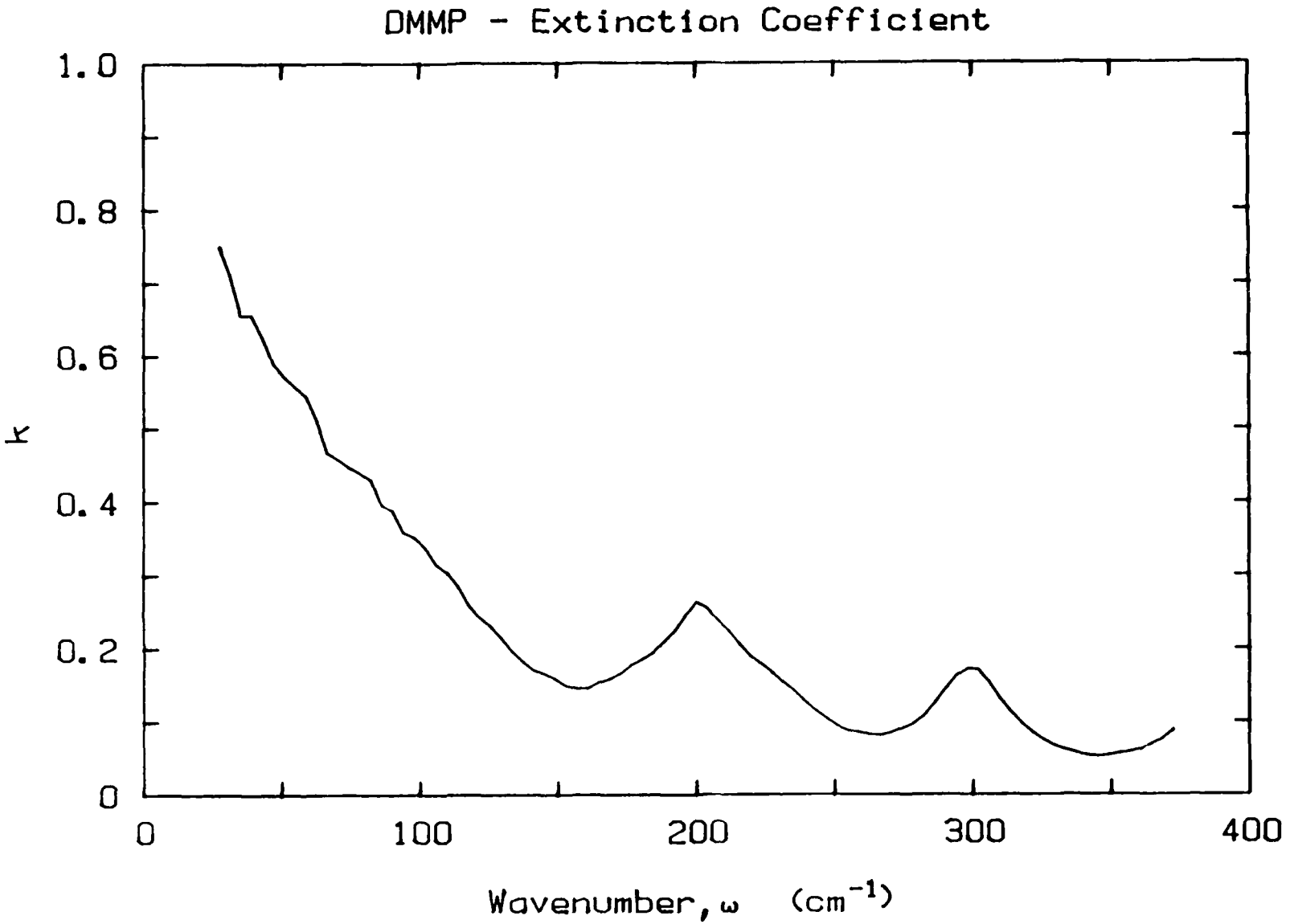

Fig. 36 Imaginary Part of the Refractive Index versus wavenumber for DMMP.

2.6 TABLES.

1. Oscillator Fit Parameters for Gypsum (in text).
2. Oscillator Fit arameters for Fluorapatite (in text).
3. Real and Imaginary Parts of the Refractive Index, n and k, for Quartz.
4. Oscillator Fit Parameters for Quartz (in text).

TABLE 3: n and k for Quartz

Quartz (two orientations)
No - index of refraction for ordinary ray
Ko - extinction coefficient for ordinary ray
Ne - index of refraction for extraordinary ray
Ke - extinction coefficient for extraordinary ray

Source of data:
20 - 370 /cm: E.E. Russell and E.E. Bell, "JOSA", vol. 57, no.3, March, 1967, p.341

370-1600 /cm: W.G. Spitzer and D.A. Kleinman, "Phys. Rev.", vol. 121, no. 5, March 1, 1961, p.1324

Wn	No	Ne	Ko	Ke
20	2.1073			
22	2.1074	2.1551		
24	2.1076	2.1558		
26	2.1076	2.1562		
28	2.1076	2.1561		
30	2.1076	2.1560	0.2644E-03	
32	2.1078	2.1561	0.2570E-03	0.2488E-03
34	2.1081	2.1562	0.2518E-03	0.2354E-03
36	2.1084	2.1565	0.2489E-03	0.2249E-03
38	2.1088	2.1569	0.2480E-03	0.2172E-03
40	2.1092	2.1572	0.2491E-03	0.2121E-03
42	2.1097	2.1575	0.2524E-03	0.2095E-03
44	2.1102	2.1578	0.2578E-03	0.2092E-03
46	2.1106	2.1581	0.2669E-03	0.2111E-03
48	2.1110	2.1585	0.2818E-03	0.2151E-03
50	2.1113	2.1589	0.2993E-03	0.2209E-03
52	2.1117	2.1594	0.3192E-03	0.2284E-03
54	2.1121	2.1599	0.3411E-03	0.2376E-03
56	2.1125	2.1603	0.3648E-03	0.2481E-03
58	2.1129	2.1608	0.3895E-03	0.2599E-03
60	2.1133	2.1614	0.4147E-03	0.2728E-03
62	2.1138	2.1619	0.4321E-03	0.2867E-03
64	2.1143	2.1625	0.4455E-03	0.3014E-03
66	2.1148	2.1630	0.4572E-03	0.3165E-03
68	2.1153	2.1636	0.4674E-03	0.3320E-03
70	2.1157	2.1642	0.4762E-03	0.3476E-03
72	2.1163	2.1649	0.4837E-03	0.3629E-03
74	2.1170	2.1656	0.4902E-03	0.3779E-03
76	2.1176	2.1663	0.4958E-03	0.3923E-03
78	2.1182	2.1670	0.5006E-03	0.4059E-03
80	2.1188	2.1677	0.5052E-03	0.4191E-03
82	2.1195	2.1684	0.5096E-03	0.4320E-03
84	2.1202	2.1692	0.5142E-03	0.4449E-03
86	2.1210	2.1700	0.5194E-03	0.4580E-03
88	2.1218	2.1708	0.5253E-03	0.4717E-03
90	2.1225	2.1715	0.5324E-03	0.4861E-03
92	2.1233	2.1723	0.5446E-03	0.5014E-03
94	2.1241	2.1731	0.5605E-03	0.5178E-03
96	2.1249	2.1740	0.5779E-03	0.5349E-03
98	2.1257	2.1749	0.5967E-03	0.5526E-03

Wn	No	Ne	Ko	Ke
100	2.1266	2.1758	0.6164E-03	0.5708E-03
102	2.1274	2.1768	0.6370E-03	0.5892E-03
104	2.1283	2.1778	0.6580E-03	0.6077E-03
106	2.1292	2.1788	0.6752E-03	0.6261E-03
108	2.1301	2.1799	0.6813E-03	0.6442E-03
110	2.1311	2.1810	0.6888E-03	0.6615E-03
112	2.1322	2.1821	0.6969E-03	0.6777E-03
114	2.1332	2.1832	0.7048E-03	0.6922E-03
116	2.1344	2.1843	0.7142E-03	0.7047E-03
118	2.1357	2.1855	0.7270E-03	0.7148E-03
120	2.1370	2.1867	0.7520E-03	0.7219E-03
122	2.1383	2.1877	0.8480E-03	0.7257E-03
124	2.1400	2.1888	0.1219E-02	0.7269E-03
126	2.1421	2.1902	0.2716E-02	0.7268E-03
128	2.1419	2.1916	0.5284E-02	0.7269E-03
130	2.1403	2.1930	0.4346E-02	0.7287E-03
132	2.1413	2.1944	0.2833E-02	0.7337E-03
134	2.1428	2.1957	0.2138E-02	0.7433E-03
136	2.1440	2.1970	0.1650E-02	0.7591E-03
138	2.1454	2.1985	0.1588E-02	0.7821E-03
140	2.1469	2.2000	0.1547E-02	0.8110E-03
142	2.1485	2.2016	0.1528E-02	0.8441E-03
144	2.1499	2.2032	0.1507E-02	0.8797E-03
146	2.1514	2.2048	0.1489E-02	0.9158E-03
148	2.1529	2.2064	0.1478E-02	0.9508E-03
150	2.1544	2.2079	0.1470E-02	0.9829E-03
152	2.1559	2.2096	0.1485E-02	0.1010E-02
154	2.1575	2.2112	0.1510E-02	0.1033E-02
156	2.1590	2.2129	0.1528E-02	0.1051E-02
158	2.1607	2.2147	0.1542E-02	0.1068E-02
160	2.1624	2.2165	0.1553E-02	0.1084E-02
162	2.1641	2.2183	0.1562E-02	0.1101E-02
164	2.1658	2.2201	0.1569E-02	0.1121E-02
166	2.1675	2.2219	0.1578E-02	0.1144E-02
168	2.1694	2.2239	0.1588E-02	0.1174E-02
170	2.1713	2.2259	0.1601E-02	0.1207E-02
172	2.1731	2.2280	0.1619E-02	0.1244E-02
174	2.1750	2.2300	0.1642E-02	0.1281E-02
176	2.1769	2.2321	0.1672E-02	0.1319E-02
178	2.1790	2.2344	0.1711E-02	0.1354E-02
180	2.1811	2.2367	0.1759E-02	0.1385E-02
182	2.1832	2.2382	0.1817E-02	0.1411E-02
184	2.1854	2.2381	0.1885E-02	0.1436E-02
186	2.1876	2.2376	0.1954E-02	0.1461E-02
188	2.1899	2.2373	0.2021E-02	0.1485E-02
190	2.1923	2.2378	0.2088E-02	0.1510E-02
192	2.1948	2.2395	0.2155E-02	0.1535E-02
194	2.1976	2.2420	0.2222E-02	0.1559E-02
196	2.2000	2.2446	0.2290E-02	0.1584E-02
198	2.2003	2.2472	0.2357E-02	0.1608E-02
200	2.2006	2.2499	0.2424E-02	0.1633E-02
202	2.2029	2.2526	0.2491E-02	0.1658E-02
204	2.2060	2.2554	0.2558E-02	0.1682E-02

Wn	No	Ne	Ko	Ke
206	2.2090	2.2583	0.2626E-02	0.1707E-02
208	2.2119	2.2613	0.2693E-02	0.1732E-02
210	2.2149	2.2644	0.2760E-02	0.1756E-02
212	2.2180	2.2675	0.2827E-02	0.1781E-02
214	2.2212	2.2708	0.2895E-02	0.1806E-02
216	2.2246	2.2742	0.2962E-02	0.1830E-02
218	2.2281	2.2777	0.3029E-02	0.1855E-02
220	2.2320	2.2812	0.3096E-02	0.1880E-02
222	2.2360	2.2849	0.3163E-02	0.1904E-02
224	2.2402	2.2887	0.3231E-02	0.1929E-02
226	2.2445	2.2926	0.3298E-02	0.1954E-02
228	2.2489	2.2965	0.3365E-02	0.1979E-02
230	2.2535	2.3006	0.3432E-02	0.2002E-02
232	2.2581	2.3047	0.3500E-02	0.2027E-02
234	2.2630	2.3090	0.3567E-02	0.2054E-02
236	2.2683	2.3133	0.3634E-02	0.2080E-02
238	2.2742	2.3178	0.3701E-02	0.2094E-02
240	2.2810	2.3223	0.3815E-02	0.2113E-02
242	2.2888	2.3269	0.4068E-02	0.2178E-02
244	2.2981	2.3316	0.4669E-02	0.2225E-02
246	2.3090	2.3365	0.7560E-02	0.2277E-02
248	2.3216	2.3414	0.1033E-01	0.2546E-02
250	2.3363	2.3465	0.1435E-01	0.2948E-02
252	2.3532	2.3517	0.2105E-01	0.3136E-02
254	2.3732	2.3571	0.2904E-01	0.3231E-02
256	2.3976	2.3626	0.4411E-01	0.3308E-02
258	2.4294	2.3682	0.9314E-01	0.3415E-02
260	2.4745	2.3740	0.1960E+00	0.3571E-02
261	2.5049	2.3770	0.2399E+00	0.3670E-02
262	2.3845	2.3800	0.2623E+00	0.3782E-02
264	2.0371	2.3862	0.2371E+00	0.4042E-02
265	1.9466	2.3894	0.2094E+00	0.4186E-02
266	1.9831	2.3926	0.1724E+00	0.4337E-02
268	2.0469	2.3992	0.1123E+00	0.4651E-02
270	2.0986	2.4060	0.7484E-01	0.4971E-02
272	2.1396	2.4131	0.5302E-01	0.5281E-02
274	2.1716	2.4205	0.4002E-01	0.5571E-02
276	2.1964	2.4281	0.3185E-01	0.5834E-02
278	2.2159	2.4360	0.2631E-01	0.6067E-02
280	2.2315	2.4442	0.2228E-01	0.6273E-02
282	2.2445	2.4527	0.1922E-01	0.6455E-02
284	2.2559	2.4616	0.1689E-01	0.6620E-02
286	2.2666	2.4709	0.1518E-01	0.6779E-02
288	2.2768	2.4805	0.1401E-01	0.6942E-02
290	2.2869	2.4905	0.1328E-01	0.7119E-02
292	2.2971	2.5010	0.1289E-01	0.7320E-02
294	2.3072	2.5119	0.1272E-01	0.7555E-02
296	2.3173	2.5233	0.1268E-01	0.7830E-02
298	2.3274	2.5353	0.1268E-01	0.8151E-02
300	2.3372	2.5478	0.1267E-01	0.8519E-02
302	2.3469	2.5610	0.1261E-01	0.8937E-02
304	2.3563	2.5749	0.1250E-01	0.9404E-02
306	2.3655	2.5896	0.1236E-01	0.9921E-02

Wn	No	Ne	Ko	Ke
308	2.3746	2.6051	0.1223E-01	0.1049E-01
310	2.3836	2.6216	0.1213E-01	0.1112E-01
312	2.3926	2.6393	0.1210E-01	0.1182E-01
314	2.4018	2.6581	0.1216E-01	0.1261E-01
316	2.4113	2.6784	0.1231E-01	0.1354E-01
318	2.4211	2.7002	0.1255E-01	0.1465E-01
320	2.4314	2.7239	0.1284E-01	0.1602E-01
322	2.4422	2.7497	0.1315E-01	0.1777E-01
324	2.4534	2.7778	0.1347E-01	0.2003E-01
326	2.4651	2.8087	0.1375E-01	0.2300E-01
328	2.4772	2.8426	0.1399E-01	0.2691E-01
330	2.4897	2.8801	0.1418E-01	0.3206E-01
332	2.5026	2.9216	0.1434E-01	0.3883E-01
334	2.5158	2.9677	0.1448E-01	0.4766E-01
336	2.5293	3.0124	0.1457E-01	0.5911E-01
338	2.5432	3.0662	0.1466E-01	0.7381E-01
340	2.5575	3.1236	0.1475E-01	0.7971E-01
342	2.5723	3.1896	0.1488E-01	0.9320E-01
344	2.5879	3.2676	0.1506E-01	0.1052E+00
346	2.6044	3.3621	0.1531E-01	0.1278E+00
348	2.6222	3.4793	0.1566E-01	0.1462E+00
350	2.6415	3.6265	0.1613E-01	0.1812E+00
352	2.6627	3.8128	0.1673E-01	0.2132E+00
354	2.6858	4.0494	0.1750E-01	0.2886E+00
356	2.7113	4.3493	0.1845E-01	0.4002E+00
358	2.7392	4.7281	0.1960E-01	0.6095E+00
360	2.7697	5.2028	0.2096E-01	0.9226E+00
362	2.8027	5.8986	0.2252E-01	0.1457E+01
364	2.8419	5.0007	0.2433E-01	0.2868E+01
366	2.8786	2.9309	0.2645E-01	0.4726E+01
367	2.8928	2.0664	0.2766E-01	0.5123E+01
368	2.9059	1.4647	0.2898E-01	0.4944E+01
370	2.9322	0.9441	0.3200E-01	0.4248E+01
372	2.9659	0.7171	0.3562E-01	0.3654E+01
374	3.0156	0.5463	0.4001E-01	0.3111E+01
376	3.0878	0.4246	0.4544E-01	0.2618E+01
378	3.1692	0.3505	0.5251E-01	0.2173E+01
380	3.2660	0.3224	0.6241E-01	0.1775E+01
382	3.3919	0.3395	0.7735E-01	0.1422E+01
384	3.5666	0.3889	0.1088E+00	0.1113E+01
386	3.8213	0.4895	0.1544E+00	0.8471E+00
388	4.2025	0.6516	0.2085E+00	0.6225E+00
390	4.7747	0.8351	0.3039E+00	0.4380E+00
392	6.0429	1.0053	0.5834E+00	0.2926E+00
394	4.6037	1.1402	0.1106E+01	0.1911E+00
396	1.4389	1.2511	0.3620E+01	0.1468E+00
398	0.8228	1.3423	0.4697E+01	0.1182E+00
400	0.5958	1.4201	0.3803E+01	0.9802E-01
402	0.7696	1.4893	0.2456E+01	0.8331E-01
404	1.2032	1.5533	0.9260E+00	0.7246E-01
406	1.5843	1.6140	0.4406E+00	0.6432E-01
408	1.8425	1.6721	0.2533E+00	0.5797E-01
410	2.0358	1.7278	0.1825E+00	0.5275E-01

Wn	No	Ne	Ko	Ke
412	2.2022	1.7792	0.1485E+00	0.4828E-01
414	2.3420	1.8227	0.1200E+00	0.4442E-01
416	2.4528	1.8648	0.1079E+00	0.4116E-01
418	2.5472	1.9047	0.1030E+00	0.3851E-01
420	2.6459	1.9410	0.9963E-01	0.3639E-01
422	2.7604	1.9822	0.1005E+00	0.3470E-01
424	2.8884	2.0225	0.1053E+00	0.3324E-01
426	3.0219	2.0611	0.1118E+00	0.3186E-01
428	3.1595	2.0976	0.1215E+00	0.3052E-01
430	3.3115	2.1317	0.1331E+00	0.2925E-01
432	3.4911	2.1633	0.1478E+00	0.2820E-01
434	3.7010	2.1927	0.1664E+00	0.2749E-01
436	3.9312	2.2204	0.1898E+00	0.2713E-01
438	4.1788	2.2470	0.2172E+00	0.2693E-01
440	4.4863	2.2734	0.2695E+00	0.2659E-01
442	4.9651	2.3006	0.3483E+00	0.2659E-01
444	5.7460	2.3296	0.4485E+00	0.2673E-01
446	6.7875	2.3614	0.7116E+00	0.2687E-01
448	7.5365	2.3969	0.9683E+00	0.2714E-01
450	6.1593	2.4368	0.1893E+01	0.2761E-01
452	2.3621	2.4818	0.4468E+01	0.2831E-01
454	1.1100	2.5319	0.6405E+01	0.2922E-01
455	0.9653	2.5590	0.6621E+01	0.2974E-01
456	0.8765	2.5873	0.6339E+01	0.3032E-01
458	0.6093	2.6476	0.5620E+01	0.3159E-01
460	0.3577	2.7126	0.4996E+01	0.3304E-01
462	0.2913	2.7816	0.4455E+01	0.3469E-01
464	0.2243	2.8544	0.3988E+01	0.3661E-01
466	0.1766	2.9309	0.3585E+01	0.3892E-01
468	0.1450	3.0116	0.3238E+01	0.4180E-01
470	0.1233	3.0981	0.2940E+01	0.4547E-01
472	0.1067	3.1931	0.2683E+01	0.5023E-01
474	0.0922	3.3011	0.2461E+01	0.5645E-01
476	0.0780	3.4290	0.2269E+01	0.6459E-01
478	0.0634	3.5865	0.2101E+01	0.7514E-01
480	0.0482	3.7870	0.1954E+01	0.8870E-01
482	0.0330	4.0479	0.1822E+01	0.1090E+00
484	0.0187	4.3919	0.1703E+01	0.1350E+00
486	0.0176	4.8475	0.1594E+01	0.1697E+00
488	0.0000	5.4455	0.1491E+01	0.2238E+00
490	0.0000	6.2334	0.1393E+01	0.3079E+00
492	0.0000	7.6673	0.1297E+01	0.4651E+00
494	0.0000	9.2817	0.1202E+01	0.8736E+00
496	0.0126	5.4787	0.1107E+01	0.5209E+01
498	0.0316	1.3849	0.1011E+01	0.8021E+01
499	0.0415	0.8611	0.9619E+00	0.8391E+01
500	0.0606	0.6567	0.9124E+00	0.7874E+01
502	0.0833	0.5429	0.8116E+00	0.6664E+01
503	0.0999	0.4367	0.7601E+00	0.5998E+01
504	0.1182	0.4811	0.7080E+00	0.5366E+01
506	0.1447	0.5587	0.6017E+00	0.4269E+01
508	0.2395	0.7224	0.4928E+00	0.3501E+01
510	0.3087	0.6231	0.3818E+00	0.3026E+01

Wn	No	Ne	Ko	Ke
511	0.3506	0.5399	0.3255E+00	0.2978E+01
512	0.3983	0.4537	0.2690E+00	0.3053E+01
514	0.4933	0.3068	0.1552E+00	0.3093E+01
516	0.5847	0.2119	0.9946E-01	0.2851E+01
518	0.6672	0.1629	0.8795E-01	0.2633E+01
520	0.7379	0.1433	0.7475E-01	0.2434E+01
522	0.7960	0.1387	0.6437E-01	0.2254E+01
524	0.8408	0.1368	0.5617E-01	0.2091E+01
526	0.8894	0.1326	0.4967E-01	0.1941E+01
528	0.9310	0.1247	0.4446E-01	0.1804E+01
530	0.9673	0.1147	0.4024E-01	0.1678E+01
532	1.0004	0.1049	0.3678E-01	0.1561E+01
534	1.0407	0.0964	0.3390E-01	0.1451E+01
536	1.0599	0.0895	0.3147E-01	0.1347E+01
538	1.0853	0.0826	0.2937E-01	0.1247E+01
540	1.1145	0.0747	0.2754E-01	0.1150E+01
542	1.1371	0.0659	0.2593E-01	0.1055E+01
544	1.1595	0.0579	0.2449E-01	0.9596E+00
546	1.1807	0.0581	0.2320E-01	0.8635E+00
548	1.2009	0.0721	0.2203E-01	0.7652E+00
550	1.2200	0.1118	0.2098E-01	0.6635E+00
552	1.2383	0.1874	0.2002E-01	0.5574E+00
554	1.2556	0.2963	0.1915E-01	0.4458E+00
556	1.2722	0.4235	0.1837E-01	0.3277E+00
558	1.2880	0.5234	0.1765E-01	0.2021E+00
560	1.3031	0.6084	0.1700E-01	0.1108E+00
562	1.3176	0.6776	0.1641E-01	0.7615E-01
564	1.3314	0.7365	0.1586E-01	0.6141E-01
566	1.3446	0.7881	0.1536E-01	0.5349E-01
568	1.3574	0.8346	0.1489E-01	0.4768E-01
570	1.3696	0.8766	0.1444E-01	0.4261E-01
572	1.3813	0.9153	0.1402E-01	0.3812E-01
574	1.3925	0.9514	0.1362E-01	0.3430E-01
576	1.4033	0.9852	0.1324E-01	0.3119E-01
578	1.4137	1.0171	0.1287E-01	0.2873E-01
580	1.4236	1.0472	0.1251E-01	0.2676E-01
582	1.4332	1.0757	0.1217E-01	0.2513E-01
584	1.4425	1.1027	0.1185E-01	0.2372E-01
586	1.4513	1.1283	0.1155E-01	0.2243E-01
588	1.4599	1.1524	0.1127E-01	0.2122E-01
590	1.4681	1.1752	0.1102E-01	0.2009E-01
592	1.4760	1.1968	0.1079E-01	0.1903E-01
594	1.4837	1.2172	0.1060E-01	0.1807E-01
596	1.4910	1.2366	0.1043E-01	0.1722E-01
598	1.4982	1.2549	0.1030E-01	0.1647E-01
600	1.5050	1.2723	0.1015E-01	0.1583E-01
602	1.5117	1.2889	0.9978E-02	0.1528E-01
604	1.5181	1.3048	0.9798E-02	0.1479E-01
606	1.5244	1.3201	0.9628E-02	0.1437E-01
608	1.5304	1.3347	0.9481E-02	0.1397E-01
610	1.5363	1.3489	0.9362E-02	0.1360E-01
612	1.5421	1.3627	0.9274E-02	0.1323E-01
614	1.5478	1.3760	0.9216E-02	0.1287E-01

Wn	No	Ne	Ko	Ke
616	1.5533	1.3891	0.9184E-02	0.1252E-01
618	1.5587	1.4019	0.9174E-02	0.1219E-01
620	1.5641	1.4143	0.9181E-02	0.1187E-01
622	1.5695	1.4266	0.9198E-02	0.1157E-01
624	1.5748	1.4386	0.9222E-02	0.1131E-01
626	1.5802	1.4503	0.9246E-02	0.1108E-01
628	1.5855	1.4617	0.9268E-02	0.1088E-01
630	1.5909	1.4729	0.9286E-02	0.1072E-01
632	1.5964	1.4838	0.9300E-02	0.1059E-01
634	1.6020	1.4944	0.9313E-02	0.1048E-01
636	1.6077	1.5046	0.9331E-02	0.1039E-01
638	1.6136	1.5145	0.9361E-02	0.1030E-01
640	1.6196	1.5240	0.9416E-02	0.1023E-01
642	1.6259	1.5331	0.9509E-02	0.1015E-01
644	1.6324	1.5418	0.9662E-02	0.1007E-01
646	1.6391	1.5501	0.9705E-02	0.9984E-02
648	1.6462	1.5579	0.9898E-02	0.9894E-02
650	1.6535	1.5653	0.1032E-01	0.9801E-02
652	1.6613	1.5723	0.1087E-01	0.9709E-02
654	1.6694	1.5789	0.1143E-01	0.9623E-02
656	1.6779	1.5851	0.1190E-01	0.9547E-02
658	1.6869	1.5910	0.1229E-01	0.9485E-02
660	1.6964	1.5965	0.1266E-01	0.9441E-02
662	1.7064	1.6018	0.1312E-01	0.9418E-02
664	1.7170	1.6068	0.1375E-01	0.9417E-02
666	1.7282	1.6117	0.1458E-01	0.9439E-02
668	1.7399	1.6164	0.1555E-01	0.9481E-02
670	1.7524	1.6210	0.1658E-01	0.9543E-02
672	1.7655	1.6257	0.1761E-01	0.9621E-02
674	1.7794	1.6303	0.1867E-01	0.9711E-02
676	1.7941	1.6351	0.1986E-01	0.9810E-02
678	1.8095	1.6401	0.2138E-01	0.9915E-02
680	1.8258	1.6453	0.2342E-01	0.1002E-01
682	1.8430	1.6508	0.2610E-01	0.1013E-01
684	1.8611	1.6566	0.2946E-01	0.1025E-01
686	1.8802	1.6627	0.3386E-01	0.1036E-01
688	1.9012	1.6693	0.4098E-01	0.1048E-01
690	1.9211	1.6763	0.5596E-01	0.1061E-01
692	1.9202	1.6838	0.1152E+00	0.1076E-01
694	1.9539	1.6918	0.1853E+00	0.1092E-01
696	1.9586	1.7002	0.2416E+00	0.1110E-01
698	1.9594	1.7091	0.2843E+00	0.1130E-01
700	1.9268	1.7185	0.3134E+00	0.1154E-01
702	1.6934	1.7283	0.3502E+00	0.1181E-01
704	1.6729	1.7386	0.3254E+00	0.1211E-01
706	1.6613	1.7492	0.2941E+00	0.1244E-01
708	1.6573	1.7602	0.2317E+00	0.1280E-01
710	1.6595	1.7715	0.1124E+00	0.1320E-01
712	1.6670	1.7830	0.5992E-01	0.1362E-01
714	1.6786	1.7948	0.4391E-01	0.1407E-01
716	1.6934	1.8066	0.3672E-01	0.1454E-01
718	1.7107	1.8186	0.3289E-01	0.1503E-01
720	1.7297	1.8306	0.3022E-01	0.1555E-01

Wn	No	Ne	Ko	Ke
722	1.7498	1.8425	0.2804E-01	0.1610E-01
724	1.7704	1.8545	0.2626E-01	0.1668E-01
726	1.7911	1.8664	0.2486E-01	0.1731E-01
728	1.8115	1.8783	0.2377E-01	0.1801E-01
730	1.8312	1.8901	0.2285E-01	0.1877E-01
732	1.8501	1.9020	0.2204E-01	0.1965E-01
734	1.8679	1.9139	0.2139E-01	0.2065E-01
736	1.8846	1.9261	0.2092E-01	0.2181E-01
738	1.9001	1.9385	0.2062E-01	0.2317E-01
740	1.9143	1.9515	0.2052E-01	0.2477E-01
742	1.9274	1.9654	0.2060E-01	0.2667E-01
744	1.9395	1.9802	0.2087E-01	0.2892E-01
746	1.9507	1.9965	0.2131E-01	0.3159E-01
748	1.9613	2.0147	0.2171E-01	0.3476E-01
750	1.9714	2.0351	0.2270E-01	0.3854E-01
752	1.9814	2.0585	0.2410E-01	0.4304E-01
754	1.9916	2.0855	0.2551E-01	0.4841E-01
756	2.0023	2.1167	0.2669E-01	0.5481E-01
758	2.0140	2.1533	0.2773E-01	0.6242E-01
760	2.0270	2.1959	0.2898E-01	0.7146E-01
762	2.0419	2.2459	0.3083E-01	0.8216E-01
764	2.0591	2.3042	0.3347E-01	0.9472E-01
766	2.0791	2.3723	0.3677E-01	0.1094E+00
768	2.1026	2.4518	0.4029E-01	0.1262E+00
770	2.1299	2.5439	0.4360E-01	0.1455E+00
772	2.1617	2.6756	0.4670E-01	0.1862E+00
774	2.1986	2.8354	0.5041E-01	0.2483E+00
776	2.2413	2.9599	0.5645E-01	0.3067E+00
777	2.2650	2.9950	0.6098E-01	0.3275E+00
778	2.2903	2.8074	0.6675E-01	0.3522E+00
780	2.3463	2.3488	0.8145E-01	0.4457E+00
782	2.4100	1.8786	0.9405E-01	0.6458E+00
784	2.4820	1.4716	0.1216E+00	0.9514E+00
786	2.5630	1.1566	0.1442E+00	0.1311E+01
788	2.6537	0.9344	0.1656E+00	0.1654E+01
790	2.7549	0.7950	0.2005E+00	0.1861E+01
792	2.8672	0.7910	0.2605E+00	0.1778E+01
794	2.9977	0.8392	0.3640E+00	0.1588E+01
796	3.1484	0.9066	0.5272E+00	0.1226E+01
798	3.2081	0.9769	0.7589E+00	0.7716E+00
800	3.0588	1.0459	0.1056E+01	0.4185E+00
802	2.5876	1.1169	0.1400E+01	0.2406E+00
804	1.9481	1.1843	0.1750E+01	0.1803E+00
806	1.3477	1.2441	0.2048E+01	0.1555E+00
808	0.9518	1.2989	0.2185E+01	0.1273E+00
810	0.7625	1.3483	0.1919E+01	0.1001E+00
812	0.7728	1.3915	0.1587E+01	0.8069E-01
814	0.8443	1.4294	0.1[illegible]E+01	0.6732E-01
816	0.9343	1.4625	0.9080E+00	0.5920E-01
818	1.0239	1.4917	0.6208E+00	0.5128E-01
820	1.1098	1.5173	0.3934E+00	0.4477E-01
822	1.1894	1.5397	0.2376E+00	0.3968E-01
824	1.2617	1.5599	0.1445E+00	0.3570E-01

Wn	No	Ne	Ko	Ke
826	1.3257	1.5783	0.9987E-01	0.3258E-01
828	1.3813	1.5952	0.8436E-01	0.3013E-01
830	1.4290	1.6108	0.7296E-01	0.2817E-01
832	1.4695	1.6260	0.6378E-01	0.2659E-01
834	1.5037	1.6406	0.5640E-01	0.2529E-01
836	1.5326	1.6547	0.5046E-01	0.2418E-01
838	1.5570	1.6686	0.4564E-01	0.2322E-01
840	1.5779	1.6824	0.4170E-01	0.2237E-01
842	1.5962	1.6960	0.3843E-01	0.2159E-01
844	1.6126	1.7094	0.3568E-01	0.2087E-01
846	1.6277	1.7228	0.3332E-01	0.2019E-01
848	1.6420	1.7360	0.3125E-01	0.1957E-01
850	1.6559	1.7489	0.2943E-01	0.1898E-01
852	1.6697	1.7615	0.2779E-01	0.1844E-01
854	1.6836	1.7738	0.2631E-01	0.1795E-01
856	1.6978	1.7856	0.2499E-01	0.1750E-01
858	1.7122	1.7971	0.2381E-01	0.1709E-01
860	1.7269	1.8080	0.2278E-01	0.1673E-01
862	1.7418	1.8183	0.2182E-01	0.1641E-01
864	1.7568	1.8282	0.2114E-01	0.1613E-01
866	1.7720	1.8375	0.2062E-01	0.1588E-01
868	1.7870	1.8462	0.2022E-01	0.1566E-01
870	1.8019	1.8544	0.1990E-01	0.1546E-01
872	1.8165	1.8621	0.1963E-01	0.1528E-01
874	1.8307	1.8694	0.1937E-01	0.1510E-01
876	1.8445	1.8761	0.1911E-01	0.1492E-01
878	1.8577	1.8825	0.1883E-01	0.1475E-01
880	1.8704	1.8886	0.1850E-01	0.1457E-01
882	1.8824	1.8944	0.1813E-01	0.1440E-01
884	1.8938	1.9000	0.1770E-01	0.1429E-01
886	1.9047	1.9054	0.1743E-01	0.1427E-01
888	1.9149	1.9107	0.1725E-01	0.1425E-01
890	1.9246	1.9160	0.1711E-01	0.1423E-01
892	1.9338	1.9213	0.1699E-01	0.1422E-01
894	1.9426	1.9267	0.1690E-01	0.1422E-01
896	1.9510	1.9321	0.1683E-01	0.1423E-01
898	1.9591	1.9378	0.1679E-01	0.1426E-01
900	1.9671	1.9437	0.1677E-01	0.1429E-01
902	1.9749	1.9497	0.1677E-01	0.1435E-01
904	1.9827	1.9560	0.1680E-01	0.1441E-01
906	1.9906	1.9625	0.1684E-01	0.1450E-01
908	1.9986	1.9693	0.1691E-01	0.1460E-01
910	2.0067	1.9764	0.1699E-01	0.1471E-01
912	2.0151	1.9837	0.1709E-01	0.1485E-01
914	2.0237	1.9912	0.1721E-01	0.1500E-01
916	2.0327	1.9990	0.1734E-01	0.1516E-01
918	2.0420	2.0070	0.1749E-01	0.1535E-01
920	2.0517	2.0152	0.1766E-01	0.1555E-01
922	2.0617	2.0235	0.1784E-01	0.1576E-01
924	2.0721	2.0320	0.1803E-01	0.1599E-01
926	2.0828	2.0406	0.1823E-01	0.1623E-01
928	2.0938	2.0493	0.1845E-01	0.1649E-01
930	2.1051	2.0580	0.1867E-01	0.1677E-01

Wn	No	Ne	Ko	Ke
932	2.1167	2.0668	0.1891E-01	0.1705E-01
934	2.1284	2.0756	0.1915E-01	0.1736E-01
936	2.1404	2.0844	0.1941E-01	0.1767E-01
938	2.1524	2.0932	0.1972E-01	0.1800E-01
940	2.1645	2.1019	0.2001E-01	0.1834E-01
942	2.1767	2.1107	0.2028E-01	0.1870E-01
944	2.1888	2.1194	0.2056E-01	0.1907E-01
946	2.2009	2.1281	0.2086E-01	0.1945E-01
948	2.2129	2.1369	0.2122E-01	0.1984E-01
950	2.2249	2.1456	0.2166E-01	0.2025E-01
952	2.2367	2.1544	0.2218E-01	0.2067E-01
954	2.2484	2.1633	0.2278E-01	0.2111E-01
956	2.2600	2.1723	0.2344E-01	0.2156E-01
958	2.2715	2.1814	0.2414E-01	0.2203E-01
960	2.2830	2.1908	0.2485E-01	0.2252E-01
962	2.2944	2.2004	0.2555E-01	0.2302E-01
964	2.3059	2.2103	0.2623E-01	0.2355E-01
966	2.3174	2.2206	0.2687E-01	0.2409E-01
968	2.3291	2.2314	0.2748E-01	0.2466E-01
970	2.3410	2.2426	0.2808E-01	0.2525E-01
972	2.3532	2.2543	0.2868E-01	0.2586E-01
974	2.3658	2.2667	0.2930E-01	0.2651E-01
976	2.3789	2.2796	0.2996E-01	0.2718E-01
978	2.3926	2.2934	0.3069E-01	0.2788E-01
980	2.4071	2.3078	0.3149E-01	0.2861E-01
982	2.4223	2.3230	0.3236E-01	0.2938E-01
984	2.4385	2.3390	0.3331E-01	0.3019E-01
986	2.4557	2.3560	0.3431E-01	0.3104E-01
988	2.4740	2.3738	0.3536E-01	0.3193E-01
990	2.4936	2.3925	0.3642E-01	0.3287E-01
992	2.5145	2.4121	0.3751E-01	0.3386E-01
994	2.5368	2.4326	0.3861E-01	0.3490E-01
996	2.5606	2.4540	0.3974E-01	0.3600E-01
998	2.5860	2.4763	0.4093E-01	0.3716E-01
1000	2.6129	2.4995	0.4221E-01	0.3838E-01
1002	2.6416	2.5236	0.4363E-01	0.3967E-01
1004	2.6719	2.5484	0.4523E-01	0.4103E-01
1006	2.7041	2.5741	0.4705E-01	0.4246E-01
1008	2.7381	2.6005	0.4909E-01	0.4398E-01
1010	2.7739	2.6277	0.5135E-01	0.4558E-01
1012	2.8114	2.6556	0.5377E-01	0.4726E-01
1014	2.8508	2.6843	0.5628E-01	0.4904E-01
1016	2.8921	2.7136	0.5878E-01	0.5092E-01
1018	2.9353	2.7434	0.6119E-01	0.5289E-01
1020	2.9805	2.7741	0.6343E-01	0.5498E-01
1022	3.0276	2.8056	0.6552E-01	0.5717E-01
1024	3.0770	2.8382	0.6760E-01	0.5949E-01
1026	3.1285	2.8718	0.6990E-01	0.6192E-01
1028	3.1824	2.9058	0.7282E-01	0.6448E-01
1030	3.2390	2.9413	0.7677E-01	0.6718E-01
1032	3.2985	2.9788	0.8205E-01	0.7002E-01
1034	3.3612	3.0185	0.8847E-01	0.7298E-01
1036	3.4279	3.0608	0.9433E-01	0.7604E-01

Wn	No	Ne	Ko	Ke
1038	3.4987	3.1049	0.9813E-01	0.7969E-01
1040	3.5745	3.1524	0.1026E+00	0.8660E-01
1042	3.6563	3.2044	0.1078E+00	0.9404E-01
1044	3.7448	3.2617	0.1138E+00	0.1004E+00
1046	3.8414	3.3251	0.1204E+00	0.1054E+00
1048	3.9473	3.3952	0.1278E+00	0.1104E+00
1050	4.0641	3.4733	0.1359E+00	0.1169E+00
1052	4.1938	3.5609	0.1447E+00	0.1264E+00
1054	4.3383	3.6595	0.1549E+00	0.1398E+00
1056	4.5000	3.7709	0.1816E+00	0.1569E+00
1058	4.6817	3.8970	0.2278E+00	0.1772E+00
1060	4.8868	4.0423	0.2958E+00	0.1993E+00
1062	5.1183	4.2070	0.3867E+00	0.2226E+00
1064	5.3915	4.3932	0.5004E+00	0.2470E+00
1066	5.8107	4.6037	0.6361E+00	0.2742E+00
1068	6.1615	4.8416	0.7922E+00	0.3080E+00
1070	6.2521	5.1683	0.9665E+00	0.3546E+00
1072	5.8914	5.7243	0.1156E+01	0.4222E+00
1074	5.3468	6.2999	0.1359E+01	0.5213E+00
1076	4.7516	6.8315	0.1571E+01	0.6628E+00
1078	4.1730	7.2376	0.1790E+01	0.8579E+00
1080	3.5630	7.4285	0.2012E+01	0.1116E+01
1082	2.9101	7.3536	0.2236E+01	0.1444E+01
1084	2.2775	6.9168	0.2457E+01	0.1841E+01
1086	1.7544	6.0947	0.2674E+01	0.2303E+01
1088	1.3545	4.4582	0.2886E+01	0.2816E+01
1090	1.0586	2.0352	0.3091E+01	0.3359E+01
1092	0.8398	1.0851	0.3289E+01	0.3904E+01
1094	0.6843	0.8502	0.3480E+01	0.4419E+01
1096	0.5745	0.7317	0.3666E+01	0.4869E+01
1098	0.4957	0.6344	0.3848E+01	0.5227E+01
1100	0.4436	0.5516	0.4026E+01	0.5482E+01
1102	0.4096	0.4879	0.4235E+01	0.5649E+01
1104	0.3845	0.4411	0.4235E+01	0.5788E+01
1106	0.3632	0.4049	0.4143E+01	0.5789E+01
1108	0.3427	0.3730	0.4041E+01	0.5645E+01
1110	0.3219	0.3423	0.3938E+01	0.5403E+01
1112	0.2962	0.3132	0.3833E+01	0.5110E+01
1114	0.2665	0.2876	0.3727E+01	0.4811E+01
1116	0.2396	0.2672	0.3620E+01	0.4554E+01
1118	0.2204	0.2526	0.3513E+01	0.4354E+01
1120	0.2089	0.2425	0.3405E+01	0.4163E+01
1122	0.1978	0.2348	0.3297E+01	0.3982E+01
1124	0.1869	0.2272	0.3189E+01	0.3808E+01
1126	0.1760	0.2181	0.3081E+01	0.3644E+01
1128	0.1659	0.2068	0.2974E+01	0.3487E+01
1130	0.1566	0.1938	0.2868E+01	0.3338E+01
1132	0.1482	0.1804	0.2762E+01	0.3197E+01
1134	0.1411	0.1680	0.2658E+01	0.3063E+01
1136	0.1355	0.1575	0.2555E+01	0.2937E+01
1138	0.1316	0.1481	0.2453E+01	0.2817E+01
1140	0.1296	0.1309	0.2353E+01	0.2704E+01
1142	0.1298	0.1172	0.2255E+01	0.2597E+01

Wn	No	Ne	Ko	Ke
1144	0.1331	0.1056	0.2159E+01	0.2497E+01
1146	0.1398	0.0954	0.2065E+01	0.2402E+01
1148	0.1499	0.0865	0.1973E+01	0.2313E+01
1150	0.1641	0.0783	0.1884E+01	0.2229E+01
1152	0.1839	0.0707	0.1797E+01	0.2150E+01
1154	0.2091	0.0621	0.1714E+01	0.2076E+01
1156	0.2407	0.0544	0.1633E+01	0.2007E+01
1158	0.2791	0.0474	0.1556E+01	0.1942E+01
1160	0.3255	0.0413	0.1483E+01	0.1880E+01
1162	0.3808	0.0360	0.1475E+01	0.1823E+01
1164	0.4455	0.0313	0.1494E+01	0.1768E+01
1166	0.5558	0.0272	0.1506E+01	0.1717E+01
1168	0.5856	0.0234	0.1507E+01	0.1669E+01
1170	0.6021	0.0202	0.1503E+01	0.1624E+01
1172	0.6098	0.0177	0.1494E+01	0.1581E+01
1174	0.5719	0.0157	0.1519E+01	0.1541E+01
1176	0.5842	0.0142	0.1556E+01	0.1502E+01
1178	0.4636	0.0132	0.1545E+01	0.1465E+01
1180	0.4020	0.0128	0.1541E+01	0.1430E+01
1182	0.3420	0.0133	0.1519E+01	0.1396E+01
1184	0.2867	0.0141	0.1491E+01	0.1364E+01
1186	0.2376	0.0153	0.1461E+01	0.1332E+01
1188	0.1954	0.0170	0.1430E+01	0.1301E+01
1190	0.1602	0.0191	0.1394E+01	0.1271E+01
1192	0.1337	0.0217	0.1355E+01	0.1242E+01
1194	0.1131	0.0247	0.1312E+01	0.1213E+01
1196	0.0977	0.0280	0.1268E+01	0.1184E+01
1198	0.0874	0.0319	0.1222E+01	0.1156E+01
1200	0.0829	0.0365	0.1176E+01	0.1127E+01
1202	0.0811	0.0417	0.1131E+01	0.1099E+01
1204	0.0815	0.0477	0.1087E+01	0.1070E+01
1206	0.0838	0.0545	0.1045E+01	0.1041E+01
1208	0.0877	0.0620	0.1006E+01	0.1012E+01
1210	0.0928	0.0697	0.9693E+00	0.9828E+00
1212	0.0987	0.0781	0.9347E+00	0.9529E+00
1214	0.1038	0.0871	0.9022E+00	0.9226E+00
1216	0.1089	0.0966	0.8714E+00	0.8918E+00
1218	0.1140	0.1065	0.8417E+00	0.8606E+00
1220	0.1189	0.1169	0.8128E+00	0.8289E+00
1222	0.1231	0.1274	0.7839E+00	0.7968E+00
1224	0.1275	0.1366	0.7547E+00	0.7642E+00
1226	0.1323	0.1452	0.7248E+00	0.7312E+00
1228	0.1385	0.1536	0.6937E+00	0.6978E+00
1230	0.1464	0.1618	0.6613E+00	0.6641E+00
1232	0.1548	0.1700	0.6274E+00	0.6302E+00
1234	0.1633	0.1783	0.5921E+00	0.5961E+00
1236	0.1690	0.1869	0.5554E+00	0.5619E+00
1238	0.1735	0.1965	0.5176E+00	0.5277E+00
1240	0.1787	0.2089	0.4791E+00	0.4936E+00
1242	0.1856	0.2224	0.4403E+00	0.4597E+00
1244	0.1995	0.2368	0.4016E+00	0.4263E+00
1246	0.2175	0.2523	0.3637E+00	0.3933E+00
1248	0.2388	0.2689	0.3270E+00	0.3610E+00

Wn	No	Ne	Ko	Ke
1250	0.2627	0.2864	0.2922E+00	0.3295E+00
1252	0.2862	0.3050	0.2597E+00	0.2990E+00
1254	0.3109	0.3244	0.2299E+00	0.2697E+00
1256	0.3366	0.3446	0.2032E+00	0.2417E+00
1258	0.3628	0.3656	0.1799E+00	0.2154E+00
1260	0.3884	0.3873	0.1600E+00	0.1908E+00
1262	0.4139	0.4096	0.1434E+00	0.1681E+00
1264	0.4392	0.4323	0.1300E+00	0.1479E+00
1266	0.4639	0.4554	0.1194E+00	0.1305E+00
1268	0.4879	0.4786	0.1113E+00	0.1250E+00
1270	0.5113	0.5009	0.1049E+00	0.1171E+00
1272	0.5338	0.5220	0.9987E-01	0.1103E+00
1274	0.5556	0.5426	0.9544E-01	0.1038E+00
1276	0.5765	0.5626	0.9110E-01	0.9779E-01
1278	0.5966	0.5821	0.8648E-01	0.9222E-01
1280	0.6159	0.6008	0.8143E-01	0.8704E-01
1282	0.6342	0.6189	0.7567E-01	0.8224E-01
1284	0.6518	0.6361	0.7061E-01	0.7777E-01
1286	0.6686	0.6526	0.6645E-01	0.7363E-01
1288	0.6846	0.6681	0.6299E-01	0.6979E-01
1290	0.6997	0.6829	0.6005E-01	0.6623E-01
1292	0.7143	0.6969	0.5750E-01	0.6293E-01
1294	0.7281	0.7103	0.5524E-01	0.5987E-01
1296	0.7413	0.7231	0.5318E-01	0.5704E-01
1298	0.7539	0.7358	0.5128E-01	0.5441E-01
1300	0.7659	0.7480	0.4950E-01	0.5197E-01
1302	0.7775	0.7597	0.4781E-01	0.4971E-01
1304	0.7885	0.7709	0.4619E-01	0.4761E-01
1306	0.7991	0.7817	0.4463E-01	0.4566E-01
1308	0.8093	0.7921	0.4312E-01	0.4386E-01
1310	0.8191	0.8020	0.4168E-01	0.4217E-01
1312	0.8286	0.8116	0.4029E-01	0.4061E-01
1314	0.8378	0.8211	0.3895E-01	0.3915E-01
1316	0.8467	0.8304	0.3767E-01	0.3780E-01
1318	0.8554	0.8393	0.3645E-01	0.3653E-01
1320	0.8638	0.8480	0.3529E-01	0.3534E-01
1322	0.8720	0.8563	0.3418E-01	0.3423E-01
1324	0.8800	0.8644	0.3313E-01	0.3318E-01
1326	0.8879	0.8722	0.3213E-01	0.3220E-01
1328	0.8956	0.8798	0.3118E-01	0.3128E-01
1330	0.9032	0.8871	0.3027E-01	0.3040E-01
1332	0.9106	0.8944	0.2941E-01	0.2957E-01
1334	0.9179	0.9014	0.2858E-01	0.2879E-01
1336	0.9251	0.9083	0.2779E-01	0.2804E-01
1338	0.9322	0.9149	0.2702E-01	0.2732E-01
1340	0.9392	0.9213	0.2628E-01	0.2664E-01
1342	0.9461	0.9276	0.2556E-01	0.2598E-01
1344	0.9530	0.9337	0.2486E-01	0.2535E-01
1346	0.9597	0.9397	0.2418E-01	0.2475E-01
1348	0.9664	0.9454	0.2351E-01	0.2416E-01
1350	0.9730	0.9512	0.2285E-01	0.2360E-01
1352	0.9795	0.9568	0.2221E-01	0.2305E-01
1354	0.9859	0.9622	0.2158E-01	0.2252E-01

Wn	No	Ne	Ko	Ke
1356	0.9922	0.9675	0.2097E-01	0.2201E-01
1358	0.9984	0.9727	0.2037E-01	0.2151E-01
1360	1.0046	0.9778	0.1979E-01	0.2102E-01
1362	1.0106	0.9828	0.1923E-01	0.2055E-01
1364	1.0166	0.9877	0.1869E-01	0.2009E-01
1366	1.0224	0.9925	0.1817E-01	0.1964E-01
1368	1.0281	0.9972	0.1768E-01	0.1920E-01
1370	1.0338	1.0019	0.1721E-01	0.1877E-01
1372	1.0393	1.0064	0.1677E-01	0.1836E-01
1374	1.0447	1.0109	0.1635E-01	0.1796E-01
1376	1.0500	1.0153	0.1595E-01	0.1757E-01
1378	1.0552	1.0196	0.1559E-01	0.1719E-01
1380	1.0602	1.0239	0.1524E-01	0.1682E-01
1382	1.0652	1.0281	0.1491E-01	0.1647E-01
1384	1.0700	1.0322	0.1460E-01	0.1612E-01
1386	1.0747	1.0363	0.1431E-01	0.1579E-01
1388	1.0792	1.0404	0.1403E-01	0.1547E-01
1390	1.0837	1.0444	0.1375E-01	0.1516E-01
1392	1.0880	1.0483	0.1349E-01	0.1486E-01
1394	1.0921	1.0522	0.1323E-01	0.1458E-01
1396	1.0962	1.0560	0.1297E-01	0.1431E-01
1398	1.1001	1.0598	0.1272E-01	0.1405E-01
1400	1.1039	1.0636	0.1246E-01	0.1380E-01
1402	1.1076	1.0673	0.1221E-01	0.1357E-01
1404	1.1112	1.0710	0.1197E-01	0.1334E-01
1406	1.1146	1.0746	0.1174E-01	0.1313E-01
1408	1.1180	1.0782	0.1151E-01	0.1293E-01
1410	1.1212	1.0818	0.1131E-01	0.1274E-01
1412	1.1243	1.0853	0.1112E-01	0.1256E-01
1414	1.1273	1.0888	0.1095E-01	0.1239E-01
1416	1.1302	1.0923	0.1081E-01	0.1223E-01
1418	1.1330	1.0958	0.1067E-01	0.1208E-01
1420	1.1358	1.0992	0.1055E-01	0.1193E-01
1422	1.1384	1.1025	0.1040E-01	0.1179E-01
1424	1.1410	1.1059	0.1022E-01	0.1166E-01
1426	1.1434	1.1092	0.9944E-02	0.1153E-01
1428	1.1458	1.1125	0.9518E-02	0.1140E-01
1430	1.1482	1.1158		0.1128E-01
1432	1.1505	1.1191		0.1115E-01
1434	1.1527	1.1223		0.1102E-01
1436	1.1549	1.1255		0.1089E-01
1438	1.1570	1.1287		0.1076E-01
1440	1.1591	1.1319		0.1061E-01
1442	1.1611	1.1350		0.1046E-01
1444	1.1631	1.1381		0.1029E-01
1446	1.1651	1.1412		
1448	1.1670	1.1443		
1450	1.1690	1.1473		
1452	1.1709	1.1503		
1454	1.1728	1.1533		
1456	1.1747	1.1563		
1458	1.1766	1.1593		
1460	1.1785	1.1622		

Wn	No	Ne
1462	1.1804	1.1651
1464	1.1823	1.1680
1466	1.1843	1.1708
1468	1.1862	1.1737
1470	1.1881	1.1765
1472	1.1901	1.1793
1474	1.1920	1.1820
1476	1.1940	1.1848
1478	1.1960	1.1875
1480	1.1980	1.1902
1482	1.2000	1.1929
1484	1.2021	1.1955
1486	1.2042	1.1982
1488	1.2062	1.2008
1490	1.2083	1.2033
1492	1.2104	1.2059
1494	1.2125	1.2084
1496	1.2147	1.2109
1498	1.2168	1.2134
1500	1.2189	1.2159
1502	1.2211	1.2183
1504	1.2232	1.2207
1506	1.2254	1.2231
1508	1.2275	1.2254
1510	1.2296	1.2278
1512	1.2317	1.2301
1514	1.2338	1.2323
1516	1.2359	1.2346
1518	1.2380	1.2368
1520	1.2400	1.2390
1522	1.2421	1.2412
1524	1.2441	1.2433
1526	1.2460	1.2455
1528	1.2479	1.2475
1530	1.2498	1.2496
1532	1.2517	1.2517
1534	1.2535	1.2537
1536	1.2552	1.2557
1538	1.2569	1.2577
1540	1.2586	1.2596
1542	1.2602	1.2615
1544	1.2617	1.2634
1546	1.2632	1.2653
1548	1.2646	1.2672
1550	1.2660	1.2690
1552	1.2673	1.2708
1554	1.2686	1.2726
1556	1.2697	1.2743
1558	1.2709	1.2761
1560	1.2719	1.2778
1562	1.2729	1.2795
1564	1.2739	1.2811
1566	1.2747	1.2828

Wn	No	Ne
1568	1.2755	1.2844
1570	1.2763	1.2860
1572	1.2770	1.2876
1574	1.2777	1.2892
1576	1.2783	1.2907
1578	1.2788	1.2923
1580	1.2793	1.2938
1582	1.2798	1.2953
1584	1.2802	1.2968
1586	1.2806	1.2982
1588	1.2810	1.2997
1590	1.2813	1.3011
1592	1.2817	1.3026
1594	1.2820	1.3040
1596	1.2823	1.3054
1598	1.2826	1.3068
1600	1.2830	1.3081
1602	1.2833	1.3095
1604	1.2836	1.3109
1606	1.2840	1.3122
1608	1.2843	1.3136
1610	1.2848	1.3149
1612	1.2852	1.3163
1614	1.2857	1.3176
1616	1.2862	1.3189
1618	1.2868	1.3202
1620	1.2875	1.3216
1622	1.2882	1.3229
1624	1.2890	1.3242
1626	1.2898	1.3255
1628	1.2907	1.3268
1630	1.2917	1.3282
1632	1.2928	1.3295
1634	1.2940	1.3308
1636	1.2952	1.3322
1638	1.2965	1.3336
1640	1.2978	1.3350
1642	1.2993	1.3364
1644	1.3008	1.3378
1646	1.3024	1.3392
1648	1.3041	1.3406
1650	1.3057	1.3421
1652	1.3074	1.3435
1654	1.3092	1.3449
1656	1.3109	1.3464
1658	1.3126	1.3478
1660	1.3143	1.3493
1662	1.3161	
1664	1.3179	
1666	1.3197	

Blank

G. REFERENCES

1. Larry L. Long, R. J. Bell, R. W. Alexander, Jr., and Marvin R. Querry, "Preparation dependent properties of pressed pellets of montmorillonite in the far infrared", Applied Optics 26, 1372 (1987).

2. L. L. Long, R. J. Bell, R. W. Alexander, Jr., and M. R. Querry, "Optical Constants of Gypsum and Calcite Single Crystals and Powders", to be published.

3. G. Brandli and A. J. Sievers, "Absolute Measurement of the Far-Infrared Surface Resistance of Pb," Phys. Rev. B5, 3550 (1972).

4. M. A. Ordal, Robert J. Bell, R. W. Alexander, Jr., L. L. Long, and M. R. Querry, "Optical Properties of fourteen metals in the infrared and far infrared: Al, Co, Cu, Fe, Pb, Mo, Ni, Pd, Pt, Ag, Ti, V, and W", Applied Optics 24, 4493 (1985).

5. Mark A. Ordal, Robert J. Bell, Ralph W. Alexander, Jr., Larry L. Long, and Marvin R. Querry, "Optical Properties of Au, Ni, and Pb at submillimeter wavelengths", Applied Optics, 26, 744 (1987).

6. Mark A. Ordal, Robert J. Bell, Ralph W. Alexander, Jr., and Raymond E. Paul, "Absorption Coefficient of Dupont Teflon FEP in the 20 - 130 wave-number range, Appl. Opt. 24, 2746 (1985).

7. E. E. Russell and E. E. Bell, J. Opt. Soc. Am. 57, 341 (1967).

8. W. G. Spitzer and D. A. Kleinman, Phys. Rev. 121, 1324 (1961).

9. R. J. Bell, R. Van Diver, and R. W. Alexander, Jr., Proceedings of the CRDEC Scientific Conference on Obscuration and Aerosol Research, E. Steubbing, editor, Aberdeen, MD, June 1987 (to be published.)

10. J. H. Weaver, C. Krafka, D. W. Lynch, and D. D. Koch, Physics Data, Optical Properties of Metals, Part I: The Transition Metals and Part II: The Noble Metals, Aluminum, Scandium, Yttrium, The Lanthanides, and the Actinides, (Fachinformationszentrum, Karlsruhe, Federal Republic of Germany, 1981).

11. L. A. Newquist, R. J. Bell, and R. W. Alexander, Jr., Proceedings of the CRDEC Scientific Conference on Obscuration and Aerosol Research, E. Stuebbing, editor, Aberdeen, MD, June 1987 (to be published).

Blank

III. PAPERS PUBLISHED UNDER THIS CONTRACT

1. M. A. Ordal, R. J. Bell, Ralph W. Alexander, Jr., and R. E. Paul, "Absorption coefficient of Dupont Teflon FEP in the 20-130 wave-number range", Appl. Opt. 24, 2746 (1985).

2. R. J. Bell, M. A. Ordal, and R. W. Alexander, Jr., "Equations Linking Different Sets of Optical Constants for Nonmagnetic Materials," Appl. Opt. 24, 3680 (1985).

3. M. A. Ordal, R. J. Bell, R. W. Alexander, Jr., L. L. Long, and M. R. Querry, Optical Properties of fourteen metals in the infrared and far infrared: Al, Co, Cu, Au, Fe, Pb, Mo, Ni, Pd, Pt, Ag, Ti, V, and W", Appl. Opt. 24, 4493 (1985).

4. M. A. Ordal, R. J. Bell, R. W. Alexander, L. L. Long, and M. R. Querry, "Optical Properties of Au, Ni, and Pb at Submillimeter Wavelengths", Appl. Opt. 26, 744 (1987).

5. L. L. Long, R. J. Bell, R. W. Alexander, Jr., and M. R. Querry, "Preparation Dependent Properties of Pressed Pellets of Montmorillonite in the Far Infrared," Appl. Opt. 26, 1372 (1987).

Papers in the Procedings of the CRDEC Scientific Conference on Obscuration and Aerosol Research.

1. L. L. Long, R. J. Bell, M. A. Ordal, R. W. Alexander, Jr., and M. R. Querry, "Optical properties of natural minerals in the far infrared and submillimeter wavelength regions, Proceedings of the 1985 CRDC Scientific Conference on Obscuration and Aerosol Research, Ronald H. Kohl, editor, p. 255.

2. R. J. Bell, R. W. Alexander, Jr., M. A. Ordal, L. L. Long, and M. R. Querry, "Optical properties of NI: Cavity measurements at FIR and submm wavelength ranges; resistivity ratios, and linkage equations," Proceedings of the 1985 CRDC Scientific Conference on Obscuration and Aerosol Research, Ronald H. Kohl, editor, p. 275.

3. R. W. Alexander, Jr., R. W. Bell, L. L. Long, M. A. Ordal, L. Newquist, and M. R. Querry, "Optical Properties of Powders, Liquids, and Metals at Millimeter and Submillimeter Wavelengths," Proceedings of the 1986 CRDEC Scientific Conference on Obscuration and Aerosol Research, R. W. Kohl, editor.

4. R. J. Bell, R. W. Alexander, Jr., Larry Newquist, and Mark A. Ordal, "Methods for measuring surface impedances in the submillimeter and far infrared," Proceedings of the 1986 CRDEC Scientific Conference on Obscuration and Aerosol Research.

Blank

2.7 References.

1. Larry L. Long, R. J. Bell, R. W. Alexander, Jr., and Marvin R. Querry, "Preparation dependent properties of pressed pellets of montmorillonite in the far infrared", Applied Optics 26, 1372 (1987).

2. L. L. Long, R. J. Bell, R. W. Alexander, Jr., and M. R. Querry, "Optical Constants of Gypsum and Calcite Single Crystals and Powders", to be published.

3. G. Brandli and A. J. Sievers, "Absolute Measurement of the Far-Infrared Surface Resistance of Pb," Phys. Rev. B5, 3550 (1972).

4. M. A. Ordal, Robert J. Bell, R. W. Alexander, Jr., L. L. Long, and M. R. Querry, "Optical Properties of fourteen metals in the infrared and far infrared: Al, Co, Cu, Fe, Pb, Mo, Ni, Pd, Pt, Ag, Ti, V, and W", Applied Optics 24, 4493 (1985).

5. Mark A. Ordal, Robert J. Bell, Ralph W. Alexander, Jr., Larry L. Long, and Marvin R. Querry, "Optical Properties of Au, Ni, and Pb at submillimeter wavelengths", Applied Optics, 26, 744 (1987).

6. Mark A. Ordal, Robert J. Bell, Ralph W. Alexander, Jr., and Raymond E. Paul, "Absorption Coefficient of Dupont Teflon FEP in the 20 - 130 wave-number range, Appl. Opt. 24, 2746 (1985).

7. E. E. Russell and E. E. Bell, J. Opt. Soc. Am. 57, 341 (1967).

8. W. G. Spitzer and D. A. Kleinman, Phys. Rev. 121, 1324 (1961).

9. R. J. Bell, R. Van Diver, and R. W. Alexander, Jr., Proceedings of the CRDEC Scientific Conference on Obscuration and Aerosol Research, E. Steubbing, editor, Aberdeen, MD, June 1987 (to be published.)

10. J. H. Weaver, C. Krafka, D. W. Lynch, and D. D. Koch, Physics Data, Optical Properties of Metals, Part I: The Transition Metals and Part II: The Noble Metals, Aluminum, Scandium, Yttrium, The Lanthanides, and the Actinides, (Fachinformationszentrum, Karlsruhe, Federal Republic of Germany, 1981)

11. L. A. Newquist, R. J. Bell, and R. W. Alexander, Jr., Proceedings of the CRDEC Scientific Conference on Obscuration and Aerosol Research, E. Stuebbing, editor, Aberdeen, MD, June 1987 (to be published).

3. PAPERS PUBLISHED UNDER THIS CONTRACT

1. M. A. Ordal, R. J. Bell, Ralph W. Alexander, Jr., and R. E. Paul, "Absorption coefficient of Dupont Teflon FEP in the 20-130 wave-number range", Appl. Opt. 24, 2746 (1985).

2. R. J. Bell, M. A. Ordal, and R. W. Alexander, Jr., "Equations Linking Different Sets of Optical Constants for Nonmagnetic Materials," Appl. Opt. 24, 3680 (1985).

3. M. A. Ordal, R. J. Bell, R. W. Alexander, Jr., L. L. Long, and M. R. Querry, Optical Properties of fourteen metals in the infrared and far infrared: Al, Co, Cu, Au, Fe, Pb, Mo, Ni, Pd, Pt, Ag, Ti, V, and W", Appl. Opt. 24, 4493 (1985).

4. M. A. Ordal, R. J. Bell, R. W. Alexander, L. L. Long, and M. R. Querry, "Optical Properties of Au, Ni, and Pb at Submillimeter Wavelengths", Appl. Opt. 26, 744 (1987).

5. L. L. Long, R. J. Bell, R. W. Alexander, Jr., and M. R. Querry, "Preparation Dependent Properties of Pressed Pellets of Montmorillonite in the Far Infrared," Appl. Opt. 26, 1372 (1987).

Papers in the Procedings of the CRDEC Scientific Conference on Obscuration and Aerosol Research.

1. L. L. Long, R. J. Bell, M. A. Ordal, R. W. Alexander, Jr., and M. R. Querry, "Optical properties of natural minerals in the far infrared and submillimeter wavelength regions, Proceedings of the 1985 CRDC Scientific Conference on Obscuration and Aerosol Research, Ronald H. Kohl, editor, p. 255.

2. R. J. Bell, R. W. Alexander, Jr., M. A. Ordal, L. L. Long, and M. R. Querry, "Optical properties of NI: Cavity measurements at FIR and submm wavelength ranges; resistivity ratios, and linkage equations," Proceedings of the 1985 CRDC Scientific Conference on Obscuration and Aerosol Research, Ronald H. Kohl, editor, p. 275.

3. R. W. Alexander, Jr., R. W. Bell, L. L. Long, M. A. Ordal, L. Newquist, and M. R. Querry, "Optical Properties of Powders, Liquids, and Metals at Millimeter and Submillimeter Wavelengths," Proceedings of the 1986 CRDEC Scientific Conference on Obscuration and Aerosol Research, R. W. Kohl, editor.

4. R. J. Bell, R. W. Alexander, Jr., Larry Newquist, and Mark A. Ordal, "Methods for measuring surface impedances in the submillimeter and far infrared," Proceedings of the 1986 CRDEC Scientific Conference on Obscuration and Aerosol Research.

APPENDIX A

REPRINTS OF PAPERS

PUBLISHED

Reprinted from Applied Optics, Vol. 24, page 2746, September 1, 1985

Absorption coefficient of Dupont Teflon FEP in the 20–130 wave-number range

Mark A. Ordal, Robert J. Bell, Ralph W. Alexander, Jr., and Raymond E. Paul

When this work was done all the authors were with University of Missouri-Rolla, Physics Department, Rolla, Missouri 65401; R. E. Paul is now with Naval Underwater Systems Center, New London, Connecticut 06320.
Received 1 June 1985.
0003-6935/85/172746-01$02.00/0.

Table I. Measured Values of the Absorption Coefficient of Teflon FEP Film

ω (cm^{-1})	λ (μm)	α (Npr/cm)	Stand. Dev. of α
22	465	0.505	0.059
32	310	0.676	0.047
43	232	0.936	0.042
54	186	1.212	0.041
65	155	1.480	0.040
75	133	1.804	0.037
86	116	2.156	0.034
97	103	2.509	0.036
108	93	2.985	0.040
118	85	3.712	0.042
129	78	4.646	0.053

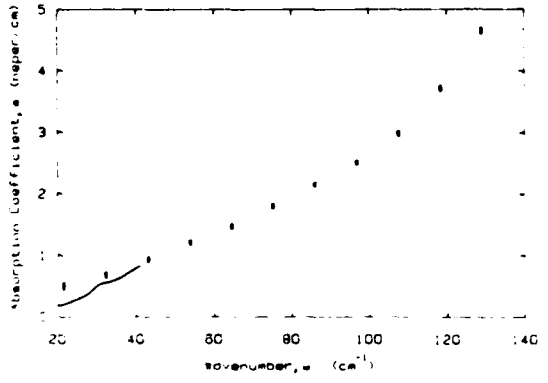

Fig. 1. $\alpha(\omega)$ for Teflon. The solid circles with error bars are the data of Table I for Teflon FEP. The solid line is the data of Chantry[5] for Teflon TFE.

In certain applications[1,2] one needs to know the absorption coefficient of a dielectric film for radiation propagating through it parallel to the surface of the film. We have made such measurements on Dupont Teflon FEP (fluorinated ethylene propylene).[3]

The absorption coefficient of Teflon FEP was measured with a RIIC FS-720 Fourier spectrometer in the 20–130-cm^{-1} region. Samples consisted of 2.5-cm high × 5-cm wide stacks of 25.4-μm Teflon FEP film clamped between thick metal plates. Radiation passed through the stacks parallel to the layers of Teflon FEP film. Three samples were used with lengths of 0.724, 0.916, and 1.782 cm.

Samples were run in permuted order to obtain 18 runs for each of the three pairings of samples. This procedure resulted in 54 data points at each frequency ω. These data points defined the ratio of measured intensities as a function of ΔL, the difference in sample length. The absorption coefficient $\alpha(\omega)$ was obtained by fitting the 54 data points at each frequency ω to the function

$$(I_1/I_2) = \exp[\alpha(\omega)(L_2 - L_1)] = \exp[\alpha(\omega)(\Delta L)], \quad (1)$$

where I_1 was the intensity measured through a sample of length L_1 cm, I_2 is the intensity for a sample of length L_2 cm, etc.

Table I lists our values for the absorption coefficient α of Teflon FEP along with the standard deviation obtained from our fit program.[4] Figure 1 shows α vs ω, with the error bars representing the standard deviation in our measurements.

The values for the absorption coefficient of Teflon TFE (polytetrafluorethylene) found in the literature[5] differ somewhat from our values for the absorption coefficient of Teflon FEP. The solid line in Fig. 1 is the data on Teflon TFE of Chantry.[5]

This work was supported in part by U.S. Army CRDC grant DAAA-15-85-K-0004 (M. Milham).

References

1. G. Brändli and A. J. Sievers, "Absolute Measurement of the Far-Infrared Surface Resistance of Pb," Phys Rev. B 5, 3550 (1972).
2. M. von Ortenberg, "Application of the Strip Transmission Line in Submillimetre Spectroscopy," Infrared Phys. 18, 735 (1978).
3. "Teflon FEP Fluorocarbon Film: Optical Properties," *Dupont Technical Bulletin T-5A*, E.I. Du Pont De Nemours & Co. (Inc.), Plastics Products and Resins Department, Fluorocarbons Division, Wilmington, Del. 19898.
4. M. S. Caceci and W. P. Cacheris, "Fitting Curves to Data: The Simplex Algorithm is the Answer," Byte 9, 340 (1984).
5. G. W. Chantry, in *Infrared and Millimeter Waves*, Vol. 8, K. J. Button, Ed. (Academic, New York, 1983), Chap. 1, p. 44.

Reprinted from Applied Optics, Vol. 24, page 3680, November 15, 1985

Equations linking different sets of optical properties for nonmagnetic materials

Robert J. Bell, Mark A. Ordal, and Ralph W. Alexander, Jr.
University of Missouri-Rolla, Physics Department, Rolla, Missouri 65401.
Received 12 August 1985.
0003-6935/85/223680-03$02.00/0.

Four different quantities are frequently used to characterize the optical properties of materials.[1-10] This Letter presents the relations among these four quantities. In addition, these four quantities are given in terms of the Drude model for metals.

The four complex quantities used to summarize the dielectric properties of materials are the complex index of refraction,

$$n_c = n + ik = \sqrt{\epsilon_c} = 1/z_c = [\epsilon_\infty + i2\sigma_c/(\omega c)]^{1/2}, \quad (1)$$

the complex dielectric function,

$$\epsilon_c = \epsilon_1 + i\epsilon_2 = n_c^2 = 1/z_c^2 = \epsilon_\infty + i2\sigma_c/(\omega c), \quad (2)$$

the normalized complex impedance,

$$z_c = \frac{Z}{4\pi/c} = r + ix = 1/n_c = 1/\sqrt{\epsilon_c} = 1/[\epsilon_\infty + i2\sigma_c/(\omega c)]^{1/2}, \quad (3)$$

and the complex conductivity,

$$\sigma_c = \sigma_1 + i\sigma_2 = i(\epsilon_\infty - n_c^2)c\omega/2$$

$$= i(\epsilon_\infty - \epsilon_c)c\omega/2 = \frac{i(\epsilon_\infty z_c^2 - 1)c\omega}{2z_c^2}. \quad (4)$$

The signs of the imaginary parts of these quantities have been chosen to correspond to the choice of traveling waves of the form

$$\exp \cdot [i(\mathbf{q} \cdot \mathbf{r} - 2\pi c\omega t)]. \quad (5)$$

In the above equations, n is the index of refraction, k is the extinction index, z_c is the normalized complex impedance, r is the normalized resistance, and x is the normalized reactance. The normalization of the complex impedance consists in dividing the impedance by its vacuum value $4\pi/c$. For metals, the angle of refraction is nearly zero for wavelengths in the IR and longer. In this case the normalized surface impedance is nearly identical to the bulk impedance, and the above expression for the bulk impedance[6,7] is used for the complex normalized surface impedance. In this Letter ϵ_∞ is the high frequency dielectric constant usually taken as unity.

Table I summarizes the relations among n_c, ϵ_c, z_c, and σ_c. All frequencies are assumed to be in units of cm^{-1}, and conductivities are in units of sec^{-1}.

If the Drude model is assumed, the complex quantities n_c, ϵ_c, z_c, and σ_c take the form

Table I. Linkage Equations

$$0 \geq \epsilon_1 = (n^2 - k^2) = \left(\frac{r^2 - x^2}{(r^2 + x^2)^2}\right) = \epsilon_\infty - \frac{2\sigma_2}{c\omega},$$

$$0 \leq \epsilon_2 = 2nk = \left[\frac{-2rx}{(r^2 + x^2)^2}\right] = \frac{2\sigma_1}{c\omega},$$

$$0 \leq n = \sqrt{\frac{\epsilon_1 + \sqrt{\epsilon_1^2 + \epsilon_2^2}}{2}} = \left(\frac{r}{r^2 + x^2}\right) = \sqrt{\frac{2\sigma_2 - c\omega\epsilon_\infty}{2\omega c}}\left[-1 + \sqrt{1 + \left(\frac{2\sigma_1}{c\omega\epsilon_\infty - 2\sigma_2}\right)^2}\right]^{1/2},$$

$$0 \leq K = \sqrt{\frac{-\epsilon_1 + \sqrt{\epsilon_1^2 + \epsilon_2^2}}{2}} = \left(\frac{-x}{r^2 + x^2}\right) = \sqrt{\frac{2\sigma_2 - c\omega\epsilon_\infty}{2\omega c}}\left[1 + \sqrt{1 + \left(\frac{2\sigma_1}{c\omega\epsilon_\infty - 2\sigma_2}\right)^2}\right]^{1/2},$$

$$0 \leq r = \left(\frac{n}{n^2 + k^2}\right) = \sqrt{\frac{\epsilon_1 + \sqrt{\epsilon_1^2 + \epsilon_2^2}}{2(\epsilon_1^2 + \epsilon_2^2)}} = \sqrt{\frac{c\omega}{2}}\left[\frac{-(2\sigma_2 - c\omega\epsilon_\infty) + \sqrt{(2\sigma_2 - c\omega\epsilon_\infty)^2 + 4\sigma_1^2}}{(2\sigma_2 - c\omega\epsilon_\infty\omega)^2 + 4\sigma_1^2}\right]^{1/2},$$

$$0 \geq X = \left(\frac{-k}{n^2 + k^2}\right) = -\sqrt{\frac{-\epsilon_1 + \sqrt{\epsilon_1^2 + \epsilon_2^2}}{2(\epsilon_1^2 + \epsilon_2^2)}} = -\sqrt{\frac{c\omega}{2}}\left[\frac{(2\sigma_2 - c\omega\epsilon_\infty) + \sqrt{(2\sigma_2 - c\epsilon_\infty\omega)^2 + 4\sigma_1^2}}{(2\sigma_2 - c\epsilon_\infty\omega)^2 + 4\sigma_1^2}\right]^{1/2},$$

$$0 \leq \sigma_1 = \frac{c\omega\epsilon_2}{2} = c\omega nk = \frac{-c\omega rx}{(r^2 + x^2)^2},$$

$$0 \leq \sigma_2 = \frac{c\omega}{2}(\epsilon_\infty - \epsilon_1) = \frac{c\omega}{2}(\epsilon_\infty - n^2 + k^2) = \frac{c\omega}{2}\left[\epsilon_\infty + \frac{x^2 - r^2}{(r^2 + x^2)^2}\right].$$

Appendix A

Table II. In the Drude Model the Real and Imaginary Parts of n_c, ϵ_c, z_c, and σ_c are Presented in Terms of ω, ω_τ, ω_p, and ϵ_∞.[a]

$$0 \le n = \left\{\frac{[(\omega_\tau^2+\omega^2)\epsilon_\infty - \omega_p^2] + \sqrt{[(\omega_\tau^2+\omega^2)\epsilon_\infty - \omega_p^2]^2 + \omega_p^4\omega_\tau^2/\omega^2}}{2(\omega_\tau^2+\omega^2)}\right\}^{1/2},$$

$$0 \le K = \left\{\frac{-[(\omega_\tau^2+\omega^2)\epsilon_\infty - \omega_p^2] + \sqrt{[(\omega_\tau^2+\omega^2)\epsilon_\infty - \omega_p^2]^2 + \omega_p^4\omega_\tau^2/\omega^2}}{2(\omega_\tau^2+\omega^2)}\right\}^{1/2},$$

$$0 \le \epsilon_1 = \left(\epsilon_\infty - \frac{\omega_p^2/\omega_\tau^2}{1+\omega^2/\omega_\tau^2}\right),$$

$$0 \le \epsilon_2 = \left(\frac{\omega_p^2/(\omega_\tau\omega)}{1+\omega^2/\omega_\tau^2}\right),$$

$$0 \le r = \sqrt{\frac{\omega_\tau^2+\omega^2}{2}}\left\{\frac{[(\omega_\tau^2+\omega^2)\epsilon_\infty - \omega_p^2] + \sqrt{[(\omega_\tau^2+\omega^2)\epsilon_\infty - \omega_p^2]^2 + \omega_p^4\omega_\tau^2/\omega^2}}{[(\omega_\tau^2+\omega^2)\epsilon_\infty - \omega_p^2]^2 + \omega_p^4\omega_\tau^2/\omega^2}\right\}^{1/2},$$

$$0 \ge x = -\sqrt{\frac{\omega_\tau^2+\omega^2}{2}}\left\{\frac{-[(\omega_\tau^2+\omega^2)\epsilon_\infty - \omega_p^2] + \sqrt{[(\omega_\tau^2+\omega^2)\epsilon_\infty - \omega_p^2]^2 + \omega_p^4\omega_\tau^2/\omega^2}}{[(\omega_\tau^2+\omega^2)\epsilon_\infty - \omega_p^2]^2 + \omega_p^4\omega_\tau^2/\omega^2}\right\}^{1/2},$$

$$0 \le \sigma_1\,(\mathrm{sec}^{-1}) = \frac{c\omega_p^2}{2\omega_\tau(1+\omega^2/\omega_\tau^2)},$$

$$0 \le \sigma_2\,(\mathrm{sec}^{-1}) = \frac{c\omega_p^2\omega}{2\omega_\tau^2(1+\omega^2/\omega_\tau^2)},$$

$$0 \le \omega_\tau = \left(\frac{\omega\epsilon_2}{\epsilon_\infty - \epsilon_1}\right) = \left(\frac{2nk\omega}{\epsilon_\infty + k^2 - n^2}\right) = \left(\frac{-2rx\omega}{(r^2+x^2)^2\epsilon_\infty + x^2 - r^2}\right) = \frac{\omega\sigma_1}{\sigma_2},$$

$$0 \le \omega_p = \omega\sqrt{\frac{(\epsilon_\infty - \epsilon_1)^2 + \epsilon_2^2}{\epsilon_\infty - \epsilon_1}} = \omega\left(\frac{(\epsilon_\infty + k^2 - n^2)^2 + 4n^2k^2}{\epsilon_\infty + k^2 - n^2}\right)^{1/2} = \omega\left\{\frac{[(x^2+r^2)^2\epsilon_\infty + x^2 - r^2]^2 + 4x^2r^2}{(r^2+x^2)^2[(x^2+r^2)^2\epsilon_\infty + x^2 - r^2]}\right\}^{1/2}$$

$$= \sqrt{\frac{2\omega(\sigma_1^2+\sigma_2^2)}{c\sigma_2}},$$

$$\rho_{\mathrm{opt}}\,(\Omega\text{-cm}) = \frac{2\times10^{-9}c\omega_\tau}{\omega_p^2} = \frac{2\times10^{-9}c\epsilon_2}{\omega[(\epsilon_\infty - \epsilon_1)^2 + \epsilon_2^2]} = \frac{4\times10^{-9}cnk}{\omega[(\epsilon_\infty + k^2 - n^2)^2 + (2nk)^2]}$$

$$= \frac{-120rx(r^2+x_2^2)^2}{\omega\{[\epsilon_\infty(r^2+x^2)^2 + x^2 - r^2]^2 + 4r^2x^2\}},$$

$$\sigma_0(\mathrm{sec}^{-1}) = \frac{10^{-9}c^2}{\rho_0(\Omega\text{-cm})} = 2\pi c\sigma_0(\mathrm{cm}^{-1}).$$

[a] The scattering ω_τ and plasma ω_p frequencies are given in terms of the real and imaginary parts of n_c, ϵ_c, z_c, and σ_c. The high frequency resistivity, the real part of the complex optical resistivity, is given in the four sets of parameters. Also the dc conductivity, σ_0 (sec^{-1}), is related to the dc resistivity ρ_0 (Ω-cm).

Table III. Reflectances at Normal Incidence (Vacuum Overlayer) for any Material.[a]

$$R = \frac{(n-1)^2+k^2}{(n+1)^2+k^2} = \frac{(r^2+x^2-r)^2+x^2}{(r^2+x^2+r)^2+x^2} = \frac{1+\sqrt{\epsilon_1^2+\epsilon_2^2} - \sqrt{2}\sqrt{\epsilon_1+\sqrt{\epsilon_1^2+\epsilon_2^2}}}{1+\sqrt{\epsilon_1^2+\epsilon_2^2} + \sqrt{2}\sqrt{\epsilon_1+\sqrt{\epsilon_1^2+\epsilon_2^2}}}$$

$$= \left[\frac{c\omega + \sqrt{(c\omega\epsilon_\infty - 2\sigma_2)^2 + 4\sigma_1^2} - \sqrt{2c\omega}\sqrt{(c\omega\epsilon_\infty - 2\sigma_2) + \sqrt{(c\omega\epsilon_\infty - 2\sigma_2)^2 + 4\sigma_1^2}}}{c\omega + \sqrt{(c\omega\epsilon_\infty - 2\sigma_2)^2 + 4\sigma_1^2} + \sqrt{2c\omega}\sqrt{(c\omega\epsilon_\infty - 2\sigma_2) + \sqrt{(c\omega\epsilon_\infty - 2\sigma_2)^2 + 4\sigma_1^2}}}\right]$$

$$= \frac{\sqrt{1+\omega^2/\omega_\tau^2} + [\omega_p^2/(\omega_\tau\omega)] - \sqrt{2}\sqrt{\omega_p^2/(\omega_\tau\omega)}\sqrt{-(\omega/\omega_\tau) + \sqrt{1+\omega^2/\omega_\tau^2}}}{\sqrt{1+\omega^2/\omega_\tau^2} + [\omega_p^2/(\omega_\tau\omega)] + \sqrt{2}\sqrt{\omega_p^2/(\omega_\tau\omega)}\sqrt{-(\omega/\omega_\tau) + \sqrt{1+\omega^2/\omega_\tau^2}}}$$

[a] For $R(\omega,\omega_\tau,\omega_p)$ there is an approximation [as stated in the text in Eq. (17)].

Appendix A

$$n_c = \left[\epsilon_\infty + \frac{i\omega_p^2/(\omega_\tau\omega)}{1 - i\omega/\omega_\tau}\right]^{1/2}, \quad (6)$$

$$\epsilon_c = \epsilon_\infty + \frac{i\omega_p^2/(\omega_\tau\omega)}{1 - i\omega/\omega_\tau}, \quad (7)$$

$$z_c = \frac{1}{\left[\epsilon_\infty + \frac{i\omega_p^2/(\omega_\tau\omega)}{1 - i\omega/\omega_\tau}\right]^{1/2}}, \quad (8)$$

$$\sigma_c(\text{sec}^{-1}) = \frac{c\omega_p^2}{2\omega_\tau(1 - i\omega/\omega_\tau)} = \frac{\sigma_0(\text{sec}^{-1})}{1 - i\omega/\omega_\tau}, \quad (9)$$

where ϵ_∞ is the real part of the high frequency dielectric function, ω_p is the plasma frequency, ω_τ is the scattering frequency, and $\sigma_0 = 1/\rho_0$ is the dc conductivity in esu (sec^{-1}). The high frequency or optical conductivity is defined as

$$\sigma_{opt}(\text{sec}^{-1}) = 1/\rho_{opt}(\text{sec}) = \frac{c\omega_p^2}{2\omega_\tau} = \frac{10^{-9}c^2}{\rho_{opt}(\Omega\ \text{cm})}. \quad (10)$$

If the simple Drude model were correct, σ_{opt} should equal σ_0. However, for many metals this is not true.[8,9]

The real and imaginary parts of n_c, ϵ_c, z_c, and σ_c are given in Table II for the Drude model. Also shown in Table II are the expressions for ω_τ and ω_p and ρ_{opt}, the real part of the complex resistivity.

The plasma frequency ω_p and scattering frequency ω_τ are related to the electron density N (cm^{-3}) and the electron scattering time τ (sec) by

$$\omega(\text{cm}^{-1}) = \omega(rad/\text{sec})/(2\pi c), \quad (11)$$

$$\omega_\tau(\text{cm}^{-1}) = 1/[2\pi c\tau(\text{sec})], \quad (12)$$

and[3]

$$\omega_p(\text{cm}^{-1}) = [Ne^2/(\pi c^2 m^*)]^{1/2}, \quad (13)$$

where m^*(g) is the effective mass of the electrons, and e is the electron charge in esu.

Table III gives the reflectance at a vacuum–medium interface for normal incidence. Also shown is the same reflectance for a Drude model material. For this equation (and only this equation), the approximation

$$\epsilon_\infty \ll [(\omega_p^2/\omega_\tau^2)/(1 + \omega^2/\omega_\tau^2)] \quad (14)$$

has been made. In general, for a metal, this approximation holds to better than 1% for frequencies of $<10^3\ \text{cm}^{-1}$.

The information in these tables can be used to obtain other frequently used quantities in terms of n_c, ϵ, z_c, or σ_c. For example, the absorption coefficient α given by

$$\alpha = 4\pi k\omega \quad (15)$$

can be obtained in terms of the components of ϵ_c, z_c, or σ_c using line 4 of Table I. The relations[8,9]

$$\omega_\tau = \frac{\omega\epsilon_2}{\epsilon_\infty - \epsilon_1}, \quad (16)$$

$$\omega_p^2 = (\epsilon_\infty - \epsilon_1)(\omega_\tau^2 + \omega^2) = \omega^2\left[\frac{(\epsilon_\infty - \epsilon_1)^2 + \epsilon_2^2}{\epsilon_\infty - \epsilon_1}\right] \quad (17)$$

can be obtained from lines 9 and 10 of Table II. Equations (16) and (17) are a way to find the Drude model parameters ω_τ and ω_p at a given frequency.

This work was partially supported by the U.S. Army [DAAA-15-85-K-0004 (M. Milham)]. We wish to thank Lola Cook for typing the tables.

References

1. F. Wooten, *Optical Properties of Solids* (Academic, New York, 1972), p. 90*ff*.
2. J. D. Jackson, *Classical Electrodynamics* (Wiley, New York, 1975), p. 296.
3. C. Kittel, *Introduction to Solid State Physics* (Wiley, New York, 1976), Chap. 10.
4. A. H. Wilson, *The Theory of Metals* (Cambridge U. P. London, 1953).
5. B. Donovan, *Elementary Theory of Metals, Vol. 2*, in *The International Encyclopedia of Physical Chemistry and Chemical Physics*, Topic 11; *The Ideal Crystalline State*, M. Blackman, Ed. (Pergamon, Oxford, 1967). Note, he uses waves of the form $\exp.[i(-\mathbf{q}\cdot\mathbf{r} + 2\pi c\omega t)]$.
6. F. E. Pinkerton and A. J. Sievers, "Quantitative FIR Absorptivity Measurements of Metals with Dual Non-Resonant Cavities," Infrared Phys. **22**, 377 (1982).
7. J. Stone, *Radiation and Optics* (McGraw-Hill, New York, 1963).
8. M. A. Ordal, L. L. Long, R. J. Bell, S. E. Bell, R. R. Bell, R. W. Alexander, Jr., and C. A. Ward, "Optical Properties of the Metals Al, Co, Cu, Au, Fe, Pb, Ni, Pd, Pt, Ag, Ti, and W in the Infrared and Far Infrared," Appl. Opt. **22**, 1099 (1983).
9. M. A. Ordal, R. J. Bell, R. W. Alexander, Jr., and M. R. Querry, "Optical Properties of Fourteen Metals in the Infrared and Far Infrared: Al, Co, Cu, Au, Fe, Pb, Mo, Ni, Pd, Pt, Ag, Ti, V, and W," Appl. Opt. **24**, (15 Dec. 1985).
10. S. Perkowitz, G. L. Carr, B. Subramaniam, and B. Mitrović, "Far-infrared Determination of Scattering Behavior and Plasma Frequency in V_3Si, Nb_3Ge, and Nb," Phys. Rev. B **32**, 153 (1985).

Table II. In the Drude Model the Real and Imaginary Parts of n_c, ϵ_c, z_c, and σ_c are Presented in Terms of ω, ω_τ, ω_p, and ϵ_∞.[a]

$$0 \le n = \left\{\frac{[(\omega_\tau^2+\omega^2)\epsilon_\infty - \omega_p^2] + \sqrt{[(\omega_\tau^2+\omega^2)\epsilon_\infty - \omega_p^2]^2 + \omega_p^4\omega_\tau^2/\omega^2}}{2(\omega_\tau^2+\omega^2)}\right\}^{1/2},$$

$$0 \le K = \left\{\frac{-[(\omega_\tau^2+\omega^2)\epsilon_\infty - \omega_p^2] + \sqrt{[(\omega_\tau^2+\omega^2)\epsilon_\infty - \omega_p^2]^2 + \omega_p^4\omega_\tau^2/\omega^2}}{2(\omega_\tau^2+\omega^2)}\right\}^{1/2},$$

$$0 \le \epsilon_1 = \left(\epsilon_\infty - \frac{\omega_p^2/\omega_\tau^2}{1+\omega^2/\omega_\tau^2}\right),$$

$$0 \le \epsilon_2 = \left(\frac{\omega_p^2/(\omega_\tau\omega)}{1+\omega^2/\omega_\tau^2}\right),$$

$$0 \le r = \sqrt{\frac{\omega_\tau^2+\omega^2}{2}}\left\{\frac{[(\omega_\tau^2+\omega^2)\epsilon_\infty - \omega_p^2] + \sqrt{[(\omega_\tau^2+\omega^2)\epsilon_\infty - \omega_p^2]^2 + \omega_p^4\omega_\tau^2/\omega^2}}{[(\omega_\tau^2+\omega^2)\epsilon_\infty - \omega_p^2]^2 + \omega_p^4\omega_\tau^2/\omega^2}\right\}^{1/2},$$

$$0 \ge x = -\sqrt{\frac{\omega_\tau^2+\omega^2}{2}}\left\{\frac{-[(\omega_\tau^2+\omega^2)\epsilon_\infty - \omega_p^2] + \sqrt{[(\omega_\tau^2+\omega^2)\epsilon_\infty - \omega_p^2]^2 + \omega_p^4\omega_\tau^2/\omega^2}}{[(\omega_\tau^2+\omega^2)\epsilon_\infty - \omega_p^2]^2 + \omega_p^4\omega_\tau^2/\omega^2}\right\}^{1/2},$$

$$0 \le \sigma_1\,(\mathrm{sec}^{-1}) = \frac{c\omega_p^2}{2\omega_\tau(1+\omega^2/\omega_\tau^2)},$$

$$0 \le \sigma_2\,(\mathrm{sec}^{-1}) = \frac{c\omega_p^2\omega}{2\omega_\tau^2(1+\omega^2/\omega_\tau^2)},$$

$$0 \le \omega_\tau = \left(\frac{\omega\epsilon_2}{\epsilon_\infty - \epsilon_1}\right) = \left(\frac{2nk\omega}{\epsilon_\infty + k^2 - n^2}\right) = \left(\frac{-2rx\omega}{(r^2+x^2)^2\epsilon_\infty + x^2 - r^2}\right) = \frac{\omega\sigma_1}{\sigma_2},$$

$$0 \le \omega_p = \omega\sqrt{\frac{(\epsilon_\infty-\epsilon_1)^2+\epsilon_2^2}{\epsilon_\infty-\epsilon_1}} = \omega\left(\frac{(\epsilon_\infty+k^2-n^2)^2+4n^2k^2}{\epsilon_\infty+k^2-n^2}\right)^{1/2} = \omega\left\{\frac{[(x^2+r^2)^2\epsilon_\infty + x^2 - r^2]^2 + 4x^2r^2}{(r^2+x^2)^2[(x^2+r^2)^2\epsilon_\infty + x^2 - r^2]}\right\}^{1/2}$$

$$= \sqrt{\frac{2\omega(\sigma_1^2+\sigma_2^2)}{c\sigma_2}},$$

$$\rho_{\mathrm{opt}}\,(\Omega\text{-cm}) = \frac{2\times10^{-9}c\omega_\tau}{\omega_p^2} = \frac{2\times10^{-9}c\epsilon_2}{\omega[(\epsilon_\infty-\epsilon_1)^2+\epsilon_2^2]} = \frac{4\times10^{-9}cnk}{\omega[(\epsilon_\infty+k^2-n^2)^2+(2nk)^2]}$$

$$= \frac{-120rx(r^2+x_2^2)^2}{\omega\{[\epsilon_\infty(r^2+x^2)^2 + x^2 - r^2]^2 + 4r^2x^2\}},$$

$$\sigma_0(\mathrm{sec}^{-1}) = \frac{10^{-9}c^2}{\rho_0(\Omega\text{-cm})} = 2\pi c\sigma_0(\mathrm{cm}^{-1}).$$

[a] The scattering ω_τ and plasma ω_p frequencies are given in terms of the real and imaginary parts of n_c, ϵ_c, z_c, and σ_c. The high frequency resistivity, the real part of the complex optical resistivity, is given in the four sets of parameters. Also the dc conductivity, σ_0 (sec^{-1}), is related to the dc resistivity ρ_0 (Ω-cm).

Table III. Reflectances at Normal Incidence (Vacuum Overlayer) for any Material.[a]

$$R = \frac{(n-1)^2+k^2}{(n+1)^2+k^2} = \frac{(r^2+x^2-r)^2+x^2}{(r^2+x^2+r)^2+x^2} = \frac{1+\sqrt{\epsilon_1^2+\epsilon_2^2}-\sqrt{2}\sqrt{\epsilon_1+\sqrt{\epsilon_1^2+\epsilon_2^2}}}{1+\sqrt{\epsilon_1^2+\epsilon_2^2}+\sqrt{2}\sqrt{\epsilon_1+\sqrt{\epsilon_1^2+\epsilon_2^2}}},$$

$$= \left[\frac{c\omega+\sqrt{(c\omega\epsilon_\infty-2\sigma_2)^2+4\sigma_1^2}-\sqrt{2c\omega}\sqrt{(c\omega\epsilon_\infty-2\sigma_2)+\sqrt{(c\omega\epsilon_\infty-2\sigma_2)^2+4\sigma_1^2}}}{c\omega+\sqrt{(c\omega\epsilon_\infty-2\sigma_2)^2+4\sigma_1^2}+\sqrt{2c\omega}\sqrt{(c\omega\epsilon_\infty-2\sigma_2)+\sqrt{(c\omega\epsilon_\infty-2\sigma_2)^2+4\sigma_1^2}}}\right]$$

$$= \frac{\sqrt{1+\omega^2/\omega_\tau^2}+[\omega_p^2/(\omega_\tau\omega)]-\sqrt{2}\sqrt{\omega_p^2/(\omega_\tau\omega)}\sqrt{-(\omega/\omega_\tau)+\sqrt{1+\omega^2/\omega_\tau^2}}}{\sqrt{1+\omega^2/\omega_\tau^2}+[\omega_p^2/(\omega_\tau\omega)]+\sqrt{2}\sqrt{\omega_p^2/(\omega_\tau\omega)}\sqrt{-(\omega/\omega_\tau)+\sqrt{1+\omega^2/\omega_\tau^2}}}$$

[a] For $R(\omega,\omega_\tau,\omega_p)$ there is an approximation [as stated in the text in Eq. (17)].

Appendix A

Reprinted from Applied Optics, Vol. 24, page 4493, December 15, 1985

Optical properties of fourteen metals in the infrared and far infrared: Al, Co, Cu, Au, Fe, Pb, Mo, Ni, Pd, Pt, Ag, Ti, V, and W.

M. A. Ordal, Robert J. Bell, R. W. Alexander, Jr, L. L. Long, and M. R. Querry

Infrared optical constants collected from the literature are tabulated for Mo and V. New data are presented for Cu, Fe, and Ni. Drude model parameters ω_τ and ω_p are given for the fourteen metals Al, Co, Cu, Au, Fe, Pb, Mo, Ni, Pd, Pt, Ag, Ti, V, and W. The Drude model parameters for Cu are revised from our earlier tabulation due to the availability of additional data. Refinements in our fitting technique have resulted in only slight changes in the Drude model parameters for Al, Au, Ag, and W. The Drude model parameters for Pb correct a numerical error in our earlier tabulation. For all fourteen metals, the optical resistivity has been calculated from the Drude model parameters ω_τ and ω_p and compared to handbook values for the dc resistivity.

I. Introduction

In our earlier tabulation of the optical constants of twelve metals[1] we showed that the Drude model provided a useful parametrization for the optical constants of six metals; Al, Cu, Au, Pb, Ag, and W. Since then we have parametrized the other six metals in our earlier tabulation; Fe, Co, Ni, Pd, Pt, and Ti. We have expanded our earlier tabulation by adding data on Mo and V from Weaver *et al.*[2]; our recently acquired data on Cu, Fe, and Ni; and data on V from Johnson and Christy.[3]

In general, the Drude model is not expected to be appropriate for transition metals in the near IR. Nevertheless, a Drude model parametrization of the dielectric function is a useful approximation (sometimes over a surprisingly large frequency range) for these metals.

II. Definitions

In keeping with IR spectroscopic notation, all frequencies will be expressed in cm^{-1}. The complex dielectric function ϵ_c and the complex index of refraction n_c are defined as [1]

$$\epsilon_c \equiv \epsilon_1 + i\epsilon_2 \equiv n_c^2 \equiv (n + ik)^2. \tag{1}$$

The Drude model dielectric function is

$$\epsilon_c = \epsilon_\infty - \frac{\omega_p^2}{\omega^2 + i\omega\omega_\tau}, \tag{2}$$

where ω, ω_p, and ω_τ have units of cm^{-1}. Separating real and imaginary parts yields

$$\epsilon_1 = \epsilon_\infty - \frac{\omega_p^2}{\omega^2 + \omega_\tau^2}, \tag{3}$$

$$\epsilon_2 = \frac{\omega_\tau\omega_p^2}{\omega(\omega^2 + \omega_\tau^2)}. \tag{4}$$

In these equations, the plasma frequency is

$$\omega_p(cm^{-1}) = \frac{1}{2\pi c}\left(\frac{4\pi Ne^2}{m^*}\right)^{1/2}, \tag{5}$$

where in cgs units N is the free electron density, e is the electronic charge, m^* is the effective mass of the electrons, and c is the speed of light in vacuum. Equation (5) corrects the like numbered equation in our earlier publication.[1]

The damping frequency ω_τ is

$$\omega_\tau(cm^{-1}) = \frac{1}{2\pi c\tau}, \tag{6}$$

where τ is the electron lifetime in seconds.

The high or optical frequency conductivity σ_{opt} is related to ω_p and ω_τ by

$$\sigma_{opt} = \frac{\omega_p^2}{4\pi\omega_\tau}, \tag{7}$$

where σ_{opt} has units of cm^{-1}. This optical conductiv

M. R. Querry is with University of Missouri-Kansas City, Physics Department, Kansas City, Missouri 64110; the other authors are with University of Missouri-Rolla, Physics Department, Rolla, Missouri 65401.

Received 11 June 1985.
0003-6935/85/244493-07$02.00/0.

Appendix A

ity should also be equal to the dc conductivity which can be expressed in terms of the dc resistivity ρ_0:

$$\sigma_0(\mathrm{cm}^{-1}) = \frac{1}{2\pi c[\rho_0(\mathrm{sec})]} = \frac{9\times10^{11}}{2\pi c[\rho_0(\Omega\mathrm{cm})]}. \quad (8)$$

We note that these two conductivities are not always equal as can later be seen in Table I.

Using the sign convention adopted in Eq. (1) we can write the surface impedance, $Z(\omega) \equiv R(\omega) + iX(\omega)$, for the Drude model:

$$Z(\omega) = \frac{4\pi}{c}(1-i)\sqrt{\left(\frac{\omega\omega_\tau}{2\omega_p^2}\right)\left(1-\frac{i\omega}{\omega_\tau}\right)}. \quad (9)$$

Extracting the real and imaginary parts we get

$$R(\omega) = \frac{4\pi}{c}\sqrt{\frac{\omega\omega_\tau}{2\omega_p^2}}\left(\frac{-\omega}{\omega_\tau}+\sqrt{1+\frac{\omega^2}{\omega_\tau^2}}\right)^{1/2}. \quad (10)$$

$$X(\omega) = \frac{-4\pi}{c}\sqrt{\frac{\omega\omega_\tau}{2\omega_p^2}}\left(\frac{\omega}{\omega_\tau}+\sqrt{1+\frac{\omega^2}{\omega_\tau^2}}\right)^{1/2}. \quad (11)$$

Taking the other sign convention (i.e., $n - ik$) leaves the expression for $R(\omega)$ unchanged, multiplies the expression for $X(\omega)$ by -1, and replaces $-i$ by i in the expression for $Z(\omega)$. Equation (9) corrects Eq. (10) in our earlier publication.[1] Since Eq. (10) remains the same for either sign convention, the numerical results given in our Ref. 1 remain unchanged.

III. Determination of Drude Model Parameters

Equations (3) and (4) can be solved for[1] for ω_τ to obtain

$$\omega_\tau = \frac{\omega\epsilon_2}{(\epsilon_\infty - \epsilon_1)}. \quad (12)$$

Equation (12) was used to obtain ω_τ using ϵ_1 and ϵ_2 at some frequency ω. Then ω_p was obtained from

$$\omega_p^2 = (\epsilon_\infty - \epsilon_1)(\omega^2 + \omega_\tau^2). \quad (13)$$

Equations (12) and (13) were applied to the lowest frequency data with ϵ_∞ taken to be unity.

We attempted to refine the values for ω_τ and ω_p obtained with the aforementioned method by fitting a function of ϵ_1 and ϵ_2. We tried various functions including ϵ_1/ϵ_2, ϵ_2/ϵ_1, $\epsilon_1\epsilon_2$ and $|\epsilon_c|$. The function $|\epsilon_c|$ worked better than the others but was surpassed slightly by the similar function

$$\sqrt{(\epsilon_1-\epsilon_\infty)^2+\epsilon_2^2} = \frac{\omega_p^2}{\omega^2+\omega_\tau^2}\sqrt{1+\left(\frac{\omega_\tau}{\omega}\right)^2}. \quad (14)$$

In cases where the data did not extend to frequencies both higher and lower than ω_τ, this fit method returned reasonable results in only a few cases. A major problem seems to be the large (orders of magnitude) difference in the values of $-\epsilon_1$ and ϵ_2 at frequencies away from ω_τ. It should be noted that a formal fit method worked well in those cases where data extend to frequencies both higher and lower than ω_τ. However, in such cases it is more convenient to obtain the value of ω_τ from Eqs. (3) and (4) with $\omega = \omega_\tau$. That is

$$-\epsilon_1 = \epsilon_2 - \epsilon_\infty \ (\text{for } \omega = \omega_\tau). \quad (15)$$

Table I. Results of a Drude Model Fit to the Dielectric Function of Fourteen Metals.[a]

Metal	$10^{-2}\omega_\tau$ (cm^{-1})	$10^{-4}\omega_p$ (cm^{-1})	ρ_{opt} ($\mu\Omega$ cm)	ρ_0[a] ($\mu\Omega$ cm)	$\frac{\rho_0}{\rho_{opt}}$
Al	6.60	11.9	2.80	2.74	0.98
Co	2.95	3.20	17.3	5.80	0.34
Cu	0.732	5.96	1.24	1.70	1.3
Au	2.15	7.28	2.43	2.20	0.91
Fe	1.47	3.30	8.10	9.80	1.20
Pb	16.3	5.94	27.7	21.0	0.76
Mo	4.12	6.02	6.82	5.33	0.78
Ni	3.52	3.94	13.3	7.04	0.52
Pd	1.24	4.40	3.84	10.55	2.8
Pt	5.58	4.15	19.4	10.42	0.54
Ag	1.45	7.27	1.65	1.61	0.98
Ti	3.82	2.03	55.6	43.1	0.78
V	4.89	4.16	17.0	19.9	1.2
W	4.87	5.17	10.9	5.33	0.49

[a] Ref. 5, pp. 9-39,9-40.

With ω_τ known, either ϵ_1 or ϵ_2 can be fit to obtain ω_p (although ϵ_1 is preferred since it tends to closely fit the Drude model to higher frequencies than ϵ_2).

Our fits are good enough for us to conclude that ϵ_∞ is much less than ϵ_1 or ϵ_2—that is, ϵ_∞ does not need to be taken as a third adjustable parameter in the fitting process.

The fit method used to obtain the values given in Table I remains a trial and error eyeball technique. The values of ω_τ and ω_p obtained from the lowest frequency data were changed by trial and error to obtain curves most closely matching the data for $-\epsilon_1$ and ϵ_2 in both magnitude and slope. In certain cases the need for lower frequency data is readily apparent. In such cases (e.g., Pd) the Drude model fit gives a reasonable estimate for $-\epsilon_1$ but not for ϵ_2. In other cases band structure, combined with a lack of very low frequency data, limits the Drude model fit to a fairly narrow frequency range (e.g.,Ti).

IV. Data

For our own measurements on Cu, Fe, and Ni the power reflectance was measured using an Al mirror as a standard. The measured reflectance of the samples was corrected for the absolute reflectance of this particular Al mirror using values measured by us. A Perkin-Elmer 580 was used in the 180–4000-cm^{-1} range, and a Varian model 2300 was used for the 4000–50,000-cm^{-1} range.

The Kramers-Kronig analysis of the reflectance data yielded n and k from which ϵ_1 and ϵ_2 were calculated. High and low frequency wing corrections were handled in various ways. At the low end we tried a constant wing where the zero frequency reflectance was assumed to equal the measured reflectance at 180 cm^{-1}. For the low frequency wing correction, we also tried a Drude model extrapolation down to 1 cm^{-1} and assumed a constant reflectance below 1 cm^{-1}. The Drude model parameters used for the low wing were found by trial and error starting with the values that best fit the higher frequency results of others. Trial and error adjustment of ω_τ and ω_p was necessary to

Appendix A

Table II. Copper

ω (cm^{-1})	λ (μm)	$-\epsilon_1$	ϵ_2	n	k
1.80E + 2	5.56E + 1	9.40E + 4	3.83E + 4	6.12E + 1	3.13E + 2
2.00E + 2	5.00E + 1	7.82E + 4	2.84E + 4	5.00E + 1	2.84E + 2
2.20E + 2	4.55E + 1	6.47E + 4	2.11E + 4	4.09E + 1	2.58E + 2
2.40E + 2	4.17E + 1	5.53E + 4	1.72E + 4	3.62E + 1	2.38E + 2
2.60E + 2	3.85E + 1	4.70E + 4	1.40E + 4	3.19E + 1	2.19E + 2
2.80E + 2	3.57E + 1	4.06E + 4	1.16E + 4	2.85E + 1	2.03E + 2
3.00E + 2	3.33E + 1	3.54E + 4	9.74E + 3	2.57E + 1	1.90E + 2
3.20E + 2	3.13E + 1	3.11E + 4	8.31E + 3	2.34E + 1	1.78E + 2
3.40E + 2	2.94E + 1	2.74E + 4	7.37E + 3	2.21E + 1	1.67E + 2
3.60E + 2	2.78E + 1	2.46E + 4	6.65E + 3	2.10E + 1	1.58E + 2
3.80E + 2	2.63E + 1	2.22E + 4	5.86E + 3	1.95E + 1	1.50E + 2
4.00E + 2	2.50E + 1	1.99E + 4	5.43E + 3	1.91E + 1	1.42E + 2
4.20E + 2	2.38E + 1	1.81E + 4	4.99E + 3	1.84E + 1	1.36E + 2
4.40E + 2	2.27E + 1	1.66E + 4	4.59E + 3	1.77E + 1	1.30E + 2
4.60E + 2	2.17E + 1	1.52E + 4	4.22E + 3	1.70E + 1	1.24E + 2
4.80E + 2	2.08E + 1	1.40E + 4	4.02E + 3	1.68E + 1	1.20E + 2
5.00E + 2	2.00E + 1	1.30E + 4	3.73E + 3	1.62E + 1	1.15E + 2
5.50E + 2	1.82E + 1	1.09E + 4	3.24E + 3	1.54E + 1	1.05E + 2
6.00E + 2	1.67E + 1	9.34E + 3	2.87E + 3	1.47E + 1	9.77E + 1
6.50E + 2	1.54E + 1	8.11E + 3	2.52E + 3	1.38E + 1	9.11E + 1
7.00E + 2	1.43E + 1	7.15E + 3	2.25E + 3	1.32E + 1	8.56E + 1
7.50E + 2	1.33E + 1	6.37E + 3	1.97E + 3	1.22E + 1	8.08E + 1
8.00E + 2	1.25E + 1	5.72E + 3	1.74E + 3	1.14E + 1	7.65E + 1
8.50E + 2	1.18E + 1	5.17E + 3	1.53E + 3	1.05E + 1	7.26E + 1
9.00E + 2	1.11E + 1	4.67E + 3	1.35E + 3	9.77E + 0	6.91E + 1
9.50E + 2	1.05E + 1	4.26E + 3	1.19E + 3	9.00E + 0	6.59E + 1
1.00E + 3	1.00E + 1	3.90E + 3	1.05E + 3	8.31E + 0	6.30E + 1
1.10E + 3	9.09E + 0	3.27E + 3	8.31E + 2	7.21E + 0	5.77E + 1
1.20E + 3	8.33E + 0	2.79E + 3	6.85E + 2	6.43E + 0	5.32E + 1
1.30E + 3	7.69E + 0	2.42E + 3	5.68E + 2	5.74E + 0	4.95E + 1
1.40E + 3	7.14E + 0	2.11E + 3	4.71E + 2	5.10E + 0	4.62E + 1
1.50E + 3	6.67E + 0	1.85E + 3	3.95E + 2	4.57E + 0	4.33E + 1
1.60E + 3	6.25E + 0	1.64E + 3	3.38E + 2	4.16E + 0	4.07E + 1
1.70E + 3	5.88E + 0	1.45E + 3	2.95E + 2	3.84E + 0	3.83E + 1
1.80E + 3	5.56E + 0	1.30E + 3	2.65E + 2	3.65E + 0	3.63E + 1
1.90E + 3	5.26E + 0	1.18E + 3	2.39E + 2	3.45E + 0	3.45E + 1
2.00E + 3	5.00E + 0	1.08E + 3	2.15E + 2	3.26E + 0	3.30E + 1
2.25E + 3	4.44E + 0	8.21E + 2	1.49E + 2	2.58E + 0	2.88E + 1
2.50E + 3	4.00E + 0	6.98E + 2	1.19E + 2	2.25E + 0	2.65E + 1
2.75E + 3	3.64E + 0	5.83E + 2	9.60E + 1	1.98E + 0	2.42E + 1
3.00E + 3	3.33E + 0	4.93E + 2	7.90E + 1	1.77E + 0	2.23E + 1
3.25E + 3	3.08E + 0	4.22E + 2	6.67E + 1	1.62E + 0	2.06E + 1
3.50E + 3	2.86E + 0	3.63E + 2	5.57E + 1	1.46E + 0	1.91E + 1
3.75E + 3	2.67E + 0	3.20E + 2	4.69E + 1	1.31E + 0	1.79E + 1
4.00E + 3	2.50E + 0	2.82E + 2	3.97E + 1	1.18E + 0	1.68E + 1
4.26E + 3	2.35E + 0	2.49E + 2	3.44E + 1	1.09E + 0	1.58E + 1
4.51E + 3	2.22E + 0	2.22E + 2	3.00E + 1	1.00E + 0	1.49E + 1
4.74E + 3	2.11E + 0	2.00E + 2	2.67E + 1	9.42E − 1	1.42E + 1
5.00E + 3	2.00E + 0	1.79E + 2	2.36E + 1	8.79E − 1	1.34E + 1
5.99E + 3	1.67E + 0	1.24E + 2	1.82E + 1	8.16E − 1	1.12E + 1
6.99E + 3	1.43E + 0	9.04E + 1	1.33E + 1	6.99E − 1	9.53E + 0
8.00E + 3	1.25E + 0	6.86E + 1	1.03E + 1	6.20E − 1	8.31E + 0
9.01E + 3	1.11E + 0	5.33E + 1	8.34E + 0	5.70E − 1	7.32E + 0
1.00E + 4	1.00E + 0	4.23E + 1	7.02E + 0	5.38E − 1	6.53E + 0
1.49E + 4	6.70E − 1	1.56E + 1	3.17E + 0	3.99E − 1	3.97E + 0
1.94E + 4	5.17E − 1	5.65E + 0	6.14E + 0	1.16E + 0	2.64E + 0

Table III. Nickel

ω (cm^{-1})	λ (μm)	$-\epsilon_1$	ϵ_2	n	k
1.80E + 2	5.56E + 1	9.07E + 3	2.12E + 4	8.37E + 1	1.27E + 2
2.00E + 2	5.00E + 1	9.28E + 3	1.84E + 4	7.52E + 1	1.22E + 2
2.20E + 2	4.55E + 1	9.18E + 3	1.58E + 4	6.75E + 1	1.17E + 2
2.40E + 2	4.17E + 1	8.91E + 3	1.37E + 4	6.08E + 1	1.12E + 2
2.60E + 2	3.85E + 1	8.51E + 3	1.18E + 4	5.50E + 1	1.07E + 2
2.80E + 2	3.57E + 1	8.06E + 3	1.03E + 4	5.00E + 1	1.03E + 2
3.00E + 2	3.33E + 1	7.62E + 3	8.95E + 3	4.55E + 1	9.84E + 1
3.20E + 2	3.13E + 1	7.16E + 3	7.85E + 3	4.16E + 1	9.43E + 1
3.40E + 2	2.94E + 1	6.70E + 3	6.88E + 3	3.81E + 1	9.03E + 1
3.60E + 2	2.78E + 1	6.23E + 3	6.10E + 3	3.53E + 1	8.65E + 1
3.80E + 2	2.63E + 1	5.80E + 3	5.44E + 3	3.28E + 1	8.29E + 1
4.00E + 2	2.50E + 1	5.40E + 3	4.88E + 3	3.06E + 1	7.96E + 1
4.20E + 2	2.38E + 1	5.05E + 3	4.43E + 3	2.89E + 1	7.67E + 1
4.40E + 2	2.27E + 1	4.74E + 3	3.98E + 3	2.69E + 1	7.39E + 1
4.60E + 2	2.17E + 1	4.42E + 3	3.64E + 3	2.56E + 1	7.12E + 1
4.80E + 2	2.08E + 1	4.16E + 3	3.31E + 3	2.41E + 1	6.88E + 1
5.00E + 2	2.00E + 1	3.89E + 3	3.05E + 3	2.30E + 1	6.65E + 1
5.50E + 2	1.82E + 1	3.33E + 3	2.51E + 3	2.05E + 1	6.13E + 1
6.00E + 2	1.67E + 1	2.90E + 3	2.14E + 3	1.87E + 1	5.71E + 1
6.50E + 2	1.54E + 1	2.57E + 3	1.84E + 3	1.72E + 1	5.35E + 1
7.00E + 2	1.43E + 1	2.30E + 3	1.61E + 3	1.59E + 1	5.06E + 1
7.50E + 2	1.33E + 1	2.10E + 3	1.40E + 3	1.46E + 1	4.80E + 1
8.00E + 2	1.25E + 1	1.91E + 3	1.21E + 3	1.32E + 1	4.57E + 1
8.50E + 2	1.18E + 1	1.74E + 3	1.05E + 3	1.21E + 1	4.34E + 1
9.00E + 2	1.11E + 1	1.59E + 3	9.09E + 2	1.10E + 1	4.13E + 1
9.50E + 2	1.05E + 1	1.44E + 3	7.89E + 2	1.00E + 1	3.93E + 1
1.00E + 3	1.00E + 1	1.31E + 3	6.96E + 2	9.33E + 0	3.73E + 1
1.10E + 3	9.09E + 0	1.08E + 3	5.66E + 2	8.36E + 0	3.39E + 1
1.20E + 3	8.33E + 0	9.05E + 2	4.84E + 2	7.79E + 0	3.11E + 1
1.30E + 3	7.69E + 0	7.79E + 2	4.21E + 2	7.29E + 0	2.89E + 1
1.40E + 3	7.14E + 0	6.78E + 2	3.66E + 2	6.79E + 0	2.69E + 1
1.50E + 3	6.67E + 0	5.93E + 2	3.19E + 2	6.35E + 0	2.52E + 1
1.60E + 3	6.25E + 0	5.18E + 2	2.86E + 2	6.08E + 0	2.36E + 1
1.70E + 3	5.88E + 0	4.59E + 2	2.60E + 2	5.86E + 0	2.22E + 1
1.80E + 3	5.56E + 0	4.09E + 2	2.38E + 2	5.66E + 0	2.10E + 1
1.90E + 3	5.26E + 0	3.65E + 2	2.20E + 2	5.53E + 0	1.99E + 1
2.00E + 3	5.00E + 0	3.27E + 2	2.06E + 2	5.45E + 0	1.89E + 1
2.25E + 3	4.44E + 0	2.57E + 2	1.79E + 2	5.30E + 0	1.69E + 1
2.50E + 3	4.00E + 0	2.12E + 2	1.60E + 2	5.19E + 0	1.54E + 1
2.75E + 3	3.64E + 0	1.77E + 2	1.42E + 2	5.01E + 0	1.42E + 1
3.00E + 3	3.33E + 0	1.51E + 2	1.29E + 2	4.87E + 0	1.32E + 1
3.25E + 3	3.08E + 0	1.31E + 2	1.17E + 2	4.73E + 0	1.24E + 1
3.50E + 3	2.86E + 0	1.14E + 2	1.07E + 2	4.60E + 0	1.16E + 1
3.75E + 3	2.67E + 0	1.01E + 2	9.82E + 1	4.46E + 0	1.10E + 1
4.00E + 3	2.50E + 0	9.07E + 1	9.08E + 1	4.34E + 0	1.05E + 1
4.25E + 3	2.35E + 0	8.03E + 1	8.38E + 1	4.23E + 0	9.91E + 0
4.50E + 3	2.22E + 0	7.11E + 1	7.91E + 1	4.20E + 0	9.42E + 0
4.75E + 3	2.10E + 0	6.55E + 1	7.55E + 1	4.15E + 0	9.10E + 0
5.00E + 3	2.00E + 0	6.09E + 1	7.06E + 1	4.02E + 0	8.78E + 0
6.00E + 3	1.67E + 0	4.44E + 1	5.63E + 1	3.69E + 0	7.62E + 0
7.00E + 3	1.43E + 0	3.42E + 1	4.61E + 1	3.41E + 0	6.77E + 0
8.01E + 3	1.25E + 0	2.69E + 1	3.95E + 1	3.23E + 0	6.11E + 0
9.00E + 3	1.11E + 0	2.16E + 1	3.49E + 1	3.12E + 0	5.60E + 0
1.00E + 4	1.00E + 0	1.83E + 1	3.11E + 1	2.99E + 0	5.21E + 0
1.50E + 4	6.65E − 1	1.05E + 1	1.82E + 1	2.29E + 0	3.97E + 0
2.00E + 4	4.99E − 1	6.05E + 0	1.15E + 1	1.87E + 0	3.09E + 0

match as nearly as possible both the magnitude and slope of the measured reflectance.

For Cu, we tried a constant low frequency wing correction as well as a Drude model extrapolation down to 1 cm^{-1} with a constant reflectance assumed below 1 cm^{-1}. The use of a Drude model low frequency wing changed the values of the optical constants at 180 cm^{-1} by at most 4% relative to the case of a constant wing. There was a <1% difference in the optical constants at 500 cm^{-1}, with the difference becoming correspondingly smaller at higher frequencies. The numbers in Table II were obtained using the Drude model low frequency wing correction described above.

For Ni, the use of a constant low frequency wing correction resulted in a pronounced downward hook in $-\epsilon_1$ at frequencies below ~300 cm^{-1}. Using the same type of Drude model low frequency wing correction we used for Cu almost completely removed the downward hook in $-\epsilon_1$. The numbers in Table III were obtained

Appendix A

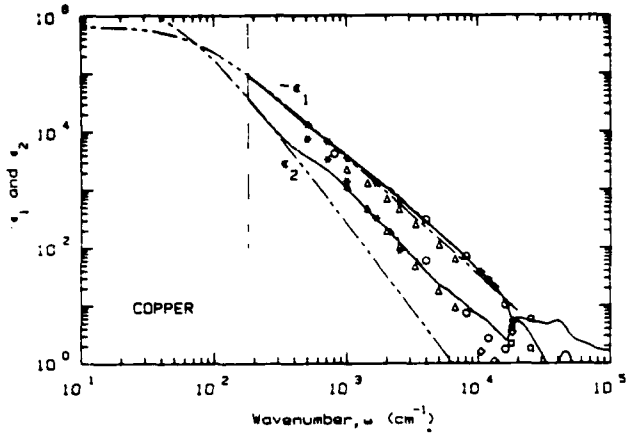

Fig. 1. Copper: $-\epsilon_1(\omega)$ and $\epsilon_2(\omega)$ vs frequency. The dashed lines are the Drude model fit. The solid lines are our data. Data from Ref. 1: Schulz, ◇ for both $-\epsilon_1$ and ϵ_2; Lenham and Treherne, • for $-\epsilon_1$ and ϵ_2; Robusto and Braunstein, □ for both; Hagemann *et al.*, ○ for both; and Dold and Mecke, △ for both. The dashed vertical line at 180 cm^{-1} marks the low frequency limit of our data.

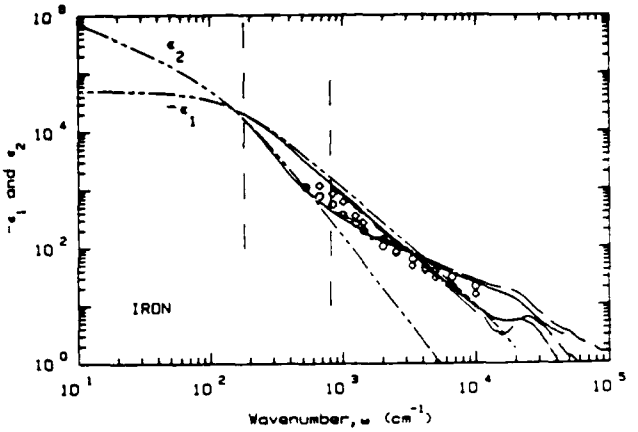

Fig. 2. Iron: $-\epsilon_1(\omega)$ and $\epsilon_2(\omega)$ vs frequency. The dashed lines are the Drude model fit. The solid lines are our data. The data from Ref. 2 are: Weaver *et al.*, dash–dot line for both $-\epsilon_1$ and ϵ_2; Bolotin *et al.*, ◇, for $-\epsilon_1$, and ○ for ϵ_2. The dashed vertical line at 180 cm^{-1} marks the low frequency limit of our data. The dashed vertical line at 807 cm^{-1} marks the low frequency limit of the Weaver *et al.* data.

using such a Drude model low frequency wing correction.

For Cu we found essentially perfect agreement in the 17,000–23,000-cm^{-1} range with the data of Weaver *et al.*[2] We arbitrarily used 20,000 cm^{-1} as a cutoff for our data and the higher frequency data from Weaver *et al.* as the first part of our high frequency wing correction. At the high frequency limit of the Weaver *et al.* data we assumed an inverse fourth-power dependence on the energy in electron volts. After this part of the high frequency wing fell to $\sim 4 \times 10^{-4}$ we assumed the reflectance remained constant at that value.

For Ni we found essentially perfect agreement in the 17,000–23,000-cm^{-1} range with the data of Lynch *et al.*[2] We arbitrarily used 20,000 cm^{-1} as a cutoff for our data and used the higher frequency data from Lynch *et al.* as the first part of our high frequency wing correction. At the high frequency limit of the Lynch *et al.* data we used the same wing correction described earlier for Cu.

For the high frequency wing correction for Fe we used the data of Moravec *et al.*[4] There was good agreement between our data and theirs with only a slight crossover between the two sets of data at 517 nm (~19,340 cm^{-1}). We used the Moravec *et al.* data as a high frequency wing correction starting at 517 nm. A constant low frequency wing correction was used for Fe.

The data of Weaver *et al.*[2] were converted from n, k, ϵ_1, and ϵ_2 vs energy (eV) to n, k, $-\epsilon_1$ and ϵ_2 vs both wave number (cm^{-1}) and wavelength (μm).

Figures 1–9 are plots of $-\epsilon_1(\omega)$ and $\epsilon_2(\omega)$ for nine metals. The dashed lines are calculated using Eqs. (3) and (4) using the Drude model parameters ω_τ and ω_p listed in Table I. Table I summarizes the results of our Drude model fit to the dielectric function of fourteen metals. Table I also includes the dc resistivity[5] ρ_0 and the optical resistivity ρ_{opt}. The optical resistivity ρ_{opt}

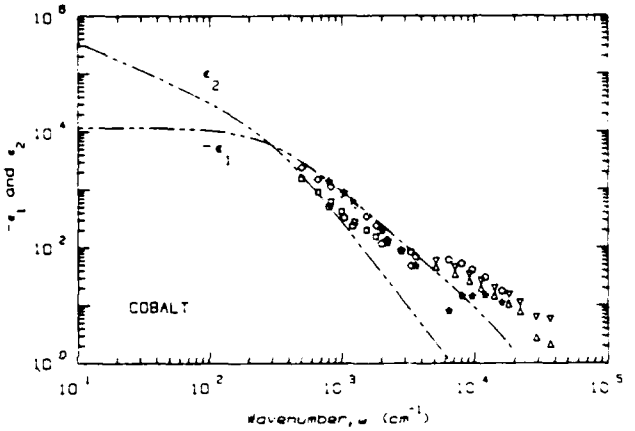

Fig. 3. Cobalt: $-\epsilon_1(\omega)$ and $\epsilon_2(\omega)$ vs frequency. The dashed lines are the Drude model fit. Data from Ref. 1: Johnson and Christy, △ for $-\epsilon_1$; X for ϵ_2; Weaver *et al.*, ★ for $-\epsilon_1$, ○ for ϵ_2.

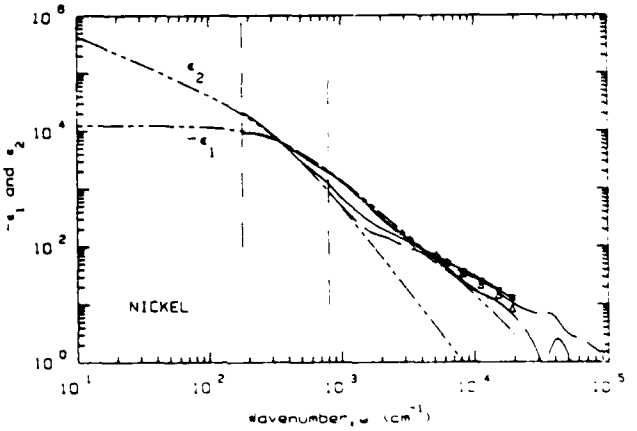

Fig. 4. Nickel: $-\epsilon_1(\omega)$ and $\epsilon_2(\omega)$ vs frequency. The dashed lines are the Drude model fit. The data from Ref. 1 are: Johnson and Christy, △ for $-\epsilon_1$ and X for ϵ_2. The solid line shows our data. The dashed vertical line at 180 cm^{-1} markes the low frequency limit of our data. The dash–dot lines are the data from Ref. 2: Lynch *et al.* The dashed vertical line at 807 cm^{-1} marks the low frequency limit of the Lynch *et al.* data.

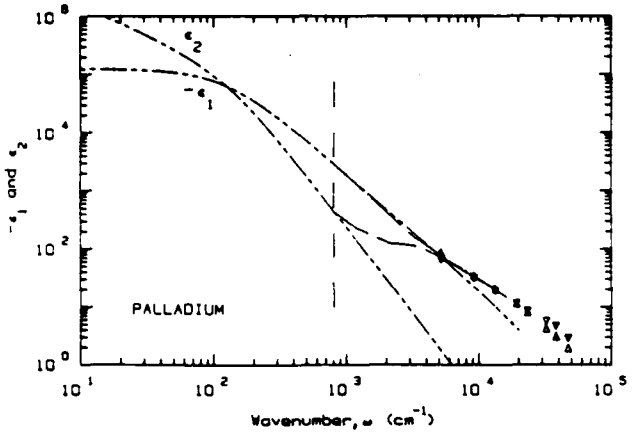

Fig. 5. Palladium: $-\epsilon_1(\omega)$ and $\epsilon_2(\omega)$ vs frequency. The dashed lines are the Drude model fit. The data from Ref. 1 are: Weaver and Benbow, dash–dot line for both $-\epsilon_1$ and ϵ_2; Johnson and Christy, △ for $-\epsilon_1$ and X for ϵ_2. The dashed vertical line at 807 cm^{-1} marks the low frequency limit of the Weaver and Benbow data.

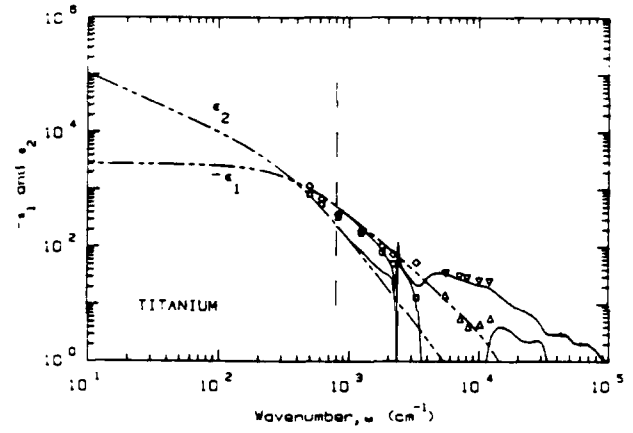

Fig. 6. Titanium: $-\epsilon_1(\omega)$ and $\epsilon_2(\omega)$ vs frequency. The dashed lines are the Drude model fit. The data from Ref. 1 are: Kirillova and Charikov (Opt. Spectrosc.), □ for $-\epsilon_1$ and ◇ for ϵ_2; Johnson and Christy, △ for $-\epsilon_1$ and X for ϵ_2. The dash–dot lines are the data from Ref. 2: Lynch *et al.* The dashed vertical line at 807 cm^{-1} marks the low frequency limit of the Lynch *et al.* data.

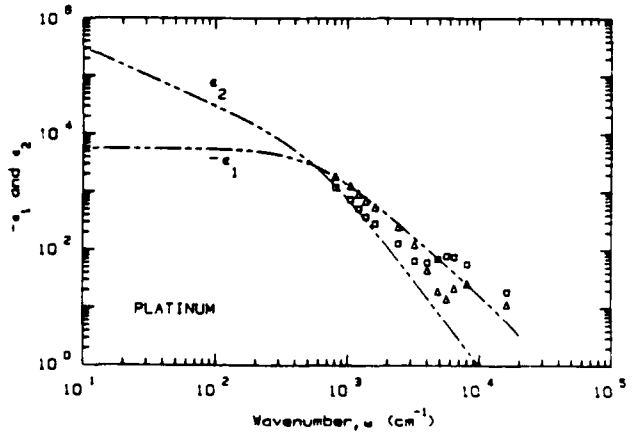

Fig. 7. Platinum: $-\epsilon_1(\omega)$ and $\epsilon_2(\omega)$ vs frequency. The dashed lines are the Drude model fit. The data from Ref. 1 are: Weaver *et al.*, ◇ for $-\epsilon_1$ and □ for ϵ_2.

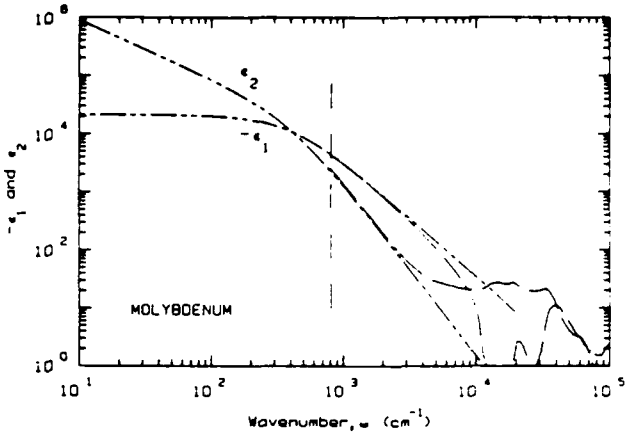

Fig. 8. Molybdenum: $-\epsilon_1(\omega)$ and $\epsilon_2(\omega)$ vs frequency. The dashed lines are the Drude model fit. The dash–dot lines are the data from Ref. 2: Weaver *et al.* The dashed vertical line at 807 cm^{-1} marks the low frequency limit of the Weaver *et al.* data.

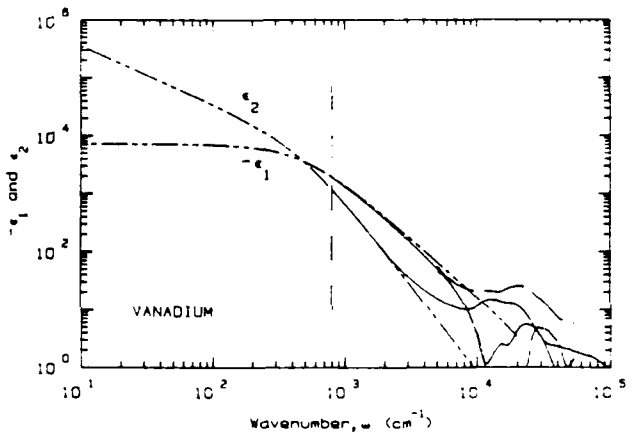

Fig. 9. Vanadium: $-\epsilon_1(\omega)$ and $\epsilon_2(\omega)$ vs frequency. The dashed lines are the Drude model fit. The solid lines are the data from Ref. 2: Weaver *et al.* The dash–dot lines are the data from Ref. 4: Johnson and Christy. The dashed vertical line at 807 cm^{-1} marks the low frequency limit of the Weaver *et al.* data.

in units of ohm cm was calculated from ω_τ and ω_p using

$$\rho_{opt} = \frac{60\omega_\tau}{\omega_p^2}. \tag{16}$$

Tables II, III, and IV present our new values of $-\epsilon_1$, ϵ_2, n, and k for Cu, Fe, and Ni. Table V presents the values of $-\epsilon_1$, ϵ_2, n, and k for Mo from Weaver *et al.*[2] Table VI presents the values of $-\epsilon_1$, ϵ_2, n, and k for V from Weaver *et al.*[2]

V. Summary

Infrared optical constants for Mo and V have been collected from the literature. New data for the optical constants Cu, Fe, and Ni are reported. The Drude model has been fit to the optical constants of the fourteen metals, Al, Co, Cu, Au, Fe, Pb, Mo, Ni, Pd, Pt, Ag, Ti, V, and W, to obtain ω_τ and ω_p. Our new data for

Table IV. Iron

ω (cm^{-1})	λ (μm)	$-\epsilon_1$	ϵ_2	n	k
1.80E + 2	5.56E + 1	2.02E + 4	1.65E + 4	5.42E + 1	1.52E + 2
2.00E + 2	5.00E + 1	1.78E + 4	1.29E + 4	4.57E + 1	1.41E + 2
2.20E + 2	4.55E + 1	1.55E + 4	1.01E + 4	3.86E + 1	1.30E + 2
2.40E + 2	4.17E + 1	1.37E + 4	8.16E + 3	3.36E + 1	1.22E + 2
2.60E + 2	3.85E + 1	1.21E + 4	6.61E + 3	2.91E + 1	1.14E + 2
2.80E + 2	3.57E + 1	1.07E + 4	5.37E + 3	2.52E + 1	1.06E + 2
3.00E + 2	3.33E + 1	9.52E + 3	4.50E + 3	2.25E + 1	1.00E + 2
3.20E + 2	3.13E + 1	8.53E + 3	3.76E + 3	1.99E + 1	9.45E + 1
3.40E + 2	2.94E + 1	7.66E + 3	3.16E + 3	1.77E + 1	8.93E + 1
3.60E + 2	2.78E + 1	6.88E + 3	2.66E + 3	1.57E + 1	8.45E + 1
3.80E + 2	2.63E + 1	6.17E + 3	2.27E + 3	1.42E + 1	7.98E + 1
4.00E + 2	2.50E + 1	5.56E + 3	1.98E + 3	1.30E + 1	7.57E + 1
4.20E + 2	2.38E + 1	5.03E + 3	1.73E + 3	1.20E + 1	7.19E + 1
4.40E + 2	2.27E + 1	4.57E + 3	1.55E + 3	1.13E + 1	6.86E + 1
4.60E + 2	2.17E + 1	4.16E + 3	1.40E + 3	1.07E + 1	6.54E + 1
4.80E + 2	2.08E + 1	3.81E + 3	1.29E + 3	1.03E + 1	6.26E + 1
5.00E + 2	2.00E + 1	3.51E + 3	1.19E + 3	9.87E + 0	6.01E + 1
5.50E + 2	1.82E + 1	2.91E + 3	9.89E + 2	9.04E + 0	5.47E + 1
6.00E + 2	1.67E + 1	2.46E + 3	8.43E + 2	8.38E + 0	5.03E + 1
6.50E + 2	1.54E + 1	2.10E + 3	7.17E + 2	7.71E + 0	4.65E + 1
7.00E + 2	1.43E + 1	1.81E + 3	6.31E + 2	7.30E + 0	4.32E + 1
7.50E + 2	1.33E + 1	1.58E + 3	5.55E + 2	6.88E + 0	4.03E + 1
8.00E + 2	1.25E + 1	1.38E + 3	4.89E + 2	6.48E + 0	3.77E + 1
8.50E + 2	1.18E + 1	1.24E + 3	4.51E + 2	6.31E + 0	3.57E + 1
9.00E + 2	1.11E + 1	1.10E + 3	4.12E + 2	6.12E + 0	3.37E + 1
9.50E + 2	1.05E + 1	9.88E + 2	3.80E + 2	5.95E + 0	3.20E + 1
1.00E + 3	1.00E + 1	8.92E + 2	3.53E + 2	5.81E + 0	3.04E + 1
1.10E + 3	9.09E + 0	7.39E + 2	3.11E + 2	5.59E + 0	2.78E + 1
1.20E + 3	8.33E + 0	6.28E + 2	2.75E + 2	5.37E + 0	2.56E + 1
1.30E + 3	7.69E + 0	5.36E + 2	2.42E + 2	5.10E + 0	2.37E + 1
1.40E + 3	7.14E + 0	4.61E + 2	2.15E + 2	4.89E + 0	2.20E + 1
1.50E + 3	6.67E + 0	3.99E + 2	1.95E + 2	4.75E + 0	2.05E + 1
1.60E + 3	6.25E + 0	3.47E + 2	1.80E + 2	4.69E + 0	1.92E + 1
1.70E + 3	5.88E + 0	3.05E + 2	1.69E + 2	4.66E + 0	1.81E + 1
1.80E + 3	5.56E + 0	2.72E + 2	1.58E + 2	4.63E + 0	1.71E + 1
1.90E + 3	5.26E + 0	2.42E + 2	1.49E + 2	4.60E + 0	1.62E + 1
2.00E + 3	5.00E + 0	2.18E + 2	1.42E + 2	4.59E + 0	1.54E + 1
2.25E + 3	4.44E + 0	1.71E + 2	1.27E + 2	4.59E + 0	1.38E + 1
2.50E + 3	4.00E + 0	1.39E + 2	1.15E + 2	4.54E + 0	1.26E + 1
2.75E + 3	3.64E + 0	1.14E + 2	1.05E + 2	4.51E + 0	1.16E + 1
3.00E + 3	3.33E + 0	9.70E + 1	9.62E + 1	4.45E + 0	1.08E + 1
3.25E + 3	3.08E + 0	8.31E + 1	8.88E + 1	4.39E + 0	1.01E + 1
3.50E + 3	2.86E + 0	7.27E + 1	8.20E + 1	4.30E + 0	9.55E + 0
3.75E + 3	2.67E + 0	6.35E + 1	7.62E + 1	4.22E + 0	9.02E + 0
4.02E + 3	2.49E + 0	5.67E + 1	7.10E + 1	4.13E + 0	8.59E + 0
4.26E + 3	2.35E + 0	5.05E + 1	6.60E + 1	4.04E + 0	8.18E + 0
4.51E + 3	2.22E + 0	4.50E + 1	6.21E + 1	3.98E + 0	7.80E + 0
4.74E + 3	2.11E + 0	4.08E + 1	5.88E + 1	3.92E + 0	7.50E + 0
5.00E + 3	2.00E + 0	3.66E + 1	5.50E + 1	3.84E + 0	7.16E + 0
5.99E + 3	1.67E + 0	2.51E + 1	4.56E + 1	3.67E + 0	6.21E + 0
6.99E + 3	1.43E + 0	1.82E + 1	3.91E + 1	3.53E + 0	5.54E + 0
8.00E + 3	1.25E + 0	1.37E + 1	3.45E + 1	3.42E + 0	5.04E + 0
9.01E + 3	1.11E + 0	1.06E + 1	3.09E + 1	3.32E + 0	4.65E + 0
1.00E + 4	1.00E + 0	8.49E + 0	2.81E + 1	3.23E + 0	4.35E + 0
1.49E + 4	6.70E − 1	4.34E + 0	2.05E + 1	2.88E + 0	3.55E + 0
1.92E + 4	5.20E − 1	2.08E + 0	3.11E + 0	5.36E + 0	1.30E + 1

Cu caused a revision in the Drude model parameters presented in our previous tabulation.[1] The experimentally determined values of $-\epsilon_1$ and ϵ_2 are plotted along with the Drude model values for these quantities. This allows one to see how well the Drude model parametrizes the data for these metals. At the higher frequencies the free electron model is sometimes poor (exceptions[1] are Ag, Au, and Al) because of intraband effects or surface quality of samples.

Table V. Molybdenum: Weaver *et al.*[a]

ω (cm^{-1})	λ (μm)	$-\epsilon_1$	ϵ_2	n	k
8.07E + 2	1.24E + 1	4.35E + 3	2.54E + 3	1.85E + 1	6.85E + 1
8.87E + 2	1.13E + 1	3.73E + 3	1.97E + 3	1.56E + 1	6.31E + 1
9.68E + 2	1.03E + 1	3.23E + 3	1.57E + 3	1.34E + 1	5.84E + 1
1.05E + 3	9.54E + 0	2.83E + 3	1.24E + 3	1.14E + 1	5.44E + 1
1.13E + 3	8.86E + 0	2.47E + 3	1.01E + 3	9.96E + 0	5.07E + 1
1.21E + 3	8.27E + 0	2.18E + 3	8.34E + 2	8.78E + 0	4.75E + 1
1.29E + 3	7.75E + 0	1.94E + 3	6.92E + 2	7.74E + 0	4.47E + 1
1.37E + 3	7.29E + 0	1.73E + 3	5.82E + 2	6.91E + 0	4.22E + 1
1.45E + 3	6.89E + 0	1.55E + 3	4.95E + 2	6.21E + 0	3.99E + 1
1.53E + 3	6.53E + 0	1.40E + 3	4.25E + 2	5.61E + 0	3.79E + 1
1.61E + 3	6.20E + 0	1.27E + 3	3.67E + 2	5.10E + 0	3.60E + 1
1.69E + 3	5.90E + 0	1.15E + 3	3.19E + 2	4.65E + 0	3.43E + 1
1.77E + 3	5.64E + 0	1.05E + 3	2.79E + 2	4.26E + 0	3.27E + 1
1.86E + 3	5.39E + 0	9.65E + 2	2.45E + 2	3.92E + 0	3.13E + 1
1.94E + 3	5.17E + 0	8.86E + 2	2.17E + 2	3.61E + 0	3.00E + 1
2.02E + 3	4.96E + 0	8.15E + 2	1.93E + 2	3.36E + 0	2.88E + 1
3.07E + 3	3.26E + 0	3.37E + 2	6.28E + 1	1.70E + 0	1.84E + 1
4.03E + 3	2.48E + 0	1.82E + 2	3.71E + 1	1.37E + 0	1.36E + 1
5.00E + 3	2.00E + 0	1.07E + 2	2.87E + 1	1.38E + 0	1.04E + 1
5.97E + 3	1.68E + 0	6.97E + 1	2.54E + 1	1.51E + 0	8.38E + 0
8.07E + 3	1.24E + 0	2.74E + 1	2.17E + 1	1.94E + 0	5.58E + 0
1.05E + 4	9.54E − 1	6.34E + 0	2.07E + 1	2.77E + 0	3.74E + 0
1.54E + 4	6.53E − 1	−1.17E + 0	2.68E + 1	3.74E + 0	3.58E + 0
2.02E + 4	4.96E − 1	2.61E + 0	2.50E + 1	3.36E + 0	3.73E + 0

[a] Ref. 2, p. 148.

Table VI. Vanadium: Weaver *et al.*[a]

ω (cm^{-1})	λ (μm)	$-\epsilon_1$	ϵ_2	n	k
8.07E + 2	1.24E + 1	1.94E + 3	1.18E + 3	1.28E + 1	4.59E + 1
9.68E + 2	1.03E + 1	1.43E + 3	7.47E + 2	9.51E + 0	3.90E + 1
1.29E + 3	7.75E + 0	8.69E + 2	3.47E + 2	5.77E + 0	3.00E + 1
1.61E + 3	6.20E + 0	5.75E + 2	1.86E + 2	3.90E + 0	2.43E + 1
1.94E + 3	5.17E + 0	4.05E + 2	1.15E + 2	2.82E + 0	2.03E + 1
2.90E + 3	3.44E + 0	1.75E + 2	4.10E + 1	1.54E + 0	1.33E + 1
3.87E + 3	2.58E + 0	9.39E + 1	2.33E + 1	1.19E + 0	9.77E + 0
5.16E + 3	1.94E + 0	4.85E + 1	1.50E + 1	1.07E + 0	7.04E + 0
6.13E + 3	1.63E + 0	3.10E + 1	1.23E + 1	1.08E + 0	5.67E + 0
7.26E + 3	1.38E + 0	1.88E + 1	1.06E + 1	1.18E + 0	4.50E + 0
8.07E + 3	1.24E + 0	1.26E + 1	1.02E + 1	1.34E + 0	3.80E + 0
8.87E + 3	1.13E + 0	8.06E + 0	1.04E + 1	1.60E + 0	3.26E + 0
1.01E + 4	9.92E − 1	3.31E + 0	1.16E + 1	2.09E + 0	2.77E + 0
1.49E + 4	6.70E − 1	2.43E + 0	1.38E + 1	2.41E + 0	2.87E + 0
2.02E + 4	4.96E − 1	4.36E + 0	1.18E + 1	2.02E + 0	2.91E + 0
5.16E + 3	1.94E + 0	5.46E + 1	4.41E + 1	2.79E + 0	7.90E + 0
6.21E + 3	1.61E + 0	3.25E + 1	3.51E + 1	2.77E + 0	6.34E + 0
7.18E + 3	1.39E + 0	1.96E + 1	2.72E + 1	2.64E + 0	5.15E + 0
8.23E + 3	1.22E + 0	1.15E + 1	2.34E + 1	2.70E + 0	4.33E + 0
9.20E + 3	1.09E + 0	6.05E + 0	2.17E + 1	2.87E + 0	3.78E + 0
1.05E + 4	9.84E − 1	3.61E + 0	2.06E + 1	2.94E + 0	3.50E + 0
1.52E + 4	6.59E − 1	−1.01E + 0	2.01E + 1	3.25E + 0	3.09E + 0
2.02E + 4	4.96E − 1	−4.74E + 0	2.56E + 1	3.92E + 0	3.26E + 0
2.52E + 4	3.97E − 1	2.69E + 0	2.14E + 1	3.07E + 0	3.48E + 0
3.02E + 4	3.32E − 1	4.75E + 0	1.53E + 1	2.37E + 0	3.22E + 0
3.52E + 4	2.84E − 1	3.96E + 0	1.02E + 1	1.87E + 0	2.73E + 0
4.02E + 4	2.49E − 1	2.68E + 0	7.33E + 0	1.60E + 0	2.29E + 0
4.52E + 4	2.21E − 1	1.26E + 0	6.45E + 0	1.63E + 0	1.98E + 0
5.02E + 4	1.99E − 1	1.14E + 0	6.29E + 0	1.62E + 0	1.94E + 0
5.32E + 4	1.88E − 1	1.45E + 0	5.59E + 0	1.47E + 0	1.90E + 0

[a] Ref. 2, p. 50.

The optical resistivities ρ_{opt} have been computed [using Eq. (16)] and compared with the handbook values of the dc resistivities ρ_0. The ratios of these two resistivities are of the order of unity for Al, Au, Fe, Pb, Mo, Ag, Ti, and V. We suggest, however, that new measurements of ρ_0 would be useful for a number of these fourteen metals.

We want to thank M. Milham and E. Steubing for encouraging and supporting this work. We would also like to express our appreciation to C. A. Ward (Krebs) for helping to lay the groundwork for this endeavor.

This work was partially supported by grant DAAA-15-85-K-0004 (M. Milham).

References

1. M. A. Ordal, L. L. Long, R. J. Bell, S. E. Bell, R. R. Bell, R. W. Alexander, and C. A. Ward, "Optical Properties of the Metals Al, Co, Cu, Au, Fe, Pb, Ni, Pt, Ag, Ti, and W in the Infrared and Far Infrared," Appl. Opt. 22, 1099 (1983).
2. J. H. Weaver, C. Krafka, D. W. Lynch, and E. E. Koch, *Physics Data, Optical Properties of Metals, Part I: The Transition Metals* (Fachinformationszentrum, 7514 Eggenatein-Leopoldshafen 2, Karlsruhe, Federal Republic of Germany, 1981).
3. P. B. Johnson and R. W. Christy, "Optical Constants of Transition Metals: Ti, V, Cr, Mn, Fe, Co, Ni, and Pd," Phys. Rev. 9, 5056 (1974).
4. T. J. Moravec, J. C. Rife, and R. N. Dexter, "Optical Constants of Nickel, Iron, and Nickel-Iron Alloys in the Vacuum Ultraviolet," Phys. Rev. B 13, 3297 (1976).
5. J. Babiskin and J. R. Anderson, Eds., *American Institute of Physics Handbook* (McGraw-Hill, New York, 1972), pp. 9-39, 9-40.
6. S. Perkowitz, G. L. Carr, B. Subramaniam, and B. Mitrovic, "Far-infrared Determination of Scattering Behavior and Plasma Frequency in V_3Si, Nb_3Ge, and Hb," Phys. Rev. B 32, 153 (1985).

Reprinted from Applied Optics, Vol. 26, Page 744, February 15, 1987

Optical properties of Au, Ni, and Pb at submillimeter wavelengths

Mark A. Ordal, Robert J. Bell, Ralph W. Alexander, Jr., Larry L. Long, and Marvin R. Querry

Measurements of the optical properties, and thus the optical constants, of metals at submillimeter wavelengths are almost nonexistent. We used a nonresonant cavity to measure at ambient temperature the angle averaged absorptance spectra $P(\omega)$ of gold, nickel, and lead in the 30–300-cm^{-1} wave-number region. The real part of the normalized surface impedance spectrum $z(\omega) = r(\omega) + ix(\omega)$ was determined from $P(\omega)$. The $r(\omega)$ spectrum was combined with previous measurements by others at higher frequencies, and Kramers-Kronig analyses of the resultant $r(\omega)$ spectra provided $\epsilon(\omega) = \epsilon_1(\omega) + i\epsilon_2(\omega)$ and $N(\omega) = n(\omega) + ik(\omega)$ for gold and nickel in the 35–15,000-cm^{-1} region and for lead in the 15–15,000-cm^{-1} region. We also derived an exact analytical expression for $P(\omega)$ of a metal.

I. Introduction

The extremely high reflectivity of metals at submillimeter wavelengths generally precludes direct measurement of the reflectance or absorptance as is customary at shorter wavelengths.[1,2] It is more practical to employ one of several methods to obtain the normalized surface resistance $r(\omega)$ of a metal. Two of the methods available for measuring the normalized surface resistance of a metal are the nonresonant cavity approach of Pinkerton *et al.*[3,4] and the parallel plate transmission line technique of Brandli and Sievers.[5] In our work a nonresonant cavity was used to obtain the normalized surface resistance of metal samples at ambient temperature. We made use of parallel plate transmission line results of Brandli and Sievers for Au to calibrate our nonresonant cavity. We also made use of the Brandli and Sievers measurements on Pb to extend the normalized surface resistance of Pb to frequencies lower than our own measurements.

The analysis of the nonresonant cavity of Pinkerton *et al.*[3,4] can be improved in several ways. The most significant improvement is use of an exact expression (instead of an approximate one) for the angle averaged absorptance of a metal. The accuracy of the analysis of the experimental data is much better when using an exact expression.

Making the measurements at room temperature allowed us to improve the design, fabrication, and use of the nonresonant cavity itself. The goal of the prior work of Sievers and co-workers was to make measurements of the surface resistance at cryogenic temperatures.

II. Analysis

A nonresonant cavity by definition has no preferred standing wave modes. This requires that all wavelengths of interest be much smaller than any of the dimensions of the cavity. Thus the cavity has a large number of closely spaced and nearly identically excited modes. The radiation in the cavity can be thought of as a uniformly distributed photon gas. This problem was originally studied by Lamb.[6]

The cavity used is essentially a right cylinder with plane end caps. Radiation enters the cavity through a small input hole and exits through another small output hole. One removable endplate of the cavity is made from either a reference metal or the sample metal. We measure the transmission spectrum of the cavity with a reference metal endplate to obtain $I_r(\omega)$ and again with the sample metal endplate to obtain $I_s(\omega)$. It is the ratio $I_s(\omega)/I_r(\omega)$ that we need for the analysis. We follow the approach used by Pinkerton and Sievers[3] with some changes because they changed both endplates of the cavity and with an improved calculation of the angle averaged absorption. We used numeric subscripts to denote various areas of the cavity walls, and we defined $P(\omega)$ to be the angle averaged

Marvin Querry is with University of Missouri-Kansas City, Physics Department, Kansas City, Missouri 64110; when this work was done all the other authors were with University of Missouri-Rolla, Physics Department, Rolla, Missouri 65401; M. A. Ordal is now with North Dakota State University, Physics Department, Fargo, North Dakota 58105, and L. L. Long is now with McDonnell Douglas Corporation, P.O. Box 516, St. Louis, Missouri 63166.

Received 22 February 1986.
0003-6935/87/040744-09$02.00/0.

absorptance. Calculating the ratio of detected intensities for sample and reference configurations of the nonresonant cavity gave[3]

$$\frac{I_s(\omega)}{I_r(\omega)} - \frac{[2S_1 + (S_2 + S_3)P_r(\omega)] + S_4P_r(\omega)}{[2S_1 + (S_2 + S_3)P_r(\omega)] + S_4P_s(\omega)} = 0, \quad (1)$$

where S_1 ≡ cross-sectional area of an input or output hole,
S_2 ≡ area of the cavity sidewalls (excluding input and output holes),
S_3 ≡ area of the bottom plate (which on our cavity is not normally removable),
S_4 ≡ area of the removable top plate,
$P_r(\omega)$ ≡ angle averaged absorptance of the reference metal,
$P_s(\omega)$ ≡ angle averaged absorptance of the sample metal,
$I_s(\omega)$ ≡ intensity at frequency ω measured at the output hole of the cavity when the top plate of area S_4 is made of the sample metal, and
$I_r(\omega)$ ≡ intensity at frequency ω measured at the output hole of the cavity when the cavity consists entirely of the reference metal.

For $P_r(\omega)$ we used an exact expression derived in the Appendix and presented in Eq. (A4), instead of the approximate expression used by Pinkerton and Sievers. We made the approximation $\xi = 1$ in Eq. (A4) for $P_s(\omega)$ equivalent to setting the refractive index $N = n + ik = n(1 + i)$ for the sample metal. Equation (1) is thus a fraction of only one unknown—the normalized surface resistance r_s of the sample metal. No further manipulation of Eq. (1) is required since numerous library routines[7] are available for solving an equation of the form $F(r_s) = 0$.

We tested this analysis by taking values of n and k from the literature or Drude model parameters ω_p and ω_τ representative of samples of interest[8] and calculating the normalized surface resistance—call it r_s'—and the intensity ratio I_s/I_r. Treating the calculated intensity ratio as if it were an actual measurement we solved Eq. (1) for r_s. If everything were exact, we should have found $r_s = r_s'$. As it was, we typically found r_s to differ from r_s' by about one-tenth of a percent. For the 10–350-cm^{-1} spectral range we found agreement that, in the worst case, was slightly better than 1%. Better than 1% agreement included the effect of setting $\xi = 1$ for the sample metal (when for typical samples it can range from 2 to 15 at 350 cm^{-1}). Using an approximate expression for the angle averaged absorptance, Pinkerton and Sievers[3] found a worst case effect of 4% for setting $\xi = 1$. One can use the approximation that $\xi = 1$ as long as $1/\sqrt{(\epsilon_1^2 + \epsilon_2^2)} \ll 1$, even if $\xi \gg 1$.

III. Experiment

The ready access to the cavity afforded by a room temperature environment made it practical to use a single nonresonant cavity with removable endplate(s). By using a single cavity we were certain that the geometry and surface finish of the fixed reference portion of the cavity was identical for sample and reference spectra. It was also possible to machine input and output cones integral to the cavity body, thus eliminating cone-to-cavity joints that constitute a possible loss mechanism not accounted for in the analysis of the data.

Without the severe space constraints imposed by a cryostat, our room temperature nonresonant cavity could be made much larger than the cavities used by Pinkerton and Sievers. The internal surface area of our cavity was more than an order of magnitude larger than that of the Pinkerton and Sievers cavities (62.93 vs 5.97 cm^2). With entrance and exit holes of 5.7-mm diameter, our larger cavity had sufficient throughput to permit the use of a Golay cell detector.

The additional space afforded by a room temperature environment made a genuinely effective sample clamping system easy to implement. We chose to make only a single endplate of our cavity removable. In this arrangement an inverted U frame bolted to the cavity body carried a single bolt projecting downward over the center of the 47-mm diam opening in the cavity body. Samples (thin plates or foils) were mounted to a stiff carrier block of 3/8-in. aluminum alloy. The bolt carried by the inverted U frame was screwed down against the back of the sample carrier forcing the sample into intimate contact with the open end of the cavity body.

In fabricating the cavity body, we avoided rounded edges at the ends of the cavity by attaching false endfaces before machining and polishing a slightly tapered bore. After polishing the interior surfaces of the cavity body with successively finer grits (terminating with a 1-μm diamond abrasive) the false endfaces were removed leaving virtually knife sharp edges at the ends of the hole through the cavity body.

On the input side of our cavity body, a large brass input cone adapted the small machined-in-place input cone to a larger diameter input beam.

Our cavity was bolted to a base of the proper height, which in turn was bolted to the bottom of the oversized sample chamber on a modified RIIC (Beckman) FS-720 Fourier spectrometer. The sample chamber was normally under a vacuum of ~0.04 Torr. Changing samples required breaking the vacuum. Using dry nitrogen to vent the chamber and maintaining a flow of nitrogen through the instrument while changing samples resulted in good run-to-run repeatability and minimal pumping time to regain the previous vacuum level.

IV. Calibration

A significant improvement was made in calibrating the cavity, i.e., in determining the optical properties of the reference metal. Pinkerton and Sievers used brass to make their cavities. Using the parallel plate transmission line method, they measured the normalized surface resistance of brass foil of similar composition to their cavity body. Finally, Pinkerton and Sievers compared these parallel plate transmission line measurements to Drude model calculations which used the

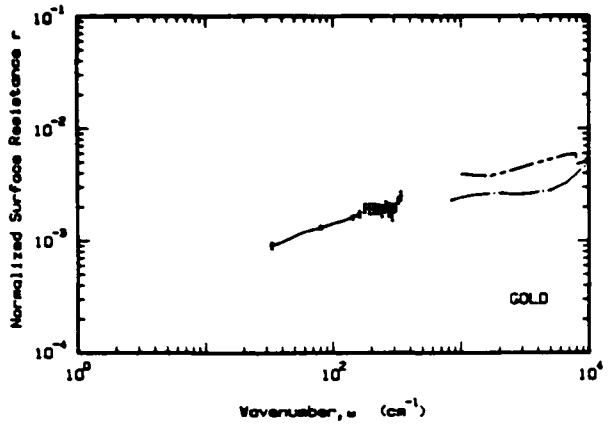

Fig. 1. Normalized surface resistance of Au: solid circles, nonresonant cavity results; dashed line, Lynch and Hunter (tabulated in Ref. 1); dash–dot line, Motulevich *et al.* (tabulated in Ref. 2); solid line, Brandli and Sievers.[5]

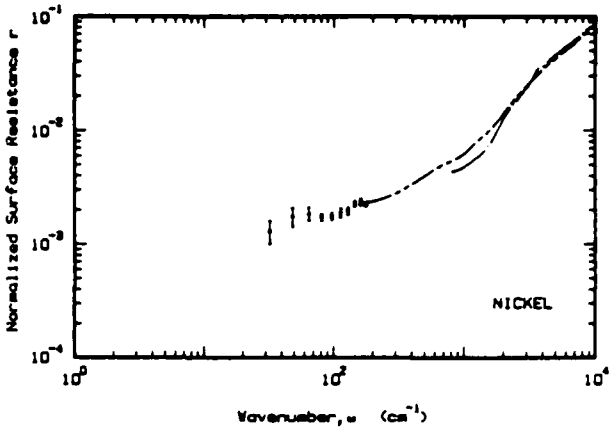

Fig. 2. Normalized surface resistance of Ni: solid circles, nonresonant cavity results; dash–dot line, Lynch and Hunter (tabulated in Ref. 1); dash line, average of the results in Ref. 7 with previously unpublished measurements.

measured dc resistivity of the brass. Deciding the parallel plate transmission line measurements and the Drude model calculations to be in sufficiently good agreement, they used the Drude model calculations over the entire range of their nonresonant cavity experiment (a range considerably broader than covered by their actual parallel plate transmission line measurements).

A better approach to calibration of our nonresonant cavity involved the use of a sample with known optical properties. The optical properties of the reference portion of the nonresonant cavity are taken as adjustable parameters to make the measured normalized surface resistance of the calibration sample agree with the known values. As calibration samples we used 0.127-mm thick 99.9985% pure Au foil and 0.025-mm 99.9992% pure Ni foil. The parallel plate transmission line measurements of Brandli and Sievers on Au foil provided known values of the optical properties with which to compare in the 35–145-cm^{-1} range. Kramers-Kronig analysis of reflectance measurements on Ni provided known values of the optical properties with which to compare in the 193–339-cm^{-1} range. The reflectance of Ni from 180 to 20,000 cm^{-1} was taken as the average of previously published measurements[8] and measurements on an equally pure sample from a different supplier. We reduced the problem from a two-parameter fit to a single-parameter fit by calculating the plasma frequency ω_p of our Al reference metal from handbook quantities. Adjusting the scattering frequency ω_τ at each spectral point of interest until agreement with the known values was reached completed the calibration procedure.

It is important to note that we did not assume Drude model behavior for the reference metal because the fitting process is repeated at each spectral point of interest. Also, the fit need not involve adjusting the Drude model parameters ω_p and ω_τ; these parameters were just easier to work with when one wanted to fix one and adjust the other. Using n and k or r and x would be equally appropriate in the calibration procedure, where x is the imaginary part of the complex surface impedance $z = r + ix$.

V. Results

Figure 1 shows the normalized surface resistance of Au obtained from the measurements made by selected investigators. The solid line with error bars of 4–7% represents the parallel plate transmission line measurements of Brandli and Sievers.[5] The solid circles with error bars of 6–17% show our nonresonant cavity measurements in the 161–339-cm^{-1} range. As mentioned earlier, the calibration of our cavity in that range stems from measurements made on a sample of high-purity nickel. The dashed line at higher frequencies shows the normalized surface resistance derived from the absorption measurements of Lynch and Hunter (tabulated in Ref. 1) and the dash–dot line the surface impedance from the measurements of Motulevich *et al.* (tabulated in Ref. 2).

Figure 2 shows the normalized surface resistance of Ni obtained from the measurements made by selected investigators. The solid circles with error bars of 4–23% show our nonresonant cavity measurements in the 32–177-cm^{-1} range. As mentioned earlier, the calibration of our cavity in that range stems from measurements made on a sample of high-purity gold: the values of the normalized surface resistance for Au resulting from those measurements were forced to agree with the parallel plate transmission line measurements of Brandli and Sievers[5] by treating the optical properties of the reference portions of the cavity walls as adjustable parameters. For comparison we also show the normalized surface resistance derived from absorption measurements by Lynch and Hunter[1] (dash–dot) and Ref. 8 (dash).

Figure 3 shows the normalized surface resistance of Pb obtained from the measurements made by selected investigators. The solid line with error bars of 3–6% represents the parallel plate transmission line measurements of Brandli and Sievers.[5] The solid circles

Appendix A

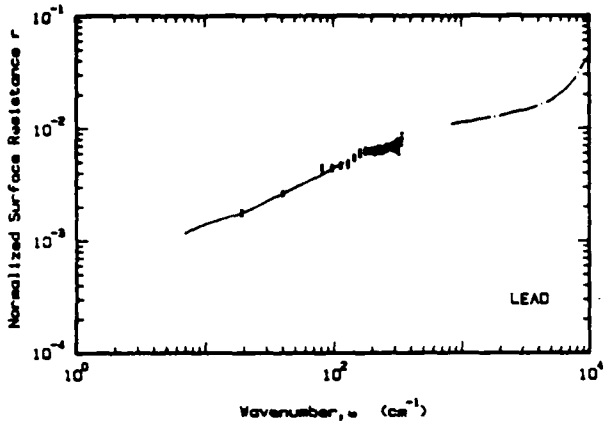

Fig. 3. Normalized surface resistance of Pb: solid circles, nonresonant cavity results; dash–dot line, Motulevich *et al.*[9]; solid line, Brandli and Sievers.[5]

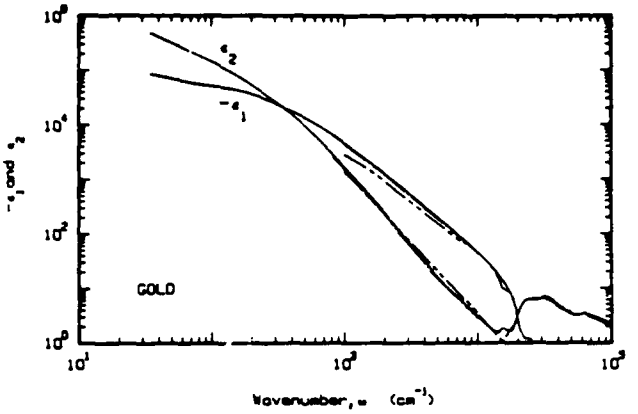

Fig. 4. Kramers-Kronig results for $-\epsilon_1$ and ϵ_2 of Au: solid line, results obtained by combining nonresonant cavity measurements with the results of Motulevich *et al.*[9]; dash line for Lynch and Hunter (tabulated in Ref. 1); dash–dot line for Motulevich *et al.*[9]

with error bars of 6–16% show our nonresonant cavity measurements in the 81–339-cm^{-1} range.

Figure 4 shows $-\epsilon_1$ and ϵ_2 for Au obtained from Kramers-Kronig analysis of the normalized surface resistance. For Kramers-Kronig analysis, we used the results of Motulevich *et al.* (tabulated in Ref. 2) from 833 to 1×10^4 cm^{-1} (the dash–dot line in Fig. 1). From 1×10^4 to 8×10^7 cm^{-1} we used the composite tabulation by Lynch and Hunter.[1] The data of Motulevich were used because it agreed better with the nonresonant cavity measurements than did the data at the low-frequency end of the Lynch and Hunter table. A spline fit was used to bridge the three sets of data. Because of this use of the data of Motulevich *et al.*, combined with our nonresonant cavity data, the values of ϵ_2 reported in Table I are higher than those given in Lynch and Hunter at the small wavenumber end of their table. We used the Drude model with $\omega_\tau = 300$ cm^{-1} and $\omega_p = 7.25 \times 10^4$ cm^{-1} as a low-frequency extrapolation down to 0.05 cm^{-1}. Table I lists values of $-\epsilon_1$ and ϵ_2 at various frequencies in the 35–1.5×10^4-cm^{-1} range. Also listed in Table I are the reflectance R and the real and imaginary parts of the complex index of refraction $N \equiv n + ik$. We terminate the table at 1.5×10^4 cm^{-1} because our values for the optical constants at higher frequencies were not significantly different from those in the tabulation used to calculate high-frequency values for the normalized surface resistance r.

Figure 5 shows $-\epsilon_1$ and ϵ_2 for Ni obtained from Kramers-Kronig analysis of the normalized surface resistance. For Kramers-Kronig analysis, we used the results from our Kramers-Kronig analysis of reflectance measurements from 190 to 20,000 cm^{-1} (the dashed line in Fig. 2). From 2.09×10^4 to 9.28×10^5 cm^{-1} we used the composite tabulation by Lynch and Hunter.[1] We used the Drude model with $\omega_\tau = 178$ cm^{-1} and $\omega_p = 3.94 \times 10^4$ cm^{-1} as a low-frequency extrapolation down to 0.05 cm^{-1}. Table II lists values of $n, k, -\epsilon_1, \epsilon_2$, and the reflectance R at various frequencies in the 35–1.5×10^4-cm^{-1} range. As with Au, we terminate the table at 1.5×10^4 cm^{-1}.

Figure 6 shows $-\epsilon_1$ and ϵ_2 for Pb obtained from the Kramers-Kronig analysis of the normalized surface resistance. For Kramers-Kronig analysis, we used the results of Motulevich *et al.*[9] from 1430 to 1.82×10^4 cm^{-1} (the dash–dot line in Fig. 3). Above 1.82×10^4 cm^{-1} we used the behavior of the normalized surface resistance of other metals to draw an arbitrary high-frequency extrapolation to 1×10^5 cm^{-1}. Small adjustments were made to this extrapolation until the n and k values at frequencies above 1.7×10^4 cm^{-1} resulting from our Kramers-Kronig analysis of the normalized surface resistance were in reasonable agreement with the tabulated values of Motulevich *et al.*[9] We used the parallel plate transmission line measurements of Brandli and Sievers[5] from 23 to 119 cm^{-1}. We used the Drude model with $\omega_\tau = 1175$ cm^{-1} and $\omega_p = 5.94 \times 10^4$ cm^{-1} as a low-frequency extrapolation down to 0.05 cm^{-1}. Table III lists values of $-\epsilon_1$ and ϵ_2 at various frequencies in the 15–1.5×10^4-cm^{-1} range. Also listed are the reflectance R and the real and imaginary parts of the complex index of refraction $N \equiv n + ik$. We start the table at 15 cm^{-1}, since the low-frequency Drude model wing falls well within the error bars on the Brandli and Sievers measurements in the 15–23-cm^{-1} range.

VI. Summary

The normalized surface impedance $r(\omega)$ of gold, nickel, and lead have been determined at submillimeter wavelengths using a nonresonant cavity. Very few optical constants for metals exist for this region of the spectrum. We have improved the analysis of the experiment by deriving an exact expression for the angle averaged absorptance. We demonstrated that the nonresonant cavity can be used to obtain reasonably accurate values for the real part of the surface impedance (the surface resistance) in the submillimeter. When combined with measurements by others (see Refs. 1 and 2, for example) at shorter wavelengths, the Kramers-Kronig relation can be used to obtain the imaginary part of the surface impedance $x(\omega)$. The

Table I. Optical Constants of Au Obtained from Kramers-Kronig Analysis of the Normalized Surface Resistance

ω (cm^{-1})	n	k	$-\epsilon_1$	ϵ_2	R
35	4.47E + 02	5.34E + 02	8.47E + 04	4.77E + 05	0.9963
50	3.56E + 02	4.44E + 02	7.01E + 04	3.16E + 05	0.9956
65	3.02E + 02	3.90E + 02	6.09E + 04	2.35E + 05	0.9950
80	2.63E + 02	3.53E + 02	5.55E + 04	1.86E + 05	0.9946
100	2.25E + 02	3.19E + 02	5.11E + 04	1.43E + 05	0.9941
125	1.88E + 02	2.88E + 02	4.74E + 04	1.08E + 05	0.9937
150	1.60E + 02	2.63E + 02	4.39E + 04	8.41E + 04	0.9933
175	1.37E + 02	2.43E + 02	4.03E + 04	6.66E + 04	0.9930
200	1.19E + 02	2.25E + 02	3.66E + 04	5.37E + 04	0.9927
225	1.05E + 02	2.10E + 02	3.31E + 04	4.41E + 04	0.9924
250	9.35E + 01	1.97E + 02	2.99E + 04	3.67E + 04	0.9921
300	7.64E + 01	1.75E + 02	2.46E + 04	2.67E + 04	0.9916
350	6.43E + 01	1.58E + 02	2.07E + 04	2.03E + 04	0.9912
400	5.48E + 01	1.44E + 02	1.79E + 04	1.58E + 04	0.9909
450	4.68E + 01	1.33E + 02	1.56E + 04	1.25E + 04	0.9907
500	3.99E + 01	1.24E + 02	1.38E + 04	9.89E + 03	0.9906
600	2.98E + 01	1.08E + 02	1.07E + 04	6.42E + 03	0.9905
700	2.30E + 01	9.49E + 01	8.48E + 03	4.37E + 03	0.9904
800	1.82E + 01	8.47E + 01	6.84E + 03	3.08E + 03	0.9903
900	1.47E + 01	7.63E + 01	5.60E + 03	2.24E + 03	0.9903
1000	1.21E + 01	6.92E + 01	4.64E + 03	1.67E + 03	0.9902
1250	8.29E + 00	5.62E + 01	3.09E + 03	9.32E + 02	0.9898
1500	6.03E + 00	4.74E + 01	2.21E + 03	5.71E + 02	0.9895
1750	4.54E + 00	4.10E + 01	1.66E + 03	3.72E + 02	0.9894
2000	3.50E + 00	3.60E + 01	1.29E + 03	2.52E + 02	0.9894
2250	2.74E + 00	3.21E + 01	1.02E + 03	1.76E + 02	0.9895
2500	2.20E + 00	2.89E + 01	8.33E + 02	1.27E + 02	0.9896
2750	1.81E + 00	2.63E + 01	6.89E + 02	9.50E + 01	0.9897
3000	1.52E + 00	2.41E + 01	5.79E + 02	7.33E + 01	0.9896
3250	1.31E + 00	2.22E + 01	4.93E + 02	5.81E + 01	0.9895
3500	1.14E + 00	2.06E + 01	4.24E + 02	4.70E + 01	0.9894
3750	1.00E + 00	1.92E + 01	3.69E + 02	3.86E + 01	0.9893
4000	8.90E − 01	1.80E + 01	3.24E + 02	3.21E + 01	0.9892
4250	7.93E − 01	1.70E + 01	2.87E + 02	2.69E + 01	0.9891
4500	7.10E − 01	1.60E + 01	2.55E + 02	2.27E + 01	0.9890
4750	6.40E − 01	1.51E + 01	2.28E + 02	1.94E + 01	0.9889
5000	5.81E − 01	1.43E + 01	2.05E + 02	1.67E + 01	0.9888
5500	4.92E − 01	1.30E + 01	1.68E + 02	1.28E + 01	0.9885
6000	4.30E − 01	1.19E + 01	1.40E + 02	1.02E + 01	0.9879
6500	3.84E − 01	1.09E + 01	1.18E + 02	8.36E + 00	0.9873
7000	3.48E − 01	1.01E + 01	1.01E + 02	7.00E + 00	0.9865
7500	3.19E − 01	9.35E + 00	8.72E + 01	5.97E + 00	0.9857
8000	2.96E − 01	8.71E + 00	7.59E + 01	5.15E + 00	0.9848
8500	2.76E − 01	8.15E + 00	6.64E + 01	4.50E + 00	0.9838
9000	2.58E − 01	7.65E + 00	5.85E + 01	3.95E + 00	0.9828
9500	2.43E − 01	7.20E + 00	5.18E + 01	3.50E + 00	0.9818
10000	2.29E − 01	6.79E + 00	4.60E + 01	3.11E + 00	0.9807
11000	2.05E − 01	6.06E + 00	3.67E + 01	2.49E + 00	0.9785
12000	1.88E − 01	5.44E + 00	2.95E + 01	2.05E + 00	0.9757
13000	1.79E − 01	4.88E + 00	2.38E + 01	1.75E + 00	0.9717
14000	1.77E − 01	4.38E + 00	1.92E + 01	1.55E + 00	0.9656
15000	2.19E − 01	3.91E + 00	1.53E + 01	1.72E + 00	0.9477

complex surface impedance $z(\omega) = r(\omega) + ik(\omega)$ can then be used to find the complex dielectric constant $\epsilon(\omega) = \epsilon_1(\omega) + i\epsilon_2(\omega)$ or complex refractive index $N(\omega) = n(\omega) + ik(\omega)$.

This work was supported in part by the U.S. Army Chemical Research, Development and Engineering Command (DAAA-15-85-K-0004).

Appendix: Calculation of the Angle Averaged Absorptance

To use the nonresonant cavity method one needs an expression for the angle averaged absorptance as a function of the optical constants. We could start with the Fresnel equations in their usual formulation[10] in terms of n and k and the angle of incidence θ. However, we choose to make the change of variable $\eta \equiv \cos(\theta)$. To avoid unnecessary algebra later, we also make the changes of variable given by $r \equiv n/(n^2 + k^2)$, $x \equiv -k/(n^2 + k^2)$, and $\xi = k/n = -x/r$. (Note that the complex index of refraction is taken to be $N \equiv n + ik$, and the normalized surface impedance of a metal is taken to be $z = r + ix$.) The absorptances for the p and s polarizations (the TM and TE modes, respectively, of Pinkerton and Sievers[3]) become

$$A_p(\eta) = 1 - R_p(\eta) = \frac{4\eta}{\left(\frac{1}{r}\right)\eta^2 + 2\eta + r(1+\xi^2)},$$

$$A_s(\eta) = 1 - R_s(\eta) = \frac{4\eta}{r(1+\xi^2)\eta^2 + 2\eta + \frac{1}{r}}.$$

Note that both $A_p(\eta)$ and $A_s(\eta)$ have the same form when considered as functions of η. Both $\int_0^1 A_p(\eta)\eta d\eta$ and $\int_0^1 A_s(\eta)\eta d\eta$ are of the form

$$4\int \frac{y^2 dy}{ay^2 + by + c}.$$

From a table of integrals[11] we find

$$\int \frac{y^2 dy}{ay^2 + by + c} = \frac{y}{a} - \frac{b}{2a^2}\ln(ay^2 + by + c) + \frac{b^2 - 2ac}{2a^2}\int \frac{dy}{ay^2 + by + c},$$

with

$$\int \frac{dy}{ay^2 + by + c} = \begin{cases} \frac{2}{\sqrt{4ac - b^2}} \arctan\left(\frac{2ay + b}{\sqrt{4ac - b^2}}\right), \\ \frac{1}{\sqrt{b^2 - 4ac}} \ln\left(\frac{2ay + b - \sqrt{b^2 - 4ac}}{2ay + b + \sqrt{b^2 - 4ac}}\right). \end{cases}$$

For the p polarization $a \equiv 1/r$, $b \equiv 2$, and $c \equiv r(1 + \xi^2)$. For the s polarization $a \equiv r(1 + \xi^2)$, $b \equiv 2$, and $c \equiv 1/r$. For both the s and p polarizations the product $ac = 1 + \xi^2$ makes $b^2 - 4ac = -4\xi^2 < 0$. Consequently, we must use the arctan form of the integral.

Define $d \equiv \sqrt{4ac - b^2} = 2\xi$. For both polarizations we have to evaluate an expression of the form

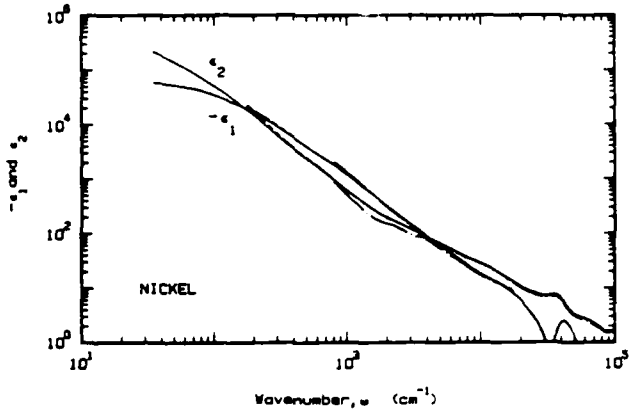

Fig. 5. Kramers-Kronig results for $-\epsilon_1$ and ϵ_2 of Ni: solid line, results obtained by combining nonresonant cavity measurements with the Kramers-Kronig results obtained from our reflectance measurements (with the values of Lynch and Hunter from Ref. 1 used above 20,000 cm^{-1}); dash–dot line for Lynch and Hunter (tabulated in Ref. 1); and dash line for the Kramers-Kronig results from averaging the reflectance in Ref. 8 with previously unpublished reflectance measurements.

$$\int_0^1 A(\eta)\eta d\eta = 4\left[\frac{\eta}{a} - \frac{b}{2a^2}\ln(a\eta^2 + b\eta + c) + \left(\frac{b^2 - 2ac}{a^2 d}\right)\tan^{-1}\left(\frac{2a\eta + b}{d}\right)\right]_{\eta=0}^{\eta=1}$$

$$= 4\left\{\frac{1}{a} - \frac{b}{2a^2}\ln\left(\frac{a+b+c}{c}\right) + \left(\frac{b^2 - 2ac}{a^2 d}\right)\left[\tan^{-1}\left(\frac{2a+b}{d}\right) - \tan^{-1}\left(\frac{b}{d}\right)\right]\right\}$$

$$= 4\left\{\frac{1}{a} - \frac{b}{2a^2}\ln\left(\frac{a+b+c}{c}\right) + \left(\frac{b^2 - 2ac}{a^2 d}\right)\tan^{-1}\left[\frac{2ad}{d^2 + b(2a+b)}\right]\right\}. \quad \text{(A1)}$$

where we have made use of the identity

$$\tan^{-1}(A) - \tan^{-1}(B) = \tan^{-1}\left(\frac{A - B}{1 + AB}\right).$$

For both polarizations,

$$ac = \left(\frac{1}{r}\right)[r(1 + \xi^2)] = 1 + \xi^2,$$

$$b^2 - 2ac = 2^2 - 2(1 + \xi^2) = 2(1 - \xi^2).$$

A. *P*-Polarization Integral

For the p polarization $a \equiv 1/r$, $b \equiv 2$, and $c \equiv r(1 + \xi^2)$. The coefficients in Eq. (A1) become

Appendix A

Table II. Optical Constants of Ni Obtained from Kramers-Kronig Analysis of the Normalized Surface Resistance

ω (cm^{-1})	n	k	$-\epsilon_1$	ϵ_2	R
35	2.86E + 02	3.75E + 02	5.90E + 04	2.15E + 05	0.9949
50	2.19E + 02	3.17E + 02	5.26E + 04	1.39E + 05	0.9941
65	1.76E + 02	2.79E + 02	4.71E + 04	9.83E + 04	0.9936
80	1.44E + 02	2.50E + 02	4.19E + 04	7.19E + 04	0.9931
100	1.16E + 02	2.19E + 02	3.46E + 04	5.07E + 04	0.9925
125	9.20E + 01	1.91E + 02	2.80E + 04	3.51E + 04	0.9919
150	7.51E + 01	1.70E + 02	2.32E + 04	2.55E + 04	0.9913
175	6.25E + 01	1.53E + 02	1.96E + 04	1.91E + 04	0.9909
200	5.27E + 01	1.39E + 02	1.66E + 04	1.47E + 04	0.9905
225	4.51E + 01	1.27E + 02	1.42E + 04	1.15E + 04	0.9902
250	3.91E + 01	1.17E + 02	1.22E + 04	9.16E + 03	0.9898
300	3.08E + 01	1.01E + 02	9.17E + 03	6.20E + 03	0.9889
350	2.56E + 01	8.78E + 01	7.05E + 03	4.50E + 03	0.9878
400	2.25E + 01	7.81E + 01	5.60E + 03	3.52E + 03	0.9865
450	2.00E + 01	7.07E + 01	4.60E + 03	2.83E + 03	0.9853
500	1.81E + 01	6.46E + 01	3.85E + 03	2.33E + 03	0.9841
600	1.52E + 01	5.55E + 01	2.85E + 03	1.69E + 03	0.9818
700	1.30E + 01	4.90E + 01	2.23E + 03	1.28E + 03	0.9800
800	1.10E + 01	4.38E + 01	1.80E + 03	9.66E + 02	0.9787
900	9.55E + 00	3.95E + 01	1.47E + 03	7.54E + 02	0.9771
1000	8.42E + 00	3.57E + 01	1.20E + 03	6.01E + 02	0.9752
1250	7.12E + 00	2.90E + 01	7.87E + 02	4.12E + 02	0.9685
1500	6.05E + 00	2.44E + 01	5.59E + 02	2.95E + 02	0.9625
1750	5.45E + 00	2.10E + 01	4.10E + 02	2.28E + 02	0.9547
2000	5.30E + 00	1.85E + 01	3.12E + 02	1.95E + 02	0.9443
2250	5.11E + 00	1.66E + 01	2.49E + 02	1.69E + 02	0.9347
2500	4.95E + 00	1.51E + 01	2.04E + 02	1.50E + 02	0.9250
2750	4.79E + 00	1.39E + 01	1.71E + 02	1.34E + 02	0.9158
3000	4.67E + 00	1.29E + 01	1.46E + 02	1.21E + 02	0.9066
3250	4.53E + 00	1.21E + 01	1.26E + 02	1.10E + 02	0.8979
3500	4.40E + 00	1.14E + 01	1.11E + 02	1.01E + 02	0.8896
3750	4.28E + 00	1.08E + 01	9.81E + 01	9.25E + 01	0.8814
4000	4.16E + 00	1.02E + 01	8.75E + 01	8.52E + 01	0.8734
4250	4.06E + 00	9.73E + 00	7.82E + 01	7.90E + 01	0.8651
4500	4.03E + 00	9.30E + 00	7.03E + 01	7.49E + 01	0.8559
4750	3.95E + 00	8.95E + 00	6.46E + 01	7.07E + 01	0.8491
5000	3.83E + 00	8.63E + 00	5.98E + 01	6.61E + 01	0.8434
5500	3.64E + 00	8.01E + 00	5.09E + 01	5.84E + 01	0.8300
6000	3.51E + 00	7.49E + 00	4.37E + 01	5.26E + 01	0.8161
6500	3.36E + 00	7.05E + 00	3.84E + 01	4.74E + 01	0.8044
7000	3.23E + 00	6.65E + 00	3.37E + 01	4.30E + 01	0.7917
7500	3.14E + 00	6.30E + 00	2.98E + 01	3.96E + 01	0.7786
8000	3.05E + 00	5.98E + 00	2.65E + 01	3.65E + 01	0.7663
8500	2.99E + 00	5.70E + 00	2.36E + 01	3.40E + 01	0.7530
9000	2.95E + 00	5.48E + 00	2.13E + 01	3.23E + 01	0.7415
9500	2.87E + 00	5.28E + 00	1.96E + 01	3.03E + 01	0.7320
10000	2.82E + 00	5.11E + 00	1.81E + 01	2.88E + 01	0.7224
11000	2.69E + 00	4.80E + 00	1.58E + 01	2.58E + 01	0.7062
12000	2.56E + 00	4.57E + 00	1.43E + 01	2.34E + 01	0.6949
13000	2.40E + 00	4.34E + 00	1.31E + 01	2.08E + 01	0.6840
14000	2.25E + 00	4.11E + 00	1.18E + 01	1.85E + 01	0.6718
15000	2.15E + 00	3.88E + 00	1.04E + 01	1.67E + 01	0.6553

$$\frac{b}{2a^2} = r^2, \qquad 2ab = \frac{4}{r},$$

$$2ad = \frac{4\xi}{r}, \qquad \frac{b^2 - 2ac}{a^2 d} = \left(\frac{r^2}{\xi}\right)(1 - \xi^2),$$

$$\frac{a + b + c}{c} = \frac{1 + 2r + r^2(1 + \xi^2)}{r^2(1 + \xi^2)}, \qquad \frac{2ad}{d^2 + b(2a + b)} = \frac{\xi}{1 + r(1 + \xi^2)}.$$

In terms of r and ξ we get

Appendix A

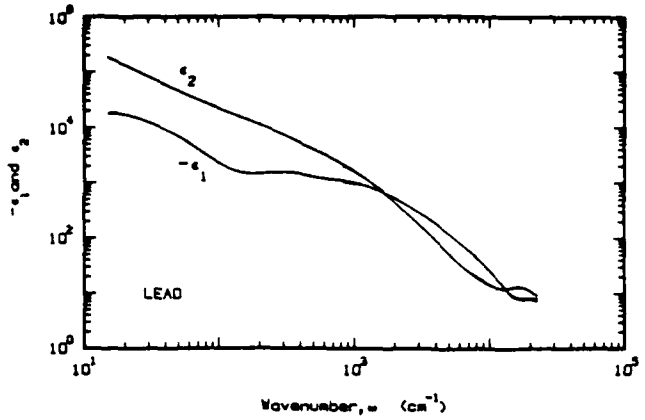

Fig. 6. Kramers-Kronig results for $-\epsilon_1$ and ϵ_2 of Pb: solid line, results obtained by combining nonresonant cavity measurements with the results of Motulevich *et al.*[9]; dash–dot line for the results of Motulevich *et al.*[9]

$$\int_0^1 A_p(\eta)\eta d\eta = 4\left\{r - r^2 \ln\left[\frac{1 + 2r + r^2(1+\xi^2)}{r^2(1+\xi^2)}\right] + \frac{r^2(1-\xi^2)}{\xi}\tan^{-1}\left(\frac{\xi}{1 + r + r\xi^2}\right)\right\}. \quad \text{(A2)}$$

Except for the additional 1 (one) in the numerator of the argument of the log function and the combining of the arctan terms into a single expression, Eq. (A2) is identical to Eq. (22) of Pinkerton and Sievers.[3]

B. *S*-Polarization Integral

For the *s* polarization $a \equiv r(1 + \xi^2)$, $b \equiv 2$, and $c \equiv 1/r$. The coefficients in Eq. (A1) become

$$\frac{b}{2a^2} = \frac{1}{r^2(1+\xi^2)^2}, \qquad 2ab = 4r(1+\xi^2),$$

$$\frac{b^2 - 2ac}{a^2 d} = \frac{(1-\xi^2)}{\xi r^2(1+\xi^2)^2},$$

$$2ad = 4\xi r(1+\xi^2), \qquad \frac{a+b+c}{c} = 1 + 2r + r^2(1+\xi^2),$$

$$\frac{2ad}{d^2 + b(2a+b)} = \frac{r\xi}{1+r}.$$

In terms of r and ξ we get

$$\int_0^1 A_s(\eta)\eta d\eta = 4\left\{\frac{1}{r(1+\xi^2)} - \frac{1}{r^2(1+\xi^2)^2} \times \ln[1 + 2r + r^2(1+\xi^2)] + \frac{(1-\xi^2)}{\xi r^2(1+\xi^2)^2}\tan^{-1}\left(\frac{r\xi}{1+r}\right)\right\}. \quad \text{(A3)}$$

Equation (A3) differs considerably in form from Eq. (23) of Pinkerton and Sievers[3] [where they approximated the denominator of the integrand function as 1 + 2r cos(θ) and then expanded the integrand function in an infinite series].

In our notation, we define $P(\omega)$ to be the angle averaged absorptance at frequency ω. Adding Eqs. (A2) and (A3) yields $P(\omega)$ in terms of r and ξ as

$$P(\omega) \equiv 4r\left\{\left[1 + \frac{1}{r^2(1+\xi^2)}\right] - \left[r + \frac{1}{r^3(1+\xi^2)^2}\right] \times \ln[1 + 2r + r^2(1+\xi^2)] + r\ln[r^2(1+\xi^2)] + \frac{(1-\xi^2)}{\xi}\left\{r\tan^{-1}\left[\frac{\xi}{1 + r(1+\xi^2)}\right] + \frac{1}{r^3(1+\xi^2)^2}\tan^{-1}\left(\frac{r\xi}{1+r}\right)\right\}\right\}. \quad \text{(A4)}$$

Note that only the first three terms remain in Eq. (A4) if one assumes $\xi \equiv 1$ ($n = k$).

Sievers[12] has shown that Eq. (A4) simplifies considerably under the assumption that $n \simeq k$ (and hence $r \ll 1$). He found

$$r(\omega) = \frac{3}{16}P(\omega)[1 + 1.6P(\omega)]. \quad \text{(A5)}$$

When analyzing our measurements, Eq. (A4) was used for P_r since both the real and imaginary parts of refractive index were known for the reference material (and hence ξ). For the sample material, the much simpler Eq. (A5) was used since only a quantity is measured at each frequency. Note that $P(\omega)$ is typically 10^{-3}–10^{-4} at the long wavelengths in question.

Working with the exact expression for the angle averaged absorptance [Eq. (A4)] results in improved accuracy over both the original approximation of Pinkerton and Sievers[3] and the improved expression of Pinkerton *et al.*[4] The exact expression has the disadvantage of requiring double-precision computations along with careful grouping of terms. Using the grouping of terms shown in Eq. (A4) operations proceed as nearly as possible on operands of like magni-

Table III. Optical Constants of Pb Obtained from Kramers-Kronig Analysis of the Normalized Surface Resistance

ω (cm^{-1})	n	k	$-\epsilon_1$	ϵ_2	R
15	2.89E + 02	3.19E + 02	1.82E + 04	1.84E + 05	0.9938
25	2.11E + 02	2.44E + 02	1.48E + 04	1.03E + 05	0.9919
50	1.41E + 02	1.64E + 02	6.95E + 03	4.62E + 04	0.9860
75	1.14E + 02	1.29E + 02	3.65E + 03	2.95E + 04	0.9848
100	9.95E + 01	1.11E + 02	2.31E + 03	2.20E + 04	0.9822
125	8.95E + 01	9.87E + 01	1.74E + 03	1.77E + 04	0.9800
150	8.18E + 01	9.06E + 01	1.52E + 03	1.48E + 04	0.9783
175	7.55E + 01	8.46E + 01	1.46E + 03	1.28E + 04	0.9768
200	7.02E + 01	8.00E + 01	1.47E + 03	1.12E + 04	0.9755
225	6.55E + 01	7.61E + 01	1.50E + 03	9.97E + 03	0.9743
250	6.14E + 01	7.27E + 01	1.52E + 03	8.93E + 03	0.9733
300	5.45E + 01	6.71E + 01	1.54E + 03	7.31E + 03	0.9713
350	4.90E + 01	6.25E + 01	1.50E + 03	6.12E + 03	0.9694
400	4.47E + 01	5.85E + 01	1.43E + 03	5.23E + 03	0.9676
450	4.12E + 01	5.52E + 01	1.35E + 03	4.55E + 03	0.9659
500	3.84E + 01	5.25E + 01	1.28E + 03	4.03E + 03	0.9643
600	3.39E + 01	4.83E + 01	1.19E + 03	3.27E + 03	0.9618
700	3.00E + 01	4.53E + 01	1.15E + 03	2.71E + 03	0.9601
800	2.65E + 01	4.26E + 01	1.11E + 03	2.26E + 03	0.9587
900	2.38E + 01	4.01E + 01	1.05E + 03	1.91E + 03	0.9572
1000	2.14E + 01	3.81E + 01	9.94E + 02	1.63E + 03	0.9562
1250	1.66E + 01	3.37E + 01	8.59E + 02	1.12E + 03	0.9540
1500	1.35E + 01	3.01E + 01	7.22E + 02	8.09E + 02	0.9516
1750	1.10E + 01	2.72E + 01	6.20E + 02	6.00E + 02	0.9503
2000	9.02E + 00	2.48E + 01	5.32E + 02	4.47E + 02	0.9495
2250	7.58E + 00	2.26E + 01	4.53E + 02	3.43E + 02	0.9481
2500	6.54E + 00	2.07E + 01	3.88E + 02	2.71E + 02	0.9463
2750	5.72E + 00	1.92E + 01	3.36E + 02	2.20E + 02	0.9447
3000	5.01E + 00	1.79E + 01	2.95E + 02	1.79E + 02	0.9437
3250	4.39E + 00	1.67E + 01	2.59E + 02	1.46E + 02	0.9428
3500	3.94E + 00	1.56E + 01	2.28E + 02	1.23E + 02	0.9411
3750	3.58E + 00	1.47E + 01	2.03E + 02	1.05E + 02	0.9394
4000	3.18E + 00	1.38E + 01	1.81E + 02	8.79E + 01	0.9389
4250	2.98E + 00	1.31E + 01	1.62E + 02	7.78E + 01	0.9361
4500	2.70E + 00	1.24E + 01	1.46E + 02	6.68E + 01	0.9354
4750	2.49E + 00	1.17E + 01	1.32E + 02	5.85E + 01	0.9336
5000	2.31E + 00	1.12E + 01	1.19E + 02	5.15E + 01	0.9318
5500	2.04E + 00	1.01E + 01	9.84E + 01	4.13E + 01	0.9270
6000	1.85E + 00	9.27E + 00	8.24E + 01	3.42E + 01	0.9214
6500	1.69E + 00	8.53E + 00	6.99E + 01	2.88E + 01	0.9154
7000	1.57E + 00	7.88E + 00	5.96E + 01	2.47E + 01	0.9086
7500	1.48E + 00	7.31E + 00	5.12E + 01	2.17E + 01	0.9004
8000	1.42E + 00	6.80E + 00	4.42E + 01	1.93E + 01	0.8907
8500	1.38E + 00	6.35E + 00	3.84E + 01	1.76E + 01	0.8795
9000	1.36E + 00	5.94E + 00	3.35E + 01	1.62E + 01	0.8668
9500	1.35E + 00	5.58E + 00	2.93E + 01	1.51E + 01	0.8525
10000	1.36E + 00	5.26E + 00	2.58E + 01	1.43E + 01	0.8367
11000	1.39E + 00	4.70E + 00	2.01E + 01	1.30E + 01	0.8001
12000	1.46E + 00	4.25E + 00	1.59E + 01	1.24E + 01	0.7576
13000	1.55E + 00	3.85E + 00	1.24E + 01	1.20E + 01	0.7086
14000	1.74E + 00	3.58E + 00	9.82E + 00	1.25E + 01	0.6579
15000	1.88E + 00	3.49E + 00	8.62E + 00	1.31E + 01	0.6323

tude. The calculation reduces to the difference of two large numbers (of the order of 10^5) identical in their first six to eight significant digits.

References

1. E. D. Palik, *Handbook of Optical Constants of Solids* (Academic, New York, 1985).
2. J. H. Weaver, C. Krafka, D. W. Lynch, and E. E. Koch, *Physics Data, Optical Properties of Metals, Part 1: The Transition Metals* and *Physics Data, Optical Properties of Metals, Part 2: The Noble Metals, Aluminum, Scandium, Yttrium, the Lanthanides, and the Actinides* (Fachinformationszentrum, 7514 Eggenatein-Leopoldshafen 2, Karlsruhe, F.R.G., 1981).
3. F. E. Pinkerton and A. J. Sievers, "Quantitative FIR Absorptivity Measurements of Metals with Dual Nonresonant Cavities," Infrared Phys. **22**, 377 (1982).
4. F. E. Pinkerton, A. J. Sievers, M. B. Maple, and B. C. Sales, "Enhanced Far-Infrared Absorption in $CdPd_3$ and $YbCuSi_2$ Experiment," Phys. Rev. B **29**, 609 (1984).
5. G. Brandli and A. J. Sievers, "Absolute Measurement of the Far-Infrared Surface Resistance of Pb," Phys. Rev. B **5**, 3550 (1972).
6. W. E. Lamb, Jr., "Theory of a Microwave Spectroscope," Phys. Rev. **70**, 308 (1946).
7. W. H. Press, B. P. Flannery, S. A. Teukolsky, and W. T. Vetterling, *Numerical Recipes: the Art of Scientific Computing* (Cambridge U.P., New York, 1986).
8. M. A. Ordal, R. J. Bell, R. W. Alexander, Jr., L. L. Long, and M. R. Querry, "Optical Properties of Fourteen Metals in the Infrared and Far Infrared: Al, Co, Cu, Au, Fe, Pb, Mo, Ni, Pd, Pt, Ag, Ti, V, and W," Appl. Opt. **24**, 4493 (1985).
9. A. I. Golovashkin and G. P. Motulevich, "Optical Properties of Lead in the Visible and Infrared Spectral Ranges," Sov. Phys. JETP **26**, 881 (1968).
10. R. J. Bell, M. A. Ordal, and R. W. Alexander, Jr., "Equations Linking Different Sets of Optical Properties for Nonmagnetic Materials," Appl. Opt. **24**, 3680 (1985).
11. M. R. Spiegel, *Mathematical Handbook of Formulas and Tables*, Schaum's Outline Series (McGraw-Hill, New York, 1968), p. 71; G. A. Korn and T. M. Korn, *Mathematical Handbook of Scientists and Engineers* (McGraw-Hill, New York, 1968), pp. 931–2.
12. A. J. Sievers, "Thermal Radiation from Metal Surfaces," J. Opt. Soc. Am. **68**, 1505 (1978).

Reprinted from Applied Optics, Vol. 26, Page 1372, April 15, 1987

Preparation dependent properties of pressed pellets of montmorillonite in the far infrared

Larry L. Long, R. J. Bell, R. W. Alexander, Jr., and Marvin R. Querry

Marvin Querry is with University of Missouri—Kansas City, Physics Department, Kansas City, Missouri 64110. When this work was done all the other authors were with University of Missouri—Rolla, Physics Department, Rolla, Missouri 65401; L. L. Long is now with McDonnell Douglas Corporation, Physics Laboratories, St. Louis, Missouri 63166.
Received 24 November 1986.
0003-6935/87/081372-03$02.00/0.

The technique of pressing powdered sample material into a pellet without the use of a supporting matrix[1,2] has been developed from interest in measuring the optical constants of materials normally unavailable in large crystalline form.[3,4]

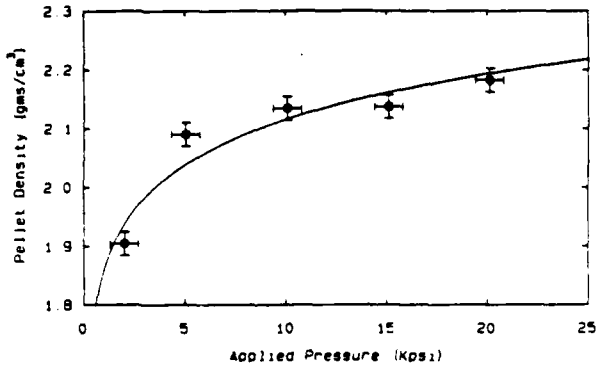

Fig. 1. Pellet density for pressed pellets of montmorillonite. The squares represent the data and the solid line is a logarithmic fit.

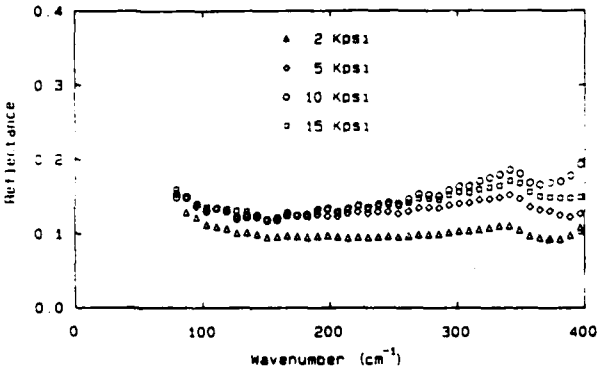

Fig. 2. Specular reflectance of montmorillonite pellets prepared at different pressures.

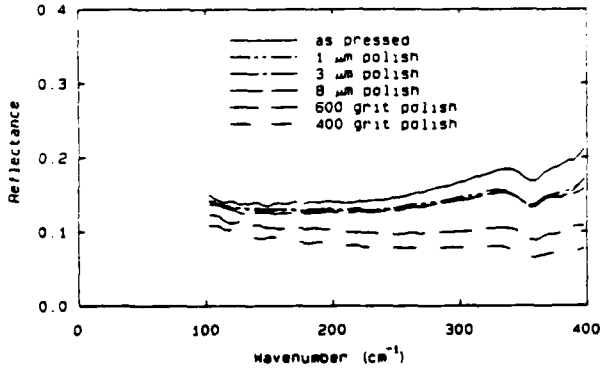

Fig. 3. Specular reflectance of montmorillonite for different surface roughnesses.

Although the principal materials of interest are clays, this method has applications whenever examining the optical properties of crystals unavailable in large enough physical size to perform reflectivity measurements. Toon *et al.* stated that it required approximately three years to grow acceptable crystals of ammonium sulfate, $(NH_4)_2SO_4$.[5] In such situations, the pressed pellet technique is useful for initial measurements. While reflectivity measurements on orientated crystals are preferred, measurements of the reflectivity of pressed pellets should be as useful, if not more so, than transmission measurements of powdered sample material embedded in a supporting matrix in determining the optical constants. Both methods will mix the optical properties for all orientations, however, reflectivity measurements have the advantage of producing better results for the imaginary part of the index of refraction k, when $k > 0.05$, than transmission measurements, which are limited to moderately small k values.[5]

The pressed pellet technique assumes two properties of the sample, a specular surface and a unique or complete mixing of all orientations of the material. These two requirements must be fulfilled to determine the optical constants of the material from standard reflectivity measurements. A complete or unique mixing of orientations means that a pressed pellet will have a unique representation of all orientations and that pressing the pellet does not make one orientation preferred over another in a nonreproducible way. For example, if a sample forms platelets when powdered, a larger representation of orientations parallel to the surface of the platelet, rather than perpendicular, would appear in the spectrum. The surface of the sample is assumed to have no diffuse component, meaning that none of the incident flux is scattered by a rough surface. A rough, nonspecular surface is created by the particle size of the powder, hardness of the particles, and failure of the particles to fuse when pressed, resulting in voids in the sample surface.

The sample pellets for reflectance studies are formed by applying several tons of force to the die containing the sample material. The die consists of a cylinder, plunger, and anvil with the sample material placed between the plunger and anvil. For the pressure-dependent studies a die with a 2.86-cm (1.125-in.) diameter was required to obtain low enough pressures to create a discernible difference in the reflectance spectrum. The samples produced were ~1 cm thick. Since the reflectance is dependent on the forming pressure, the pressure at which the reflectance reaches an asymptotic value must be determined. Some work has been done to determine the effect of pressure on the reflectance of compacted powder in the 0.23–2.65-μm wavelength range and on particle size effects in the compression of powders.[6–8] In this shorter wavelength region, different physical processes are occurring at the surface, since the wavelength is smaller than the particle size. In the far infrared, ≥ 25 μm, the wavelength is much larger than the particle size (~1-μm diameter). Therefore, an increase in sample preparation pressure is expected to produce an increase in the bulk density of the pellet and in the reflectance.

The near-normal reflectance measurements with an angle of incidence of ~15° were performed on an RIIC FTS-720 interferometer supplied by Beckman Instruments, Inc. These measurements were taken so that the Fourier transform of the double sided interferogram produced a spectral point approximately every 4 cm^{-1} with an apodized resolution of around 8 cm^{-1}. The measurements covered the spectral range of 400–100 cm^{-1} (25–100 μm), using a diamond window Golay cell detector. A first surface gold mirror was used as a standard (with an assumed reflectance of 1.0).

Figure 1 represents the bulk density as a function of applied pressure. To obtain this data samples were prepared at 2, 5, 10, 15, and 20 kpsi, producing a resultant bulk density of 1.90, 2.09, 2.13, 2.14, and 2.18 gm/cm^3, respectively. Huffine and Bonilla[7] determined that the bulk density of compressed powders is a logarithmic function of the applied pressure. This indicates that the density of the pressed sample should converge to a density representative of the individual particles in the powder, which is 2–3 gm/cm^3 for

montmorillonite. The data in Fig. 1 have the functional form of density = $A + B \ln(PC)$, where A and B are constants determined from the least-squares fit to the data, P represents the applied pressure, and the constant C has the units of inverse pressure.

To determine if the bulk density of the entire pellet is representative of the surface density, the specular reflectance is measured for the 2-, 5-, 10-, and 15-kpsi pressing force samples. The reflectance of the 20-kpsi pressing force sample is excluded, because at high pressure this clay material has a tendency to adhere to the plunger and anvil, producing a surface roughness larger than the wavelength. Figure 2 shows the reflectance for different pressures. The 15-kpsi sample has a lower reflectance than the 10-kpsi sample, due to a rough surface obtained from material adhering to the plunger and anvil of the die. The 2-kpsi sample has the lowest reflectance, with the reflectance for the 5 kpsi much higher. The 10- and 15-kpsi samples approach the same reflectance at 250 cm^{-1} even with the surface roughness problem indicated earlier with the 15-kpsi sample. At 200 cm^{-1} the reflectance of the 5-kpsi sample approaches the same reflectance as the 10- and 15-kpsi samples. At 100 cm^{-1} the reflectance for the 15-, 10-, and 5-kpsi samples is indistinguishable and the reflectance for the 2-kpsi sample is within 10% of the other three. This indicates that in the far infrared the reflectance may be considered independent of the preparation pressure, as long as the forming pressure is in excess of 10 kpsi.

For pressures greater than the 10-kpsi minimum, an increase in the preparation pressure resulted in higher bulk densities, however, a corresponding increase in the reflectance was not observed. This indicates that the material near the surface of the pellet was at a higher density than that interior to the pellet, suggesting the creation of a surface skin, and that increasing the preparation pressure only increased the bulk density in the interior of the pellet. A higher bulk density implies fewer microscopic voids in the pellet. To examine the effect of the surface skin on the reflectance, the reflectance was measured for a polished pressed pellet of montmorillonite. The pellet was successively polished with sandpaper of the following grit sizes: 400 and 600 grit, 8, 3, and 1 μm. After each polish the specular reflectance was measured. By polishing the sample the surface skin was removed and a surface of known roughness was created. The removal of the surface skin was evidenced by the lack of a glossy surface that could be visually observed before the sample was polished. Much work has been done on the effect of surface roughness on the reflectance.[6–12] If the surface roughness was much smaller than the wavelength, to a first approximation the surface could be considered completely specular, with no diffuse component. As the roughness increased the specular reflectance decreased due to scattering at the surface. Usually the surface can be considered completely specular if the rms surface roughness is an order of magnitude smaller than the wavelength.

Figure 3 represents the specular reflectance at several surface roughnesses. The specular reflectance obtained for a sample polished at either 400 or 600 grit is lower by as much as 50% from the reflectance obtained for the pellet before being polished. This is expected since the surface roughness is larger than the wavelength. After the sample was again polished with 8-μm sandpaper, the reflectance increased by a substantial amount. Repeated polishing with 3- and 1-μm sandpaper increased the reflectance by only a small amount. This indicates that the surface of the polished pellet was smooth enough to be considered specular for these wavelengths. Therefore, the reflectances obtained with 1-μm grit polish represents the reflectance for the bulk of the pellet, which would indicate that the surface of the pellet is at a higher density than the bulk. This also indicates that bulk density measurements may not represent the density of the surface as seen by the incident radiation.

In conclusion, it was determined for montmorillonite, and presumably for all clays, that a sample preparation pressure in excess of 10 kpsi was sufficient for the reflectance spectrum to reach a stable value for wavelengths as short as 30 μm. For longer wavelengths pressing pressures <10 kpsi could be used to reach a stable reflectance value. In addition, the surface of the sample was found to be specular in the far infrared. Due to a surface skin, the density of the surface seen by the incident radiation was higher than that indicated by density measurements that included the entire pellet. This skin layer is probably representative of the density of the naturally occurring mineral, indicating that bulk densities of pressed pellets do not necessarily represent the surface density seen by the incident radiation. From this work it appears that the pellets produced are of high enough quality to measure the reflectivity and thereby ascertain the optical constants with the understanding that the optical constants will contain a mixture of all orientations.

This work was partially supported by the U.S. Army CRDEC grants DAAD-11-85-K-0004 and DAAA-15-85-K-00004 (M. Milham and J. Embury).

References

1. F. E. Volz, "Infrared Specular Reflectance of Pressed Crystal Powders and Mixtures," Appl. Opt. **22**, 1842 (1983).
2. M. R. Querry, "Optical Properties of Natural Minerals and Other Materials in the 350–50,000 cm Spectral Region," Final Report of Contract DAAG-29-79-C0131 (Aug. 1983).
3. R. G. Pinnick, S. G. Jennings, D. C. Boice, and J. P. Cruncleton, "Attenuated Total Reflectance Measurements of the Complex Refractive Index of Kaolinite Powder at CO_2 Laser Wavelengths," Appl. Opt. **24**, 3274 (1985).
4. J. E. Eberhardt, J. G. Haub, and A. W. Pryor, "Reflectivity of Natural and Powdered Minerals at CO_2 Laser Wavelengths," Appl. Opt. **24**, 388 (1985).
5. O. B. Toon, J. B. Pollack, and B. N. Khare, "The Optical Constants of Several Atmospheric Aerosol Species: Ammonium Sulfate, Aluminum Oxide, and Sodium Chloride," J. Geophys. Res. **81**, 5733 (1976).
6. E. A. Schatz, "Effect of Pressure on Reflectance of Powders," J. Opt. Soc. Am. **56**, 389 (1966).
7. C. L. Huffine and C. F. Bonilla, "Particle-Size Effects in the Compression of Powders," AIChE J. **8**, 490 (1962).
8. R. Dejir, A. Aszodi, R. Beiguieu, and C. N. Turcanu, "Study of Density Distribution in Cylindrical UO Compacts by Means of the Autoradiographic Method," Rev. Roum. Phys. **26**, 397 (1981).
9. H. E. Bennett and J. O. Porteus, "Relation Between Surface Roughness and Specular Reflectance at Normal Incidence," J. Opt. Soc. Am. **51**, 123 (1961).
10. H. E. Bennett, "Specular Reflectance of Aluminized Ground Glass and the Height Distribution of Surface Irregularities," J. Opt. Soc. Am. **53**, 1389 (1963).
11. J. O. Porteus, "Relation Between the Height Distribution of a Rough Surface and the Reflectance at Normal Incidence," J. Opt. Soc. Am. **53**, 1394 (1963).
12. C. A. Depew and R. D. Weir, "Surface Roughness Determination by the Measurement of Reflectance," Appl. Opt. **10**, 969 (1971).

APPENDIX B
PREPRINT OF PAPER
TO BE SUBMITTED

The optical properties of Al, Fe, Ti, Ta, W, and Mo at submillimeter wavelengths

by

Mark A. Ordal,* Robert J. Bell, Ralph W. Alexander, Jr.
and Lawrence A. Newquist
Physics Department, University of Missouri-Rolla, Rolla, MO 65401
and
Marvin R. Querry
Physics Department, University of Missouri-Kansas City,
Kansas City, MO 64110

ABSTRACT

Measurements of the optical constants of metals at submillimeter wavelengths are sparse. We have used a nonresonant cavity to measure, at room temperature, the angle averaged absorptance spectra $P(\omega)$ of molybdenum, tantalum, titanium, tungsten, and iron in the 30 to 300 cm^{-1} wavenumber region. The real part of the normalized surface impedance spectrum $z(\omega) = r(\omega) + ix(\omega)$ was determined from $P(\omega)$. Measurements were also made on iron from 400 cm^{-1} to 4,000 cm^{-1} using standard reflectance techniques. The $r(\omega)$ spectrum was combined with previous measurements by others at higher frequencies and Kramers-Kronig analyses of the resultant combined $r(\omega)$ spectra provided $\varepsilon(\omega) = \varepsilon_1(\omega) + i\varepsilon_2(\omega)$ and $N(\omega) = n(\omega) + ik(\omega)$.

I. INTRODUCTION

The extremely high reflectivity of metals at submillimeter wavelengths generally precludes direct measurement of the reflectance or absorptance as is customary at shorter wavelengths. As a result, most of the measurements for metals have been made at wavelengths shorter than 5 or 10 micrometers. See references 1-3, for example. Sievers and coworkers have pioneered measurements in the far infrared using two methods. They have measured the transmission of either nonresonant cavities[4,5] or plane parallel waveguides[6] from which they could derive the real part of the normalized surface resistance. Their measurements were made at liquid helium temperatures.

We have recently reported measurements at room temperature for gold, nickel and lead using a nonresonant cavity.[7] The measured transmission of the nonresonant cavity was used to calculate $r(\omega)$, the real part of the normalized surface impedance $z(\omega) = r(\omega) + ix(\omega)$ from 30 to 300 cm^{-1}. We then used optical constants from the literature to calculate $r(\omega)$ at shorter wavelenths. The resulting $r(\omega)$ spectrum was Kramers-Kronig analyzed to obtain $x(\omega)$. By thus combining our far infrared measurements with the literature for shorter wavelengths, we obtain the real and imaginary parts of the normalized surface impedance [or, equivalently, the real and imaginary parts of the dielectric function $\varepsilon(\omega) = \varepsilon_1(\omega) + i\varepsilon_2(\omega)$ or the real and imaginary parts of the refractive index $N(\omega) = n(\omega) + ik(\omega)$.]

A Perkin-Elmer model 580 spectrophotometer was used to measure the reflectance of the iron samples from 400 cm^{-1} to 4,000 cm^{-1} using a standard reflectance attachment. A Varian

model 2300 was used for the 4,000-50,000 cm^{-1} range.[3] An aluminum mirror, corrected for absolute reflectance, was used as a standard.

This paper extends three previous papers[3,7,8], (which summarized data available in the literature for a number of metals and reported Drude model fits to this data), by providing long wavelength data for additional metals.

II. EXPERIMENT

A nonresonant cavity has no preferred standing wave modes and hence its dimensions must be large compared to all wavelengths of interest. Our cavity is cylindrical with plane end caps. The cylinder axis makes an angle of four degrees with the plane of the endcaps. One end plate was removable and was made either of the reference metal or the sample metal. The body and other endplate are made of the reference metal (aluminum in our case). Radiation enters through a small input hole and exits through another small hole. The transmission spectrum with the sample metal endplate, $I_s(\omega)$, and the transmission spectrum with the reference endplate, $I_r(\omega)$, were measured. Pinkerton and Sievers showed that[4]

$$\frac{I_s(\omega)}{I_r(\omega)} - \frac{\left[2S_1+(S_2+S_3)P_r(\omega)\right] + S_4P_r(\omega)}{\left[2S_1+(S_2+S_3)P_r(\omega)\right] + S_4P_s(\omega)} = 0 \qquad (1)$$

where

S_1 = cross sectional area of an input or output hole.

S_2 = area of the cavity sidewalls (exluding input and output holes).

S_3 = area of the bottom plate (which on our cavity is not normally removable).

S_3 = area of the removable top plate.

$P_r(\omega)$ = angle averaged absorptance of the reference metal.

$P_s(\omega)$ = angle averaged absorptance of the sample metal.

$I_s(\omega)$ = intensity at frequency ω measured at the output hole of the cavity when the top plate of area S_4 is made of

the sample metal.

$I_r(\omega)$ = intensity at frequency ω measured at the output hole of the cavity when the cavity consists entirely of the reference metal.

For $P_s(\omega)$ and $P_r(\omega)$ we used the exact expression derived by Ordal, et al.,[7]

$$P(\omega) = 4r\left\{\left[1+\frac{1}{r^2\left[1+\xi^2\right]}\right]-\left[r+\frac{1}{r^3\left[1+\xi^2\right]}\right]\ln\left[1+2r+r^2(1+\xi^2)\right]\right.$$

$$+ r\ln\left[r^2(1+\xi^2)\right]$$

$$\left.+\frac{(1-\xi^2)}{\xi}\left[r\tan^{-1}\left[\frac{\xi}{1+r\left[1+\xi^2\right]}\right]+\frac{1}{r^3\left[1+\xi^2\right]^2}\tan^{-1}\left[\frac{r\xi}{1+r}\right]\right]\right\} \qquad (2)$$

As the optical constants for the sample are not known, and we have only one measurement (namely, the reflectance), we made the approximation $\xi = 1$ in Eq. (2) when calculating P_s, leaving one unknown, $r_s(\omega)$ for the sample metal. This approximation is equivalent to setting the complex refractive index $N = n + ik = n(1 + i)$ for the sample metal. Note that one can use the approximation $\xi = 1$ as long as $1/\sqrt{(\varepsilon_1^2+\varepsilon_2^2)} \ll 1$, even if $\xi \gg 1$. For $P_r(\omega)$, we used values of n and k for aluminum which had been measured in our laboratory. The values for aluminum were obtained using the measurements of Brandli and Sievers on gold foil and our measurements on Ni foil. This calibration procedure is described in detail in a previous paper.[7] Note that after calculating $P_r(\omega)$ and $P_s(\omega)$ in this manner and inserting them in Eq.(1), we are left with an equation in one unknown, $r_s(\omega)$.

Standard routines were used to find r_s[9].

Because a single cavity with one changeable endplate was used, the cavity body and one endplate were identical for the sample and reference measurement. The samples which were thin sheets or foils were epoxied to a plate of 3/8 inch aluminum alloy before being mounted as the cavity endplate. The cavity and samples were polished with 1 micrometer diamond abrasive.

III. RESULTS

A. ALUMINUM: The normalized surface resistance for aluminum obtained from the nonresonant cavity measurements is plotted in Fig. 1. The measurements of Shiles, et al. (tabulated in ref. 2) were used to calculate the normalized surface impedance from 322 cm^{-1} to 7 x 10^6 cm^{-1}. A Drude model with ω_τ = 408 CM^{-1} and ω_p = 92,700 CM^{-1} was used for a low frequency wing correction. The Drude model low frequency calculations, the nonresonant cavity measurements, and the Shiles, et al. measurements were combined and then the entire data set was Kramers-Kronig analyzed to obtain x, the imaginary part of the normalized surface impedance. From r and x the real and imaginary parts of the dielectric function, ε_1 and ε_2 and the real and imaginary parts of the complex refractive index, n and k, were calculated. These are displayed in Table 1, along with the calculated reflectance, R. Figure 2 shows a plot of ε_1 and ε_2.

B. IRON: Figure 3 shows the normalized surface resistance of iron measured using the nonresonant cavity from 100 cm^{-1} to 340 cm^{-1}. To combine these results with measurements at shorter wavelengths, the following procedure was used. The data of Bolotin, et al. (tabulated in Ref. 2) and of Weaver, et al. (also tabulated in Ref. 2) were used in the region from 1,000 cm^{-1} to 242,000 cm^{-1}. Our reflection measurements were used between 400 and 4,000 cm^{-1}. In regions of overlap, the various data sets were in reasonable agreement, and an average was taken. Beyond 242,000 cm^{-1} a high wing extrapolation corresponding to the reflectance falling off to one over the frequency to the

fourth power was used. Below 100 cm^{-1}, a Drude model extrapolation was made using ω_τ = 156 cm^{-1} and ω_p = 29,500 CM^{-1}. These parameters were chosen to match smoothly to the nonresonant cavity results. The Kramers-Kronig analysis of this combined set of measurements resulted in the values of ϵ_1 and ϵ_2 shown in Fig. 4. Along with n and k, and the calculated reflectance R, they are also tabulated in Table 2.

C. **TITANIUM:** Figure 5 shows the normalized surface impedance obtained from the nonresonant cavity. Again a Drude model fit was used to obtain a low frequency wing for the Kramers-Kronig analysis. The Drude model parameters were ω_τ = 372 cm^{-1} and ω_p = 25,000 cm^{-1}. At shorter wavelengths, the measurements of Lynch, et al. (tabulated in Ref. 2) were used (1,290 cm^{-1} to 24,000 cm^{-1}). The gap between our nonresonant cavity measurements and Lynch's was filled using a spline fit. Shown in Fig. 6 are ϵ_1 and ϵ_2. In Table III are the values of ϵ_1, ϵ_2, n, k, and the calculated reflectance.

D. **TANTALUM:** The normalized surface impedance of tantalum is shown in Fig. 7. In order to perform the Kramers-Kronig analysis, a Drude low frequency wing was used with ω_τ = 470 cm^{-1} and ω_p = 50,000 cm^{-1}. The data of Weaver, et al. tabulated in Ref. 2) was used from 800 cm^{-1} to 322,600 cm^{-1}. The gap between the nonresonant cavity measurements and those of Weaver was filled with a spline fit. After Kramers-Kronig analysis of this combined set of data, ϵ_1, ϵ_2, n, k and R were calculated. These are tabulated in Table IV and ϵ_1 and ϵ_2 are plotted in Fig. 8.

E. **TUNGSTEN**: Figure 9 shows the measured surface impedance for tungsten. A low frequency Drude wing was generated using ω_τ = 250 cm^{-1} and ω_p = 50,000 cm^{-1}. The data of Weaver et al. (tabulated in Ref. 2) were used from 3,700 cm^{-1} to 32,000 cm^{-1}. The region between our far infrared and Weaver's near infrared data was filled using a spline fit to the ends of both data sets. After Kramers-Kronig analysis of this joint data set, the values of the dielectric function, refractive index and reflectivity shown in Table V were calculated. Figure 10 shows ϵ_1 and ϵ_2.

F. **MOLYBDENUM**: The normalized surface impedance of molybdenum is plotted versus wavenumber in Fig. 11 from 80 to 340 cm^{-1}. For the Kramers-Kronig analysis, a low frequency Drude wing with ω_τ = 412 CM^{-1} and ω_p = 60,200 cm^{-1} was matched to the nonresonant cavity measurements. The optical constants determined by Lynch and Hunter (tabulated in Ref. 1) were used from 800 cm^{-1} to 1.6 x 10^6 cm^{-1}. As usual, a spline fit was used in the gap between these two sets of measurements. The dielectric function obtained from the Kramers-Kronig analysis is shown versus frequency in Fig. 12. Table VI contains the dielectric function, the complex refractive index and the calculated reflectance as a function of wavenumber.

This work was partially supported by the U.S. Army CRDEC contract DAAA-15-85-K-0004 (M. Milham and J. Embury).

IV. REFERENCES

1. Edward D. Palik, Handbook of Optical Constants of Solids (Academic Press, New York, 1985).

2. J. H. Weaver, C. Krafka, D. W. Lynch, and E. E. Koch, Physics Data, Optical Properties of Metals, Part I: The Transition Metals, and Physics Data, Optical Properties of Metals, Part II: The Noble Metals, Aluminum, Scandium, Yttrium, The Lanthanides, and the Actinides, (Fachinformationszentrum, 7514 Eggenatein-Leopoldshafen 2, Karlsruhe, Federal Republic of Germany, 1981).

3. M. A. Ordal, Robert J. Bell, R. W. Alexander, Jr., L. L. Long, and M. R. Querry, "Optical properties of 14 metals in the infrared and far infrared: Al, Co, Cu, Au, Fe, Pb, Mo, Ni, Pd, Pt, Ag, Ti, V, and W," Appl. Opt. 24, 4493 (1985).

4. F. E. Pinkerton, and A. J. Sievers, "Quantitative FIR Absorptivity Measurements of Metals with Dual Nonresonant Cavities," Infrared Phys. 22, 377 (1982).

5. F. E. Pinkerton, A. J. Sievers, M. B. Maple, and B. C. Sales, "Enhanced Far-infrared Absorption in $CdPd_3$ and $YbCuSi_2$ Experiment," Phys. Rev. B29, 609 (1984).

6. G. Brändli and A. J. Sievers, "Absolute Measurement of the Far-Infrared Surface Resistance of Pb," Phys. Rev. B5 (9), 3550 (1972).

7. M. A. Ordal, R. J. Bell, R. W. Alexander, and M. R. Querry, "The optical properties of Au, Ni, and Pb at submillimeter wavelengths," Appl. Opt. 26, 744 (1987).

8. M. A. Ordal, L. L. Long, R. J. Bell, S. E. Bell, R. R. Bell, R. W. Alexander, Jr., and C. A. Ward, "Optical properties of the metals Al, Co, Cu, Au, Fe, Pb, Ni, Pb, Ni, Pt, Ag, Ti, and W in the infrared and far infrared," Appl. Opt. 22, 1099 (1983).

9. William H. Press, Brian P. Flannery, Saul A. Teukolsky, and William T. Vetterling, Numerical Recipes: the Art of Scientific Computing (Cambridge University Press, New York, NY, 1986).

FIGURES

TABLES

Blank

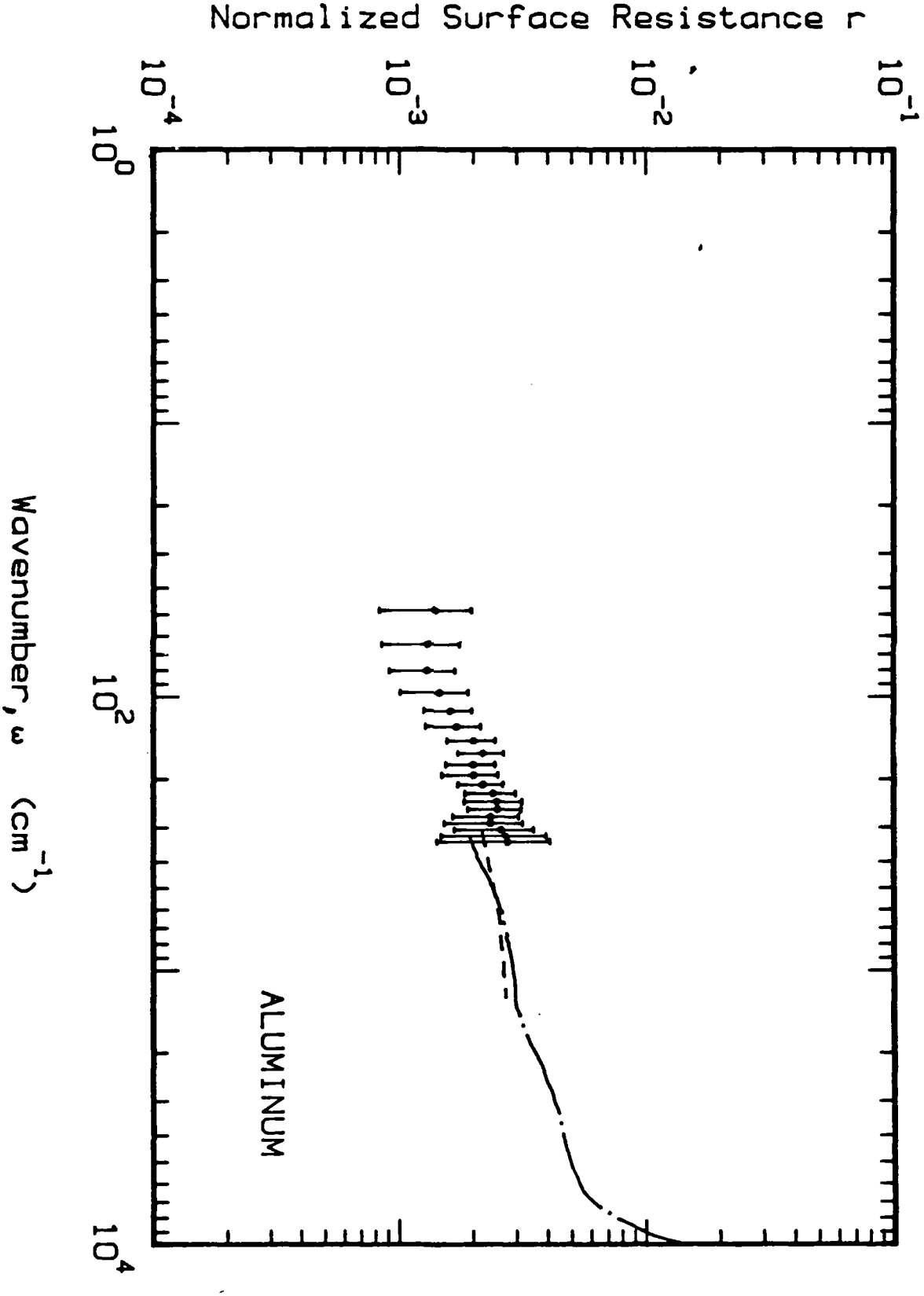
Normalized Surface Resistance r
10^{-4}
10^{-3}
10^{-2}
10^{-1}
10^{0}
10^{2}
10^{4}
Wavenumber, ω (cm^{-1})
ALUMINUM

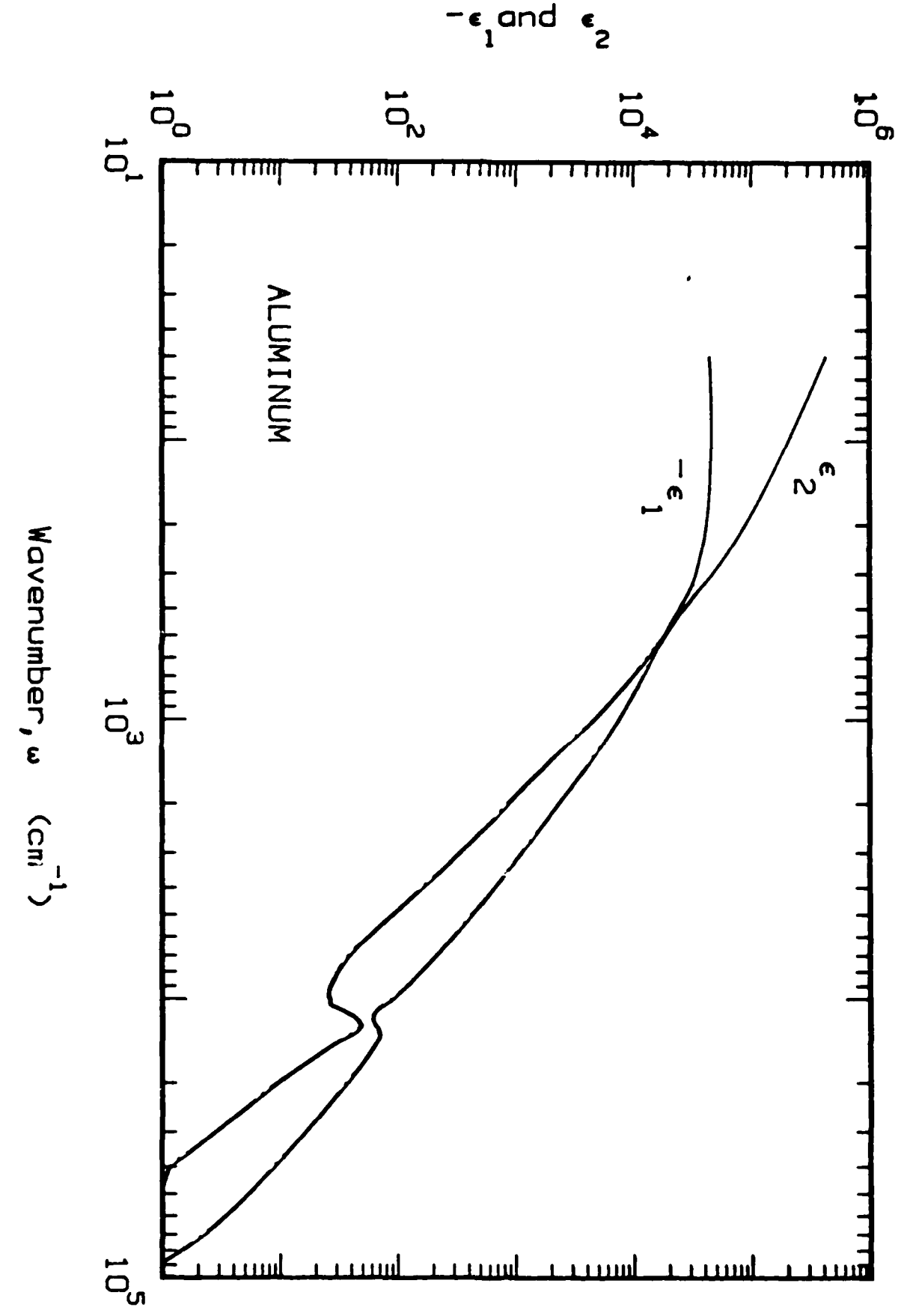
$-\epsilon_1$ and ϵ_2
10^0
10^2
10^4
10^6
10^1
10^3
10^5
ALUMINUM
$-\epsilon_1$
ϵ_2
Wavenumber, ω (cm^{-1})

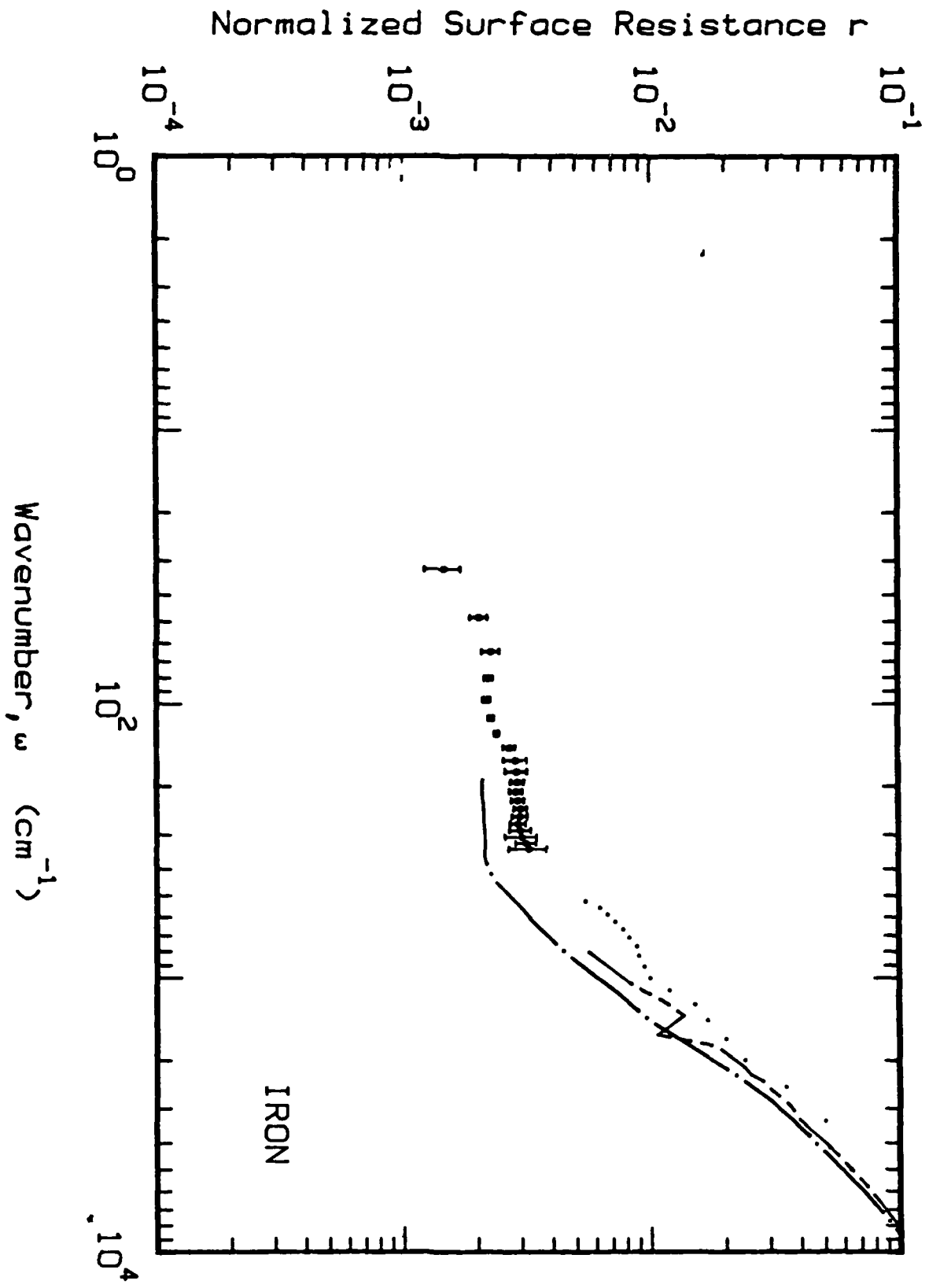
Normalized Surface Resistance r
10^{-4}
10^{-3}
10^{-2}
10^{-1}
10^{0}
10^{2}
10^{4}
Wavenumber, ω (cm^{-1})
IRON

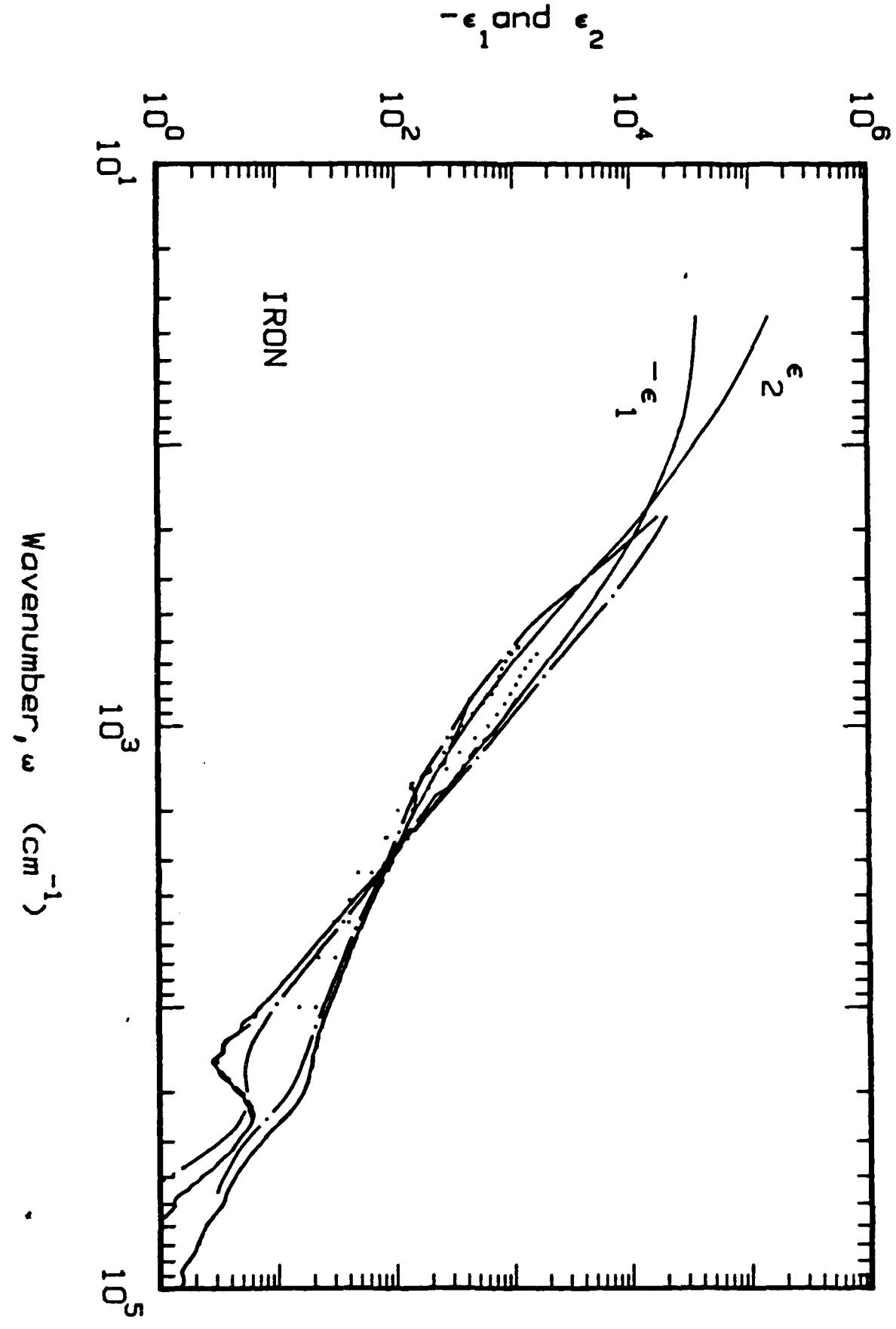
$-\epsilon_1$ and ϵ_2
10^0
10^2
10^4
10^6
10^1
10^3
10^5
IRON
$-\epsilon_1$
ϵ_2
Wavenumber, ω (cm^{-1})

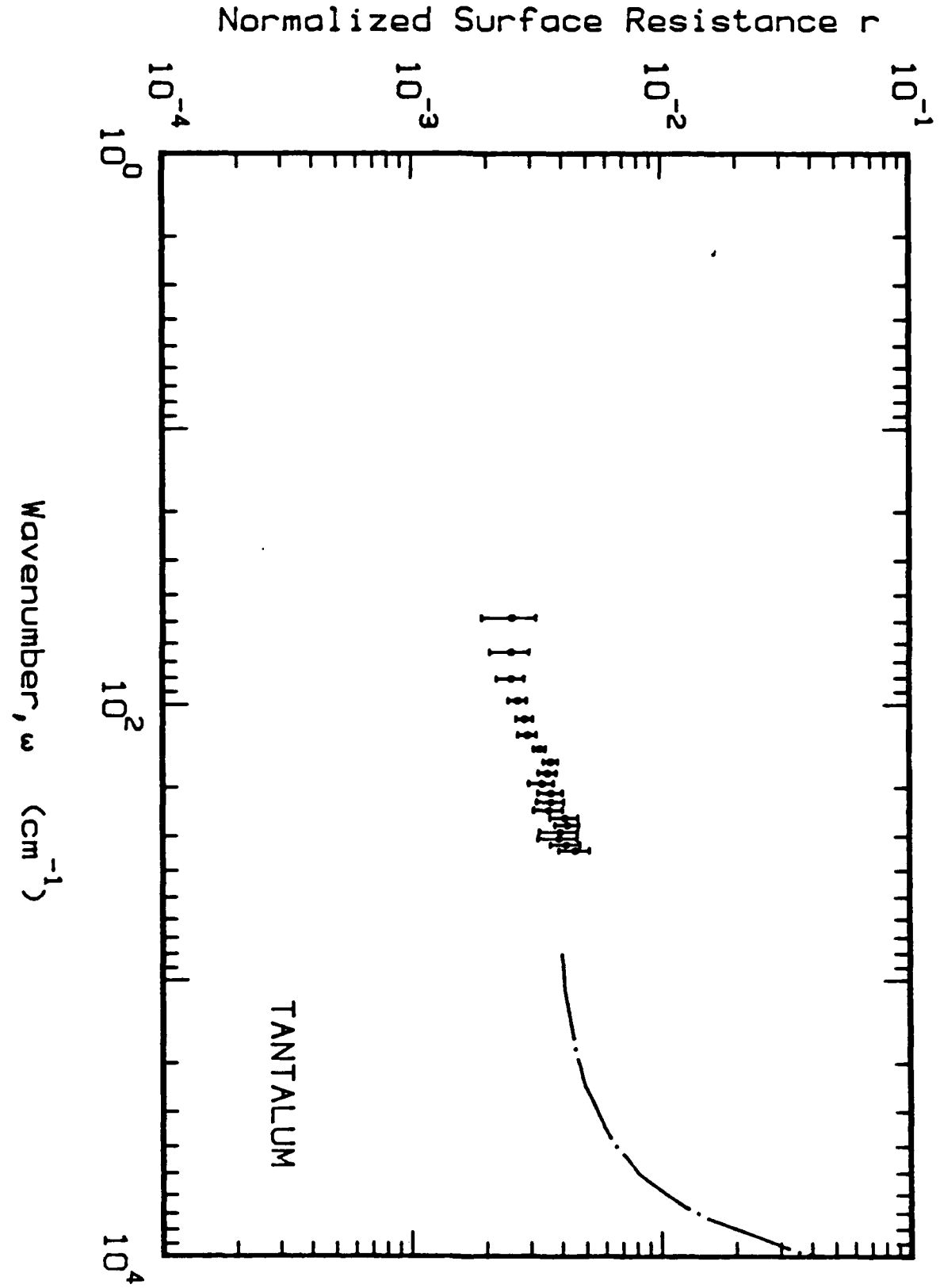
Normalized Surface Resistance r
10^{-4}
10^{-3}
10^{-2}
10^{-1}
10^{0}
10^{2}
10^{4}
Wavenumber, ω (cm^{-1})
TANTALUM

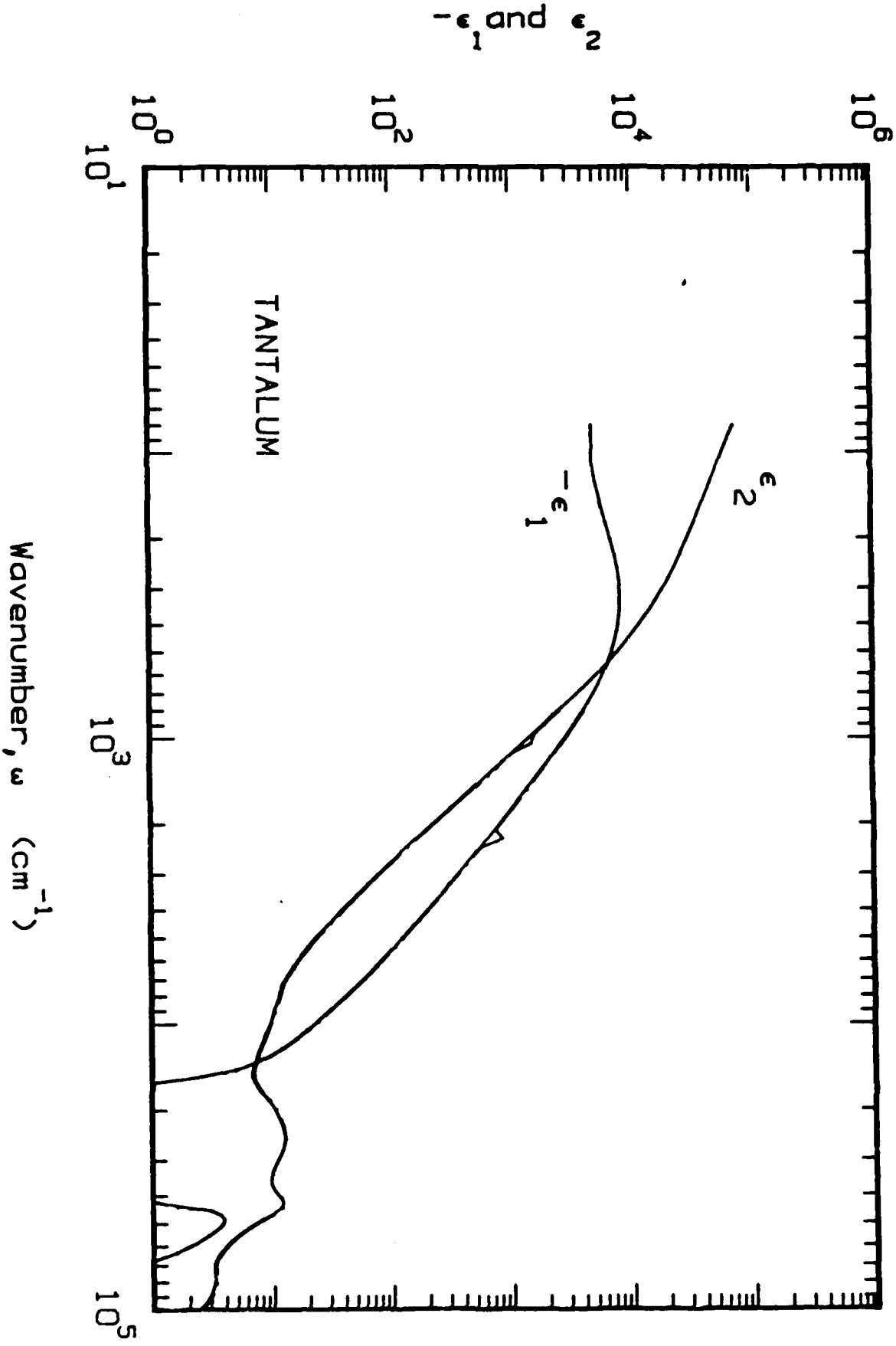
$-\epsilon_1$ and ϵ_2
10^0
10^2
10^4
10^6
10^1
10^3
10^5
TANTALUM
$-\epsilon_1$
ϵ_2
Wavenumber, ω (cm^{-1})

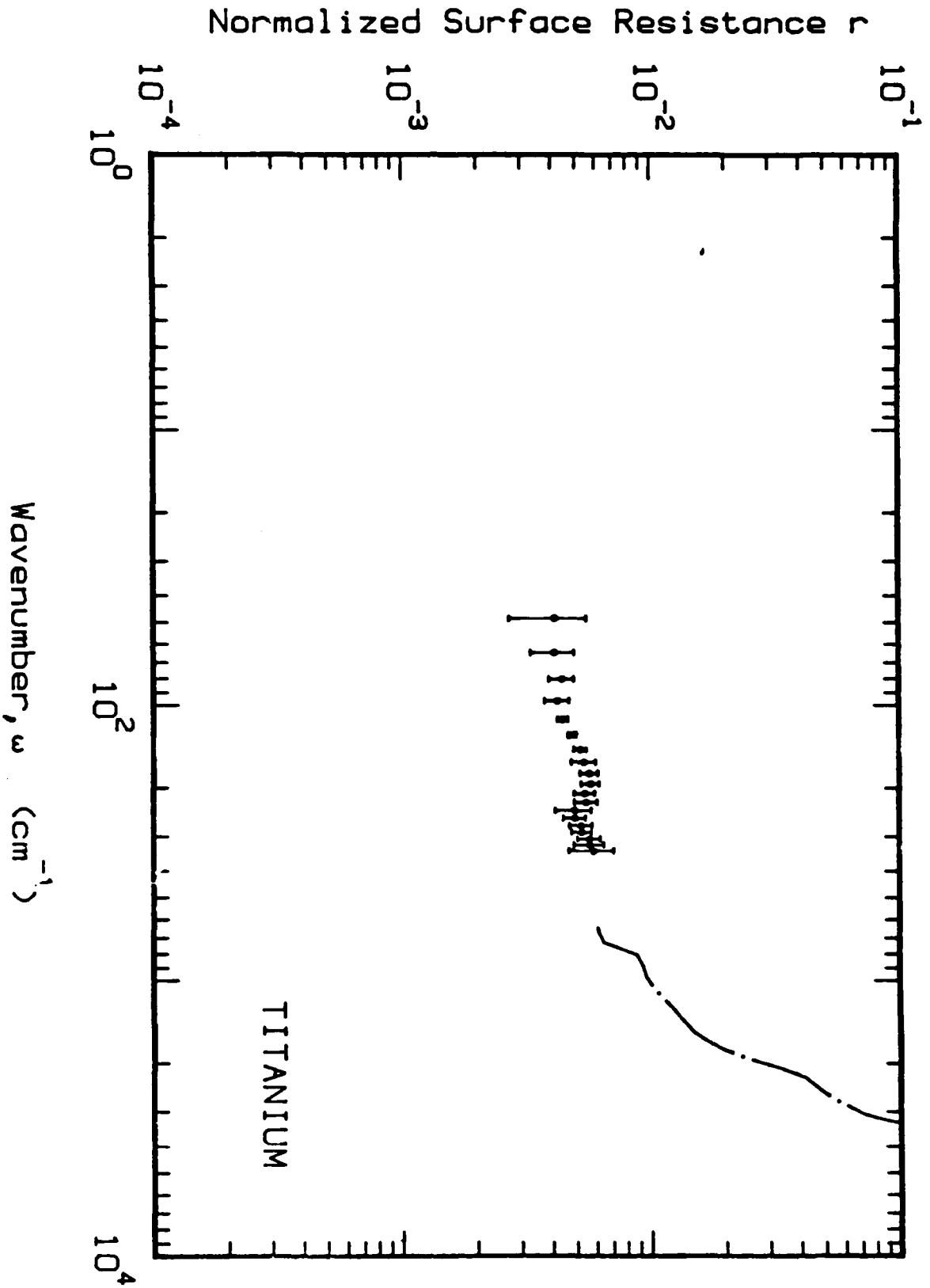
Normalized Surface Resistance r
10^{-4}
10^{-3}
10^{-2}
10^{-1}
10^{0}
10^{2}
10^{4}
Wavenumber, ω (cm^{-1})
TITANIUM

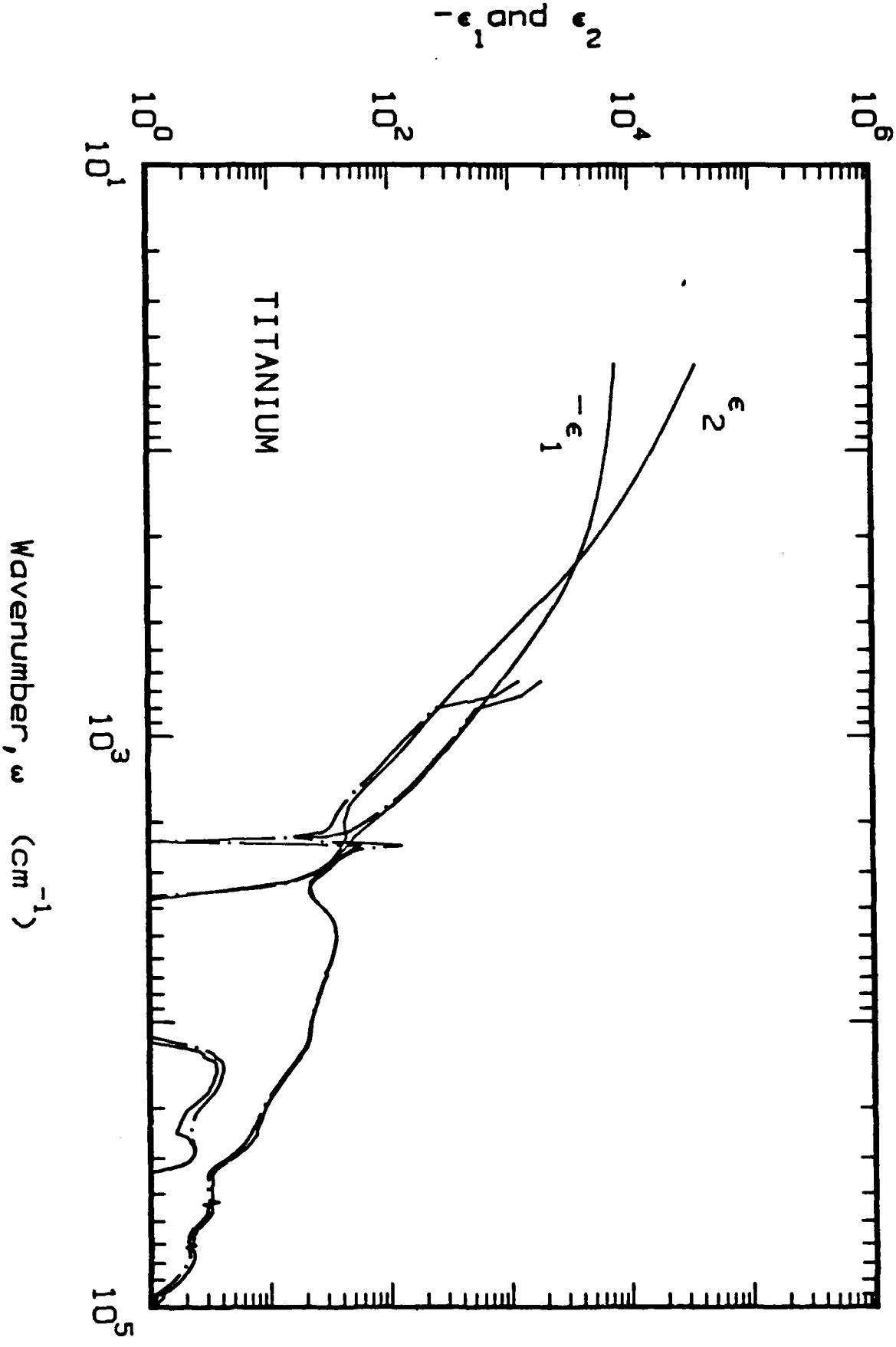
$-\epsilon_1$ and ϵ_2
10^0
10^2
10^4
10^6
10^1
10^3
10^5
TITANIUM
$-\epsilon_1$
ϵ_2
Wavenumber, ω (cm^{-1})

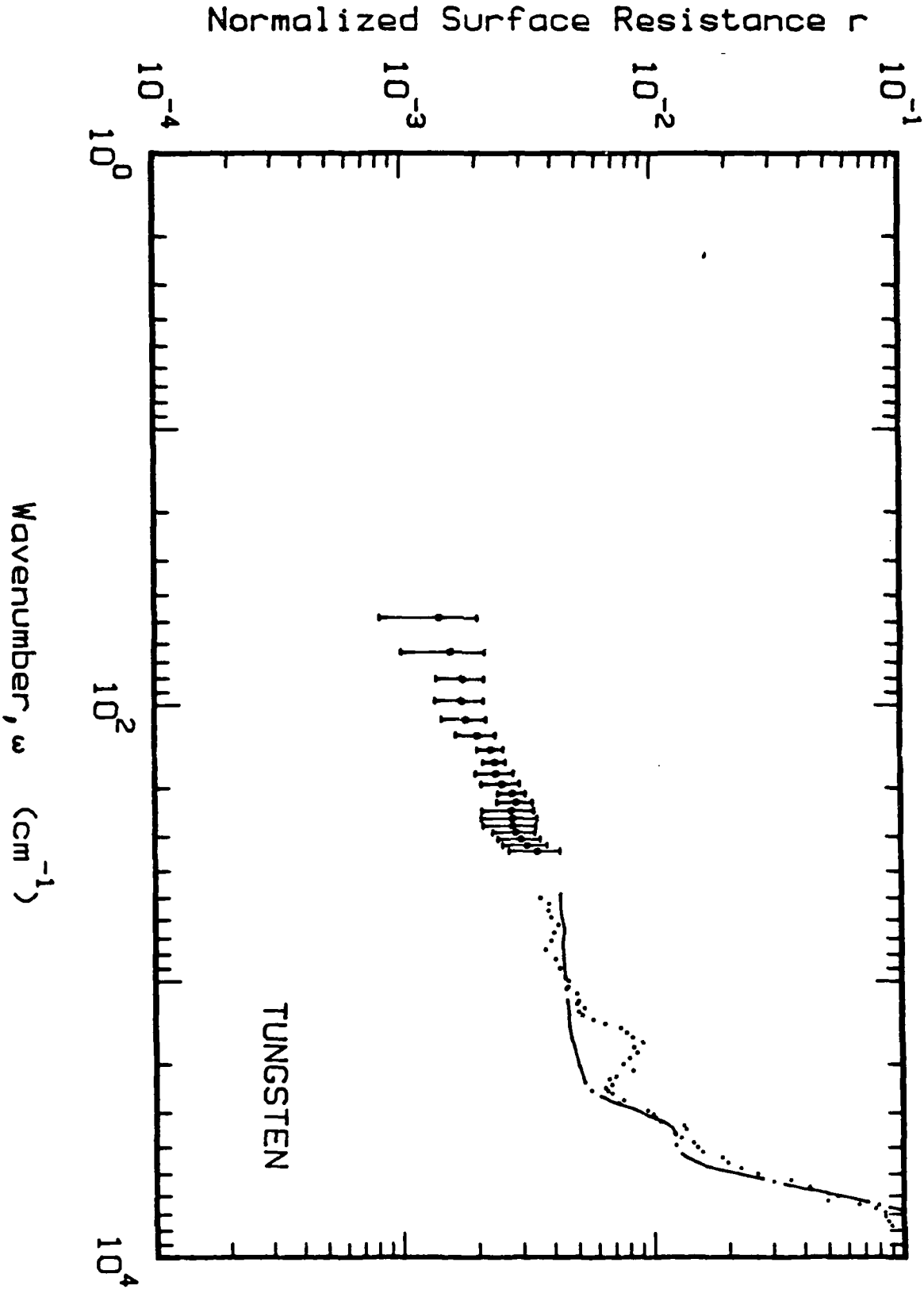
Normalized Surface Resistance r
10^{-4}
10^{-3}
10^{-2}
10^{-1}
10^{0}
10^{2}
10^{4}
Wavenumber, ω (cm^{-1})
TUNGSTEN

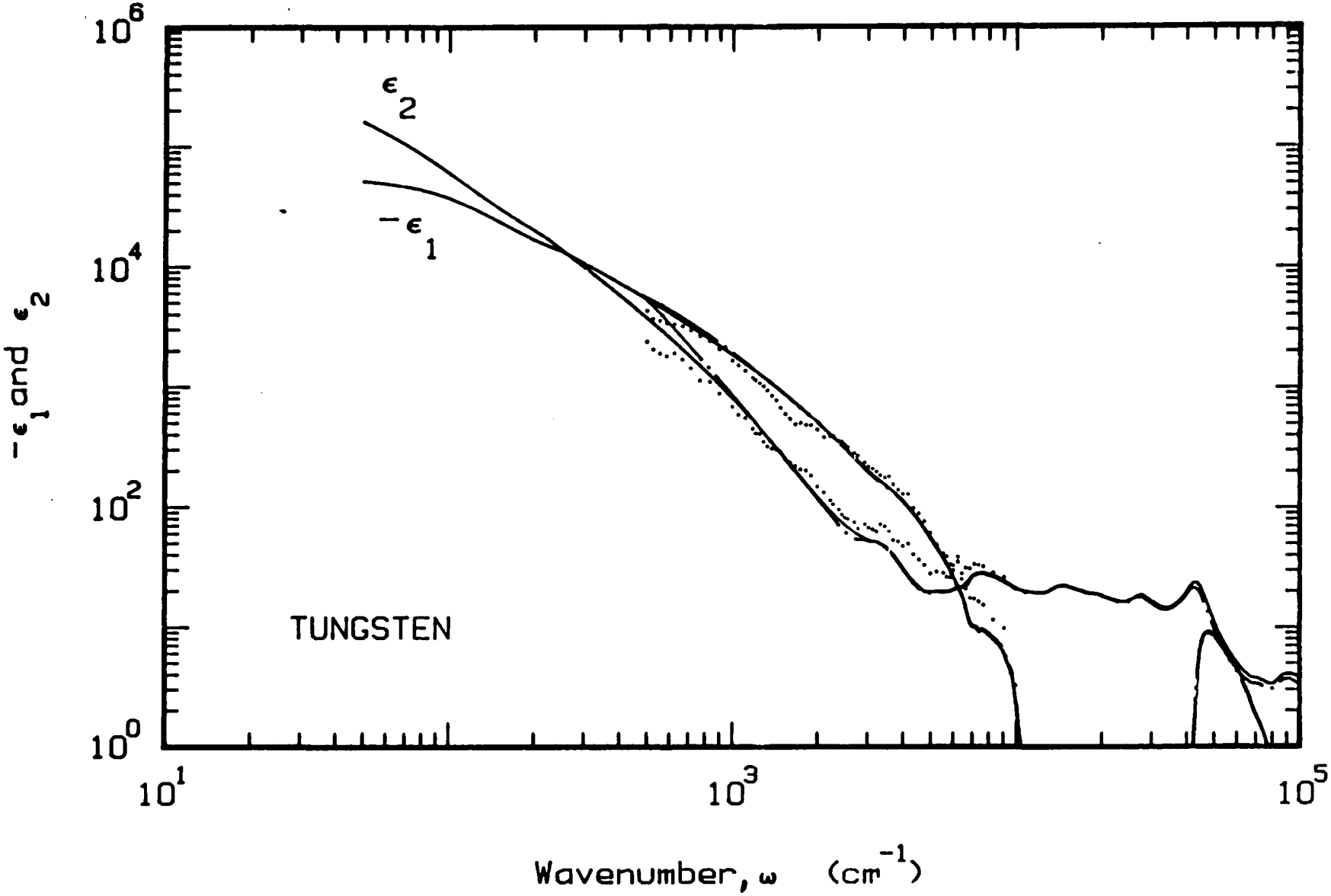
10^6
10^4
10^2
10^0
10^1
10^3
10^5
ϵ_2
$-\epsilon_1$
TUNGSTEN
$-\epsilon_1$ and ϵ_2
Wavenumber, ω (cm^{-1})

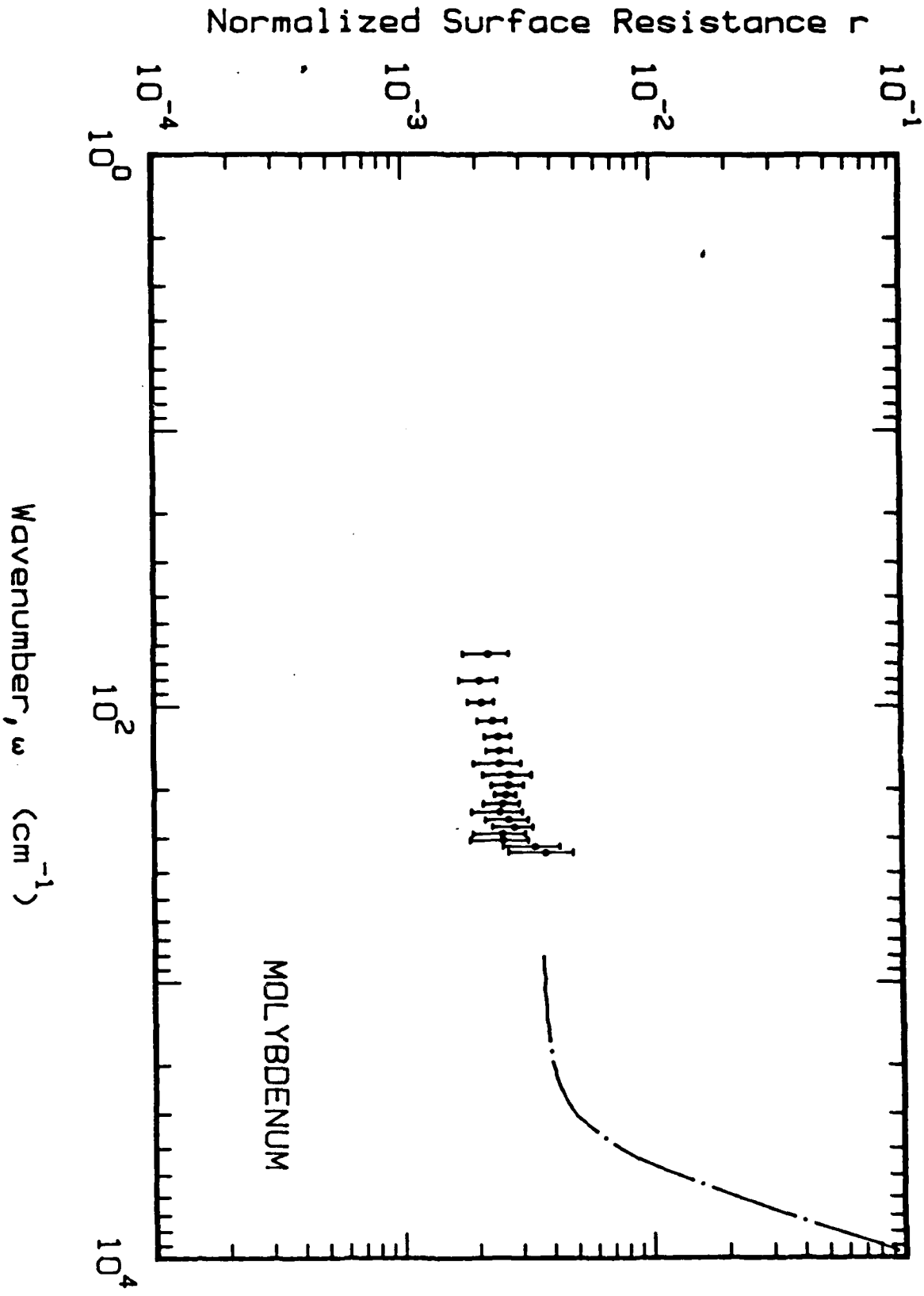
Normalized Surface Resistance r
10^{-4}
10^{-3}
10^{-2}
10^{-1}
10^{0}
10^{2}
10^{4}
Wavenumber, ω (cm^{-1})
MOLYBDENUM

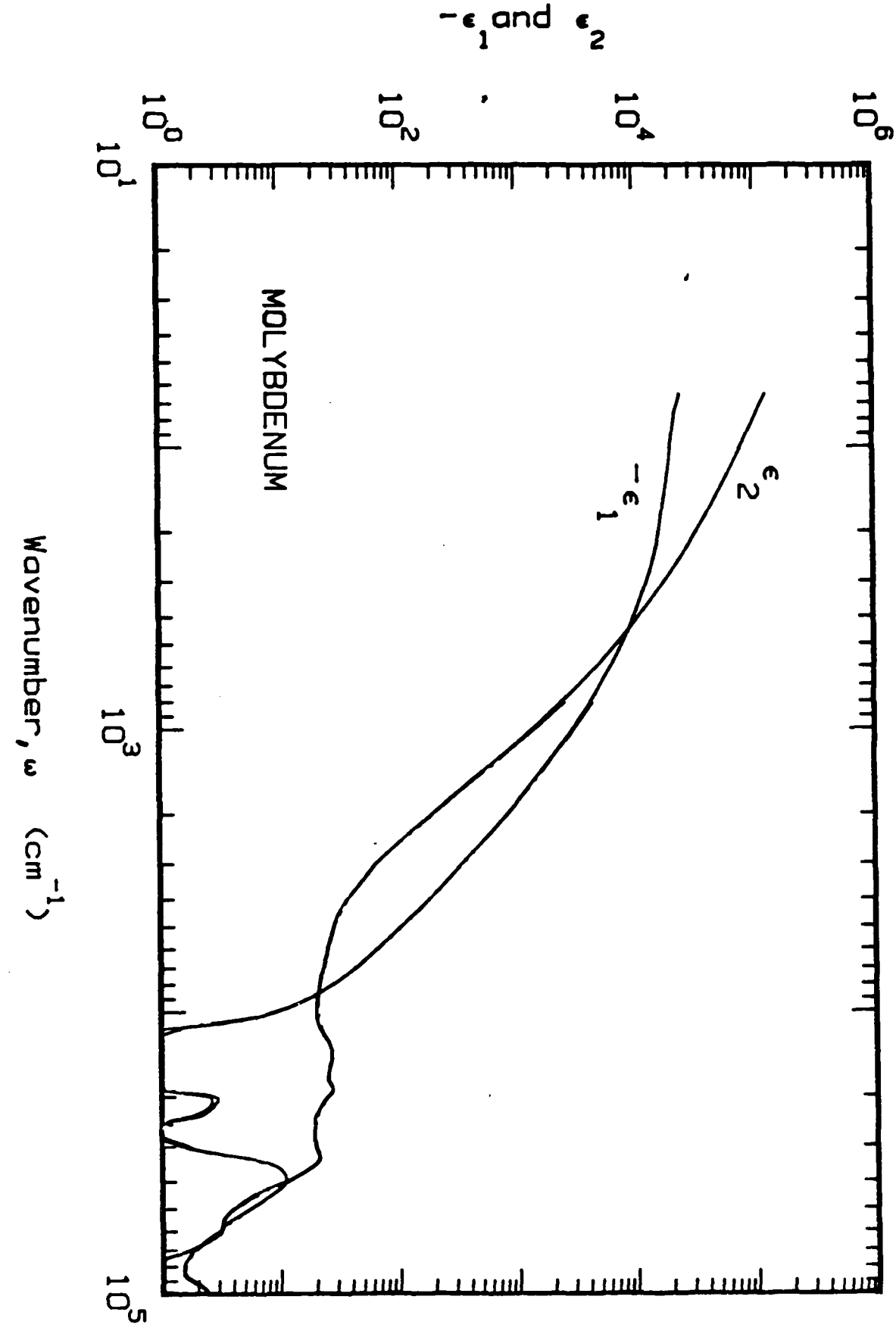
$-\epsilon_1$ and ϵ_2
10^0
10^2
10^4
10^6
10^1
10^3
10^5
MOLYBDENUM
$-\epsilon_1$
ϵ_2
Wavenumber, ω (cm^{-1})

Aluminum

Wn	n	k	-E1	E2	R
50	436.98909	485.19932	4445.8912	42405.361	0.995909
65	374.73526	431.44791	4572.0782	32335.749	0.995421
80	329.97183	393.77470	4617.7106	25986.911	0.995012
100	286.08777	357.47647	4594.3214	20453.929	0.994556
125	245.00980	324.59867	4533.4496	15905.971	0.994092
150	213.38844	299.72607	4430.1094	12791.616	0.993715
175	188.04844	279.77106	4290.9634	10522.102	0.993402
200	167.07810	263.04366	4127.6872	8789.7669	0.993141
225	149.32871	248.55977	3948.2895	7423.4221	0.992921
250	134.05166	235.70537	3758.7173	6319.3391	0.992734
300	108.95823	213.37170	3365.5586	4649.7203	0.992436
350	88.918176	192.23917	2904.9455	3418.7112	0.992103
400	76.681189	174.09538	2442.9198	2669.9682	0.991560
450	68.262241	159.23227	2069.5183	2173.9103	0.990944
500	61.871514	148.17314	1812.7196	1833.5393	0.990448
600	50.744867	131.07397	1460.5344	1330.2663	0.989778
700	42.226361	117.86671	1210.9495	995.41644	0.989283
800	35.492290	107.26425	1024.5918	761.41079	0.988941
900	30.167884	98.172167	872.76732	592.32931	0.988626
1000	25.832564	90.720430	756.28751	468.70826	0.988455
1250	17.708575	75.320562	535.95934	266.76396	0.988240
1500	13.385937	63.967532	391.26618	171.25308	0.987544
1750	10.625810	55.544522	297.22861	118.04110	0.986802
2000	8.8866481	49.131664	233.49479	873.23162	0.985847
2250	7.6669569	44.210650	189.57994	677.92230	0.984890
2500	6.5579910	40.184716	157.18041	527.06201	0.984310
2750	5.7888000	36.878956	132.65472	426.96980	0.983533
3000	5.0466806	34.058286	113.44979	343.76258	0.983129
3250	4.5104289	31.653186	981.58020	285.53889	0.982523
3500	4.0097886	29.575977	858.66002	237.18683	0.982175
3750	3.5693590	27.735962	756.54327	197.99921	0.981931
4000	3.1815630	26.073820	669.72172	165.91100	0.981750
4250	2.8842412	24.591905	596.44294	141.85797	0.981387
4500	2.6179915	23.257800	534.07140	121.77745	0.981098
4750	2.4038118	22.062867	480.99179	106.06996	0.980706
5000	2.1962737	20.969371	434.89089	92.108954	0.980475
5500	1.8892471	19.041604	359.01343	71.948588	0.979627
6000	1.6474236	17.430945	301.12384	57.432299	0.978801
6500	1.4501184	16.005291	254.06649	46.419134	0.977875
7000	1.3374754	14.766043	216.24717	39.498437	0.976063
7500	1.2712686	13.676589	185.43296	34.773235	0.973544
8000	1.2324984	12.721123	160.30791	31.357528	0.970446
8500	1.2366448	11.880035	139.60594	29.382766	0.966151
9000	1.2211025	11.108164	121.90021	27.128411	0.961937
9500	1.2553502	10.361271	105.78004	26.014047	0.955343
10000	1.3789601	9.6826848	91.852854	26.704071	0.944516
11000	2.0063894	8.4485537	67.352461	33.902178	0.900200
12000	2.7846191	8.3634734	62.193584	46.578175	0.867826
13000	2.6528613	8.7156916	68.925607	46.243043	0.881180
14000	2.0208103	8.5523233	69.058560	34.565246	0.901744
15000	1.6232262	8.0797904	62.648150	26.230654	0.910026

Iron

Wn	n	k	-E1	E2	R
35	238.51940	305.98052	36732.576	145964.88	0.993681
50	183.41621	260.36949	34150.764	95511.971	0.992793
65	147.11263	230.22637	31362.058	67738.412	0.992148
80	120.39992	207.32665	28488.201	49924.224	0.991657
100	95.357710	181.94710	24011.654	34700.117	0.991002
125	75.191427	158.19090	19370.609	23789.199	0.990244
150	61.295883	140.34826	15940.449	17205.541	0.989601
175	51.169978	126.39007	13356.084	12934.754	0.989052
200	43.260218	115.07592	11371.020	9956.4184	0.988617
225	36.866495	105.45507	9761.6343	7775.5179	0.988254
250	31.895957	97.090004	8409.1168	6193.5571	0.987859
300	24.861494	83.533158	6359.6947	4153.5182	0.986995
350	20.259827	73.149608	4940.4046	2963.9968	0.986035
400	17.093309	65.004217	3933.3670	2222.2744	0.984983
450	14.820484	58.469983	3199.0922	1733.1069	0.983843
500	13.131270	53.124410	2649.7727	1395.1820	0.982618
600	10.825531	44.921725	1900.7693	972.60302	0.979932
700	9.3532527	38.936666	1428.5806	728.36895	0.976952
800	8.3467645	34.384013	1112.5918	573.99051	0.973703
900	7.6216326	30.807425	891.00812	469.60574	0.970211
1000	7.0686579	27.901743	728.54132	394.45575	0.966484
1250	6.1662033	22.672232	476.00804	279.60318	0.956375
1500	5.6202947	19.159671	335.50527	215.36599	0.945291
1750	5.2507160	16.634437	249.13446	174.68540	0.933488
2000	4.9822242	14.731832	192.20431	146.79458	0.921172
2250	4.7769777	13.247145	152.66734	126.56263	0.908513
2500	4.6139960	12.056655	124.07398	111.25872	0.895658
2750	4.4807297	11.081212	102.71632	99.303831	0.882728
3000	4.3691978	10.267835	86.338543	89.724403	0.869826
3250	4.2740535	9.5797246	73.503589	81.888511	0.857039
3500	4.1915574	8.9905172	63.260247	75.368537	0.844443
3750	4.1189946	8.4808227	54.958237	69.864925	0.832098
4000	4.0543264	8.0360513	48.140558	65.161549	0.820056
4250	3.9959802	7.5450020	42.478198	61.098554	0.808360
4500	3.9427114	7.2989194	37.729251	57.555066	0.797041
4750	3.8935181	6.9908450	33.712430	54.437963	0.786125
5000	3.8475818	6.7151655	30.289563	51.674297	0.775627
5500	3.7628981	6.2434063	24.820721	46.986604	0.755918
6000	3.6845745	5.8553312	20.708815	43.148808	0.737893
6500	3.6099615	5.5306374	17.556128	39.930777	0.721452
7000	3.5376077	5.2542311	15.092276	37.174816	0.706403
7500	3.4671150	5.0146674	13.126002	34.772857	0.692509
8000	3.3989889	4.8032972	11.518539	32.652708	0.679513
8500	3.3344296	4.6138021	10.168749	30.768797	0.667177
9000	3.2750676	4.4419211	9.0045955	29.095184	0.655318
9500	3.2227697	4.2852453	7.9770831	27.620718	0.643845
10000	3.1837613	4.1442444	7.0384258	26.388570	0.632770
11000	3.0937414	3.8974446	5.6188386	24.115371	0.612663
12000	3.0342872	3.7486080	4.8451634	22.748707	0.599798
13000	2.9736330	3.5471579	3.7398358	21.095891	0.580766
14000	2.9443374	3.4648084	3.3357743	20.403130	0.572707
15000	2.8735043	3.3589960	3.0258269	19.304179	0.562747

Titanium

Wn	n	k	-E1	E2	R
50	119.99544	148.43379	7633.6859	35622.757	0.986912
65	100.49717	131.88977	7295.2320	26509.097	0.985486
80	86.399911	120.07897	6954.0133	20749.624	0.984332
100	72.630316	108.42373	6495.0594	15728.015	0.983096
125	59.644857	97.484039	5945.6290	11628.843	0.981900
150	49.906684	88.904473	5413.3282	8873.8550	0.980980
175	42.303853	81.834224	4907.2242	6923.8059	0.980260
200	36.217641	75.809491	4435.3614	5491.2818	0.979688
225	31.260311	70.562709	4001.8888	4411.6244	0.979228
250	27.169229	65.925258	3607.9727	3582.2769	0.978855
300	20.880752	58.046709	2933.4146	2424.1179	0.978295
350	16.284041	51.475157	2384.5218	1676.4472	0.977908
400	13.299690	45.839465	1924.3748	1219.3013	0.976928
450	11.217047	41.326081	1582.0229	927.11318	0.975840
500	9.6744916	37.605191	1320.5546	727.62220	0.974676
600	7.5817542	31.846917	956.74316	482.91100	0.972123
700	6.2397504	27.621553	724.01572	344.70319	0.969389
800	5.2931800	24.380236	566.37815	258.09795	0.966605
900	4.5921948	21.789718	453.70355	200.12526	0.963703
1000	4.0715739	19.664351	370.10899	160.12972	0.960509
1250	3.2048691	15.799043	239.33857	101.26773	0.952039
1500	2.4841185	12.895769	160.13002	64.069237	0.944315
1750	2.1867059	10.536270	106.23131	46.079449	0.927812
2000	2.3660792	8.7896083	71.658884	41.593819	0.893164
2250	2.8327334	7.7291731	51.715738	43.789373	0.847764
2500	2.7313635	7.0189943	41.805934	38.342850	0.827100
2750	2.5809283	6.2578349	32.499306	32.302046	0.801404
3000	2.3943002	5.4204022	23.648086	25.956140	0.765850
3250	2.4004043	4.4865443	14.367139	21.539041	0.697032
3500	3.0649496	3.5829978	3.4439569	21.963415	0.582456
3750	3.8144105	3.0741948	-5.0990540	23.452481	0.532393
4000	4.3647610	3.1898829	-8.8757860	27.846153	0.551827
4250	4.6520327	3.3990496	-10.087870	31.624980	0.572217
4500	4.7418094	3.6030774	-9.5025890	34.170213	0.587225
4750	4.7311251	3.7288987	-8.4788590	35.283772	0.595202
5000	4.6752372	3.8164244	-7.2927480	35.685379	0.600180
5500	4.4682212	3.8823682	-4.8922180	34.694560	0.602597
6000	4.2746437	3.8609249	-3.3658370	33.008157	0.599833
6500	4.0126191	3.8077018	-1.6025190	30.557715	0.594940
7000	3.9419174	3.7122171	-1.7581570	29.266506	0.587267
7500	3.8097162	3.5906589	-1.6211060	27.358783	0.577006
8000	3.6981480	3.5123265	-1.3398610	25.978206	0.570096
8500	3.6009322	3.4342207	-1.1728410	24.732792	0.563026
9000	3.5179021	3.3609902	-1.0793800	23.647269	0.556208
9500	3.4440424	3.2989913	-0.9780839	22.723732	0.550281
10000	3.3957928	3.2418121	-1.0220630	22.017044	0.544683
11000	3.3065327	3.2405736	-0.4318412	21.430125	0.544673
12000	3.1079186	3.3007447	1.2357575	20.516891	0.552333
13000	2.8061078	3.2717366	2.8300195	18.361692	0.554422
14000	2.5658703	3.1836237	3.5517695	16.337531	0.550850
15000	2.3704320	3.0317254	3.5724114	14.372998	0.538628

Tantalum

Wn	n	k	-E1	E2	R
80	184.49663	196.87085	4719.1248	72644.016	0.989914
100	164.07966	177.86128	4712.5008	58366.836	0.988854
125	145.58840	161.98150	5042.0233	47165.256	0.987798
150	131.25365	151.08524	5599.2281	39660.977	0.986978
175	119.43744	143.08774	6208.7985	34180.068	0.986342
200	109.23359	136.82885	6790.1559	29892.614	0.985848
225	100.17673	131.63028	7291.1522	26372.582	0.985462
250	92.016211	127.08528	7683.6846	23387.811	0.985160
300	77.867703	119.08288	8117.3521	18545.420	0.984732
350	66.138800	111.86857	8140.2353	14797.706	0.984458
400	56.428490	105.16669	7875.8590	11868.796	0.984280
450	48.392026	98.921392	7443.6535	9574.0132	0.984166
500	41.721911	93.122866	6931.1502	7770.5278	0.984101
600	31.493393	82.794230	5863.0508	5214.9424	0.984076
700	24.238520	73.949845	4881.0737	3584.8696	0.984120
800	19.058763	66.350003	4039.0864	2529.0980	0.984133
900	15.615760	59.926459	3347.3285	1871.5944	0.983848
1000	12.931507	54.673721	2821.9919	1414.0272	0.983751
1250	8.7691085	44.613332	1913.4521	782.43829	0.983183
1500	6.4122619	37.643719	1375.9325	482.76277	0.982575
1750	4.9008382	32.510917	1032.9415	318.66149	0.982045
2000	3.9020861	28.577040	801.42097	223.02015	0.981434
2250	3.1932058	25.461819	638.10767	162.60966	0.980818
2500	2.6799222	22.915456	517.93616	122.82328	0.980099
2750	2.3469537	20.845754	429.03725	97.848038	0.978939
3000	2.0587589	19.120563	361.35743	78.729256	0.978037
3250	1.8209204	17.640057	307.85584	64.242278	0.977176
3500	1.6348171	16.359682	264.96656	53.490174	0.976185
3750	1.4802727	15.240124	230.07017	45.119079	0.975165
4000	1.3499202	14.239580	200.94335	38.444593	0.974076
4250	1.2678805	13.363144	176.96610	33.885739	0.972395
4500	1.1923530	12.595572	157.22672	30.036736	0.970821
4750	1.1067824	11.896174	140.29399	26.332953	0.969668
5000	1.0326738	11.243595	125.35202	23.221933	0.968359
5500	0.9608260	10.114648	101.38292	19.436833	0.963794
6000	0.9019896	9.1771344	83.406210	16.555360	0.958925
6500	0.8564461	8.3686838	69.301368	14.334653	0.953379
7000	0.8354757	7.6548582	57.898834	12.790895	0.946069
7500	0.8414308	7.0171487	48.532371	11.808890	0.936051
8000	0.8740663	6.4776281	41.195673	11.323753	0.923111
8500	0.9012078	6.0121558	35.333842	10.836403	0.909337
9000	0.9253053	5.5894492	30.385753	10.343894	0.894096
9500	0.9603200	5.2167868	26.292650	10.019570	0.876318
10000	0.9821499	4.8873028	22.921110	9.6001281	0.858758
11000	1.0150307	4.2736932	17.234167	8.6758595	0.818134
12000	1.0730870	3.7362305	12.807903	8.0186007	0.764894
13000	1.1466787	3.2384897	9.1729431	7.4270145	0.696164
14000	1.2685432	2.7919609	6.1858440	7.0834463	0.607910
15000	1.4478379	2.3306224	3.3355663	6.7487268	0.493041

Tungsten

Wn	n	k	-E1	E2	R
50	242.14161	332.81796	52135.234	161178.15	0.994299
65	196.54283	294.94073	48242.936	116113.94	0.993758
80	163.02849	265.86909	44108.085	86688.476	0.993318
100	130.21900	234.03939	37817.448	60952.753	0.992765
125	103.53408	202.21197	30170.375	41871.663	0.992008
150	87.148396	177.92054	24060.874	31010.979	0.991158
175	76.505227	159.83902	19695.461	24457.041	0.990302
200	68.665703	146.58093	16770.990	20130.165	0.989572
225	61.731428	136.67195	14868.452	16873.909	0.989081
250	54.191208	128.08146	13468.174	13881.779	0.988856
300	44.209069	112.34062	10665.974	9932.9489	0.987941
350	37.127733	100.62038	8745.9914	7471.6129	0.987173
400	31.772550	91.217414	7311.1217	5796.4198	0.986472
450	27.599188	83.517367	6213.4354	4610.0231	0.985834
500	24.256111	77.087223	5354.0811	3739.6725	0.985255
600	19.231714	66.923752	4108.9298	2574.1169	0.984262
700	15.634532	59.208636	3261.2239	1851.3986	0.983466
800	12.935818	53.112521	2653.6045	1374.1078	0.982839
900	10.843912	48.146015	2200.4483	1044.1823	0.982356
1000	9.1935519	44.019189	1853.1676	809.38539	0.981988
1250	6.2868052	36.072044	1261.6684	453.55582	0.981431
1500	4.4961625	30.343034	900.48423	272.85443	0.981087
1750	3.3712766	26.005432	664.91701	175.34301	0.980608
2000	2.6672954	22.612178	504.19613	120.62672	0.979668
2250	2.2388765	19.898510	390.93813	89.100611	0.977966
2500	1.9949739	17.694770	309.12496	70.601208	0.975223
2750	1.8774806	15.887186	248.87776	59.655769	0.971191
3000	1.8505739	14.400460	203.94863	53.298233	0.965650
3250	1.9169200	13.261664	172.19714	50.843098	0.958414
3500	1.8748013	12.375593	149.64041	46.403556	0.953542
3750	1.6746349	11.554665	130.70589	38.699691	0.952379
4000	1.4507921	10.710594	112.61204	31.077692	0.951930
4250	1.2886548	9.8569158	95.498158	25.404325	0.949660
4500	1.2212030	9.0476312	80.368294	22.097989	0.943719
4750	1.1946455	8.2613235	66.822288	19.738707	0.934599
5000	1.2992808	7.5659499	55.555468	19.660587	0.916886
5500	1.5455798	6.4453363	39.153543	19.923564	0.871262
6000	1.8828191	5.4881071	26.574312	20.666226	0.804026
6500	2.2587782	4.7741297	17.690236	21.567400	0.729584
7000	3.0278249	4.3901355	10.105566	26.585123	0.658805
7500	3.1990778	4.4460869	9.5335904	28.446756	0.657852
8000	3.1960757	4.3367596	8.5925835	27.721224	0.648923
8500	3.1599449	4.1791582	7.4801119	26.411819	0.636480
9000	3.0821649	3.9693342	6.2558737	24.468285	0.619717
9500	3.0570934	3.7224010	4.5104492	22.759456	0.596640
10000	3.0826871	3.4208368	2.1991647	21.090740	0.565367
11000	3.2814572	3.0100921	-1.7073070	19.754977	0.520807
12000	3.5190631	2.7670600	-4.7271840	19.474918	0.498683
13000	3.7783360	2.6322954	-7.3468440	19.891393	0.492184
14000	3.9313491	2.7924078	-7.6579650	21.955860	0.510352
15000	3.8312601	2.9042727	-6.2437540	22.254049	0.517715

Molybdenum

Wn	n	k	-E1	E2	R
65	227.57460	276.18720	24489.170	125706.39	0.992917
80	200.43914	248.88501	21767.898	99772.593	0.992180
100	173.64793	224.74485	20356.642	78052.956	0.991426
125	148.54398	202.91175	19107.865	60282.639	0.990648
150	129.77236	186.39648	17902.784	48378.221	0.989988
175	114.94950	173.65334	16942.094	39922.730	0.989454
200	102.12640	163.32577	16245.505	33359.746	0.989051
225	91.330970	154.08616	15401.198	28145.676	0.988678
250	82.241906	145.83988	14505.539	23988.299	0.988334
300	67.891603	131.81545	12766.043	17898.324	0.987724
350	57.122067	120.35199	11221.672	13749.509	0.987209
400	48.760817	110.79000	9896.8064	10804.422	0.986777
450	42.092997	102.66741	8768.7765	8643.1578	0.986419
500	36.663706	95.659355	7806.4849	7014.4529	0.986124
600	28.406166	84.122793	6269.7341	4779.2120	0.985692
700	22.527740	75.010773	5119.1170	3379.6464	0.985419
800	17.948846	67.549462	4240.7687	2424.8698	0.985413
900	14.599652	61.094152	3519.3455	1783.9067	0.985312
1000	12.132436	55.822815	2968.9906	1354.5334	0.985243
1250	8.0417701	45.523100	2007.6825	732.17260	0.985067
1500	5.7374219	38.275608	1432.1042	439.20663	0.984806
1750	4.3080595	32.926140	1065.5713	283.69553	0.984508
2000	3.3460153	28.788898	817.60482	192.65619	0.984211
2250	2.7142480	25.500166	642.89134	138.42755	0.983650
2500	2.2903056	22.850789	516.91304	104.67058	0.982811
2750	1.9643186	20.649783	422.55498	81.125506	0.981946
3000	1.7296250	18.769452	349.30071	64.928225	0.980768
3250	1.6006395	17.177196	292.49402	54.988998	0.978787
3500	1.5147128	15.828837	248.25772	47.952285	0.976413
3750	1.4347181	14.654142	212.68547	42.049125	0.973994
4000	1.3719253	13.607095	183.27087	37.335836	0.971235
4250	1.3358240	12.667669	158.68541	33.843553	0.967797
4500	1.3246140	11.821314	137.98887	31.317357	0.963496
4750	1.3419643	11.064120	120.61389	29.695309	0.958031
5000	1.3787354	10.396535	106.18703	28.668141	0.951515
5500	1.4476138	9.2513402	83.491710	26.784735	0.936770
6000	1.5124883	8.2838453	66.334472	25.058437	0.919264
6500	1.6167352	7.4926629	53.526165	24.227304	0.897329
7000	1.7014062	6.7993804	43.336791	23.137016	0.872861
7500	1.7797564	6.1751066	34.964409	21.980371	0.844763
8000	1.9061057	5.6230394	27.985333	21.436215	0.809694
8500	2.0338468	5.1486289	22.371847	20.943045	0.772198
9000	2.1691522	4.7136001	17.512805	20.449032	0.731054
9500	2.3419619	4.3245235	13.216718	20.255738	0.686382
10000	2.5372515	3.9968299	9.5370042	20.281926	0.643729
11000	2.9807157	3.4956418	3.3348457	20.839029	0.575179
12000	3.4879914	3.2991627	-1.2816100	23.014903	0.550322
13000	3.7771262	3.4266289	-2.5248970	25.885619	0.562867
14000	3.8159832	3.5417088	-2.0180270	27.030203	0.572886
15000	3.7361860	3.5912220	-1.0622100	26.834947	0.576976